# Funktion oligomerer Pmp Adhäsine im Infektionsprozess von Chlamydien

Inaugural-Dissertation

zur Erlangung des Doktorgrades
der Mathematisch-Naturwissenschaftlichen Fakultät
der Heinrich-Heine-Universität Düsseldorf

vorgelegt von

Sebastian Wintgens
aus Duisburg

Düsseldorf, Mai 2023

aus dem Institut für Funktionelle Genomforschung der Mikroorganismen
der Heinrich-Heine-Universität Düsseldorf.

Gedruckt mit der Genehmigung der
Mathematisch-Naturwissenschaftlichen Fakultät der
Heinrich-Heine-Universität Düsseldorf

Berichterstatter:

1. Prof. Dr. Johannes H. Hegemann

2. Prof. Dr. Klaus Pfeffer

Tag der mündlichen Prüfung: 19.07.2023

# Inhalt

*Abkürzungsverzeichnis* ..... *5*

*Zusammenfassung* ..... *7*

*Summary* ..... *9*

*1. Einleitung* ..... *11*

1.1 Taxonomie von Chlamydien ..... 11

1.2 Pathogenität von Chlamydien ..... 12

1.2.1 *Chlamydia pneumoniae* ..... 14

1.2.2 *Chlamydia trachomatis* ..... 14

1.3 Der biphasische Entwicklungszyklus ..... 16

1.4 Adhäsion und Internalisierung von Chlamydien ..... 18

1.4.1 Die chlamydiale Adhäsion ..... 18

1.4.2 Die Internalisierung in die Wirtszelle ..... 22

1.5 Die chlamydiale Zellwand ..... 24

1.5.1 Chlamydiale äußere Membran-Komplex (COMC) ..... 26

1.5.2 Major outer membrane protein ..... 28

1.5.3 OmcA und OmcB ..... 28

1.6 Bakterielle Sekretionssysteme ..... 30

1.6.1 Das Typ-V-Sekretionssystem der Pmps ..... 30

1.7 Die Familie der Polymorphen Membranproteine ..... 33

1.7.1 Funktion innerhalb der Infektion ..... 35

1.7.2 Expression der Pmps ..... 37

1.7.3 Oligomerisierung von Pmps ..... 39

1.7.4 Prozessierung von Pmps ..... 40

1.8 Impfstoffe ..... 42

1.9 Amyloide ..... 44

1.9.1 Klassischer Aufbau amyloider Proteine ..... 44

1.9.2 Funktionelle Amyloide ..... 48

1.9.3 Toxische Amyloide ..... 49

1.9.4 Die Rolle von Amyloid-β in der Alzheimer-Erkrankung ..... 50

1.9.5 *C. pneumoniae* und die Alzheimer Erkrankung ..... 53

1.9 Ziel dieser Arbeit ..... 55

*2. Teil I Manuskript I* ..... *56*

2.1 Zusammenfassung ..... 57

*3. Teil II Manuskript II* ..... *88*

3.1 Zusammenfassung ..... 89

*4. Teil III Manuskript III* ..... *126*

4.1 Zusammenfassung ..... 127

*5. Teil IV Abschließende Diskussion* ..... *162*

5.1 Pmps favorisieren Proteine der Pmp-Familie als Interaktionspartner auf der chlamydialen Oberfläche ..... 162

5.2 *C. pneumoniae* Pmp21 und Aβ-Oligomere weisen einen ähnlichen Bindungsmodus für das zelluläre Prion Protein $PrP^C$ auf ..... 165

5.3 Ein Fünf-Komponenten-Impfstoff aus PmpA, PmpD, PmpG, PmpH und Ctad1 vermittelt einen langanhaltenden Infektionsschutz ..... 169

*Literaturverzeichnis* ..... *172*

*Abbildungsverzeichnis* ..... *193*

*Danksagung* ..... *194*

*Eidesstattliche Erklärung* ..... *195*

# Abkürzungsverzeichnis

| Begriff | Abkürzung |
|---|---|
| **3'Sulfogalactolipid** | 3'SGL |
| **aberranter Körper (aberrant body)** | AB |
| **allgemeine Sekretionsweg** | Sec-Weg |
| **Aminosäure (amino acid)** | aa |
| **Amyloid-Vorläuferprotein (Amyloid Precursor Protein)** | APP |
| **APP intrazelluläre C-terminale Domäne** | AICD |
| **Autotransporter-Untergruppe 5a** | At-5a |
| **Biofilm assoziiertes Protein** | Bap |
| **Bluthirnschranke (Blood–brain barrier)** | BBB |
| **Centers for Disease Control and Prevention** | CDC |
| **Chlamydia outer membrane complex** | COMC |
| **Früh einsetzende Alzheimer-Krankheit (Early-onset Alzheimer's disease)** | EOAD |
| **Elementarkörperchen (elementary body)** | EB |
| **Ephrin Rezeptor A2** | EPHA2 |
| **Epidermaler Wachstumsfaktor Rezeptor** | EGFR |
| **Fibroblast Wachstumsfaktor Rezeptor** | FGFR |
| **Heparansulfat-ähnliche Glykosaminoglykane** | HS-GAGs |
| **Integrin beta-1 Rezeptor** | ITGB1 |
| **Kilobasen** | Kb |
| **Spät einsetzende Alzheimer-Krankheit (Late-onset Alzheimers's disease)** | LOAD |
| **Leitsequenz (signal sequence)** | SS |
| **Lipopolysaccharid** | LPS |
| **Lymphogranuloma venereum** | LGV |
| **Major Basic Protein** | MBP |
| **Major Outer Membrane Protein** | MOMP |
| **Mannose-6-Phosphat Rezeptor** | M6PR |
| **Megabasen** | Mb |

| | |
|---|---|
| **Membranangriffskomplex/Perforinprotein** | MACPF |
| **Monozyten-Chemoattraktant-Protein-1** | MCP-1 |
| **Outer Membrane Protein** | OmcB |
| **Polyacrylamid-Gelelektrophorese** | PAGE |
| **Polymorphe Membran Protein 21** | Pmp21 |
| **polymorphes Membranprotein** | Pmp |
| **reaktive Sauerstoffspezies** | ROS |
| **Retikular Körper (reticular body)** | RB |
| **Sorting Nexin 9** | SNX9 |
| **Stunde (hour)** | h |
| **Thioflavin T** | ThT |
| **Transelektronenmikroskopie** | TEM |
| **Typ-3-Sekretionssystem** | T3SS |
| **Typ-5-Sekretionssystem** | T5SS |
| **variable Domäne 4** | VD4 |
| **Zwillings-Arginin-Translokationsweg** | Tat-Weg |
| **zystische Fibrose Transmembran Konduktanz Regulator** | CFTR |
| **α-Carboxy-terminales Protein-Fragment** | α-CFT |

# Zusammenfassung

Chlamydien sind gramnegative, obligat intrazelluläre und bakterielle Krankheitserreger, die Infektionen bei Menschen und Tieren verursachen. Wichtigster und initialer Schritt der Infektion ist die Bindung an die Wirtszelle über Adhäsine. Polymorphe Membranproteine (Pmps) sind eine hochkonservierte Familie von Proteinen, die bei allen Chlamydien in unterschiedlicher Anzahl vorkommen. Alle *C. trachomatis* Pmps sowie Pmp6, Pmp20 und Pmp21 von *C. pneumoniae* wurden als Adhäsine charakterisiert.

Untersuchungen *in vitro* zeigten, dass Pmp-Proteinfragmente aus *C. trachomatis* homomere und heteromere funktionale Oligomere und Protofibrillen generieren konnten. Es entstand die Hypothese, dass infektiöse chlamydiale EBs verschiedene Pmp-Komplexe auf der Zelloberfläche präsentieren könnten um damit eine Antigenvariation für die Immunvermeidung zu erzeugen. Projekt 1 vertiefte diese Analysen und untersuchte die *in vitro* Oligomerisation von PmpG, PmpH und PmpI in ihrer Volllänge-Form (ohne β-Fass) sowie die Kartierung des proteinösen Gebietes um PmpI. PmpG, PmpH und PmpI waren in der Lage an HEp-2 Zellen zu binden und hochmolekulare homomere und heteromere Komplexe zu generieren. Alle Pmp-Proteine zeigten eine Oligomerisations-Kinetik, vergleichbar mit anderen Oligomer bildenden Proteinen wie Amyloid-β (Aβ). Atomkraftmikroskopische Aufnahmen zeigten Oligomere und Protofibrillen für PmpG und PmpH, wohingegen PmpI Oligomere und große Proteinakkumulationen erzeugte. Zur Untersuchung der nativen räumlichen Umgebung von PmpI auf der chlamydialen Oberfläche wurden PmpI-APEX2 Fusionsproteine kloniert und von Chlamydien exprimiert. Markierte Proteine wurden analysiert und zeigten eine starke Anreicherung von Proteinen der Pmp-Familie wie PmpD, PmpG, PmpI, PmpB und PmpF. Insbesondere PmpD zeigte eine sehr starke Anreicherung was darauf hindeutet, dass es heteromere PmpI-PmpD-Komplexe auf der Oberfläche von EBs geben könnte. Dies könnte zu Clustern mit akkumulierten adhäsiven Eigenschaften führen, die eine verbesserte Bindung und Infektion bewirken.

1998 wurden von Balin *et al.* die ersten Daten veröffentlicht, die einen Zusammenhang zwischen einer *C. pneumoniae* Infektion und der spät auftretenden Alzheimer-Krankheit herstellen. Luczak *et al*. 2016 demonstrierte, dass rekombinantes Pmp21_D-wt (ein kurzer C-terminaler Teil der *C. pneumoniae* Pmp21-Passagierdomäne) oligomerisiert, in der Lage ist Protofibrillen zu generieren und Ähnlichkeiten zu dem bereits für Alzheimer beschriebenen Aβ ausweist. Projekt 2 zeigte, dass Pmp21_D-wt eine Oligomerisations-Kinetik, vergleichbar zu Aβ, aufwies. Untersuchungen mittels Atomkraftmikroskopie visualisierten Pmp21_D-wt als Oligomere und Protofibrillen. Es wurde gezeigt, dass chlamydiale EBs und das zelluläre Prion-Protein ($PrP^C$; wichtiger Rezeptor in der Pathogenese von Alzheimer) in einer Infektion kolokalisierten und $PrP^C$ mittels rekombinantem Pmp21_D-wt angereichert werden konnte. Diese

Interaktion wurde als spezifisch bestimmt, da Pmp21_D-wt Oligomere nur an PrP-Fragmente banden, welche Motive aufwiesen, die auch schon für die Bindung mit Aβ beschrieben wurden. Dies untermauert die Theorie eines möglichen chlamydialen Einflusses in der Entstehung von Alzheimer und bildet zugleich einen der ersten kausalen Erklärungsansätze.

Ein Großteil der Pmp-Proteinfamilie konnte bereits als chlamydiales Oberflächenprotein und als Adhäsin identifiziert werden. Ziel von Projekt 3 war, in einer Kooperation mit der AG Klos (Medizinische Hochschule Hannover) und AG Guzmán (Helmholtz-Zentrum für Infektionsforschung), die Entwicklung eines Multikomponenten Impfstoffes aus PmpA, PmpD, PmpG und PmpH sowie Ctad1 aus *C. trachomatis* Serovar E, verstärkt mit dem mukosalen Adjuvans zyklisches Diadenosinmonophosphat. Es wurde ein Mausmodell mit Impfung und Lungeninfektion verwendet. Wir konnten zeigen, dass eine intranasale Impfung zu serovarübergreifendem und wirkungsvollen Schutz gegen urogenitale und okuläre Stämme von *C. trachomatis* führte, welcher mindestens 5 Monate andauerte.

# Summary

*Chlamydiae* are gram-negative, obligate intracellular and bacterial pathogens that cause infections in humans and animals. The most important and initial step of infection is binding to the host cell via adhesins. Polymorphic membrane proteins (Pmps) are a highly conserved family of proteins found in varying numbers in all *Chlamydiae*. All *C. trachomatis* Pmps as well as Pmp6, Pmp20 and Pmp21 of *C. pneumoniae* have been characterized as adhesins.

Studies *in vitro* showed that Pmp protein fragments from *C. trachomatis* generate homomeric and heteromeric functional oligomers and protofibrils. The hypothesis emerged that infectious chlamydial EBs could present different Pmp complexes on the cell surface to generate antigen variation for immune evasion. Project 1 elaborated on these analyses and investigated the *in vitro* oligomerisation of PmpG, PmpH and PmpI in their full-length form (without β-barrel) and mapped the proteinaceous area around PmpI. PmpG, PmpH and PmpI were able to bind to HEp-2 cells and generate high molecular weight homomeric and heteromeric complexes. All Pmp proteins showed oligomerisation kinetics comparable to other oligomer-forming proteins such as amyloid-β (Aβ). Atomic force microscopy images showed oligomers and protofibrils for PmpG and PmpH, whereas PmpI generated oligomers and large protein accumulations. To investigate the native spatial environment of PmpI on the chlamydial surface, PmpI-APEX2 fusion proteins were cloned and expressed by *C. trachomatis*. Labeled proteins were analyzed and showed strong enrichment of Pmp family proteins such as PmpD, PmpG, PmpI, PmpB and PmpF. In particular, PmpD showed very strong enrichment suggesting that there might be heteromeric PmpI-PmpD complexes on the surface of EBs. This could lead to clusters with accumulated adhesive properties, resulting in enhanced binding and infection.

In 1998, Balin et al. published the first data linking a *C. pneumoniae* infection to late-onset Alzheimer's disease. Luczak et al. 2016 demonstrated that recombinant Pmp21_D-wt (a short C-terminal part of the *C. pneumoniae* Pmp21 passenger domain) oligomerizes, is able to generate protofibrils and may show similarities to Aβ (a toxic agent for the generation of Alzheimer's disease). Project 2 showed that Pmp21_D-wt exhibited oligomerisation kinetics comparable to Aβ. Atomic force microscopy analyses visualized Pmp21_D-wt as oligomers and protofibrils. It was shown that chlamydial EBs and the cellular prion protein ($PrP^C$; important receptor in the pathogenesis of AD) colocalized in an infection and that $PrP^C$ could be enriched using recombinant Pmp21_D-wt. This interaction was confirmed to be specific, as Pmp21_D-wt oligomers only bound to PrP fragments that exhibited motifs already described for binding with Aβ. This

supports the theory of a possible chlamydial influence in the development of Alzheimer's disease and at the same time forms one of the first causal explanations.

A large part of the Pmp protein family has already been identified as a chlamydial surface protein and as an adhesin. The aim of project 3 was, in cooperation with AG Klos (Medizinische Hochschule Hannover) and AG Guzmán (Helmholtz-Zentrum für Infektionsforschung), to develop a multicomponent vaccine consisting of PmpA, PmpD, PmpG and PmpH as well as Ctad1 from *C. trachomatis* serovar E, boosted with the mucosal adjuvant cyclic diadenosine monophosphate. A mouse model with vaccination and lung infection was used. We were able to show that intranasal vaccination resulted in cross-serovar and effective protection against urogenital and ocular strains of *C. trachomatis*, which lasted at least 5 months.

# 1. Einleitung

## 1.1 Taxonomie von Chlamydien

Bakterien, welche der Ordnung der *Chlamydiales* angehören, sind gramnegative obligate intrazelluläre Parasiten, welche eine Vielzahl von Tieren, einschließlich des Menschen, infizieren können [2]. Sie zeichnen sich in ihrer Vermehrung durch einen einzigartigen biphasischen Lebenszyklus aus, an welchem infektiöse Elementar Körper (EBs), metabolisch aktive Retikular Körper (RBs) sowie die persistenten und aberranten Körper (ABs) beteiligt sind [3]. Die Ordnung der *Chlamydiales* beinhaltet die Familie der *Chlamydiaceae*, sowie einige Chlamydien-ähnliche Familien wie die *Parachlamydiaceae*, *Waddliaceae* und *Simkaniaceae*, *Rhabdochlamydiaceae*, *Criblamydiaceae, Piscichlamydiaceae, Clavichlamydiaceae* und *Parilichlamydiaceae* [4]. Die Familie der *Chlamydiaceae* ist die bisher am besten beschriebene Familie der *Chlamydiales* Ordnung, zu welcher insgesamt 13 Spezies zählen, welche sich in drei Human- und mehrere Tier-Pathogene aufgliedern [2, 3, 5, 6]. Ihre prominentesten Mitglieder sind das Humanpathogen *Chlamydia pneumoniae* (*Cpn*), welches zu akuten respiratorischen Krankheiten der Atemwege wie Pneumonie und Bronchitis führen kann [4, 7, 8], sowie *Chlamydia trachomatis* (*Ctr*), welches je nach betrachtetem Serovar zu Entzündung der Harnröhre, Unfruchtbarkeit und Fehlgeburten bei Frauen (Serovar D bis K), Lymphogranuloma venereum (LGV, Serovar L) oder zur hochansteckenden Augenkrankheit Trachom (Serovare A bis C) führen kann [3, 9]. Auf *Cpn* und *Ctr* wird in den Kapiteln 1.2.1 und 1.2.2 noch im Detail eingegangen. *Chlamydia abortus* infiziert Säugetiere und *Chlamydia psittaci* Vögel, wobei beide auf den Menschen übertragen werden können [3, 10, 11]. Weitere bekannte chlamydiale Spezies der *Chlamydiaceae* bilden *C. muridarum*, *C. abortus* und *C. pecorum*.

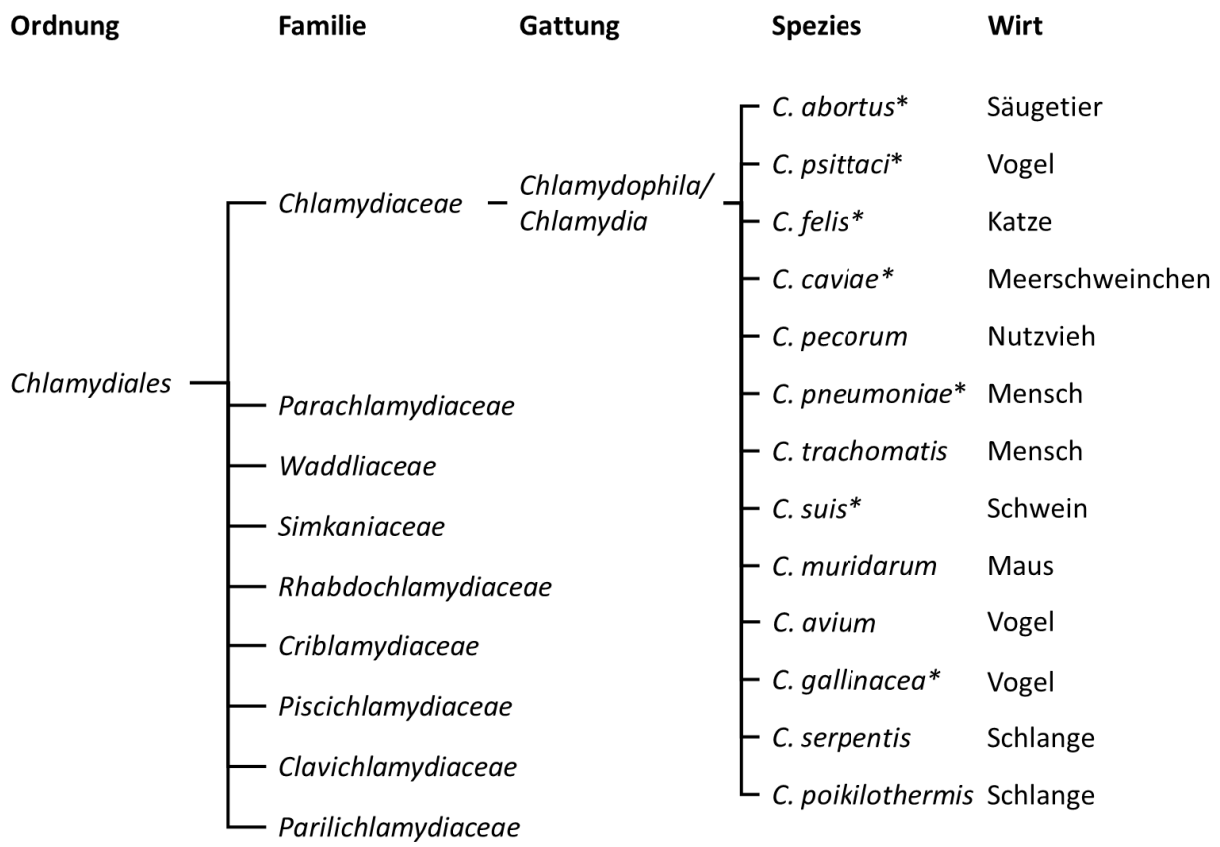


Abbildung 1: Taxonomische Einteilung der Ordnung *Chlamydiales*.

Die Ordnung der *Chlamydiales* teilt sich in 9 Familien auf, wobei auf die Familie der *Chlamydiaceae* besonderen Fokus gelegt wurde. Die Darstellung wurde in Anlehnung an [3, 5, 12, 13] erstellt. Mit (*) markierte Spezies zeigen zoonotisches Potential [3, 6, 10, 11, 14]. Die Länge der Linien stellt keine tatsächlichen phylogenetischen Abstände dar.

## 1.2 Pathogenität von Chlamydien

Die Familie der *Chlamydiaceae* ist weit verbreitet und kann durch ihre Fähigkeit die Schleimhäute zu infizieren zur Erkrankung bei Menschen und Tieren führen. Der biphasische Entwicklungszyklus, auf welchen in Kapitel 1.3 noch im Detail eingegangen wird, beinhaltet neben der EB und RB auch eine persistente Form (AB), welche bei Nährstoffentzug oder anderweitigen Stressbedingungen das langfristige Überleben und Bestehen ermöglicht. Endet die gegebene Stresssituation, redifferenziert das AB zum RB um den Entwicklungszyklus fortzusetzen [3]. Erkrankungen durch Chlamydien sind häufig asymptomatisch, wodurch sie oft nicht oder zu spät diagnostiziert werden, was zu keiner oder verspäteter Behandlung führt [6].

Innerhalb der letzten Jahrzehnte konnten insgesamt 13 chlamydiale Spezies identifiziert werden, zu denen *C. abortus*, *C. psittaci*, *C. felis*, *C. caviae*, *C. pecorum, C. pneumoniae*, *C. trachomatis*, *C. suis*, *C. muridarum*, *C. avium*, *C. gallinacea*, *C. serpentis* und *C. poikilothermis* zählen [6, 15]. Innerhalb dieser Gruppe bilden *C. pneumoniae* und *C. trachomatis* die bekanntesten Vertreter. *C. trachomatis* ist eine der weitverbreitetsten sexuell übertragbaren Krankheiten [16]. Nach der US-amerikanischen Behörde „Centers for Disease Control and Prevention" (CDC) gab es im Jahr 2018 4 Millionen chlamydiale Neuinfektionen in den USA [17]. Allerdings ist hier aufgrund der oft asymptotischen Erkrankungen mit einer großen Dunkelziffer zu rechnen. *Ctr* ist zumeist in einer relativ jungen Altersklasse vertreten, wobei 60 - 70 % aller Neuinfektionen zwischen dem 15ten und 24ten Lebensjahr stattfinden und geschätzt 5 % der sexuell aktiven Frauen im Alter von 14 - 24 Jahren infiziert sind [17, 18]. *Cpn* ist ein weltweit verbreiteter Krankheitserreger der Atemwege. Die Antikörper-Prävalenz gegen *Cpn* ist sehr hoch und steigt bei zunehmenden Alter weiter an. Neben Infektionen beim Menschen konnte *Cpn* auch in weiteren Spezies wie Koalas, Pferden, dem Beuteldachs und Reptilien wie Schlangen, Frösche, Chamäleons, Leguane und Schildköten identifiziert werden [6, 19-21]. *C. abortus* ist verantwortlich für Plazentainfektionen bei Schafen und Ziegen und führt zum namensgebenden Abbruch der Trächtigkeit oder zur Geburt schwächerer Nachkommen und bewirkt damit in vielen Ländern einen erheblichen negativen Einfluss auf die Viehwirtschaft [22-24]. Weitere mögliche Wirte können neben Geflügel, Yaks und Schweine auch die Frau darstellen. *C. muridarum* infiziert Nagetiere [25, 26]. *C. pecorum* befällt Nutzvieh sowie den Beuteldachs, Tauben und Koalas [27, 28]. Mögliche Folgen einer Infektion stellen eine Lungenentzündung, im Falle der Infektion der Augen eine mögliche Erblindung oder Darminfektionen und Infektionen der Harn- und Geschlechtsorgane da [29-32]. *C. psittaci* infiziert primär Vögel, wo es Rhinitis, Konjunktivitis, und Blepharitis auslöst. Durch Infektionen der Atemwege können zudem auch andere Organismen wie der Mensch erkranken [33]. *C. suis* befällt Schweine und führt zu Atemwegsinfektionen, Enteritis und Fortpflanzungsstörungen [34-36]. *C. felis* führt bei Katzen zur Entstehung einer Bindehautentzündung mit geringen respiratorischen Symptomen [37]. Zudem steht es im Verdacht im Menschen zur Keratoconjunctivitis zu führen [6, 14]. *C. caviae* verursacht Infektionen beim Meerschweinchen, welche asymptotisch sind oder Bindehautentzündungen mit serösem bis eitrigen Ausfluss erzeugen [38, 39]. Der Kontakt zu erkrankten Meerschweinchen kann zur Übertragung auf den Menschen führen und Konjunktivitis als Folge haben [6]. Weitere chlamydiale Erreger sind *C. avium* und *C. gallinacea*, welche Infektionen bei Vögeln verursachen, sowie die erst kürzlich entdeckten Schlangen-Pathogene *C. serpentis* und *C. poikilothermis* [5, 40].

## 1.2.1 *Chlamydia pneumoniae*

*C. pneumoniae* ist das weitverbreitetste intrazelluläre Bakterium, welches mit Infektionen des Respirationstrakts im Zusammenhang gebracht wird [41]. Die Übertragung erfolgt über Tröpfcheninfektion von Menschen zu Menschen. Länger als bei den meisten Atemwegsinfektionen beim Menschen, beträgt die Inkubationszeit *bei C. pneumoniae* etwa 3 - 4 Wochen [42]. Die Fähigkeit des Erregers, in Aerosolen in einer feuchten Umgebung zu überdauern, trägt zu seiner Verbreitung bei [43]. Die Erkrankung verläuft meist asymptomatisch oder führt zur Entwicklung von akuten Erkrankungen der oberen und unteren Atemwege, einschließlich Bronchitis, Sinusitis, Pharyngitis und Lungenentzündung [42]. Die häufig asymptomatische Erkrankung führt oft zu einer verspäteten oder keiner Diagnose und Behandlung und verstärkt auf diese Weise die globale Verbreitung der Krankheit [6]. Aufgrund seiner starken Verbreitung ist der Großteil der Bevölkerung diesem Erreger mindestens einmal im Leben ausgesetzt [44]. Zudem steht *C. pneumoniae* im Verdacht, mit einer Vielzahl chronischer Entzündungskrankheiten wie Atherosklerose, Arthritis, Asthma, Lungenkrebs sowie neurologische Krankheiten wie Alzheimer und Multiple Sklerose in Verbindung zu stehen. Allerdings konnte hier bisher kein direkter Kausalzusammenhang nachgewiesen werden [45]. Interessanterweise besitzen fast alle *C. pneumoniae* Stämme, welche aus Tieren isoliert wurden, ein zusätzliches 7,5 Kilobasen (Kb)-Plasmid, welches aber in keinem menschlichen Isolat identifiziert werden konnte [46]. Daher gibt es die Hypothese, dass der menschliche *C. pneumoniae* Stamm ursprünglich aus Tieren stammte und sich nach und nach seinem menschlichen Wirt durch den Verlust bestimmter Gene und des Plasmides anpasste [47]. Die mangelnde genetische Manipulierbarkeit von Chlamydien erschwert bisher dessen detaillierte Erforschung. Verfahren um sowohl *C. pneumoniae*, als auch *C. trachomatis* zu transformieren, versprechen dem Abhilfe zu schaffen [46, 48].

## 1.2.2 *Chlamydia trachomatis*

*C. trachomatis* ist ein gramnegatives obligat intrazelluläres Bakterium. Bisher ist nur der Mensch als sein natürlicher Wirt bekannt [49]. Innerhalb der USA ist es die am meisten gemeldete bakterielle Infektion. Global ist es der häufigste sexuell übertragene Erreger und die Ursache für die Augeninfektion Trachom, welche weltweit die häufigste infektiöse Erblindungsursache darstellt [50]. Frauen erleiden häufig

Erkrankungen des Gebärmutterhalses, welche sich in Folge als Zervizitis, Urethritis, entzündliche Beckenerkrankung, Perihepatitis oder Proktitis äußert. Chlamydieninfektionen bei Frauen verlaufen zu 70 - 80 % asymptomatisch. 15 - 40 % der Infektionen steigen bis in den oberen Genitaltrakt auf, was zu schwerwiegenden Folgeerscheinungen wie erhöhten Risiko von Unfruchtbarkeit oder Eileiterschwangerschaften führt. Auch Neugeborene sind gefährdet sich mit *Ctr* zu infizieren, wenn sie während der Geburt den kontaminierten Geburtskanal passieren [3, 51]. Folgen sind meist asymptotische Infektionen der Schleimhäute von Augen, Oropharynx, Urogenitaltrakt und Rektum, wodurch eine Erkrankung meistens erst 5 - 12 Tage nach der Geburt in Form einer Konjunktivitis entdeckt wird [52]. Zu spät entdeckte und behandelte Erkrankungen und die daraus entstehenden Komplikationen resultieren zudem in erhöhten medizinischen Kosten [50, 53]. Eine Infektion des Mannes führt zu Urethritis, Epididymitis, Prostatitis, Proktitis oder reaktiver Arthritis. Unabhängig vom Geschlecht können sowohl bei der Frau wie auch beim Mann Konjunktivitis, Pharyngitis und seltener Lymphogranuloma venereum auftreten [54]. *Ctr* lässt sich in drei Biovare unterteilen, welche wiederum nach Serovaren aufgetrennt werden können. Serovare A - C (das Trachom-Biovar) sind die führende Ursache für nicht-kongenitale Erblindung in Entwicklungsländern. Serovare D - K (das Genital-Biovar) sind die am häufigsten sexuell übertragenen Bakterien [3, 51]. Serovare L1 - L3 (das Lymphogranuloma venereum-Biovar) dringen in die Lymphgefäße und Lymphknoten ein, was zum LGV führt. Obwohl das LGV-Biovar bisher primär mit den tropischen Gebieten der Welt inklusive Indien, Westindien, Afrika, Südostasien, und Südamerika in Verbindung gebracht wird, werden zunehmend auch Ausbrüche von LGV-Infektionen in den industrialisierten Regionen Nordamerikas, Europas und Australiens registriert. Betroffen hiervon sind vor allem Männer, welche Geschlechtsverkehr mit Männern ausüben und häufig mit dem Humanen Immundefizienz-Virus (HIV) koinfiziert sind [6]. Chlamydiale Infektionen können mit Antibiotika wie Proteinsynthese-Hemmern (Tetracycline, Makrolide) oder Hemmern der Nukleinsäure-Synthese (Fluorchinolone, Rifampicin) behandelt werden. Allerdings ist dies bei asymptomatischen und damit nicht endeckten bzw. behandelten Verläufen nicht möglich. Zusätzlich wurde schon häufig von einem Therapieversagen oder möglicher chlamydialer Antibiotikaresistenz berichtet [55]. Zusammenfassend machen das zumeist asymptomatische Auftreten der Erkrankung in Kombination mit einem fehlenden Impfstoff weiterhin intensive Forschungen in diesen Organismus notwendig.

## 1.3 Der biphasische Entwicklungszyklus

*Chlamydiae* besitzen einen einzigartigen biphasischen Vermehrungszyklus, welcher vollständig innerhalb eukaryotischer Wirtszellen stattfindet. Im Laufe ihrer Entwicklung unterlagen *Chlamydiae* starken Anpassungsprozessen, was zu einer Reduzierung ihres Genoms (1,04 Megabasen (Mb) mit 895 offenen Leserahmen für *C. trachomatis*) führte und zur Folge hat, dass diese Bakterien für einen Großteil ihrer Stoffwechselprozesse auf ihren Wirt angewiesen sind [3, 56]. Der hochspezialisierte intrazelluläre Lebensstil mit dem konservierten Entwicklungszyklus resultiert in einer Gemeinsamkeit von ca. 2/3 der vorhergesagten Proteine, welche sich in allen *Chlamydia* finden [3, 4]. Die Ausnahme bildet eine Zone mit hoher genomischer Diversität (genannt Plastizitätszone), die für eine Reihe von Virulenzfaktoren kodiert. Dazu zählen Zytotoxin, Phospholipase D und Membranangriffskomplex/Perforinprotein (MACPF). Es wird vermutet, dass sie einen Einfluss auf Wirtstropismus und Nischenspezifität ausüben [3, 4]. Etwa 10 % des chlamydialen Genoms kodieren für Virulenz-Effektoren, welche über Sekretionssystem abgegeben werden [3, 57]. Das Typ-5-Sekretionssystem transportiert Effektoren zur chlamydialen Zelloberfläche, wohingegen das Typ-2-Sekretionssystem Effektoren ins Inklusion-Lumen und das Typ-3-Sekretionssystem Effektoren in das Zytosol der Wirtszelle und in die Inklusions-Membran transportiert [3, 58]. Innerhalb des biphasischen Vermehrungszyklus verwendet *Chlamydia* zwei stark morphologisch unterschiedliche und hochspezialisierte Formen, welche als EB und RB bezeichnet werden. Das EB (0,3 - 0,35 µm [59]) stellt die infektiöse, zumeist als metabolisch inaktiv beschriebene Form des Chlamydiums dar [2]. Es überlebt in der extrazellulären Umgebung aufgrund seiner extrem widerstandsfähigen Zellwand, welche ein kompliziertes Netzwerk aus mit Disulfidbindungen vernetzten Proteinen darstellt („*Chlamydia* outer membrane complex“ (COMC)) und so einen Schutz gegen osmotischen Stress und physikalischen Belastungen bietet [60]. Das EB bindet an die Wirtszelle, wo es über Phagozytose oder Endozytose aufgenommen wird und sich in Folge in einem frühen Endosom in der Wirtszelle befindet. Die Membran des Endosoms wird im Folgenden durch vom Chlamydium sekretierte Effektor-Proteine, die so genannten „inclusion membrane proteins“ (Incs) stark modifiziert, wodurch zum einen die Fusion des Endosoms mit dem Lysosom verhindert wird und zum anderen eine Kommunikationsplattform mit dem Wirt entsteht. Dieser spezialisierte chlamydiale Einschluss wird als Inklusion bezeichnet. Innerhalb der Inklusion differenzieren EBs in die nicht infektiöse metabolisch aktive RB-Form (0,5 - 2,0 µm) [2, 59, 61]. Nach mehreren Teilungen redifferenzieren RBs zurück in EBs und verlassen über Extrusion, Exozytose oder Zelllyse die Wirtszelle [62, 63]. Die nun frei gewordenen EBs können eine neue Infektionsrunde starten. Neben infektiösen EBs und metabolisch aktiven, sich teilenden RBs gibt es eine weitere, sich nicht teilende, nicht infektiöse Form,

welche als aberranter Körper (AB) bezeichnet wird. Das AB entsteht als Reaktion auf Stressbedingungen und ist charakterisiert durch vergrößerte, aberrante und sich nicht teilende RBs, welche aufgrund einer scheinbar kontinuierlichen DNA-Replikation ohne Teilung entstehen [64]. Bekannte Stressbedingungen sind die Anwesenheit von β-Lactamen wie Penicillin und Clavulansäure, weiteren Antibiotika wie Phosphomycin, Nähstoffmangel, Behandlung mit Interferon (IFN-gamma) oder die Koinfektion des Wirtes mit Viren [65-68]. Nach Beendigung der Stressbedingung können ABs in RBs reaktiviert werden [3].

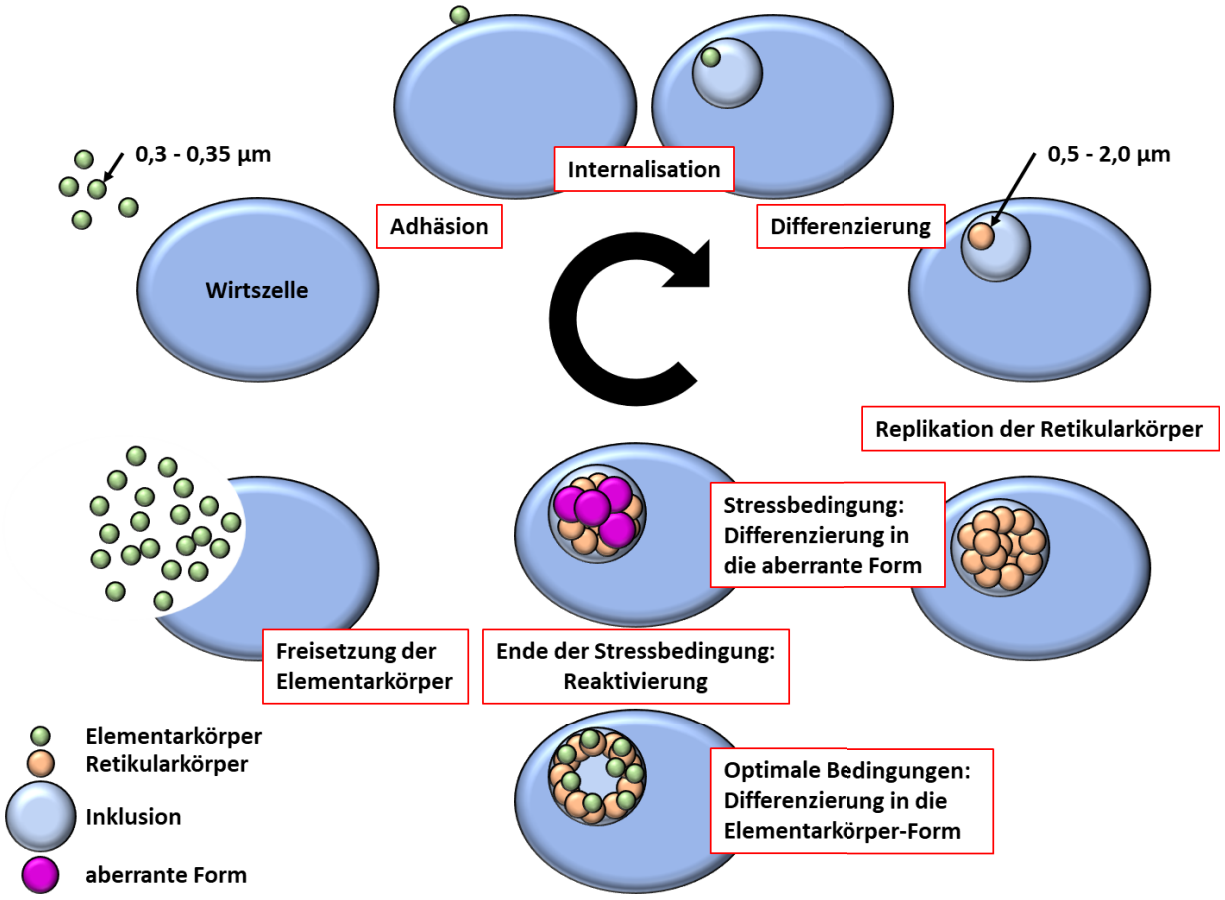


Abbildung 2: Biphasische Vermehrungszyklus von Chlamydien.

Ein infektiöses EB adhäriert an einer Wirtszelle und dringt in diese ein. Nach der Internalisierung ist das EB von einer speziellen Membran (der Inklusion) umgeben. Innerhalb der Inklusion differenziert das infektiöse, sich nicht teilende EB in seine metabolisch aktive, nicht infektiöse RB-Form. Nach einigen Teilungen differenzieren sich die RBs asynchron zurück zu EBs. Stressbedingungen resultieren stattdessen in der Differenzierung zu ABs. Sobald die Stressbedingung aufgelöst wurde, redifferenzieren ABs zu RBs. Die neu entstandenen EBs werden durch Extrusion, Verschmelzung der Inklusion mit der Membran der Wirtzelle oder durch Lyse der Wirtszelle freigesetzt und können nun einen neuen Vermehrungszyklus starten. Abhängig von der betrachteten chlamydialen Spezies variiert die notwendige Zeit für das Durchlaufen eines vollständigen Zyklus und benötigt bei *C. trachomatis* ca. 48 - 72 h [2, 3, 63].

## 1.4 Adhäsion und Internalisierung von Chlamydien

### 1.4.1 Die chlamydiale Adhäsion

Der wichtigste und initiale Schritt der Infektion durch *Chlamydia* ist die Adhäsion des EBs an die Wirtszelle. Anhand von Studien über *C. pneumoniae und C. trachomatis* konnte gezeigt werden, dass es sich bei der Anheftung von EBs an die Wirtszelle um einen mehrstufigen Prozess handelt, bei welchem zunächst eine reversible, elektrostatische Interaktion mit geringer Affinität mit heparansulfatähnlichen Glykosaminoglykanen (HS-GAGs) des Wirts stattfindet [69-73]. Bekannte Adhäsine, welche an HS-GAGs der Wirtszelle binden, sind das „Outer Membrane Protein B“ (OmcB) von *C. pneumoniae* und *C. trachomatis* und das „Major Outer Membrane Protein“ (MOMP) für *C. trachomatis* [71, 74, 75]. Diesem ersten reversiblen Schritt der Bindung folgt dann ein zweiter, irreversibler, temperaturabhängiger und heparinresistenter Bindungsschritt, welcher für *C. trachomatis* Serovar L2 beschrieben wurde aber gleichermaßen für alle chlamydialen Spezies gelten dürfte [73].

Innerhalb der letzten 20 Jahre wurden mehrere chlamydiale Adhäsine und entsprechende Wirtsrezeptoren für *C. pneumoniae* und *C. trachomatis* entdeckt und beschrieben, welche die Bindung nach der ersten reversiblen Interaktion des EBs mit HS-GAGs weiter ausbauen. Chlamydien sind gramnegative Bakterien, welche eine innere und äußere Membran besitzen. Interessanterweise konnte, trotz vorhandener Enzyme, keine Peptidoglykanschicht nachgewiesen werden. Allerdings konnten neue Untersuchungen zeigen, dass Peptidoglykan während der RB-Replikation synthetisiert wird [76-79]. Um das EB vor äußeren Einflüssen zu schützen und eine physikalische Stabilität zu verleihen, besitzen Chlamydien eine Umhüllung in Form eines stabilisierenden Netzwerkes cysteinreicher Proteine („*Chlamydia* outer membrane complex“ (COMC)), welche über Disulfid-Brücken miteinander vernetzt sind [80, 81]. Hauptbestandteil des COMCs bildet mit 60 % das Protein MOMP [82-84]. Studien an *C. pneumoniae* zeigen, dass MOMP an den Mannose-6-Phosphat Rezeptor (M6PR/IGFR2) bindet [85]. Weitere Proteine des COMCs bildet die Familie der polymorphen Membranproteine (Pmps) [86, 87]. Pmps repräsentieren die größte Proteinfamilie in *Chlamydia.* Mit mehr als 10 % in *C. pneumoniae* und *C. trachomatis* beanspruchen sie einen großen Anteil der chlamydienspezifischen Kodierungskapazität am reduzierten Genom und bekräftigen damit ihre Wichtigkeit innerhalb der chlamydialen Biologie [88]. Studien demonstrierten die adhäsiven Eigenschaften vom Polymorphen Membran Protein 21 (Pmp21) und identifizierten es zudem als Invasin mit dem Epidermalen Wachstumsfaktor Rezeptor (EGFR) als seinen

Rezeptor. Aktivierung des EGFRs führte zur Rekrutierung des Adaptoren Wachstumsfaktor-Rezeptor-Bindungsprotein 2 (Grb2) und Ligase c-Cbl und zur Aktivierung der extrazellulär signalregulierten Kinase 1 und 2 (ERK1/2) [1]. Neue Daten zeigen, dass der EGFR auch eine wichtige Rolle in der Infektion *durch C. trachomatis* darstellen könnte. Zellen, welche mit *C. trachomatis* infiziert wurden, zeigten einen Aktivierung des EGFR und seiner nachgeschalteten Effektoren Phospholipase Cγ1 (PLCγ1), Akt und Signaltransduktor und Aktivator der Transkription 5 (STAT5) [89]. Diese Aktivierung könnte womöglich durch *C. trachomatis* Pmps erfolgen. Hinweise darauf gibt eine Publikation aus 2022, in welcher das *Chlamydia psittaci* Pmp17G in der Lage war an Humanzellen zu binden, eine Folgeinfektion nach Vorbeschichtung von Zellen mit Pmp17G zu reduzieren und den EGFR zu aktivieren [90]. Neben dem zuvor erwähnten *C. pneumoniae* Pmp21 sind Pmp6, Pmp14, Pmp16, Pmp19 und Pmp20 beschriebene Adhäsine, welchen aber noch kein Rezeptor zugeordnet werden konnte [91, 92]. Auf dieselbe Weise zeigten alle *C. trachomatis* Pmps die Fähigkeit, an Wirtszellen zu adhärieren, sowie das eine Überschichtung und damit Sättigung der Oberfläche der Wirtszelle zu einer reduzierten Folgeinfektion führt [93]. Die entsprechenden humanen Interaktionspartner sind allerdings noch unbekannt.

Das „Lipid-dependent Internalization Promoting Protein“ (LipP) ist ein *C. pneumoniae* spezifisches Adhäsin und Invasin. Interessanterweise führte eine Vorbehandlung von Humanzellen mit LipP bei einer Folgeinfektion mit *C. pneumoniae* nicht zur erwarteten Infektionsminderung sondern einer Verstärkung. Obwohl die Bindung von „Lipid-Raft“-abhängig beschrieben wurde, ist noch kein humaner Interaktionspartner bekannt [94]. Das Protein GroEL1 konnte innerhalb der Infektion durch *C. pneumoniae* sowohl innerhalb der Inklusionen, als auch auf dem EB identifiziert werden. Mit GroEL1 beschichtete Latex-Kugeln, sowie GroEL1-präsentierende Hefezellen adhärierten an Humanzellen und identifizierten GroEL1 damit als Adhäsin [95]. Ein spezifischer Rezeptor für GroEL1 ist bisher unbekannt. Als mögliche Interaktoren werden CD14, TLR4 und/oder TLR2 beschrieben [96-99]. Es wurde gezeigt, dass die Gegenwart von Apolipoprotein E4 mit einem bisher noch unbekanntem *C. pneumoniae* Adhäsin die Adhäsion von *C. pneumoniae* verstärkt [100].

Das *C. trachomatis* Lipopolysaccharid (LPS) vermittelt Bindung an den zystischen Fibrose Transmembran Konduktanz Regulator (CFTR) [101]. Ctad1 ist ein beschriebenes Adhäsin und Invasin von *C. trachomatis*. Vorinkubation von Humanzellen mit Ctad1 verringert die anschließende Folgeinfektion. Mit Ctad1 beschichtete Latexkügelchen wurden von Zellen aufgenommen und demonstrierten seine Fähigkeit als Invasin. Der β-1 Integrin Rezeptor (ITGB1) konnte als sein humaner Interaktionspartner identifiziert werden [102]. Das *C. trachomatis* Hitzeschockprotein 70 (Hsp70/DnaK) bindet an den 3’Sulfogalactolipid (3’SGL) Rezeptor [103].

Neben den zuvor erwähnten Adhäsinen gibt es einige Rezeptoren, für welche eine Wichtigkeit im Infektionsprozess durch *C. trachomatis* gezeigt werden konnte, obwohl der chlamydiale Interaktionspartner noch unbekannt ist. Wirtsrezeptor mit noch fehlendem *C. trachomatis* Interaktionspartner stellt der Fibroblast Wachstumsfaktor Rezeptor (FGFR) dar. Der Fibroblasten-Wachstumsfaktor 2 (FGF2) bindet hierbei an EBs und fungiert als Brückenmolekül, um die Interaktion an den FGFR zu fördern. Dies aktiviert den FGFR und führt zur Aufnahme von EBs [104]. Ein weiterer zellseitiger Rezeptor ist der Ephrin Rezeptor A2 (EPHA2) [105]. Bindung von EBs an den EPHA2 bewirkt dessen Aktivierung, welches zur Aufnahme des Rezeptors und des EBs führt. Adhäsine mit entsprechendem Rezeptor oder Bindepartner sind in Abbildung 3 zusammengefasst. Detaillierte Informationen zu COMC, MOMP und Pmps sind in den Kapiteln 1.5.1, 1.5.2 und 1.7 enthalten.

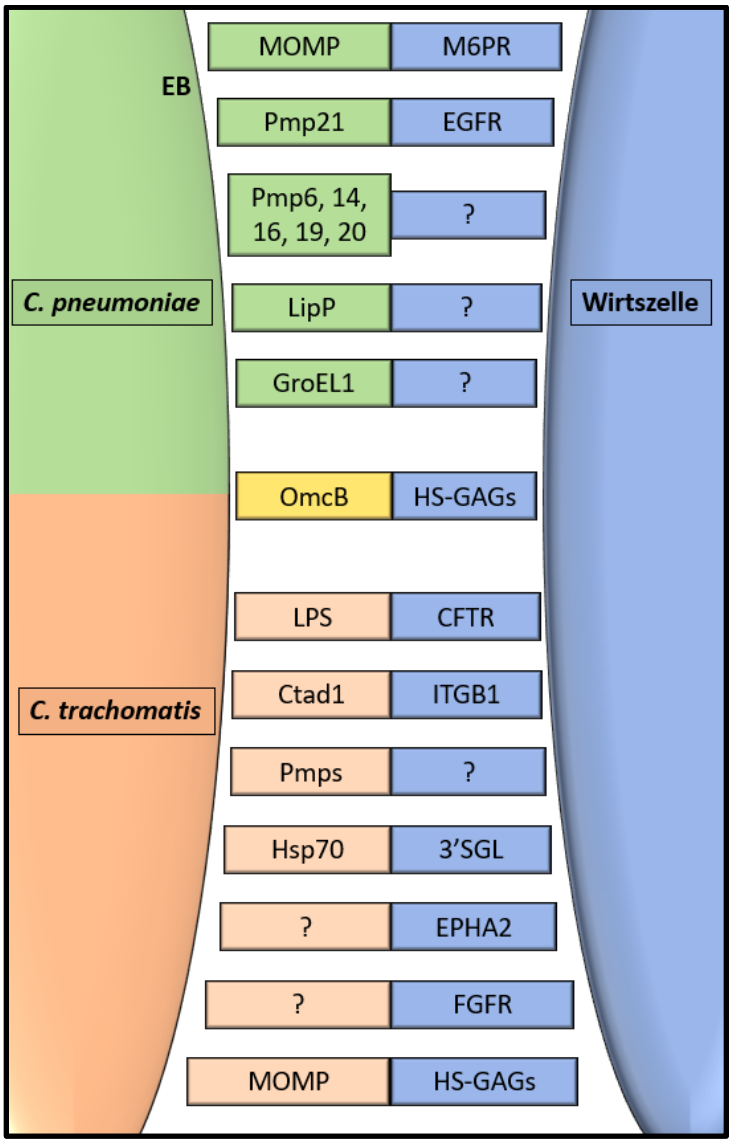


Abbildung 3: Schematisches Adhäsionsmodell für *C. pneumoniae* und *C. trachomatis*.

Publizierte Interaktoren für *C. pneumoniae* sind OmcB, welches initial an HS-GAGs bindet, sowie das Adhäsin LipP und GroEL1. Spezifische Rezeptoren für LipP und GroEL1 sind bisher nicht bekannt. Weitere proteinöse Interaktionspartner bilden MOMP an den M6PR/IGFR2, sowie Pmp21 an den EGFR. Für Pmp6, Pmp14, Pmp16, Pmp19 und Pmp20 konnte eine Bindung an Zellen gezeigt werden. Der entsprechende Wirtsrezeptor ist nicht bekannt. Wie bei *C. pneumoniae* bindet *C. trachomatis* OmcB an HS-GAGs. Weitere bekannte Interaktionen bestehen zwischen chlamydialen LPS mit dem CFTR, MOMP an HS-GAGs, Ctad1 an den ITGB1 und HSP70 an den 3'Sulfogalactolipid (3'SGL) Rezeptor. Alle *C. trachomatis* Pmps sind Adhäsine; allerdings sind die humanen Interaktionspartner unbekannt. Für die Infektion wichtige Rezeptoren mit noch fehlendem zugehörigen chlamydialen Bindepartner stellen der FGFR und EPHA2 dar. Abbildung angelehnt an [72].

## 1.4.2 Die Internalisierung in die Wirtszelle

Im Anschluss an die Adhäsion des EBs erfolgt dessen Aufnahme in die Wirtszelle. Die Adhäsion stabilisiert das EB auf der Oberfläche. Um das Eindringen in die Wirtszelle zu ermöglichen ist ein komplexer Prozess notwendig, bei welchem Signalkaskaden aktiviert werden, welche Wirtzellprozesse auslösen und final eine Aktinremoddelierung auf der Zelloberfläche hervorrufen. Diese resultiert in einer Vielzahl von Zelloberflächenstrukturen mit dem Ziel, das EB aufzunehmen.

Alle für die EB-Aufnahme beschriebenen Mechanismen haben gemein, dass am Ort und Umgebung der EB-Bindung eine Assemblierung aktinreicher Strukturen stattfindet [106, 107]. Eine Störung dieser Rekrutierung resultiert hingegen in einer reduzierten Aufnahme-Effizienz [106-108]. Um die Aktinremoddelierung zu initiieren, verwendet das EB die Translokation von Effektoren um Wirtszell-Signalkaskaden auszulösen, sowie die Bindung von Adhäsinen an ihre entsprechenden Rezeptoren [109-112]. Die Internalisierung von EBs ist bisher noch unzureichend verstanden, mögliche Abläufe stark diskutiert und daher im Fokus vieler Arbeitsgruppen.

Eine Möglichkeit der EB-Aufnahme beschreibt der Clathrin-Mechanismus. Clathrin ist an der Einstülpung von Zellmembranen sowie der Bildung von Vesikeln bei der rezeptorabhängigen Endozytose beteiligt und könnte damit einen Hauptakteur bei der EB-Aufnahme darstellen [113, 114]. Studien zeigten, dass *C. trachomatis* mit Clathrin-beschichteten Vertiefungen assoziiert und in Clathrin-beschichtete Vesikel aufgenommen wird [115-117]. Experimente, in welchen die endozytische Maschinerie gehemmt wurde, zeigten eine signifikant reduzierte Invasion durch *C. trachomatis* L2 [118], wohingegen die Aufnahme von *C. pneumoniae* Clathrin-unabhängig zu sein scheint [119], was auf eine Spezies-Spezifität hindeutet. Andere Untersuchungen zeigten hingegen eine unveränderte Aufnahme von *C. trachomatis,* wenn die Clathrin-abhängige Endozytose gehemmt wurde [120, 121].

Eine weitere Möglichkeit stellte der Caveolae-vermittelte Eintritt dar, für welchen es allerdings sowohl unterstützende als auch wiederlegende Studien gibt [122-124]. Caveolae sind eine spezialisierte Art von „lipid rafts“. Hierbei handelt es sich um 50-100 nm große flaschenförmige Einstülpungen, welche sich in „lipid rafts“ bilden sobald das Caveolae-Markerprotein Caveolin-1 exprimiert wird [123, 125]. Auf diese Weise zeigten die Inklusion aller Chlamydien Stämme, welche über „lipid rafts“ in die Zelle eingedrungen waren, Caveolin-1, welches sie beim Eintritt in die Zelle erwarben und sich im darauf folgenden Infektionsprozess mehrte [122, 126]. Entgegengesetzt zum Caveolae-vermittelten Eintritt zeigen weitere Untersuchungen, dass die Infektion durch *C. trachomatis* „lipid rafts“ unabhängig ablaufen könnte [124].

Neben den bisher genannten Mechanismen wurden Adhäsin-Rezeptor-Paare entdeckt, welche zum Eintritt des EBs in die Wirtszelle beitragen.

*C. pneumoniae* Pmp21 ist ein Adhäsin und Invasin, welches an den EGFR bindet, diesen aktiviert und in Folge zur Aufnahme vom EB führt [1]. Ein weiteres Invasin ist das *C. trachomatis* Ctad1, welches an den ITGB1 bindet [102]. Sowohl die Pmp21-EGFR-Interaktion wie auch die Ctad1-ITGB1-Interaktion führen zur Aktivierung von ERK1/2 und nachfolgender Aktinremoddelierung [1, 102].

Aktuelle Studien beschreiben die Internalisierung als einen primär Aktin-getriebenen Prozess, bei dem an die Wirtszelle adhärierende EBs über ihr Typ-3-Sekretionssystem (T3SS) vorverpackte Effektoren direkt in das Zytosol der Wirtszelle injizieren und so eine Umstrukturierung des Zytoskeletts bewirken und damit die Aufnahme des EBs fördern [127, 128].

Schlüsselproteine in diesem Prozess stellen das Aktin-Rekrutierungsphosphoprotein TarP, TmeA und CT166 dar [129-131]. TarP ist hoch konserviert und in allen chlamydialen Spezies zu finden [132]. Es ist ein Multidomänenprotein, welches Aktin durch seinen eigenen globulären Aktindomänen (G-Aktin) und filamentösen Aktindomänen (F-Aktin) nukleiert, bündelt und bei *C. trachomatis* mit dem Wirts-ARP2/3-Komplex synergiert [133, 134]. Des Weiteren ist die N-terminale Phosphorylierungsdomäne von TarP wahrscheinlich an Signalkaskaden durch Rekrutierung von Effektorproteinen wie Shc1, Sos1, Vav2 und Rac1 beteiligt [3, 133]. Homologe TarP-Proteine lassen sich in allen chlamydialen Spezies finden. Obwohl diese Proteine eine Reihe konservierter Domänen aufweisen, variiert die Aminosäuresequenz mit 40 % bis 94 % stark, wenn man das *C. trachomatis* L2 TarP mit homologen anderer chlamydialer Spezies vergleicht [132, 135, 136]. Zusätzlich konnte vor kurzem gezeigt werden, dass das *C. pneumoniae*-Ortholog von TarP (CPn0572), das Aktin-Zytoskelett über eine neu identifizierte F-Aktin-Bindungsdomäne und die Rekrutierung von Vinculin reorganisiert [3]. *C. trachomatis* TmeA interagiert mit dem Aktin-bündelnden Protein AHNAK [130]. Störungen des offenen Leserahmens von *tmeA* zeigten eine TmeA abhängige Invasion, wohingegen keine Abhängigkeit von AHNAK demonstriert werden konnte [137].

*C. trachomatis* CT166 kommt in vielen chlamydialen Spezies vor. Allerdings unterscheiden sich die Homologe stark [131]. CT166 weist ein DXD-Motiv auf, das für die enzymatische Aktivität vieler bakterieller und Säugetier-Glykosyltransferasen vom Typ A wichtig ist, was zu der Hypothese führte, dass CT166 eine Glykosyltransferase-Aktivität besitzt [138, 139]. Obwohl CT166 in der Lage ist, die Ras GTPase zu modifizieren und zu inaktivieren, sowie eine Mutation des DXD Motives zu einer verringerten Ras-Inhibierung führt, ist die Rolle von CT166 im EB-Eintritt unklar, da sowohl in DXD beinhaltenden und defizienten Stämmen eine effiziente EB-Aufnahme in Wirtszellen beobachtet werden konnte [139, 140].

Ein weiteres Effektorprotein stellt das *C. pneumoniae* CPn0678 dar, welches die Internalisierung des EBs durch Umbau der Plasmamembran der Wirtszelle und Rekrutierung von Sorting Nexin 9 (SNX9), einem zentralen multifunktionalen endozytischen Gerüstprotein fördert [141]. Die *C. pneumoniae* Proteine CPn0677 und CPn0678 stehen im Verdacht, durch Nutzung amphipathischer Helices Membranverformungen an der Innenseite der Wirtszell-Plasmamembran hervorzurufen, indem sie den humanem SNX9 rekrutieren und dadurch Einstülpungen der Plasmamembran induzieren [141-144]. Zusammenfassend geschieht die erfolgreiche Internalisierung in die Wirtszelle, die Modifikation der Inklusionsmembran und Etablierung als Interaktionsplattform mit dem Wirt durch Invasin-Wirtszell-Rezeptorinteraktionen und Effektorproteine, die über das Typ III Sekretionssystem in das Zytoplasma der Wirtszelle, die Inklusionsmembran oder ins Lumen des Inklusion sekretiert werden und in Folge Wirtszellprozesse modifizieren [3, 127, 145].

## 1.5 Die chlamydiale Zellwand

*Chlamydia* sind gramnegative obligat intrazelluläre Bakterien. Innerhalb ihres biphasischen Replikationszyklus findet ein stetiger Wechsel zwischen ihrer extrazellulären, infektiösen EB-Form und intrazellulären, nicht infektiösen sich replizierenden RB-Form statt [3]. Es ist davon auszugehen, dass die Membranen beider Formen auf ihre jeweiligen Anforderungen, Adhäsion/Infektion (EB) oder Vermehrung und das Überleben im Wirt (RB) höchst spezialisiert sind und daher spezifische Unterschiede aufweisen [81, 146]. Zu Beginn einer chlamydialen Infektion befinden sich EBs in einer rauen extrazellulären Umgebung, in welcher sie überleben und gleichzeitig in der Lage sein müssen, an einen neuen Wirt zu binden und diesen zu infizieren. *Chlamydia* sind wie andere gramnegative Bakterien von einer äußeren Membran, welche im Kontakt zum extrazellulären Raum steht, und einer zytoplasmatischen inneren Membran umgeben, zwischen denen sich der periplasmatische Zwischenraum befindet [147, 148]. Beide Membranen beinhalten Phospholipide und Proteine. Die äußere Membran beinhaltet LPS [149-151]. Die Chlamydienhülle besteht aus Lipiden, welche eine Mischung aus prokaryotischen und eukaryotischen darstellt. Während die prokaryotischen Lipide vom Chlamydium selbst synthetisiert werden können, müssen eukaryotische Lipide vom Wirt bezogen werden [152]. Vom Wirt synthetisiertes Sphingomyelin oder dessen Vorläufer sind hierbei für die Replikation der RBs als essentiell identifiziert worden [152, 153]. Womöglich aufgrund der harschen extrazellulären Außenbedingungen, besitzen EB-Membranen einen um 8 % erhöhten Anteil an Cholesterin im Vergleich zur RB Membran, was sie mit einer größeren Steifigkeit

und geringeren Durchlässigkeit gelöster Stoffe ausstattet [154]. Das LPS von Chlamydien besitzt besondere Eigenschaften, die es von anderen gramnegativen Organismen unterscheidet. Im Vergleich zu herkömmlichen gramnegativen Bakterien besitzt das Chlamydien-Lipid A nicht hydroxylierte Fettsäuren was seine Aktivität als Endotoxin deutlich reduziert [155]. Dies konnte in einer Studie bestätigt werden, bei welcher die Auslösung einer entzündlichen Zytokinreaktion durch *C. trachomatis* als ca. hundertfach weniger effektiv beschrieben wurde, als die von *Salmonella minnesota* und *Neisseria gonorrhoeae*. Dieses spezielle LPS könnte damit einen Verbergungsmechanismus gegen die Wirtsimmunantwort darstellen [81, 156]. Gramnegative Bakterien stabilisieren ihre Membran durch Peptidoglykan im periplasmatischen Raum, welches die Aufrechterhaltung von Zellform und des hydrostatischen Drucks gewährleistet [157]. Das Vorhandensein eines typischen Peptidoglykans in der chlamydialen Membran war lange umstritten. Lange Zeit wurde von einer „Chlamydienanomalie“ gesprochen, da das chlamydiale Genom für die funktionelle Peptidoglykan-Biosynthese kodiert, das Wachstum von Chlamydien durch auf die Peptidoglykan-Biosynthese gerichtete Antibiotika beeinflusst wurde und der zytosolischen Peptidoglykan-Sensor des Wirts bei Infektion aktiviert wurde, aber dennoch kein Peptidoglykan in Chlamydien nachgewiesen werden konnte [158-167]. Erst im Jahr 2014 konnte Peptidoglykan in *C. trachomatis* L2 RBs nachgewiesen werden, wo es als Ring erschien. Weiterhin deuteten gewonnene Daten auf eine Positionierung des Peptidoglykans am Septum sich teilender RBs und damit eine mögliche Rolle des Peptidoglykans bei der RB-Teilung hin [79].

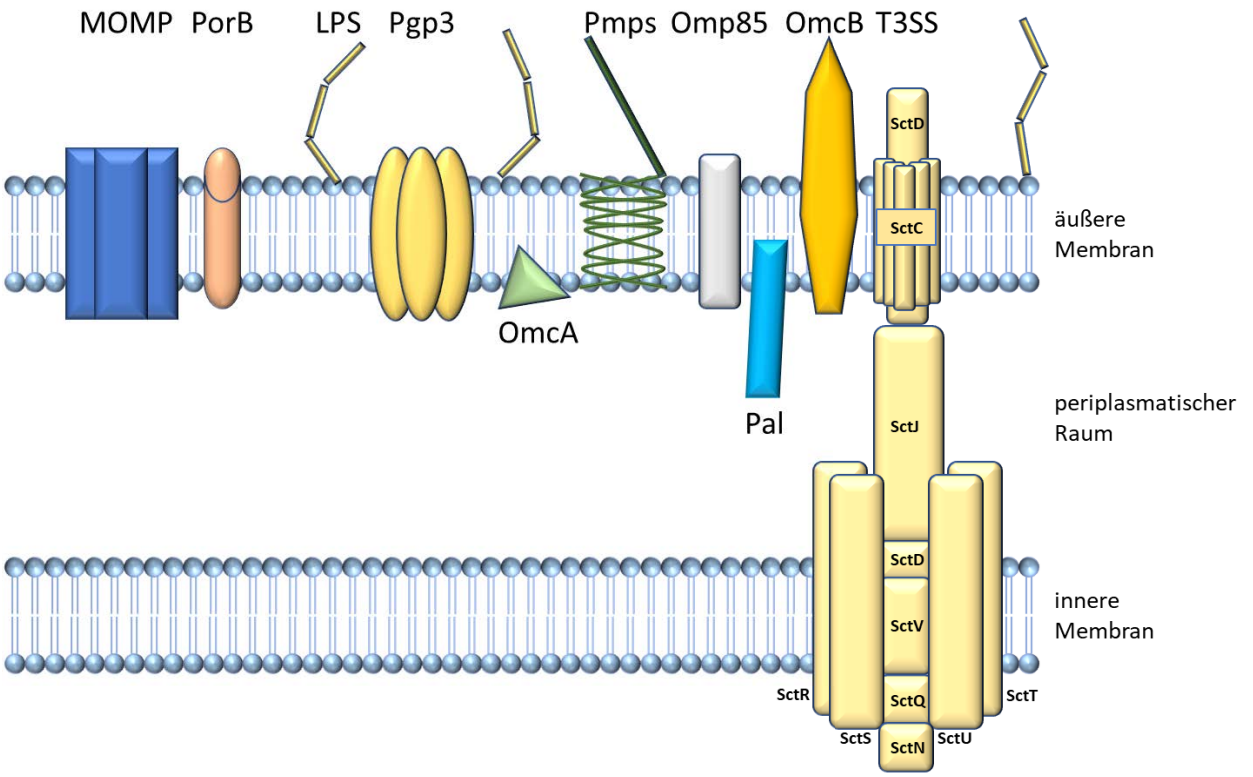


Abbildung 4: Schematische Darstellung der chlamydialen Zellwand.

MOMP ist das Hauptprotein der äußeren Membran und Großteil des „*Chlamydia* outer membrane complex“ (COMC). Ein weiterer großer Anteil der äußeren Membran bilden die Proteine OmcA und OmcB. Weitere beschriebene Bestandteile der äußeren Membran bilden chlamydiales LPS, die Mitglieder der Pmp-Familie, PorB (OmpB), Pgp3, Pal und Omp85 sowie einige weitere Adhäsine, welche bereits in Abbildung 3 gezeigt wurden. Das T3SS durchspannt innere und äußere Membran und verbindet sie. SctR, SctS, SctU und SctT sind Membranproteine, welche den Kern des Sekretionssystems umgeben. SctN interagiert mit Effektoren und Chaperonen und treibt das TS33 energetisch an. SctQ bildet eine Verbindung zu SctD. SctV bildet einen Kanal durch die innere Membran. SctD bindet sich in die innere Membran ein. SctJ bildet eine Brücke über den periplasmatischen Raum und verbindet SctD und SctC. SctC befindet sich innerhalb der äußeren Membran. Die Grafik wurde orientiert an [81] erstellt und mit den Quellen [57, 127, 168] ergänzt.

## 1.5.1 Chlamydiale äußere Membran-Komplex (COMC)

Um die Position chlamydialer Proteine innerhalb der Zellwand bzw. der chlamydialen Umhüllung genauer beschreiben zu können, wurden Extraktionsassays entwickelt, wobei EBs in unterschiedlichen Detergenzien inkubiert, dadurch bestimmte Proteine abgelöst und je nach verwendetem Detergens und dessen Eigenschaften Rückschlüsse auf die native Proteinposition möglich wurden [169-172].

Detergenzien sind Substanzen, welche unter anderem in der Zell- und Proteinbiologie zur Zellpermeabilisierung, Zelllyse sowie der Extraktion von Membranbestandteilen eingesetzt werden. Ihre amphiphilen Eigenschaften ermöglichen es ihnen Protein-Protein, Protein-Lipid sowie Lipid-Lipid Bindungen aufzulösen. Je nach Eigenschaft werden sie in die Gruppen Ionisch (z. B. Sarkosyl), Nicht-Ionisch (z. B. Triton X-100), Zwitterionisch (z. B. CHAPS) und Chaotrop (z.B. Urea) eingeteilt [173].

Caldwell *et al.* 1981 definierte die Proteine von EBs, welche nach Inkubation in Sarkosyl nicht abgelöst werden konnten, als Proteine des COMC. Das COMC ist ein stabilisierendes Netzwerk cysteinreicher Proteine, welche über Disulfid-Brücken miteinander vernetzt sind. Das COMC erhöht die Festigkeit des EBs und dessen Resistenz gegenüber physischen und osmotischen Stress und ermöglicht ihm damit das Überdauern im rauen extrazellulären Raum [80, 81]. Die bekanntesten und gleichzeitig am meisten vorkommenden Bestandteile des COMC bilden MOMP, Mitglieder der Familie der polymorphen Membranproteine (Pmps), sowie die cysteinreichen Proteine OmcA und OmcB [86, 174-176]. Weitere bekannte Proteine des COMC bilden PorB, Omp85, CTL0887, CTL0541, CTL0645, OprB, SctC, Pgp3 und Pal [86, 177-179]. *C. trachomatis* PorB ist ein, zwischen den unterschiedlichen Serovaren, hoch konserviertes Porin. Es lokalisiert zur chlamydialen Oberfläche und ist Bestandteil des COMC. Vorbehandlung chlamydialer EBs mit PorB-Antikörper führte zu einer reduzierten Folgeinfektion und machte PorB damit zu einem interessanten Target zur Impfstoffentwicklung [180-182]. Omp85 besitzt eine N-terminale, periplasmatische Domäne und eine C-terminale β-Fass-Domäne, die es in der äußeren Membran fixiert [183]. Es unterstützt den Einbau von Proteinen in die äußere Membran und ist während des Übergangs von RB- zu EB-Form, womöglich am Transport von MOMP, PorB und OprB zum COMC verantwortlich [86, 184]. CTL0887 wurde im COMC identifiziert [86, 177, 185]. Es akkumuliert in EB-, COMC- und löslichen Fraktionen. Zusätzliche Hinweise, dass es sich um ein sekretiertes Protein handelt, ein geringer Anteil von Cysteinen im Protein und ein Mangel an Transmembran-Helices lassen an einer kovalenten Bindung zu anderen COMC-Proteinen zweifeln [86, 185]. CTL0645 ist ein EB spezifisches und hoch konserviertes Protein von *C. trachomatis* [86, 186]. Birkelund *et al.* 2009 beschreibt OprB als Protein des COMCs. Fluoreszenzmikroskopische Aufnahmen infizierter Zellen mit anti-OprB resultierten in ringförmigen Strukturen (ähnlich wie bei MOMP) was für eine Lokalisation in der Membran spricht. Da Färbungen mit unfixierten Chlamydien nicht erfolgreich waren, konnte hier keine Aussage über eine Lokalisation auf der Oberflächen von EBs getroffen werden [177]. SctC ist Teil des Typ-3-Sekretionssystems [187]. Das für die Expression von Pgp3 verantwortliche Gen befindet sich auf dem Plasmid von *C. trachomatis.* Das Protein Pgp3 ist Bestandteil der äußeren Membran, wird aber auch ins Zellzytosol sekretiert. Es handelt sich um einen Virulenzfaktor und unterstützt die chlamydiale Infektion [188, 189]. Während der Infektion mit *C. trachomatis* inhibiert Pgp3 die Apoptose [190]. Zudem fördert Pgp3 über den TLR2-Signalweg sowie durch

die Aktivierung des NALP3-Inflammasons die Produktion entzündungsfördernder Zytokine [190-192] . Auf die große Familie der Pmp-Proteine wird im Folgenden im Detail eingegangen (siehe 1.6).
Pal ist ein Peptidoglykan-assoziiertes Lipoprotein der äußeren Membran [81]. Es interagiert mit Tol-Proteinen, wodurch ein membranüberspannendes Multiproteinsystem entsteht [193].
Obwohl die Hauptbestandteile des COMC in ihrer Zusammensetzung häufig ähnlich beschrieben werden, ist die genaue Zusammensetzung nicht vollkommen definierbar, da unterschiedliche Studien mit leicht unterschiedlichen EB-Präparationen und unterschiedlichen Methoden zu diversen Resultaten kamen [86, 177]. Des Weiteren werden vereinzelt Proteine wie GroEL, DnaK, RNA-Polymerase β, Elongationsfaktor Tu und Histon-H1- ähnliche Proteine Hc1 und Hc2 in COMC-Fraktionen identifiziert, bei denen es unklar ist, ob es sich um mögliche Bestandteile des COMC oder Artefakte handelt [177].

### 1.5.2 Major outer membrane protein

MOMP ist ein 39,5 kDa großes Protein und macht ca. 60 % des COMC aus. Es ist stark über Disulfidbrücken vernetzt und vermittelt damit zusätzliche Stabilität für die chlamydiale Membran [82-84]. Es ist ein Trimer mit β-Faltblattstruktur, wurde als Porin in RBs sowie Adhäsin bei EBs beschrieben und seine fünf konservierten und vier variablen Sequenzen durchspannen die äußere Membran und sind damit sowohl der extrazellulären, wie auch der periplasmatischen Seite ausgesetzt [83, 194-198]. Monoklonale und polyklonale Antikörper gegen MOMP sind in der Lage, eine Infektion mit *Chlamydia* zu reduzieren, was seine Wichtigkeit im Zusammenhang mit einer Immunrektion des Wirtes zeigt. Erste Impfstudien mit nativen oder auch rekombinant hergestellten MOMP oder DNA, welche für MOMP kodierte, erzeugte nur unvollständige oder inkonsistente Immunität [199-201]. Erst 2020 war es Pal *et al.* möglich mit einem Impfstoff aus MOMP und den zwei Adjuvanten Th1 und Th2 einen effektiven Impfstoff zu entwickeln, welcher bei Mäusen eine langanhaltende Immunität gegen *C. muridarum* vermittelte [202].

### 1.5.3 OmcA und OmcB

Neben MOMP bilden OmcA und OmcB weitere prominente Bestandteile des COMC [86]. OmcA ist ein 12-15 kDa großes hydrophiles Lipoprotein, welches mit seinen Lipidkomponenten in der äußeren Membran

verankert ist. Der proteinöse Teil des OmcA orientiert sich zum periplasmatischen Raum [146, 203, 204]. Das als 57-62 kDa beschriebene OmcB stellt ein wichtiges Adhäsin bei Chlamydien dar. Es bindet an HS-GAGs und etabliert damit die erste reversible Bindung an die Wirtszelle [74]. Seine hohe Wichtigkeit wird durch die Tatsache unterstrichen, dass es hoch konserviert zwischen den Spezies der Gattung *Chlamydia* ist. Es besitzt eine variable N-terminale Region, in der die hochkonservierte HS-Bindedomäne (aa 41 – 90) lokalisiert ist [74, 205-207]. OmcB ist mit weiteren Membranproteinen über Disulfidbindungen vernetzt und vermittelt auf diese Weise weitere osmotische Stabilität und Membran-Festigkeit [206, 208]. Seine zelluläre Lokalisation wird widersprüchlich beschrieben. Studien von Everett und Hatch 1995 mit *C. psittaci* legen eine Lokalisation im Periplasma nahe, wohingegen Studien von Ting *et al.* 1995 an *C. caviae* von einem OmcB berichten, dessen N-terminale Seite durch die äußere Membran zum extrazellulären Raum gerichtet ist [169, 209]. Das *C. trachomatis* LGV OmcB ist oberflächenlokalisiert und verfügbar für Detektion mittels Antikörper [210]. In der N-terminalen Region befindet sich die Bindedomäne für Heparin, welche außer im OmcB in *C. trachomatis* LGV auch in den Homologen in *C. trachomatis* Serovar B, *C. pneumoniae* und *C. psittaci* gefunden werden konnte [210]. Die Bindung von *C. trachomatis* Serovar L1 ist Heparin-abhängig, wohingegen die Bindung von *C. trachomatis* Serovar E als Heparin-unabhängig beschrieben wird [75, 207, 211]. Es konnte gezeigt werden, dass eine einzige Position in der Aminosäuresequenz von OmcB zwischen *C. trachomatis* Serovar L1 und *C. trachomatis* Serovar E über Heparin-abhängige bzw. unabhängige Bindung entscheidet [74, 207]. Variationen an dieser Stelle könnten daher Rückschlüsse auf Zell-, Wirtstropismus und Krankheitsbild zwischen den beiden Serovaren ermöglichen [74, 207].

## 1.6 Bakterielle Sekretionssysteme

Bakterien besitzen unterschiedlichste Methoden oder Mechanismen um Proteine für multiple Zwecke zu sekretieren. Im Allgemeinen geschieht der Transport von Proteinen durch den allgemeinen Sekretionsweg („Sec“-Weg) oder einen Zwillings-Arginin-Translokationsweg („Tat“-Weg), welche beide hoch konservierte Mechanismen der Proteinsekretion in allen Domänen darstellen [212]. In gramnegativen Bakterien werden Protein zur inneren Membran oder in den periplasmatischen Raum transportiert. In diesen Gebieten können sie verbleiben oder in Folge über weitere Sekretionssysteme aus dem Bakterium sekretiert werden [213]. Zusammenfassend werden im „Sec“- Weg Proteine in einem dreiteiligen Mechanismus bestehend aus Protein-„Targeting“-Komponente, einem Motorprotein und einem membranintegrierten leitenden Tunnel (SecYEG-Translokase) im ungefalteten Zustand translokiert [214]. Der „Tat“-Weg translokiert Proteine in einem gefalteten Zustand [215]. Dafür verwendet er eine zwei- bis drei-teilige Maschinerie, welche die Proteine TatA, TatB und TatC umfasst [216, 217]. Der „Tat“-Weg ist notwendig, da bestimmte posttranslationale Modifikationen nur im Cytoplasma erfolgen können [218]. Gramnegative Bakterien verwenden spezielle Mechanismen, um Proteine außerhalb der Zelle, in den extrazellulären Raum, zu sekretieren. Beschriebene Gründe hierfür sind Kommunikation, Virulenz, Adhäsion, Nährstoffakquirierung, sowie Wachstumshemmung konkurrierender Bakterien. Für die Ausübung dieser Funktion entwickelten gramnegative Bakterien hochspezialisierte Proteinkomplexe, welche als Sekretionssysteme bezeichnet werden und in die Gruppen 1 bis 9 eingeteilt werden [213, 219, 220]. Sekretionssysteme unterscheiden sich in ihrem Aufbau stark, zeigen unterschiedliche Grade an Komplexität, können als multiproteinöser Komplex mehrere Membranen umfassen oder wie im Fall des Typ-5-Systems nur die gramnegative äußere Membran umfassen [221].

### 1.6.1 Das Typ-V-Sekretionssystem der Pmps

Auf Basis ihrer vorhergesagten Eigenschaften identifizierten bioinformatische Untersuchungen und Genomsequenzierung Pmps als Autotransporter bzw. Typ-5a-Sekretionssystemproteine [222, 223]. Grundlage der Bezeichnung „Autotransporter“ ist der Umstand, dass bisher weder chemische Energie in Form von ATP noch Protonen oder anderweitige Ionen-Gradienten identifiziert werden konnten, welche den Transport antreiben, wodurch Typ-5-Sekretionssysteme als autarkes System erscheinen [224].

Teilnehmer und Funktionen, welche für das Typ-5-Sekretionssystem beschrieben wurden, sind mannigfaltig und beinhalten unter anderem Proteasen (EspC, EspP, Hbp und Pic von *E. coli*), Lipasen (EstA von *Pseudomonas aeruginosa*), Abwehrmechanismen gegen das Immunsystem (IgA Protease von *E. coli*) und Adhäsine (AIDA-I von *E. coli*) [219]. Eine umfassende Übersicht ist im Review von Meuskens *et al.* 2019 dargestellt [219]. Allgemein sind alle Autotransporter durch eine Sec-Leitsequenz, eine Passagierdomäne und eine β-Fassdomäne, welche sich in der äußeren Membran befindet, charakterisiert [225]. Sie werden im Zytosol translatiert, wo die Polypeptidkette durch Chaperone in einem ungefalteten Zustand gehalten wird. Die Polypeptidkette transloziert über das SecYEG-Translokon in den periplasmatischen Raum, wo die Leitsequenz in Folge abgespalten wird (siehe *Abbildung 5*) [214, 226, 227]. Innerhalb des periplasmatischen Raums bleibt die Polypeptidkette in einem ungefalteten faltungskompetenten Zustand, welcher durch Chaperone wie SurA, Skp und DegP erhalten wird [228-232]. Die Insertion der β-Fassdomäne in die äußere Membran erfolgt mit Hilfe der β-Fass-Assemblierungs-Maschinerie (BAM-Komplex; in *E. coli* BamA bis BamE) [221, 233, 234]. Mögliche Erklärungsversuche, wie die Energieversorgung des Typ-5-Sekretionsystems für einen Transport funktionieren könnten, umfassen die Energiegewinnung durch die intrinsische Faltungsfähigkeit des Autotransporters selbst („Brownian ratchet model“) oder eine asymmetrische Ladungsverteilung innerhalb der Passagierdomäne als ein möglicher Antriebsfaktor [235-237].

Abhängig von der Reihenfolge, in welcher die Passagier- und β-Fassdomäne im Vorläuferprotein erscheinen, dem oligomeren Zustand der assemblierten β-Fassdomäne (Monomer oder Trimer) und Größe des β-Fasses, lassen sich Typ-5-Sekretionssysteme in die Untergruppen 5a bis 5e einteilen [238]. Die bisher am besten untersuchte Untergruppe bildet die Autotransporter-Untergruppe 5a (At-5a). AT-5a besteht aus einer 12-strängigen β-Fassdomäne, welche als ein C-terminale Verankerung in der äußeren Membran des Bakteriums fungiert. Diese wird für den nachfolgenden Transport der N-terminalen Passagierdomäne in den extrazellulären Raum benötigt [239]. Die Passagierdomäne wird über einen „C-terminus-first“ Mechanismus transportiert. Bei diesem formt der C-Terminus der Passagierdomäne eine Haarnadelschleife („hairpin-loop“-Modell der Sekretion) im Inneren des β-Fasses. Beim Austritt aus dem β-Fass in den extrazellulären Raum, auf die Oberfläche der Membran, erfolgen vom C-Terminus aus die schrittweise Faltung der Passagierdomäne [240]. Die Passagierdomäne vermittelt die eigentliche Funktion des Proteins und wurde zumeist als wichtiger bakterieller Virulenzfaktor beschrieben [219]. In einigen Fällen kann eine Passagierdomäne auch abgespalten werden. Beispiele sind das Adhäsin *E. coli* AIDA-I oder selbstaggregierende Autotransporter wie *E. coli* Ag43 [241-243]. Autotransport der Untergruppe 5b (At-5b) werden auch als Zwei-Partner-Sekretionsweg (TPS) bezeichnet. Die Passagierdomäne wird über ein 16-strängige β-Fass in den extrazellulären Raum transportiert. Das 16-strängige β-Fass ist zudem an eine

schwankende Nummer periplasmatischer Domänen (POTRA) gebunden, welche Protein-Protein Interaktion vermitteln. Autotransport der Untergruppe 5c (At-5c) zeichnen sich durch drei identische Polypeptidketten, welche zur Bildung einer trimeren Passagierdomäne und eines einzelnen 12-strängigen β-Fasses beitragen aus. Das β - Fass weißt eine große Ähnlichkeit zu den β-Fässern der Gruppe At-5b auf. Autotransport der Untergruppe 5d (At-5d) stellen eine Kombination aus At-5a und At-5b dar. Eine Passagierdomäne ist kovalent mit einer C-terminalen Domäne verbunden, die Merkmale aufweist, die an die Transporter vom At-5b angelehnt sind. Bei Autotransport der Untergruppe 5e (At-5e; auch als Intimin/Invasin-Weg bezeichnet) befindet sich die β-Fassdomäne N-terminal zur C-terminal lokalisierten Passagierdomäne [244].

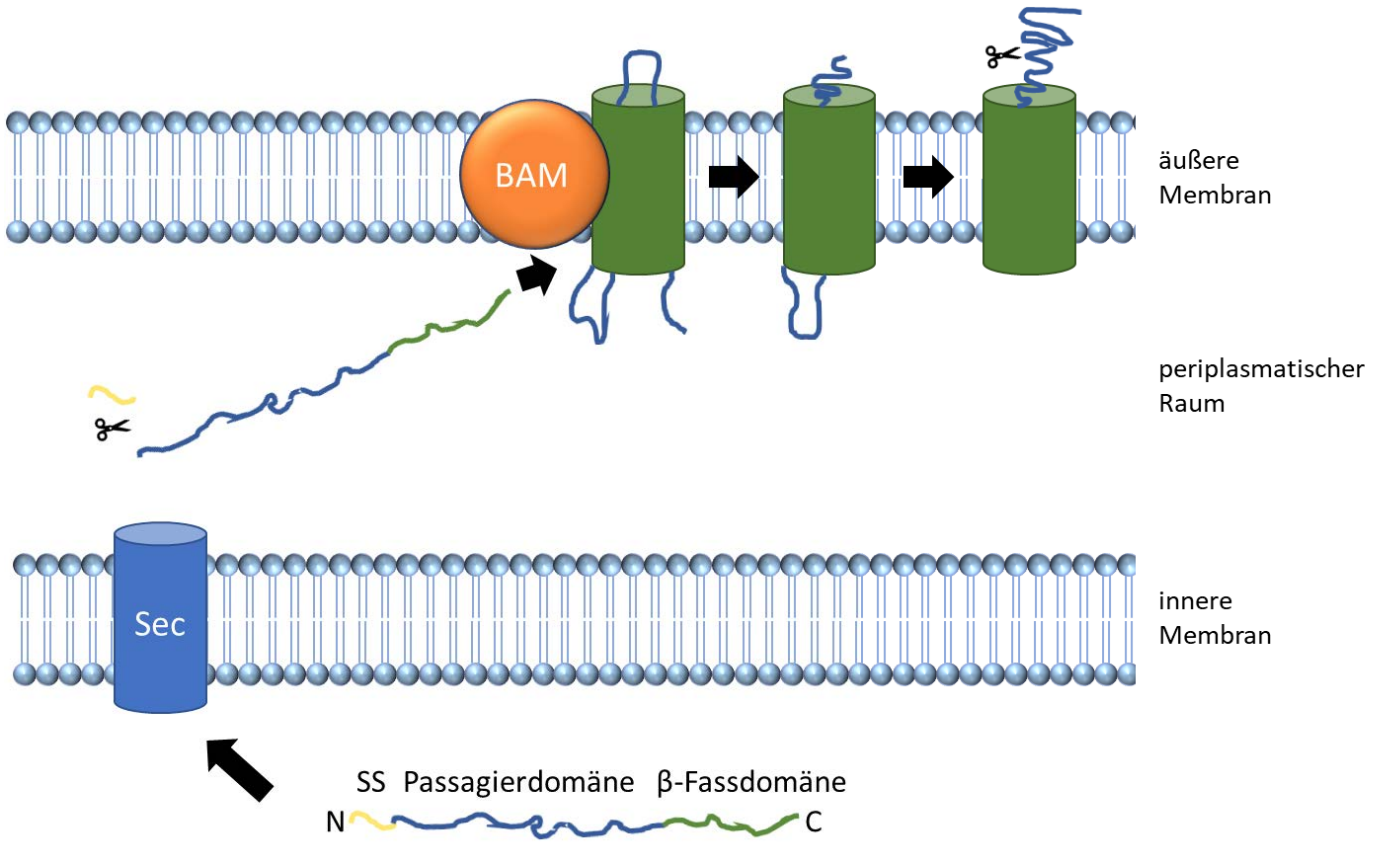


Abbildung 5: Schematische Darstellung des Typ-5-Sekretionssystems.

Intrazelluläres Autotransporterprotein translozierт durch seine Sec-Leitsequenz (gelb) über die innere Membran in den periplasmatischen Raum. Die Leitsequenz wird abgespalten. Die β-Fassdomäne (grün) lokalisiert mithilfe der β-Fass-Assemblierungs-Maschinerie (BAM) in die bakterielle äußere Membran, wo es eine Pore formt. Nach und nach passiert die ungefaltete Passagierdomäne (blau) die in der äußeren Membran lokalisierte β-Fass-Pore. Im extrazellulären Raum faltet sich die Passagierdomäne vollständig und kann je nach aktuell betrachtetem Protein auch abgespalten werden. Die Darstellung wurde nach [214, 235, 241-243] erzeugt.

## 1.7 Die Familie der Polymorphen Membranproteine

Polymorphen Membranproteine (Pmps) repräsentieren die größte Proteinfamilie in *Chlamydia.* Mit 13,6 % in *C. trachomatis* und 17,5 % in *C. pneumoniae* beanspruchen sie einen großen Anteil der chlamydienspezifischen Kodierungskapazität am stark reduzierten Genom und unterstreichen damit ihre Bedeutung innerhalb der chlamydialen Biologie [88]. Nach ihrer ursprüngliche Entdeckung als immunodominante Antigene von *C. abortus* und *C. pneumoniae* infizierten Wirten folgte durch Grimwood und Stephens 1999 ihre bioinformatische Charakterisierung und Einteilung in die sechs Subgruppen: A (PmpA), B (PmpB, PmpC), D (PmpD), E (PmpE, PmpF), G (PmpG und PmpI) und H (PmpH) [222, 245-247]. Obwohl alle chlamydialen Spezies für Pmps codieren, unterscheiden sie sich stark in ihrer Anzahl, Größe und Aminosäurensequenz. So beinhaltet die Pmp-Familie von *C. trachomatis* und *C. muridarum* die neun Mitglieder PmpA bis PmpI, wohingegen *C. caviae* für 17*, C. abortus* für 18 und *C. pneumoniae* für 21 Pmps codiert (Abbildung 7) [56, 248-251]. Es wird vermutet, dass Pmps durch Genduplikationen entstanden sind, dadurch eine funktionelle Vielfalt ermöglichten und möglicherweise unmittelbar mit den zwischen verschiedenen Serovaren beobachteten Variationen der Krankheitsschwere im Zusammenhang stehen [252]. Es wurde bereits in verschiedenen *C. trachomatis*-Serovaren, einschließlich der Serovare D, E und L2 gezeigt, dass alle 9 *pmp*-Gene *in vitro* transkribiert und die Proteine an die bakterielle Oberfläche verlagert werden [253-255]. Pmps zeigen eine große Heterogenität im Bezug zu ihrer Aminosäureidentität. Innerhalb derselben Subgruppe und chlamydialen Spezies aber auch unterschiedlichen Spezies weisen sie häufig hohe Sequenzidentitäten auf. So zeigen *C. trachomatis* Serovar E PmpB und PmpC 43 % (Subgruppe B), *C. pneumoniae* Pmp21 und *C. trachomatis* PmpD (Homolog zu Pmp21) 33% Identität wohingegen Pmp-Proteine unterschiedlichen Subgruppen wie PmpE (Subgruppe E) und PmpD (Subgruppe D) nur 18 % Identität teilen [92, 222, 256].

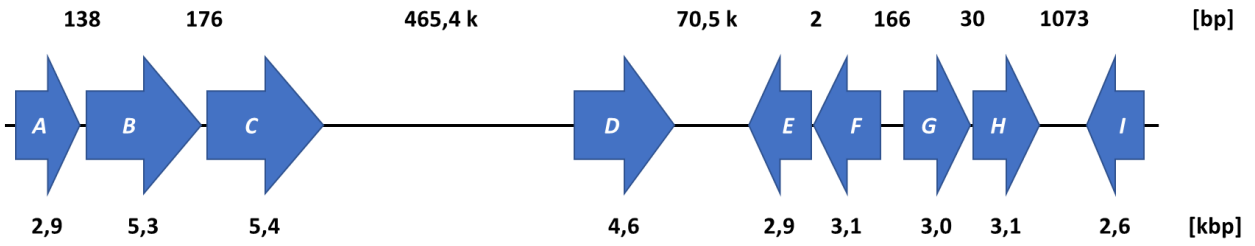


Abbildung 6: Anordnung der *pmp*-Gene im Genom von *C. trachomatis* serovar E DK-20.
Der Abstand zwischen einzelnen *pmp*-Genen (in Basenpaaren (bp)) sowie deren Größe (in Kilobasenpaaren (kbp)) werden über bzw. unter dem *pmp* angegeben. Die Grafik wurde orientiert an [257] erstellt.

Die *pmp*-Gene von *C. trachomatis* sind in 2 Genom-Clustern angeordnet, wobei *pmpA* bis *pmpC* sowie *pmpE* bis *pmpI* je ein Cluster bilden. *pmpD* liegt genetisch isoliert vor. RT-PCR Daten weisen darauf hin, dass *pmpABC*, *pmpFE* und *pmpGH* gemeinsam transkribiert werden, was vermuten lässt, dass diese Gene in Operons organisiert sind (siehe Abbildung *7*) [257]. Dabei stellt das *pmpABC*-Operon durch deutliche Unterschiede im Transkript-Profil von *pmpA* eine Besonderheit dar, welche auf das Vorhandensein eines zusätzlichen *pmpA*-spezifischen Promotors oder posttranskriptionelle Mechanismen, die die mRNA-Stabilität beeinflussen, hindeutet [257]. PmpA, PmpD und PmpI sind mit 99,6 %, 99,1 % und 99,2 % Aminosäuren-Identität die am stärksten konservierten *C. trachomatis* Pmps. Daher ist es wahrscheinlich, dass sie eine sehr große Wichtigkeit sowie serovarübergreifende Aufgaben innerhalb der chlamydialen Biologie ausüben [257, 258]. Interessanterweise zeigten Studien von Tan *et al*. 2010, in welchem unter anderen die Inklusionsspezifische-Expression von *C. trachomatis* Pmps anhand von infizierten HeLa-Zellen untersucht wurde, dass die Expression von PmpA, PmpD und PmpI mit < 1 % deutlich häufiger nicht abgeschaltet war im Verhältnis zu anderen Pmps, was zusätzlich auf ihre Wichtigkeit hindeutet [253].

Computergestützte bioinformatische Analysen identifizieren Pmps aufgrund ihrer Eigenschaften als Autotransporter (Typ-V-Sekretionssystem). Diese Eigenschaften sind eine N-terminale Sec-Leitsequenz für die Translokation zur Membran, gefolgt von einer Passagierdomäne (ausschlaggebend für die Funktion des Proteins), einem C-terminalen β-Fass und Phenylalanin am C-terminalen Ende des Proteins, was auf eine Lokalisierung in der äußeren Membran deutet [222, 223, 259]. Autotransporterproteine sind innerhalb der gramnegativen Bakterien weit verbreitet und leisten einen Beitrag zur Virulenz vieler Pathogene [235, 260, 261]. Pmps werden durch das Vorhandensein von mehreren FxxN und GGA (I, L, V) Tetrapeptidmotiven im N-terminalen Abschnitt des Proteins definiert. Diese kommen bei Pmp-Proteinen überdurchschnittlich häufig vor und sind damit ein wesentliches Merkmal dieser Familie. FxxN- und GGA (I, L, V)-Motive werden durchschnittlich 11,3 bzw. 5 Mal in *C. pneumoniae*-Pmps und 13,6 bzw. 6,5 Mal in *C. trachomatis*-Pmps gefunden, wohingegen sie nur 0,84 bzw. 0,01 Mal im gesamten *C. pneumoniae*-Proteom bzw. 0,73 bzw. 0,06 Mal im gesamten *C. trachomatis*-Proteom gefunden werden [88, 91, 222]. Außerhalb der chlamydialen Proteine sind das FxxN und GGA (I, L, V)-Motiv nur wenig verbreitet. Beispiele bilden unter anderem das Außenmembranprotein, Adhäsin und Invasin OmpA von *Rickettia conorii* (7 FxxN und 7 GGA), der *E. coli* Autotransporter YfaL (13 FxxN und 6 GGA) oder das humane Mucin 5B [262-264].

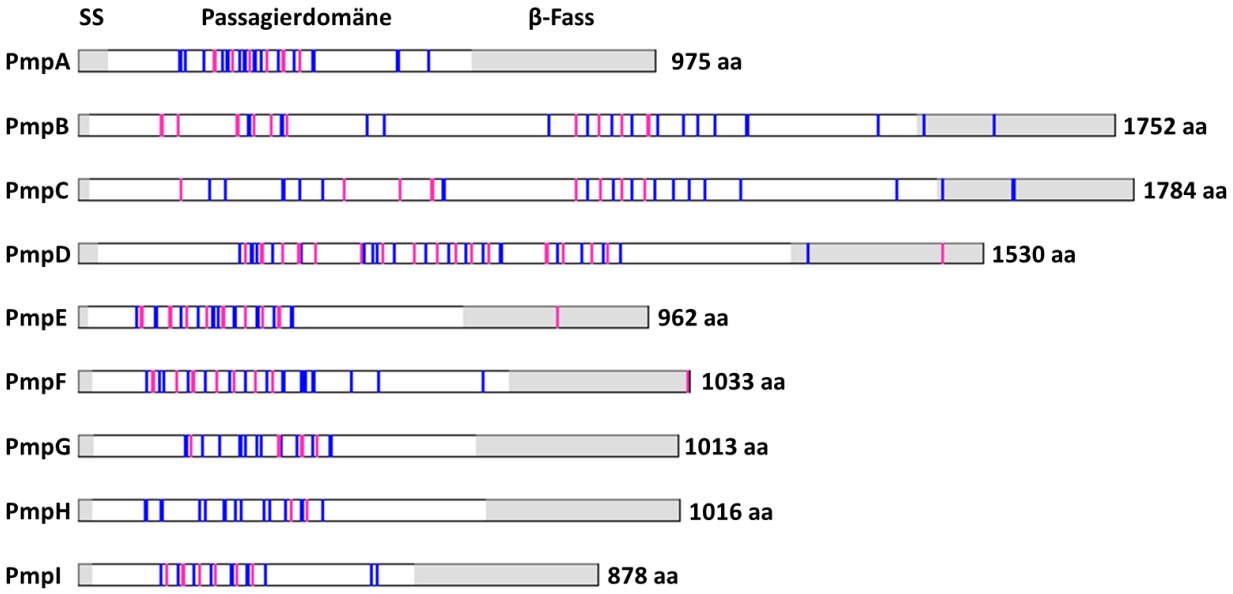


Abbildung 7: Schematische Darstellung der *C. trachomatis* Serovar E Pmps.
Die Grafik zeigt *C. trachomatis* Serovar E PmpA bis PmpI in ihrer Volllänge-Form. Sie besitzen einen N-terminale Leitsequenz (SS, grau), zentrale Passagierdomäne (weiß) und eine C-terminale β-Fass-Domäne (grau). Senkrechte Kennzeichnungen repräsentieren die Tetrapeptidmotive GGA (I, L, V; pink) und FxxN (blau). Die Länge wird in Aminosäuren (aa) angegeben. SS und β-Fass-Domänen wurden mittels der Onlinesoftware SignalIP, Phöbius, Phyre2 und RaptorX bestimmt [265-269]. Die Grafik wurde mit RStudio und auf Grundlage eines Codes von Fabienne Kocher erstellt [270].

## 1.7.1 Funktion innerhalb der Infektion

Die adhäsiven Eigenschaften der Pmps konnte erstmalig in der Studie von Mölleken *et al.* 2010 demonstriert werden, in welcher die Bindung von *C. pneumoniae* Pmp6, Pmp20 und Pmp21 (Homologe zu *C. trachomatis* PmpG, PmpB, und PmpD) an menschlichen Epithelzellen durch Pmp-präsentierende Hefezellen und mit rekombinanten Pmp beschichteten Latexkügelchen gezeigt werden konnte. Des Weiteren wurde gezeigt, dass eine Vorbehandlung menschlicher Zellen mit rekombinantem Pmp6, Pmp20 oder Pmp21 eine darauffolgende Infektion mit *C. pneumoniae* signifikant reduzierte, was mit einer verminderten Adhäsion von Chlamydien an die Wirtszellen korrelierte und damit die adhäsiven Eigenschaften von Pmp6, Pmp20 und Pmp21 verdeutlichte. Zur Identifikation adhäsionskompetenter Bereiche der Pmp21-Passagierdomäne wurden 4 Untereinheiten (Pmp21 Domänen A-D) auf ihre Bindefähigkeit getestet. Unabhängig von der getesteten Domäne vermittelten alle Pmp21-Untereinheiten Bindung an HEp-2 Zellen im Hefe-Display sowie bei mit Pmp beschichteten Latexkügelchen. Zudem reduzierte eine Vorbehandlung von Zellen mit rekombinanten Pmp21 Domäne B-D eine Folgeinfektion.

Spezifische Antikörper gegen Pmp21 waren in der Lage eine Infektion *in vitro* zu neutralisieren. Abschließend zeigte eine Kombination verschiedener Pmps einen additiven infektionsblockierenden Effekt was auf vergleichbare Funktionen hinweist [91]. Weniger Jahre später zeigten Untersuchungen von Becker und Hegemann 2014, dass auch alle löslichen, rekombinant hergestellten Pmps von *C. trachomatis* in der Lage sind, eine (in variierendem Ausmaß) Bindung an Humanzellen zu vermitteln. Vorinkubation von Pmp-Protein auf Humanzellen reduzierte eine nachfolgende Infektion mit *C. trachomatis* EBs, was auf eine wichtige Funktion der gesamten Proteinfamilie im Infektionsprozess schließen ließ. Untersuchungen mit Paaren von rekombinanten Pmps oder einer Kombination von Pmp21 und OmcB zeigten zudem, dass sich der Adhäsionsweg bzw. die verwendeten Oberflächenstrukturen der Wirtszelle, welche alle Pmps verwenden vom OmcB-GAG-Weg unterscheidet [93]. Vertiefende Untersuchungen des *C. pneumoniae* Pmp21 führten schließlich zur Identifizierung des EGFRs als humanen Rezeptor. Mit Pmp21 beschichtete Latexkügelchen wurden von menschlichen Zellen aufgenommen und demonstrierten damit dessen Funktion als Invasin. In Kurzzeitinfektionsexperimenten zeigten Immunfluoreszenz-mikroskopische Aufnahmen eine Kolokalisation von EGFR und EBs an der bakteriellen Eintrittsstelle. Aktivierung und Signalweiterleitung des EGFRs wurden sowohl bei Inkubation mit chlamydialen EBs als auch bei der Inkubation mit rekombinanten Pmp21 ausgelöst. Nicht EGFR exprimierende Hamsterzellen zeigten nach Transfektion mit einem EGFR-tragenden Plasmids eine verstärkte Adhäsion und Internalisierung an bzw. in EBs. Aktivierung des EGFR führt zu der Rekrutierung des Adaptorproteins Grb2 sowie der Ubiquitin-Ligase c-Cbl. Grb2 bindet an die Phosphotyrosine 1068 und 1086 des aktivierten EGFR und induziert über den Ras/Raf-Signalweg die ERK1/2-Signalkaskade. Dies erlaubt die Bindung von c-Cbl an Phosphotyrosin 1045. Über Clathrin-abhängiger und -unabhängiger Endozytose führt dieser Proteinkomplex zur Internalisierung des EGFR [1].

PmpD bildet das *C. trachomatis* Homolog zum *C. pneumoniae* Pmp21 (33 %ige Aminosäureidentität) [92, 222]. Studien einer *C. trachomatis* PmpD null Mutante demonstrierten, dass PmpD nicht essentiell für eine Infektion ist. Infektion mit der PmpD null Mutante zeigte keine Infektions- oder Wachstumsdefizite in kultivierten Mäusezelllinien *in vitro* oder in einem urogenitalen Infektionsmodell der Maus. Allerdings zeigte die PmpD-null Mutante eine reduzierte Adhäsion und Infektion an humanen endozervikalen und konjunktivalen Zellen sowie innerhalb eines nichtmenschlichen Primatenmodels zur Untersuchung der *C. trachomatis* Augeninfektion [271]. Viele Forschungsergebnisse weisen darauf hin, dass Pmps innerhalb der chlamydialen Infektion einen Einfluss auf die Wirtsspezifität ausüben könnten. So zeigten humane Epithelzellen, welche mit rekombinanten *C. trachomatis* Pmps vorbehandelt wurden, keine signifikant reduzierte Infektion in einer nachfolgenden Infektion mit *C. pneumoniae* EBs. Dies war auch bei der Verwendung von *C. pneumoniae* Pmps und einer Folgeinfektion mit *C. trachomatis* EBs der Fall, was darauf

schließen lässt, dass Pmps am Wirts- und Gewebetropismus beteiligt sind [93]. Vergleichbares zeigten auch Crane *et al.* 2006 mit Experimenten, in welchen anti-PmpD Antikörper in der Lage waren, eine *C. trachomatis* Infektion zu neutralisieren aber nicht eine Infektion mit *C. pneumoniae*, *C. muridarum* oder *C. caviae,* was auch hier darauf hinwies, dass PmpD ein speziesspezifisches Antigen ist [272]. Unterstützt wurden diese Observationen durch Studien von Gomes *et al.* 2006, welcher die Polymorphismen aller *C. trachomatis* Serovar Pmps untersuchte und dabei eine Korrelation der identifizierten genetischen Variationen mit bestimmten Gewebe beschrieb. Folglich waren die *pmp*-Gene von *C. trachomatis* LGV (L1, L2, L2a, L3) am engsten miteinander verwandt und zeigten gleichzeitig den stärksten Unterschied zu den nicht LGV-Serovaren, die okulären und urogenitalen Krankheitsgruppen erzeugen [258].

## 1.7.2 Expression der Pmps

*C. pneumoniae* besitzt 21 Pmps wovon 15 exprimiert werden. Bei *C. trachomatis* werden alle 9 Pmps exprimiert [253, 273, 274]. Aufgrund ihrer Anzahl ist es wahrscheinlich, dass Pmps essentielle und/oder unterschiedliche Funktionen innerhalb des Infektionszyklus ausüben und daher zu anderen Zeitpunkten in unterschiedlichem Ausmaß exprimiert werden. Manche Pmps könnten daher eine RB oder EB Spezifität aufweisen. Zusätzlich können sich die Expressionsstärke und -Zeitpunkte zwischen chlamydialen Spezies und Serovaren unterscheiden. Wann welches Pmp exprimiert wird ist immer noch Gegenstand wissenschaftlicher Untersuchungen. Nunes *et al.* 2007 untersuchte die Transkription der Pmp-Gene über den gesamten Replikationszyklus von *C. trachomatis* Serovare E und L2. Für *C. trachomatis* Serovar E zeigten *pmpB*, *C*, *D*, *E*, *F*, *G* und *H* bei 24 - 48 Stunden die größte mRNA-Menge. *PmpA* transkribierte bei 12 - 18 Stunden und *pmpI* bei 18 - 24 nach Infektion am stärksten. Für Serovar L2 zeigten *pmpA* bei 12 Stunden, *pmpB*, *E*, *G*, *H* und *I* nach 18 - 36 Stunden und *pmpC*, *D* und *F* nach bei 18 - 48 Stunden nach Infektion die meiste mRNA.

Ihre Studie zeigte, dass für alle Pmps 2 Stunden nach Beginn der Infektion mRNA detektiert werden konnte. *PmpA* zeigte hierbei die geringste Transkription, wurde allerdings 12 Stunden nach Infektion als sehr stark transkribiert detektiert, was womöglich auf einen Rolle bei der RB-Entstehung hindeutet [255]. PmpF zeigte die insgesamt stärkste Transkription und wurde je nach betrachteten Serovar 18 bis 36 Stunden nach Infektionsbeginn am stärksten detektiert, was auf eine wichtige Funktion innerhalb der RB-Form hindeutet. Diese Transkription war 20- bis 50-fach stärker als das zu diesem Zeitpunkt niedrigste transkribierte *pmp*. *PmpA* und *pmpI* zeigten insgesamt die schwächste Transkription [255].

Analysen der *pmp*-Transkription von *C. psittaci* zeigten erneut eine frühe (wenn auch sehr niedrige) Transkription aller *pmp*-Gene (2 Stunden nach Infektion). Die Mehrzahl der *pmp*-Gene (*pmpE1*, *pmpE2*, *pmpG1a*, *pmpG1b*, *pmpG1c*, *pmpG1d*, *pmpG2*, *pmpG3*, *pmpG6*, pmp*G8* und *pmpH*) zeigte die stärkste Transkription 24 Stunden nach der Infektion, welche auch bei 32 und 48 Stunden auf einem hohen Niveau blieb. *pmpA* und *pmpH* zeigten ihre stärkste Transkription bereits 2 bis 12 Stunden nach Infektionsbeginn, welche im Bereich von 12 - 18 abfiel und bei *pmpH* nach 18 Stunden wieder auf ein höheres Niveau anstieg. Die Transkription von pmpB und pmpD waren durchgehend gering und erreichten ihr Maximum bei 18 - 48 Stunden. pmpG4 und pmpG5 wurden am stärksten 48 Stunden nach Beginn der Infektion transkribiert [248].

Interessanterweise zeigen auch die Indizierung chlamydialer Stressfaktoren einen Einfluss auf das Expressionsverhalten von Pmps. Studien in welchen das Expressionsverhalten von *C. trachomatis* unter optimalen Bedingungen oder unter Einfluss von Penicillin verglichen wurde, zeigten unter Stress eine unveränderte Transkription von *pmpA*, *pmpD* und *pmpI*, wohingegen für *pmpE*, *F*, *G*, und *H* reduzierte Transkript-Level wahrgenommen wurden [257]. Dies deutet darauf hin, dass PmpA, PmpD und PmpI besonders wichtige Rollen in der Infektion durch *C. trachomatis* einnehmen [257].

Saka *et al.* 2011 untersuchten durch ihre quantitativen Proteomik-Studien die metabolischen und pathogenen Eigenschaften der Entwicklungsformen von *C. trachomatis* und verglichen dabei das Vorhandensein der Pmps in der RB und EB Form. In dieser Studie zeigten RBs ein etwa ähnliches Vorkommen (4 - 6 %) von PmpA , PmpE, PmpG und PmpH wohingegen PmpC (18 %), PmpI (22 %) und PmpD (40 %) vermehrt detektiert wurden. Die EB-Form zeigte kein bis kaum PmpA und PmpD (1 %), vergleichbare Mengen (10 - 11 %) an PmpC und PmpF, fast gleiche Mengen (17 - 18 %) an PmpB , PmpH und PmpE und am meisten PmpG (26 %) [128]. Vergleichbar mit Nunes *et al.* 2007 und Van Lent *et al.* 2016, welche eine Transkription von *pmpA* im frühen Abschnitt des chlamydialen Infektionszyklus beschrieben, waren nur in RBs PmpA Protein zu detektieren [128, 248, 255]. Transkription von *pmpD* wurde für den späten Abschnitt der Infektion beschrieben, wohingegen Saka *et al.* 2011 von einem primären Vorkommen von PmpD-Protein in der RB-Form berichtete [128, 248, 255]. Zusammenfassend unterstreichen diese Daten, dass die Pmp Expression hoch variabel ist, sich zwischen unterschiedlichen chlamydialen Spezies und Serovaren unterscheiden kann und Chlamydien damit viele unterschiedliche Antigene präsentieren. Diese hohe Antigenvariation könnte einen Abwehrmechanismus gegen das Immunsystem darstellen und so eine effektive Adaption des Immunsystems an die Infektion verhindern [256].

## 1.7.3 Oligomerisierung von Pmps

Die FxxN- und GGA (I, L, V)-Motive der Pmps befinden sich zum Großteil innerhalb der Passagierdomäne, wo sie eine ausschlaggebende Bedeutung für die Oligomerisierung als auch Funktion innerhalb der Adhäsion darstellen (siehe Abbildung 7) [91, 93, 275]. Vertiefende Deletionsanalysen mit *C. pneumoniae* Pmp21-Fragmenten offenbarten, dass wenigstens zwei repetitive Tetrapeptidmotive (ein GGA(I, L, V) und ein FxxN oder zwei FxxN Motive) essentiell für den adhäsiven Charakter des Pmp21 sind [91]. Es ist möglich, dass Tetrapeptidmotive ausschlaggebend für den hochmolekularen oligomeren Zustand von Pmp-Proteinen sind und nur oligomerisiertes Pmp an Zellen binden könnte [275].

Studien zur Suche und Identifikation chlamydialer Adhäsine resultierte bisher in nicht-filamentösen, monomeren Adhäsinen wie beispielsweise die Pmp-Familie, OmcB, *C. trachomatis* Ctad1 oder *C. pneumoniae* LipP (CPn0473) [74, 91, 93, 94, 102]. Innerhalb der letzten 15 Jahre entstanden einige Studien, welche eine Oligomerisierung auch bei Pmps vorstellbar machen könnten. Studien von Swanson *et al.* 2009 fokussierten sich auf das *C. trachomatis* PmpD. Innerhalb ihrer Studien konnten sie zeigen, dass immunaffinitätsgereinigtes natives PmpD als Oligomer mit einer ausgeprägten 23-nm-blumenartigen Struktur vorlag. Oligomeres PmpD wurde mittels „Blue Native PAGE“ aufgetrennt und erschien als Schmier einer Größe von 250 bis 1.050 kDa. Weitere Analysen mittels zweitdimensionaler SDS-PAGE identifizierten sowohl Volllänge-PmpD (155 kDa), sowie die zwei proteolytisch prozessierten Fragmente 73 kDa-Passagierdomäne (PD) und die 82 kDa-Translokatordomäne. Insgesamt zeigten ihre Resultate, dass PmpD entweder als oberflächenassoziiertes Oligomer mit blumenartiger Struktur höherer Ordnung oder in löslicher Form, welche auf infizierte Zellen beschränkt ist, vorkommt [276]. Interessanterweise zeigten auch Studien des *C. pneumoniae* Homologes Pmp21 ringartige Strukturen auf der bakteriellen Oberfläche von Chlamydien, welche als mögliche oligomere Strukturen diskutiert wurden [91]. Vertiefende Studien von Luczak *et al.* 2016 konzentrierten sich auf unterschiedliche Subfragmente von Pmp21 und ob das Vorhandensein oder Nicht-Vorhandensein von zwei FxxN-Motiven die Selbstinteraktion, Faltung und das Adhäsionsverhalten beeinflussen können. Pmp21_D-wt (ein C-terminales Fragment, das von dem natürlich vorkommenden M-Pmp21 abgeleitet ist) Moleküle generieren Oligomere, welche auch als Protofibrillen erscheinen und in der Lage sind wie das Amyloid Protein Fragment Aβ42 an Thioflavin-T zu binden. Eine mutierte Pmp21_D-wt Version (Pmp21_D-mt), in welcher die zwei FxxN Motive durch SXXV Motive ausgetauscht sind (erstmals untersucht in [91]), zeigt hingegen eine stark verringerte Fähigkeit Oligomere zu generieren, an Zellen zu binden und in Folge auch einen geringeren Infektions-blockierenden Effekt nach Vorbehandlung von Humanzellen mit rekombinanten Pmp21_D-mt Oligomeren.

Sekundärstrukturanalysen zeigen, dass Pmp21_D Monomere beider Varianten überwiegend als „random coils“ vorliegen, während die Oligomere überwiegend β-Faltblätter bilden. Daraus folgt, dass das FxxN-Motiv notwendig für die Bildung von β-Faltblatt-reichen Oligomeren ist [275]. Ergänzt wurde diese Studie durch Arbeiten von Paes *et al.* 2018 am *C. trachomatis* Homolog PmpD. Sie zeigten für die PmpD Passagierdomäne, dass zusätzlich zu nicht-kovalenten Wechselwirkungen umfangreiche disulfidvermittelte kovalente Interaktionen eine Rolle bei der Bildung von Strukturen höherer Ordnung spielen, welche womöglich einzigartig für Chlamydien sind [277]. Eine jüngste Studie untersuchte Motiv-arme und Motiv-reiche rekombinant exprimierte *C. trachomatis* Pmp-Fragmente und konnte mittels „Blue Native PAGE“, Größenausschlusschromatographie und Elektronenmikroskopie zeigen, dass alle Proteinfragmente unabhängig von ihrer Motivanzahl hoch-molekulare oligomere Strukturen generieren. Mischung und anschließende Renaturierung verschiedener Pmp-Fragmente resultieren in heteromeren Komplexen, welche Filamente von bis zu 2 µm Länge erzeugen, die damit wesentlich länger als entsprechende homomere Strukturen sind. Nur adhäsionskompetente Oligomere sind in der Lage eine Infektion nach Vorbehandlung der Humanzellen zu blockieren. Interessanterweise führt eine Vorbehandlung chlamydialer EBs mit adhäsionsinkompetenten Oligomeren ebenfalls zu einer Reduzierung in einer Folgeinfektion durch Bindung an adhäsionsfähige Pmp Strukturen auf der EB Oberfläche [278]. Obwohl noch keine protofibrillähnlichen Strukturen auf der Oberfläche von Chlamydien gezeigt werden konnten, weisen zusammenfassend die vorliegenden Studien auf ein mögliches Vorkommen oligomerer Pmps auf der Oberfläche von Chlamydien hin. Diese könnten als homomere und/oder heteromere (zusammengesetzt aus unterschiedlichen Pmps und prozessierten Pmp-Fragmenten) Oligomere vorliegen, damit eine enorme Anzahl an unterschiedlichen Antigenen präsentieren und so einen Schutzmechanismus gegen das Wirtszell-Immunsystem darstellen [278].

## 1.7.4 Prozessierung von Pmps

Viele Pmps von unterschiedlichen chlamydialen Spezies zeigen die Lokalisation auf der chlamydialen Oberfläche, begleitet von komplexen proteolytischen Prozessierungen [91, 253, 272, 274, 276, 279-281]. PmpD und sein Homolog *C. pneumoniae* Pmp21 bilden die bisher am besten untersuchten chlamydialen Proteine der Pmp-Familie.

Mithilfe von 1D- und 2D-PAGE konnte gezeigt werden, dass Pmp21 komplexen Prozessierung unterliegt. Das prozessierte N-Pmp21 wird zur chlamydialen Oberfläche transloziert, wo es an andere Komponenten der äußeren Membran bindet [281]. Die Spaltungen erfolgen direkt nach der Leitsequenz, im Zentrum der Passagierdomäne bei Aminosäure (aa) ~670 und im C-Terminalen Bereich zwischen Passagierdomäne und β-Fass bei aa 1146 und resultierten damit in das 70 kDa N-Pmp21, 55 kDa M-Pmp21 und 45 kDa C-Pmp21D (vgl. Abbildung 8). Obwohl Studien zeigen, dass Pmp21 zum Großteil prozessiert und mit der Oberfläche von chlamydialen RBs und EBs assoziiert wird ist dies nicht immer der Fall [91, 281]. So konnten während einer Infektion mit EBs, Pmp21 in voller Länge (N/M/C-Pmp21), das Zwischenprodukt N/M-Pmp21 und das vollständig prozessierte N-Pmp21 nachgewiesen werden [280, 281]. Da alle Fragmente adhäsive Eigenschaften demonstrieren, könnte dies eine mögliche Adhäsion verstärken und eine Infektion verbessern [91].

Studien an EB-Lysaten von *C. trachomatis* L2 zeigten, dass mit PmpD spezifischen Antikörper neben Volllänge PmpD (155 kDa) auch zwei weitere PmpD-Fragmente (~80 und ~42 kDa) detektiert werden können, was darauf hindeutete, das *C. trachomatis* ähnlich wie *C. pneumoniae* Pmp21 prozessiert wird [272]. Weitere Analysen mit Domänen-spezifischen anti-Peptid-Antikörpern (gerichtet gegen die N-terminale Domäne (N-PmpD), Mitte (M-PmpD) und C-Terminus (C-PmpD)) demonstrierten, dass 24 Stunden nach Infektionsbeginn und in EB-Fraktionen neben Volllänge PmpD (p155) auch ein N-terminales (p73; Passagierdomäne) und ein C-terminales (p82) Fragment detektiert werden [254, 276]. Weiterführende Sequenzanalysen von p155 und p82 erlaubten die Identifikation der Spaltungsstellen bei aa 55 (zwischen Leitsequenz und Passagierdomäne) und bei aa 762 (zwischen Passagierdomäne und C-Terminus des Proteins) [276]. Zur Analyse zum Auftreten unterschiedlicher PmpD-Fragmente während des Infektionszyklus wurden Zellen mit *C. trachomatis* infiziert, zu unterschiedlichen Zeitpunkten geerntet, aufbereitet und durch Ultrazentrifugation in lösliche und unlösliche Fraktion aufgetrennt. Visualisierung mittels Western Blot zeigt, dass 24 Stunden nach Beginn der Infektion p155, p82 und p73 in der unlöslichen Fraktion detektiert werden können. Interessanterweise sind in der löslichen Fraktion ein 111 kDa Fragment (p111), p73 und ein 30 kDa Fragment (p30) zu detektieren [276].

Zusammenfassend zeigt dies, dass sowohl Pmp21 als auch PmpD komplexen Prozessierungsmechanismen unterliegen. Da nicht bekannt ist ob Pmps eine autoproteolytische Aktivität besitzen oder chlamydiale oder humane Enzyme die Prozessierung vermitteln, ist der genaue Prozess der Pmp-Prozessierung unbekannt.

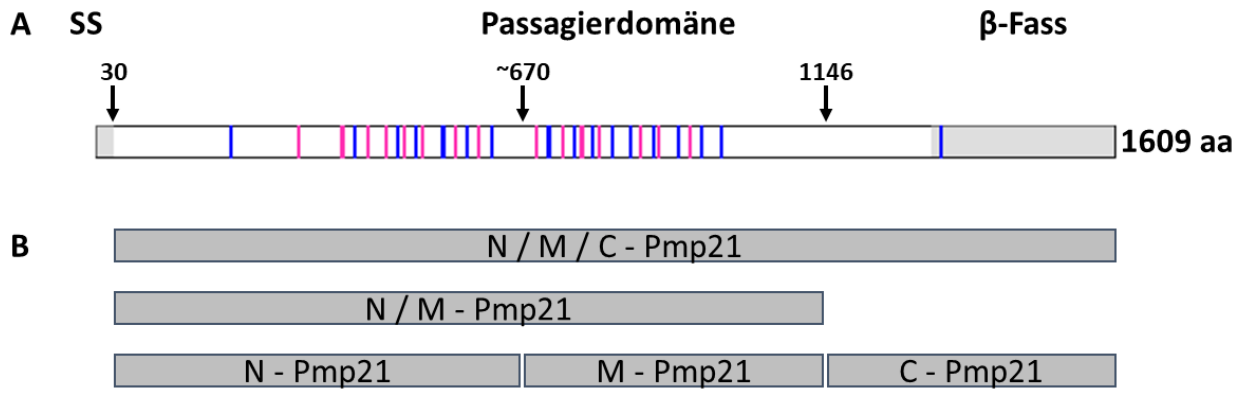


Abbildung 8: Schematische Darstellung der Prozessierung von *C. pneumoniae* Pmp21.

A. Die Grafik zeigt *C. pneumoniae* Pmp21 in seiner unprozessierten Volllänge-Form. Es besitzt eine N-terminale SS, zentrale Passagierdomäne und eine C-terminale β-Fass-Domäne. Senkrechte Kennzeichnungen repräsentieren die Tetrapeptidmotive GGA (I, L, V; pink) und FxxN (blau). Zwei identifizierten Prozessierungsstellen sind mit Pfeilen markiert [91, 280, 281]. B: Schematische Darstellung natürlich vorkommender prozessierter Pmp21-Fragmente, wie sie auf der chlamydialen Oberfläche vorkommen und auch mittels Proteomanalyse identifiziert wurden [91, 273, 280, 281]. Die Grafik wurde mit RStudio und auf Grundlage eines Codes von Fabienne Kocher erstellt [270].

## 1.8 Impfstoffe

*C. trachomatis* ist die Hauptursache für vermeidbare Erblindung und die häufigste, bakterielle, sexuell übertragbare Infektion [282]. Chlamydiale Infektionen sind grundsätzlich mit Antibiotika behandelbar. Allerdings verlaufen sie häufig ohne Symptome, wodurch eine Behandlung nicht oder zu spät durchgeführt wird. Insbesondere Frauen sind durch mögliche entzündliche Beckenerkrankungen, Unfruchtbarkeit oder Fehlgeburten als Folge einer chlamydialen Infektion einem starken Risiko ausgesetzt [3, 9, 283, 284]. Innerhalb der letzten Jahrzehnte verzeichneten Gesundheitsbehörden nur geringe Erfolge in der Eindämmung steigender *C. trachomatis* Infektionen [285]. Zusätzlich gibt es noch keine Medikamente, welche kosteneffizient genug sind um das Bakterium in den Entwicklungsländern zu eliminieren [6, 60]. Trotz langer Forschung gibt es zum aktuellen Zeitpunkt keinen chlamydialen Impfstoff. Daher ist die chlamydiale Impfstoff-Forschung ein Gebiet intensiver Forschung mit hohem Interesse. Klinische Trachom-Studien mit lebenden oder inaktivierten EBs von *C. trachomatis* resultierten in einem kurzeitigen Rückgang der Erkrankung und einer reduzierten bakteriellen Belastung [286]. Dem entgegen zeigten weitere Studien eine höhere Häufigkeit von Bindehautentzündungen bei geimpften Personen nach Exposition gegenüber *C. trachomatis* oder das eine Infektion mit einem heterologen Serovar zu einer schwereren Erkrankung

führen könnte [287-290]. Obwohl zusammenfassend diese Form der Impfung als allgemein sicher angesehen wird, ist der erzielte Schutz nur von kurzer Dauer und womöglich serovarspezifisch [291]. Da eine Impfung mit lebenden, attenuierten oder toten EBs nicht ausreichend funktioniert, muss eine Subunit-Impfung entwickelt werden. Die meisten Antigene, welche für die Impfstoffforschung von Interesse sind, sind oberflächenassoziierte Proteine, welche eine Antikörper-bildende Reaktion hervorrufen [286]. Zudem sollten sie in jeder Spezies und bei allen Serovaren, gegen die der Impfstoff wirken soll, vorkommen, ähnlich exprimiert werden sowie leicht und in hohen Mengen rekombinant herstellbar sein. Eines der meistuntersuchten chlamydialen Antigene ist MOMP. Es stellt einen Großteil der chlamydialen Membran dar (60 % des COMC), ist hoch antigenisch und beinhaltet Epitope für B- und T-Zellen [82, 292]. Pal *et al.* 2001 zeigte, dass Mäuse, welche mit nativem trimerischen MOMP (nMOMP) geimpft wurden, einen Schutz gegen „shedding“ und Unfruchtbarkeit aufbauten [293]. Zudem zeigten Untersuchungen in einem *C. muridarum* Atemwegs-Model, dass eine Impfung mit nMOMP einen signifikant stärkeren Schutz erzeugt, als eine Impfung mit rekombinanten MOMP, was darauf schließen lässt, dass die tertiär Struktur von MOMP wichtig für den Schutz ist [294]. Allerdings war es nicht möglich mit MOMP aus einem Serovar einen serovarübergreifenden Immunschutz aufzubauen. Daher wurde Herip1 entwickelt, welches aus Regionen der variablen Domäne 4 (VD4) von MOMP aus mehreren Serovaren besteht und daher breit neutralisierend wirkt [295].

Die Ergebnisse der bisherigen Pmp-Forschung mit *C. pneumoniae* und *C. trachomatis* lassen darauf schließen, dass vielleicht alle, aber mit höherer Sicherheit die meisten Pmps auf der Oberfläche von EBs vorliegen und eine wichtige Relevanz innerhalb der Infektion ausüben und damit womöglich auch immunogen sind, wodurch sie gute Ziele für die Impfstoffentwicklung darstellen könnten [91, 93, 128]. Knudsen *et al.* 1999 und Bunk *et al.* 2008 zeigten in Untersuchen von *C. pneumoniae*, dass PmpG-Homologe (Konformationsepitope von *C. pneumoniae* Pmp10 und Pmp6) immundominante Antigene darstellen [247, 296]. Interessanterweise zeigten Untersuchungen an mit *C. trachomatis* infizierten Patienten hohe Titer gegen bestimmte Pmps, welche aber zwischen den Patienten variierten und damit die Variation der Expression im Laufe des chlamydiale Replikationszyklus widerspiegeln könnten (vgl. 1.6.2) [257, 273, 280, 297-299]. Damit wären Pmps an der Antigenvariation beteiligt und würden zur Strategie der Immunvermeidung beitragen [81]. Diese Theorie wurde durch eine kürzlich veröffentliche Studie bekräftigt, welche demonstrierte, dass rekombinante Pmps *in vitro* in der Lage sind, homomere und heteromere funktionelle Oligomere zu bilden. Ist dies auch *in vivo* der Fall, wäre es vorstellbar, dass Volllänge-Pmps, welche auf der äußeren Membran verankert sind, mit weiteren Pmps ihrer Art und auch anderen Volllänge-Pmps sowie unterschiedlichen prozessierten Pmp-Fragmenten interagieren, wodurch eine Vielzahl heteromerer Komplexe entstehen würden. Dies würde in einem gewaltigen Anstieg an

Antigen-Variation auf der EB-Oberfläche resultieren und so eine Immunvermeidungs-Strategie stärken [278]. Impfstoffversuche auf Basis von Pmps sind vielversprechend und konnten bereits in einigen Studien überzeugen. So demonstrierte Paes *et al.* 2016, dass eine Immunisierung mit *C. trachomatis* PmpD mit drei verschiedenen Formulierungen eines Lipidadjuvans der zweiten Generation, eine verstärkte Infektionsresistenz und eine erhebliche Reduktion der durchschnittlichen Bakterienbelastung nach einer darauffolgenden intravaginalen Infektion mit *C. trachomatis* erzeugt [300]. Müller *et al.* 2017 impfte Mäuse mit einer Kombination aus PmpA und dem Adjuvans CpG-ODN 1826, welches in einer reduzierten Bakterienbelastung, innerhalb der ersten 10 Tage nach Infektion mit *C. muridarum*, und Verringerung von Häufigkeit und Schweregrad von Läsionen des Genitaltraktes resultierte [301]. Zur Analyse einer möglichen speziesübergreifenden schützenden Immunantworte nutzte Pal *et al.* 2017 rekombinante Fragmente aller neun *C. trachomatis* Serovar E Pmps zur Impfung von BALB/c-Mäusen, welche in Folge mit *C. muridarum* infiziert wurden. Mäuse, welche mit PmpC, PmpG oder PmpH behandelt wurden, zeigten den besten Schutz [302].

Zusammenfassend zeigt sich, dass Pmp-Proteine ein großes Potential für die mögliche Generierung eines Impfstoffes gegen unterschiedliche Spezies und Serovare aufweisen. Zukünftige Forschungen in diesem Gebiet, sowie die weitere Entschlüsselung der Funktionen der Pmp-Familie werden daher in Zukunft eine wirkungsvolle Abwehr gegen gefährliche Folgen chlamydialer Erkrankungen wie Unfruchtbarkeit oder Erblindung entgegenwirken.

## 1.9 Amyloide

### 1.9.1 Klassischer Aufbau amyloider Proteine

Als Amyloid-Fibrillen bezeichnet man homomere polymere Proteinkomplexe, welche unterschiedliche Kreuz-β Konformationen einnehmen können (*Abbildung 9*). Intermolekulare Kontakte zwischen den β-Strängen stabilisieren die nicht verzweigten Fibrillen, welche sich rechtwinklig zur Fibrillenachse ausrichten und eine Kreuz-β-Architektur ergeben [303-305].

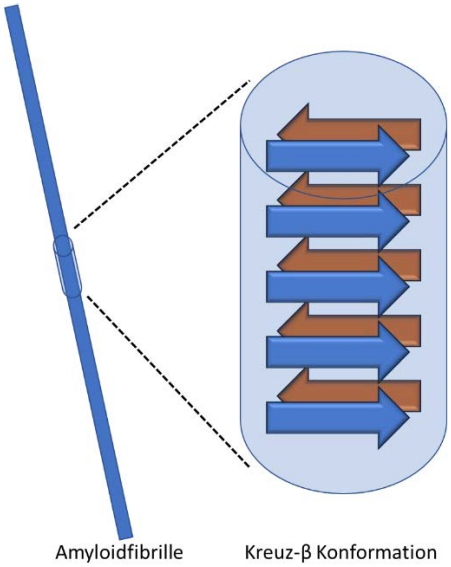


Abbildung 9: Schematische Darstellung einer Kreuz-β Konformation.
Amyloidfibrillen (links) sind fadenförmige Proteine, welche eine Architektur aufweisen, bei welcher die einzelnen β-Stränge senkrecht zur Faserachse verlaufen (rechts; Kreuz-β Konformation). Abbildung angelehnt an [306, 307].

Der Amyloid-Zustand gehört zu den stabilsten Proteinzuständen und wurde in seiner Stärke vergleichbar mit Stahl beschrieben [308, 309]. Amyloide lassen sich in funktionelle Amyloide, welche wichtige Aufgaben innerhalb der Zelle ausüben, und toxische Amyloide, die Schäden verursachen und dadurch Krankheiten erzeugen, unterscheiden. Eines der bekanntesten Beispiele für Amyloide, ihrer Entstehung und ihren potentiell toxischen Auswirkungen bildet die Amyloid-Kaskade-Hypothese für die Alzheimer Erkrankung, welche in Hardy *et al.* 1992 vorgestellt wurde [310]. Amyloid-Vorläufer-Protein (APP) wird in einer krankhaften Amyloid-fördernden Weise gespalten und erzeugt Amyloid-β (Aβ) Peptide. Ansammlungen von Aβ führen zu toxischen Aβ-Amyloiden, welche in Folge neurotoxische Schäden verursachen [310] (siehe detaillierte Erklärung in 1.9.3). In einer weiteren von Hurshman *et al.* 2004 beschriebenen „Downhill polymerisation"-Amyloidgenerierung zerfallen stabile native Transthyretin-Tetramere langsam in Monomere. Nach dieser Verzögerungsphase findet eine schnelle Formung einer amyloidogenen Konformation durch die Monomere statt [311, 312]. Die ursprüngliche Theorie zur Generierung von Amyloiden beschreibt einen kristallisationsähnlichen und nukleationsabhängigen Polymerisations-Mechanismus, in welchem Nukleation und Elongation zur Entstehung von Amyloid-Fibrillen führen [313-315] (siehe Abbildung 10). Die Überschreitung einer einzigen positiven Energiebarriere führt in einem Schritt zur Nukleation und der Erzeugung von Kernen („nuclei"). Kerne sind Oligomere, welche zur Amyloid-Fibrillen -Bildung fähig sind. Sie sind die kleinste strukturelle Einheit, welche die Entstehung von

Amyloid-Fibrillen fördern. Zwischenzustände sind thermodynamisch unvorteilhaft und werden daher nicht angesammelt. Obwohl diese Theorie allgemein akzeptiert wurde, fanden sich in frühen Stadien von Fibrillenbildungsreaktionen gleichzeitig oft eine große Anzahl oligomerähnlicher Aggregate, welche hoch unterschiedlich in Morphologie, Sekundärstruktur, Toxizität und funktionellen Eigenschaften erschienen [316-319]. Untersuchungen des Hefeproteins Sup35 führten dann zu der Hypothese, dass auch frühe Aggregate eine wichtige Rolle im Nukleationsprozess haben könnten [320, 321]. Im Gegensatz zur bisher beschriebenen Amyloidgenerierung spielt hier die untersuchte Proteinkonzentration und damit die Anzahl an Monomeren nur eine geringe Rolle. Dadurch entstand die Theorie, dass die Generierung von Kernen durch Konformationsumlagerungen („nucleated-conformational-conversion“, NCC) von Protein-Molekülen innerhalb eines Oligomers erfolgt und es sich um eine mehrstufige Keimbildung über eine Kette oligomerartiger Zwischenstufen handelt (vgl. Abbildung 10)[318]. Zudem wurden Hinweise gefunden, dass auch die Entstehung von Amyloid-β(Aβ)-Fibrillen auf diese Weise funktionieren könnte [322].

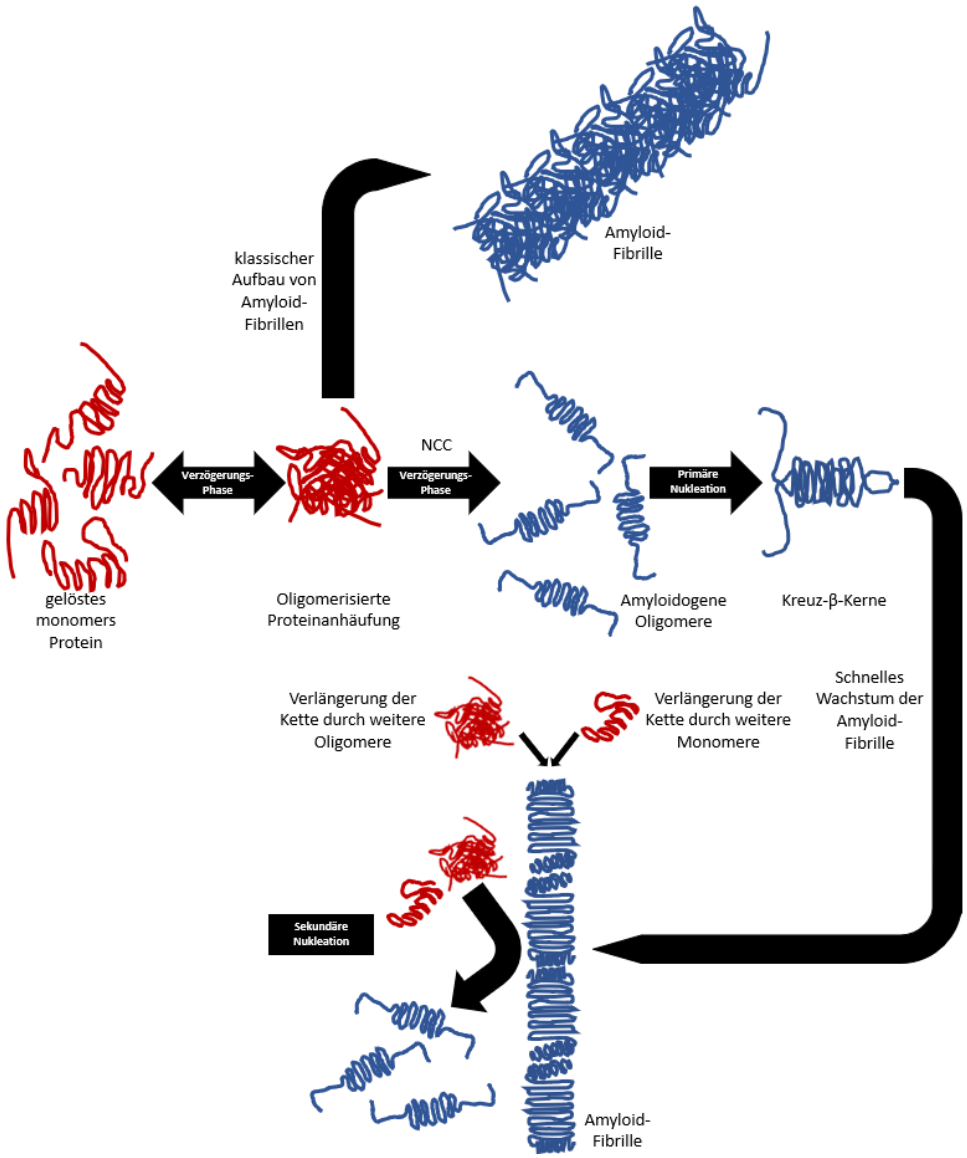


Abbildung 10: Schematische Darstellung der klassischen Amyloid-Assemblierung und der nukleierenden Konformationsumwandlung zu Amyloid-Fibrillen.

In der klassischen Theorie zur Amyloid-Assemblierung ist der Aufbau von Amyloid-Fibrillen abhängig von der Nukleation. Nach einer anfänglichen Verzögerungsphase bilden gelöste monomere Proteine oligomerisierte Proteinanhäufungen, welche im Anschluss zur Entstehung von Fibrillen führen [323]. In der nukleierenden Konformationsumwandlung (NCC) gibt es zunächst ein Gleichgewicht zwischen gelösten monomeren Protein und oligomerisiertem Protein. Während der Verzögerungsphase wandeln sich kontinuierlich Oligomere in amyloidartige Oligomere um. In einem schnellen Prozess innerhalb der primären Nukleation wandeln sich Amyloid-artige Oligomere zu Kreuz-β-Kernen. Sobald Kreuz-β-Kerne vorhanden sind, führt dies zur schnellen Assemblierung von Amyloid-Fibrillen. Die Kerne rekrutieren in Folge monomeres und oligomeres Protein in die Kreuz-β-Form um und verlängern so die wachsende Amyloid-Fibrille. Die Präsenz vorgeformter Fibrillen sorgt für eine sofortige Assemblierung. Zusätzlich werden auch an den Seitenflächen der Amyloid-Fibrille in einem Prozess der Sekundären Nukleation monomeres und oligomeres Protein in Amyloid-artige Oligomere umgewandelt. Grafik modifiziert aus [323] und [312].

## 1.9.2 Funktionelle Amyloide

Amyloide sind hauptsächlich durch ihre krankmachenden Eigenschaften bekannt geworden, wodurch der Aufbau von Amyloidfibrillen als primär pathologischer Prozess angesehen wird. Beste Beispiele hierfür sind die Alzheimer-, Parkinson- oder Huntington-Erkrankung [323]. Jedoch konnten diverse Studien demonstrieren, dass es auch „positive“ Amyloidfibrillen gibt, welche physiologische Funktionen in Prokaryoten als auch in Eukaryoten aufweisen [324, 325]. Amyloide zeichnen sich durch besondere Eigenschaften aus, die sie für biologische Prozesse interessant machen. Im Amyloid kann ein enger Abstand zwischen identischen Seitenketten innerhalb der Kreuz-β-Struktur eine neuartige Bindungsspezifität erzeugen, welche im monomeren Zustand fehlt. Wo ein einzelner β-Strang nur eine geringe Bindungsaffinität besitzt (z. B. an eine Membran), könnte eine Amyloid-Fibrille, welche aus vielen β-Strängen besteht, eine starke Bindungsaffinität aufweisen [326]. Wie in Otzen *et al.* 2019 demonstriert lassen sich funktionelle Amyloide in die 5 Untergruppen chemische Lagerung (A), Struktur (B), Information (C), Funktionsverlust (D) und Signalgebung/Funktionsgewinn (E) einteilen [326]. Prominentes Beispiel für Gruppe A sind verschiedene Peptidhormone, welche in Granula gelagert werden, oder das toxische Protein der Eosinophilen, das „Major Basic Protein“ (MBP), welches die Membranen perforiert, wenn es nicht im Amyloid-Zustand gebunden ist. Gruppe B beinhaltet Amyloide, welche strukturelle Aufgaben erfüllen. Ein hierbei oft zitiertes Protein ist Curli von *E. coli*. Curli gehören zu den wichtigste proteinösen Komponenten einer extrazellulären Matrix, wie sie von vielen *Enterobacteriaceae* gebildet wird. Neben der Biofilmbildung sind für Curli-Fasern beschriebene Funktionen unter anderem die Adhäsion an Oberflächen, Zellaggregation und Invasion von Wirtszellen [326, 327]. Weitere Vertreter Struktur-vermittelnder Amyloide sind Chaplins. Chaplins sind amphiphile Proteine, die bei *Streptomyceten* die Oberfläche von Lufthyphen unter Bildung von amyloidartigen Stäbchenschichten überschichten [328]. Gruppe C beschreibt funktionelle Prion-Proteine, welche an der epigenetischen Vererbung und dem Gedächtnis beteiligt sind. Das Orb2-Amyloid gehört zur Familie der CPEB-Proteine („cytoplasmic polyadenylation element binding“). Orb2 bildet in Drosophila-Gehirnen funktionell aktive Fibrillen und spielt eine wichtige Rolle bei der Bildung des Langzeitgedächtnisses [329]. Amyloid-Bildung der Proteine in Gruppe D führt zum Funktionsverlust des normalerweise gelösten Proteins. Bekannte Beispiele sind das Hefe-Enzym Pyruvatkinase (Cdc19) und der Terminator Sup35 [326]. Als Reaktion auf Stress (z. B. Nährstoffmangel oder Hitze) bildet Cdc19, eine Pyruvat-Kinase der Hefe, reversible, amyloidähnliche Aggregate, um so das Protein vor der Degradation zu schützen. Gleichzeitig arretieren die Hefezellen in der G1-Phase des Zellzyklus. Nach Beendigung der Stresssituation erlaubt das Auflösen der Cdc19-

Amyloide die Zurverfügungstellung funktionsfähiger Enzyme und damit einen schnellen Neustart des Zellzyklus [330, 331] . Die normale zelluläre Aufgabe von Sup35 besteht darin, die Translation zu beenden [332]. Aggregation von Sup35 führt zu dessen Funktionsverlust und resultiert in Folge zu einem erhöhten translatorischen „Read-Through“ von Stopcodons [333]. Gruppe E beschreibt Proteine, welche durch ihre Umwandlung in den Amyloidzustand aktiviert werden. HET-S und HELLP sind in Pilzen den Zelltod auslösende, porenbildende Proteine, welche durch Wechsel in den Amyloidzustand aktiviert werden [334]. Die genannten Beispiele stellen nur einen Bruchteil der inzwischen entdeckten funktionalen Amyloide dar. Die stetige Entdeckung neuer Mitglieder dieser Proteinfamilie zeigt, dass es sich bei Amyloiden nicht ausschließlich um krankheitserzeugende Proteine, sondern auch um Proteine mit wichtigen physiologischen Funktionen handelt [326, 335, 336].

### 1.9.3 Toxische Amyloide

Die Anordnung von Proteinen zu Amyloiden und Amyloid-Fibrillen, welche in Folge zu Ablagerung von Plaques, intrazellulären Einschlüssen und schließlich Gewebe- und Organschäden führen kann, ist die Grundlage und herausstechendes Kriterium für Amyloidkrankheiten (Amyloidosen) [337]. Amyloidosen sind vielfältig und erzeugen häufig pathologische Erscheinungsbilder, welche eng mit dem Alter der Spezies zusammenhängen. Bekannte Beispiele stellen Parkinson, Diabetes Typ II, Alzheimer und dialysebedingte Amyloidosen dar [338]. Amyloide weisen einige Eigenschaften auf, welche ihre Pathogenität verstärkt und zugleich ihre Bekämpfung erschwert. Amyloide zeichnen sich durch ihre hohe thermodynamische Stabilität sowie ihre Übertragbarkeit aus. Sie sind in der Lage, ursprünglich nativ gefaltetes Protein (z.B. das Prion Protein ($PrP^{C}$)) in Amyloid-Protein (z.B. $PrP^{Sc}$ (Scrapie bzw. infektiöse Form)) umzuwandeln und sich auf diese Weise zu vermehren [339]. Des Weiteren unterstützt ihre hohe Stabilität eine effektive Akkumulation und vermittelt zugleich eine Belastung für Proteasen [340, 341]. Zwei der bestuntersuchten Amyloide, welche mit neurodegenerativen Krankheiten in Verbindung gebracht werden, sind das α-Synuklein und Aβ [342-344]. α-Synuklein ist ein in großer Menge vorkommendes neuronales Protein, welches sich stark angereichert in präsynaptischen Nervenendigungen neuronaler Zellen und womöglich auch auf der Kernhülle findet. Es ist verantwortlich für Parkinson und weitere neurodegenerative Erkrankungen [342, 345]. Es ist in der Lage, an viele verschiedene Proteine zu binden und eine Reihe von Funktionen im Zusammenhang mit diesen Proteininteraktionen auszuüben, z. B. die Bindung und Hemmung von Phospholipase D, Bindung an und

Regulation von Tyrosinhydroxylase, die Bindung an das SNARE-Protein Synaptobrevin-2 und die Chaperonisierung des SNARE-Komplexes, Bindung an Synphilin und DJ-1, Regulierung von Mikrotubuli durch Bindung an Tubulin und die Verstärkung der Tau-Phosphorylierung [342]. Die physiologischen Auswirkungen dieser Interaktionen sind jedoch häufig unbekannt [342]. Diverse Studien zeigten, dass eine Überexpression von α-Synuklein neurotoxische Effekte erzeugt, dass die Neurotoxizität mit der α-Synuklein-Aggregation korreliert und sich womöglich von einem Neuron zum nächsten ausbreiten kann. Im Falle der familiären Parkinson-Erkrankung sorgen Mutationen in α-Synuklein für eine verstärkte Aggregation und damit eine verstärkte Neurotoxizität [346-354]. Auf die Bildung und Auswirkungen von Aβ wird in 1.9.4 eingegangen.

## 1.9.4 Die Rolle von Amyloid-β in der Alzheimer-Erkrankung

Die Alzheimer-Erkrankung ist eine chronische neurodegenerative Störung, welche sich in die zwei unterschiedlichen Formen der früh einsetzende Alzheimer-Krankheit („Early-onset Alzheimer's disease", EOAD) und die spät einsetzende Alzheimer-Krankheit („Late-onset Alzheimers's disease", LOAD) unterscheiden. EOAD ist die Ursache für früh auftretende neurodegenerative Demenz (unter 65 Jahre) und macht 4 - 8 % aller Alzheimer-Erkrankungen aus [355]. EOAD wird als die aggressivere der beiden Formen beschrieben, ist aber gleichzeitig allgemein weniger intensiv erforscht [356, 357]. Neben dem Alter als der Hauptrisikofaktor für die Entstehung von LOAD wurden auch andere Faktoren wie Atherosklerose, Typ-2-Diabetes, Neurotrauma und Infektionen beschrieben [358-363]. Diese Erkrankungen haben gemeinsam, dass sie systemische Entzündungen fördern, welche die Entstehung von LOAD beeinflussen könnten [45]. Schlüsselelemente der Alzheimer-Pathologie bilden Aβ, Tau-Hyperphosphorylierung und Neuroinflammation [364].

Aβ-Peptide akkumulieren und erzeugen senile Plaques was zur neuronalen und synaptischen Dysfunktion beim Fortschreiten von Alzheimer führt. Publizierte Auswirkungen und Schäden durch Aβ beschreiben eine Reduzierung der synaptische Plastizität, Hemmung der Langzeitpotenzierung (LTP) im Hippocampus, von welchem man annimmt, dass es eine wichtige Rolle im Prozess von Lernen und Gedächtnis darstellt, und die Produktion reaktiver Sauerstoffspezies (ROS)[365-367]. Grundlage für die Erzeugung von Aβ ist eine spezielle Spaltung des APP [343]. Die genaue physiologische Rolle des APP ist unbekannt. Allerdings konnte gezeigt werden, dass Überexpression von APP in einem positiven Effekt auf die Gesundheit und das Wachstum der Zellen resultieren kann [368]. APP wird primär in Neuronen produziert, wo es schnell

metabolisiert wird und final zu den synaptischen Endigungen lokalisiert [369, 370]. An der Zelloberfläche kann APP, im nicht Amyloid generierenden Pfad, durch α-Sekretase und γ-Sekretase gespalten werden, was in keiner Produktion von Aβ resultiert [343]. Im Amyloid erzeugenden Pfad wird APP von der Zelloberfläche in Clathrin-beschichteten Vertiefungen in ein endosomales Kompartiment reinternalisiert und in Folge durch β-Sekretase und γ-Sekretase zu Aβ prozessiert. Die Gründe, warum ein Teil des APPs direkt auf der Zell-Oberfläche durch α-Sekretase gespalten, wohingegen ein anderer Teil wieder in Endosomen internalisiert und in Folge zu Aβ gespalten wird, sind größtenteils unklar, obwohl „Lipid Rafts" eine wichtige Rolle dabei spielen könnten. Nach der Spaltung von APP in Aβ kehrt das Endosom zur Zelloberfläche zurück und gibt das Aβ durch Exozytose frei [343, 371].

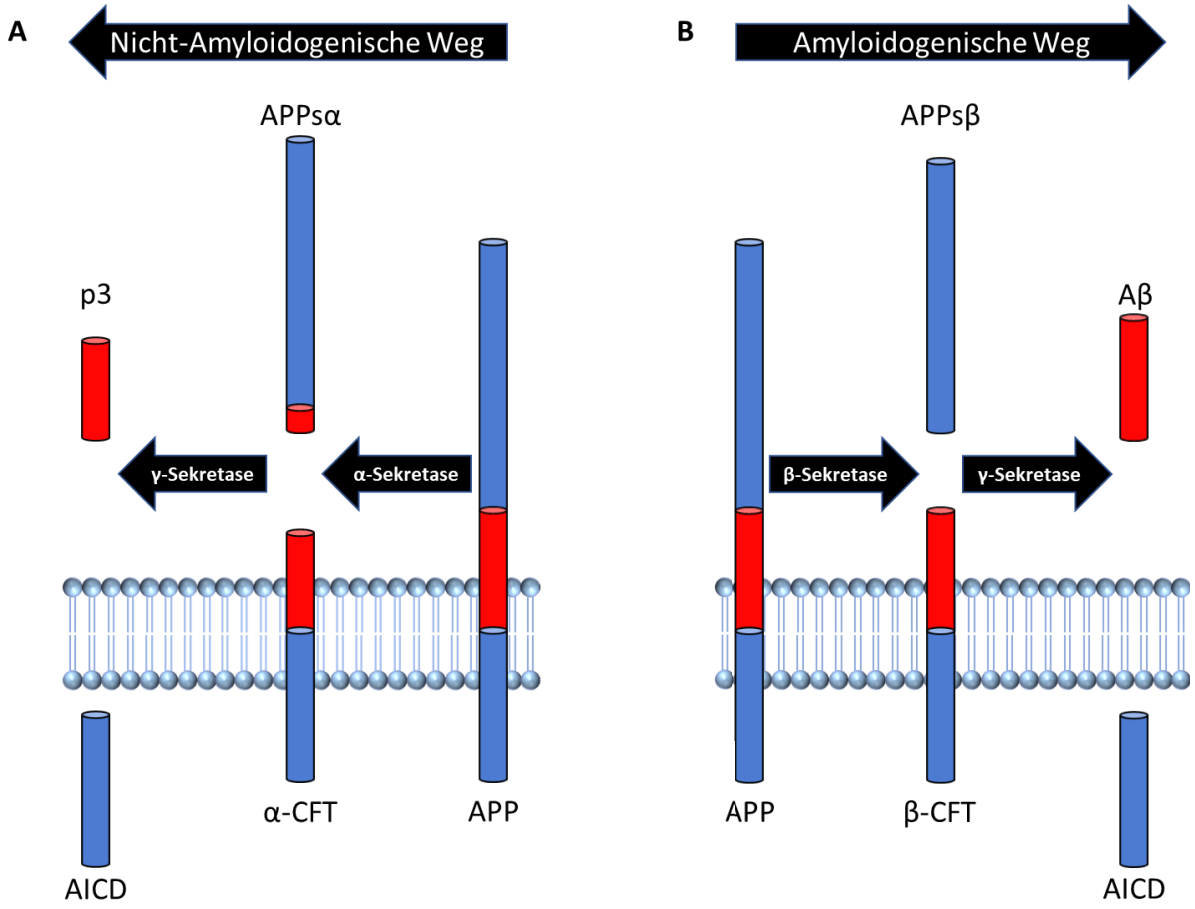


Abbildung 11: Zusammenfassende schematische Darstellung der APP-Prozessierung.

A. Im Nicht-Amyloidogenischen Weg spaltet die α-Sekretase APP zunächst in die Zwischenprodukte APPsα und α-CFT (Carboxy-terminales Fragment) bevor im nächsten Schritt α-CFT in AICD (APP intrazelluläre C-terminale Domäne) und p3 gespalten wird. B. Im Amyloidogenischen Weg erfolgt die Spaltung von APP durch die β-Sekretase in APPsβ und β-CTF. β-CTF wird in Folge von der γ-Sekretase in AICD und Aβ prozessiert. Abbildung erstellt in Anlehnung an [372].

Es gibt zwei Hauptarten von Aβ im Gehirn: Aβ40 und Aβ42. Obwohl Aβ40 in löslicher Form um ein Vielfaches häufiger vorkommt als Aβ42, ist Aβ42 der Hauptbestandteil der Amyloid-Plaques und wird als das toxischere der beiden angesehen [373, 374]. Im Prozess der darauf folgenden Fibrillogenese akkumulieren Aβ Proteine und bilden größere oligomere Spezies, die sich weiter zu kurzen, flexiblen, unregelmäßigen Protofibrillen aggregieren und zuletzt reife unlöslichen Fibrillen bilden, welche resistent gegen proteolytische Spaltung sind [375]. Die pathogenen Eigenschaften von Aβ sind vielfältig. Experimente, in welchen Neuronalzellen mit Aβ-Fibrillen behandelt wurden, zeigten ein, vermutlich apoptotisches, Absterben innerhalb von 24 h [376, 377]. Sowohl eine Toxizität für dimeres Aβ, als auch eine Toxizität, welche mit Oligomergröße zunimmt, ist für Aβ beschrieben worden [378, 379]. Allergemeiner Konsens besteht darüber, dass oligomeres Aβ und nicht Fibrill-Form-Aβ als neurotoxische Substanz in der Alzheimer Erkrankung wirkt, mit der Zellmembran interagiert und so dessen Integrität stört [379-383]. Zudem wurden in letzten Jahren immer mehr Rezeptoren wie der Nikotinischer Acetylcholinrezeptor oder Prionen-Protein-Rezeptor (PrP) entdeckt, an welche Aβ binden kann und die im Verdacht stehen sich auf die Alzheimer Erkrankung auszuwirken [384, 385].

Ein weiteres Hauptelement der Alzheimer-Erkrankung sind das Auftreten von neurofibrillären „Tangles“ (NFTs). NFTs entstehen durch Aggregierung von hyperphosphoryliertem Tau-Protein. Tau ist ein Mikrotubuli-assoziiertes Protein, dessen Hauptfunktionen Stimulierung der Tubulinpolymerisation, die Stabilisierung von Mikrotubuli sowie der Transport von intrazellulären Organellen durch Mikrotubuli ist. Hyperphosphorylierung von Tau führt zu dessen Funktionsverlust, der Entstehung von NFTs und neuronalen Schäden [386, 387].

Neben Aβ-Plaques und NFTs werden in der Alzheimer-Pathologie Entzündungen beobachtet, welche primär durch Mikroglia angetrieben werden. Studien demonstrieren, dass eine Abwehrreaktion durch das angeborene Immunsystem eine Rolle in der Alzheimer-Entstehung spielt und dem Erscheinen von Alzheimer-Pathologie voraus gehen kann. Dies deutet darauf hin, dass Immunprozesse womöglich die AD-Pathologie vorantreiben und die Zunahme an Aβ aufrechterhalten. Neben Aβ-Ablagerungen und weiteren Faktoren können Mikroglia auch durch pathogene Infektionen aktiviert werden [364, 388].

Forschungen der letzten Jahre beschreiben eine immer wichtiger werdende Rolle von Infektionen durch Bakterien, Pilzen und Viren in der Entstehung von Entzündungen und dem Auslösen von Alzheimer [389]. Prominenteste Beispiele sind *Porphyromonas gingivalis* (Parodontal-Bakterium), *Helicobacter pylori* (Magen-Darm-Bakterium) und *C. pneumoniae* (Lungenbakterium) [390]. Mögliche Zugangswege zum Gehirn sind der Trigeminusnerv, oral-olfaktorischen Weg oder systemischen Kreislauf [391]. Die Infektionshypothese beschreibt die erhöhte Menge von APP und dessen amyloidogenische Spaltung in Aβ als Reaktion auf eine Infektion des Gehirns [392, 393]. Als Verteidigungsmechanismus gegen eine

Infektion, produzieren Neuronen antimikrobiell wirkendes Aβ-Peptid [394]. Moir *et al*. 2018 beschreibt die Produktion von Aβ-Peptid als Teil der angeborenen Immunantwort, wo sie als Verteidigungsmechanismus bei mikrobiellen Infektionen im Gehirn dient. Vermehrte Aβ-Ablagerungen, Entzündungen und die vermehrte Verarbeitung von APP zu Aβ könnten durch die lange anhaltende Aktivierung dieses Verteidigungsmechanismus bedingt sein [364, 395, 396].

### 1.9.5 *C. pneumoniae* und die Alzheimer Erkrankung

Innerhalb der letzten 25 Jahre häuften sich die wissenschaftlichen Hinweise, dass eine chlamydiale Erkrankung und LOAD im Zusammenhang stehen könnten. Balin *et al.* 1998 untersuchte postmortale Hirnproben von Patienten mit und ohne LOAD auf das Vorhandensein von *C. pneumoniae* DNA mit dem Ergebnis, dass 17/19 LOAD-Patienten in Hirnarealen mit AD-bezogener Neuropathologie positiv für *C. pneumoniae* waren. Untersuchungen identischer Hirnareale bei Kontrollpatienten resultierten hingegen in 18/19 negativen Resultaten. Elektronen- und immunoelektronenmikroskopische Untersuchungen von AD-Gehirnregionen identifizierten chlamydiale RBs und EBs, während dieselben Gehirnregionen von Kontrollpatienten diese nicht aufwiesen. In AD-Gehirnen wurde *C. pneumoniae* in Perizyten, Mikroglia und Astroglia nachgewiesen und lebensfähige *C. pneumoniae* Zellen konnten aus AD-Gehirnen isoliert werden [363]. Untersuchungen von Gérard *et al.* 2006 identifizierte Gehirnproben von 20/25 AD-Patienten als positiv für die Gene *cpn1046* and *cpn0695*, wohingegen 24/27 Kontroll-Proben negativ waren. Erneut konnte gezeigt werden, dass die Chlamydien lebensfähig waren, in Gebieten mit AD-bezogener Neuropathologie gefunden wurden und dass Astrozyten, Mikroglia und Neuronen mögliche Wirte darstellen [397]. Inzwischen existieren multiple Studien, welche eine Infektion durch *C. pneumoniae* mit Alzheimer in Verbindung bringen, indem sie *C. pneumoniae* in von Alzheimer betroffenen Hirnarealen identifizierten, *C. pneumoniae* zusammen mit Aβ-Akkumulationen auftraten oder Alzheimer-ähnliche Plaques in Mäusen durch intranasale Infektion mit *C. pneumoniae* induziert werden konnten [398, 399]. Wie Chlamydien in das Gehirn kommen könnten, um dort eine Infektion des Zentralen Nervensystems auslösen, ist auf vielfache Weise vorstellbar. *C. pneumoniae* ist ein Atemwegserreger, welcher sowohl über den olfaktorischen als auch den Lungenweg Pneumonien auslöst [400]. Das olfaktorische System stellt eine Verbindung zwischen der äußeren Umgebung und dem Gehirn dar, indem Erreger über die Nase aufgenommen und anschließend über den Bulbus olfactorius ins Gehirn eindringen. Daher könnte es möglich sein, dass Chlamydien, vergleichbar zum Rabies-Virus, dem Influenza-A-Virus und dem

Parainfluenzavirus auf diese Weise das Gehirn infizieren [401, 402]. Die Tatsache, dass die intranasale Applikation von *C. pneumoniae* Alzheimer ähnliche Plaques erzeugt, unterstützt diese Theorie [399]. Eine weitere Möglichkeit wäre das Durchschreiten der Bluthirnschranke (BBB) über eine Version des „Trojan Horse“ Mechanismus, wie er für HIV beschrieben wird, bei welchem infizierte Immunzellen die BBB passieren und so das Gehirn infizieren [403, 404]. Sobald sich Chlamydien im Hirn befinden und Infektionen starten, könnte das Vorhandensein chlamydialer Antigene wie Membranproteine oder LPS zur Ausschüttung proinflammatorischer Zytokine führen [45, 405].

Amyloide weisen antimikrobielle Eigenschaften auf [392, 406]. Da Amyloid-Formen und Chlamydien in denselben Gehirn-Regionen gefunden werden konnten, könnte dies, wie in 1.9.4 beschrieben, eine Form der Abwehr vom Wirt darstellen und zum anderen der Start einer neuronalen Erkrankung wie Alzheimer sein [392, 395, 398]. Zusammenfassend muss festgehalten werden, dass eine Verbindung zwischen *C. pneumoniae* und der Alzheimer Erkrankung umstritten ist, da es auch Studien gab, welche nicht in der Lage waren, DNA oder *C. pneumoniae* in AD-Gehirnen zu identifizieren [407-410]. Gleichzeitig gibt es viele Studien, die die Anwesenheit von *C. pneumoniae* mit gleichzeitiger Anwesenheit von alzheimertypischen neuropathologischen Merkmalen demonstrierten, aber nur wenige Studien, die eine direkte Kausalität zeigten [396, 411]. Ein Beitrag von *C. pneumoniae* zur Entstehung von Alzheimer ist vorstellbar, bedarf aber noch vieler klinisch-pathologischer und experimenteller Beweise.

## 1.9 Ziel dieser Arbeit

Pmp-Proteine sind eine Gruppe von Adhäsinen, welche auf der chlamydialen Oberfläche als Volllänge-Proteine oder prozessiert, womöglich in Form von homomeren oder heteromeren Oligomeren vorkommen könnten und essentielle Funktionen innerhalb der Infektion ausüben. Wie genau sie auf der Oberfläche vorliegen und ob sie eventuell mit anderen Proteinen interagieren, ist nur wenig untersucht (vgl. 1.7.1, 1.7.2, 1.7.3, 1.7.4).

Ziel von Projekt 1 war es, die Proteine PmpG, PmpH und PmpI von *C. trachomatis* Serovar E als Volllänge-Varianten auf ihre oligomerisierenden Eigenschaften zu untersuchen. Aufgrund ihrer bisher beschriebenen biochemischen *in vitro* Eigenschaften liegt es nahe, dass Pmp-Proteine *in vivo* mit Pmp-Proteinen derselben Art oder anderen/weiteren Pmp-Proteinen interagieren und auf der chlamydialen Oberfläche präsentiert werden könnten. Zur Entschlüsselung dieser Fragestellung wurde das APEX2-Biotinylierungssystem zur Kartierung der chlamydialen Oberfläche eingesetzt. PmpI-APEX2 Fusionsproteine wurden von *C. trachomatis* Serovar L2 Transformanten exprimiert, markierten ihre räumlich nächsten Partner, wurden in Folge aufgereinigt und massenspektrometrisch analysiert. Dies erlaubte eine Einschätzung auf mögliche Bindepartner von PmpI auf der EB-Oberfläche.

Ziel von Projekt 2 war die biophysische Analyse des *C. pneumoniae* Pmp21-Subfragments, Pmp21_D-wt. Es gibt experimentelle Hinweise, dass eine Infektion mit *C. pneumoniae* einen Einfluss auf die Entstehung der Alzheimer Erkrankung haben könnte (vgl. 1.9.5). Untersuchungen von Favaroni *et al*. 2021 demonstrierten, dass *C. trachomatis* Pmp-Fragmente homomere und heteromere Oligomere und Protofibrillen generieren. Luczak *et al*. 2016 zeigte mögliche Gemeinsamkeiten zwischen oligomeren und protofibrillären Strukturen, generiert von *C. pneumoniae* Pmp21_D-wt, und Strukturen, wie sie von Aβ bekannt sind. Projekt 2 vertiefte diese Analysen, indem es die biophysischen Eigenschaften von Pmp21_D-wt anhand von Oligomerisierungskinetiken und Atomkraftmikroskopie weiter untersuchte und Gemeinsamkeiten und Unterschiede zu Aβ entschlüsselte.

Ziel von Projekt 3 war die Entwicklung eines, auf Pmp-Proteinen basierenden, Impfstoffes. Pmps sind eine hochkonservierte Familie von chlamydialen Adhäsinen, welche bisher in allen chlamydialen Spezies in unterschiedlicher Anzahl identifiziert werden konnten. Sie sind ideale Proteine für die Impfstoffentwicklung. In einer Kooperation mit der AG Klos (Medizinische Hochschule Hannover) und AG Guzmán (Helmholtz-Zentrum für Infektionsforschung) wurde daher in Projekt 3 ein neuer Multikomponenten-Impfstoff aus *C. trachomatis* Serovar E Pmps (PmpA, PmpD, PmpG und PmpH) und Ctad1 entwickelt.

# 2. Teil I Manuskript I

**Identification of *Chlamydia trachomatis* PmpI binding partners via proximity labeling**

Sebastian Wintgens and Johannes H. Hegemann

Erstautor
Beteiligungen:
Sebastian Wintgens: 90 %, Johannes H. Hegemann: 10 %

Sebastian Wintgens (SW) plante zusammen mit Prof. Johannes H. Hegemann (JHH) alle Experimente, die in diesem Manuskript dargestellt sind. SW schrieb das gesamte Manuskript, wertete die Daten aus und stellte alle Figuren und Figurlegenden zusammen. SW erbrachte die experimentellen Daten zu allen Figuren. ThT-Kinetiken wurden unter Anleitung von Filip Hasecke (FH) durchgeführt (Figur 3). AFM-Aufnahmen wurden mit Hilfe von FH erzeugt (Figur 3).

JHH übernahm als korrespondierender Autor Korrekturarbeiten am Manuskript und den Figuren & Figurlegenden. SW und JHH diskutierten während der Projektlaufzeit die Ergebnisse und entwickelten gemeinsam die Diskussion.

Hiermit bestätige ich, dass diese Angaben korrekt sind.

Düsseldorf, den 30.05.2023

Sebastian Wintgens

## 2.1 Zusammenfassung

Ein wesentlicher Schritt der Chlamydieninfektion ist die Adhäsin-vermittelte Anheftung von infektiösen Elementarkörperchen an menschliche Zellen. Die Mitglieder der Familie der polymorphen Membranproteine (Pmp) wirken als Adhäsine, sind in jeder chlamydialen Spezies vorhanden und aufgrund ihrer EB-Oberflächenlokalisation interessante Kandidaten für Impfstoffstudien. In Adhäsionsstudien zeigten *C. trachomatis* Volllänge PmpH und PmpI (ohne Signalsequenz und β-Fass) die Fähigkeit, an HEp-2-Zellen zu adhärieren. PmpG, PmpH und PmpI waren in der Lage, hochmolekulare Komplexe zu bilden, zeigten in einem ThT-Assay oligomerähnliches Wachstum und erschienen in der Atomkraftmikroskopie als Oligomere und Protofibrillen. Um potenzielle Pmp-Komplexe, die aus Pmps oder Pmps mit anderen Oberflächenproteinen bestehen, von der EB-Zelloberfläche zu isolieren und zu untersuchen, verwendeten wir die auf räumlicher Nähe basierende APEX2-Markierungstechnik, um *C. trachomatis* L2-Stämme zu erzeugen, die PmpI-APEX2-Fusionskonstrukte exprimierten. APEX2 biotinyliert Proteine in seiner Nähe. Die biotinylierten Proteine wurden isoliert und anschließend mittels Massenspektrometrie analysiert. Die Ergebnisse zeigten eine Anreicherung von Proteinen der Pmp-Familie wie PmpD, PmpG, PmpI, PmpB und PmpF sowie dem Protein YidC und Proteinen des Typ-III-Sekretionssystems. Die Funktionen solcher Komplexe sind noch weitestgehend unerforscht, könnten aber wie bereits früher postuliert adhäsionsverstärkende oder immunabwehrvermeidende Effekte ausüben. Die EB-Oberfläche präsentiert möglicherweise eine Vielzahl unterschiedlicher Pmp Komplexe mit bislang noch unbekannten Funktionen. Die weitere Aufklärung und Auswirkungen dieser Komplexe wird der Fokus zukünftiger Forschung sein.

**Identification of *Chlamydia trachomatis* PmpI binding partners via proximity labeling**

Authors

Sebastian Wintgens and Johannes H.Hegemann

Institute of Functional Microbial Genomics, Heinrich-Heine-University Düsseldorf, 40204 Düsseldorf, Germany

**Abstract:**

An essential step during the chlamydial infection is the attachment of the elementary bodies (EBs) to human cells via adhesins. The polymorphic membrane protein (Pmp) family members act as adhesins, are present in every chlamydial species and are therefore interesting candidates for vaccine studies. In adhesion studies, *Chlamydia trachomatis* (*Ctr)* full length PmpH and PmpI (without signal sequence and β-barrel) showed the ability to adhere to HEp-2 cells. PmpG, PmpH and PmpI were able to create high molecular complexes that showed oligomer-like growth in a ThT-Assay and appeared as oligomers and protofibrils when analyzed by via atomic force microscopy. In order to isolate and study potential Pmp-complexes consisting of Pmps or Pmps with other surface located proteins from the EB cell surface we utilized the well-developed APEX2 proximity labeling technique and generated *Ctr* L2 strains expressing PmpI-APEX2-fusion constructs. APEX2 biotinylates proteins in its proximity. Biotinylated proteins were isolated and then analyzed via mass spectrometry. Results showed a PmpI-specific enrichment of almost all Pmps (PmpG, PmpI, PmpD, PmpB, PmpF), YidC and some proteins of the type III secretion system. The function of such complexes is still under investigation and will offer much potential for future research.

**Introduction:**

*Chlamydia trachomatis* (*Ctr*) is an obligate intracellular gram-negative bacterium and pathogen. It infects millions of people every year and is, depending on the serovar, best known for its sexually transmitted disease or blindness-causing trachoma [1-3]. It is possible to treat a chlamydial infection effectively with antibiotics. However, up to 70 % of infections remain asymptomatic and untreated, which can lead to the development of a long-term infection [4, 5]. If left untreated, this can lead to pelvic inflammatory disease, ectopic pregnancy and infertility, and blindness [1, 6]. The chlamydial infection is characterized by an unique biphasic replication cycle. Using adhesins the chlamydial infectious elementary body (EB) attaches itself to a host cell and invades the cell via invasins. Inside the host cell, the EB is enclosed by a plasma membrane which is subsequently modified and develops into the inclusion membrane. This membrane serves as a barrier as well as interaction platform with the host cell. Within the inclusion, the EB differentiates into its replicating, metabolically active and non-infectious reticulate body (RB) form. After several divisions, the RBs redifferentiate into EBs. The mature EBs are released by fusion of the inclusion membrane with the cell membrane, extrusion or lysis of the host cell [7-9].

In the last 20 years, the *Ctr* EB cell surface molecules LPS, OmcB, Ctad1, Hsp70 and the entire Pmp family have been identified as crucial for adhesion to the host cell [10-15]. Even though each chlamydial species code for different Pmps, their number can vary greatly. *Ctr* codes for 9 Pmps, which can be further classified into the six phylogenetic subtypes A, B, D, E, G and H [16]. Binding studies have shown that all Pmps are able to adhere to host cells in varying degrees. Pre-incubation of host cells with recombinant Pmp proteins or Pmp fragments results in a reduced subsequent infection by *Ctr* showing that Pmp adhesins are essential for an infection [13, 17]. In addition to its adhesive properties, *Chlamydia pneumoniae* (*Cpn*) Pmp21 has been identified as an invasin with EGFR as its human receptor [18]. *Ctr* uses a high proportion of its coding capacity (13.6 %) for Pmp genes [16, 19-21], again indicating their importance in infection. Vaccination studies with different *Ctr* Pmp mixtures and the adhesin Ctad1 mediated significant protection in mice [22].

Pmps have characteristics of autotransporters [21, 23-25]. They have a cleavable N-terminal Sec-dependent leader sequence for translocation to the membrane, a central passenger domain and a C-terminal β-barrel domain that anchors them in the outer membrane [21, 26]. The passenger domain contains repetitive FxxN and GGA (I ,L ,A ) motifs, which are important for adhesive properties and assembly for multimeric protein complexes. At least 2 motifs are necessary for binding to cells [27].

Studies of PmpD indicate that Pmps are highly processed before they localize to the membrane where they appear as oligomers [28] or alternatively localize to the periplasmic space as a full-length protein and

undergo cleavage of the leader sequence. Next, the C-terminal segment forms a β-barrel and the N-terminal passage domain is exported and cleaved, resulting in an N-terminally oriented membrane protein [21, 25]. Luczak *et al.* demonstrated using recombinant *Cpn* Pmp21_D, a C-terminal fragment of the Pmp21 passenger domain containing 2 FxxN-Motives, that it is able to generate oligomers with protofibrillar form [29].

Recent research has demonstrated that *Ctr* Pmp fragments are able to generate functional homomers and heteromeric oligomers *in vitro* [17]. Favaroni *et al.* showed that oligomers generated by fragments of PmpA, PmpD, PmpI and PmpG show a molecular size of 1,300 kDa (PmpA, PmpD), 1,250 kDa (PmpI) and 800 kDa (PmpG). Combining these fragments resulted in fragment sizes that were approximately between those of the corresponding homomeric oligomers (Pmps A + G: 1,050 kDa) or the same size as one of the homomeric oligomers (PmpI + PmpA: 1,250 kDa) [17]. Visualized by Transmission electron microscopy (TEM) oligomeric PmpG-fragments appeared as dot-like structure (average diameter of 12 nm). Fragments of oligomeric PmpA, PmpD and PmpI appeared as protofibrils with an average length of 186 nm. In all cases, the generation of heteromeric oligomers resulted in significantly longer protofibrillar structures compared to the corresponding homomeric structures [17]. Pmp homomeric and heteromeric oligomers on the surface of EBs would result in an enormous variability of antigen presentation on the EB surface, which may represent a chlamydial protection mechanism against the immune system [17].

At this stage, it is not possible to say with certainty in which form exactly Pmps are present on the chlamydial EB surface. Homomeric oligomers [17, 29], heteromeric oligomers between different Pmps or Pmp fragments [17] or possibly between Pmps and other chlamydial membrane proteins are conceivable. Based on previous research [13, 17, 29], we show here that recombinant full-length Pmps (without signal sequence and β-barrel, Figure 1) have the potential to bind to human cells, form homomeric and heteromeric complexes and show oligomeric growth and protofibril formation.

To address the question of how Pmps appear on the chlamydial surface, we used the APEX2-based proximity labelling technique in combination with the recently developed method for transforming Chlamydia and subsequent mass spectrometric analysis. *Ctr* PmpI is an adhesin, showed the ability to reduce subsequent infection after treatment of cells [13] and has the ability to generate high molecular weight oligomeric structures [17]. Furthermore, it is the most highly conserved Pmp, together with PmpA and PmpD, and is expressed even under chlamydial stress conditions [30]. Due to its high importance in chlamydial biology and infection and its ability to form homomeric and heteromeric complexes [17], we used the PmpI protein to generate an APEX2 fusion protein (PmpI-APEX2).

APEX2 biotinylates the proteins around PmpI in a radius of 20 nm [31] and thus allows an assessment of the proteinaceous environment of natively localized PmpI in order to find out whether certain Pmps or

other membrane proteins are found more frequently than in a wild-type situation. These findings could hint to possible chlamydial binding partners.

Here we show the successful enrichment of membrane proteins with a PmpI-APEX2 fusion protein compared to APEX2 alone. Many known membrane or membrane-associated proteins were among the top findings. Additionally, our results showed a strong enrichment of PmpD and further Pmp proteins. This could mean that PmpD and possibly further pmp proteins are binding or complex partners of PmpI. Confirmation of this findings and biological consequences will be the focus of future studies.

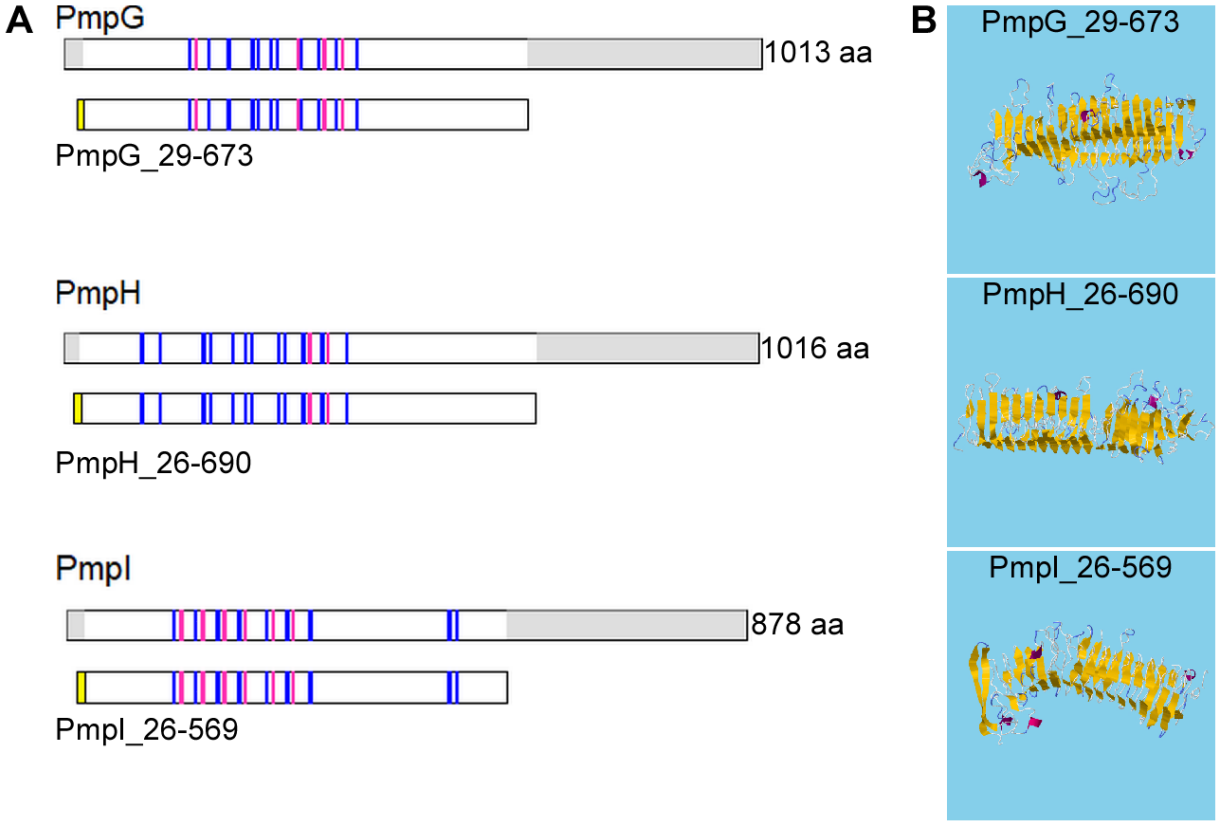


Figure 1: Schematic representation and structure prediction analysis of the proteins used.

**A**. Schematic representation of *Ctr* E PmpG, PmpH and PmpI (full length) as well as expressed full length passenger domain of PmpG_29-673, PmpH_26-690 and PmpI_26-569. N-terminal signal sequence (grey); central passage domain (white) ; C-terminal β-barrel domain (grey). The passenger domain contains FxxN (blue) and GGA (I, L, V (magenta)) motifs [27, 29]. The graphics were created with RStudio [32]. The recombinant Pmp protein fragments carry an N-terminal HIS tag (yellow). **B.** Predicted structure of PmpG_29-673, PmpH_26-690 and PmpI_26-569. Yellow arrows symbolize β-sheets whereas areas with α-helix character are labelled pink. Structure predictions were performed using RaptorX [33-38].

**Methods**:

Cloning

For the generation of plasmids used for protein expression the selected areas coding for the passenger domains of *pmpG*, *pmpH* and *pmpI* were amplified by PCR with respective primers on genomic DNA of *Ctr* E and cloned into the expression vector pKM32 via homologous recombination in yeast strain CEN.PK 2-1C [27]. Subsequently, the plasmids were isolated from yeast, amplified in *E. coli* strain XL1-Blue (Stratagene) and verified by sequencing. To construct PmpIAPEX2V1, fragments coding for the *pmpI* signal sequence, *apex2* (origin: mKate2-P2A-APEX2-2xFYVE_hrs (Addgene Plasmid #67663)) and the *pmpI* passenger domain with β-barrel were amplified by PCR and cloned into the 3x FLAG-tag containing pKM255 via homologous recombination in CEN.PK2-1C (pKM255 provided by Katja Mölleken; pKM255 is a modification of p2TK2--SW2 IncDProm-RSGFP-IncDTerm [39]). For PmpIAPEX2V2, the N-terminal part of PmpI (aa 1-373), *apex2*, and the remaining passenger domain with β-barrel (aa 374-878) were amplified and likewise cloned into pKM255. For the APEX2 construct, only the *apex2* gene was cloned into pKM255.

Bacterial and human strains

*E. coli* XL1-Blue (Stratagene) and *E. coli* GM48 (New England Biolabs) were used to amplify plasmid DNA. The proteins were expressed in *E. coli* BL21 (DE3) (Agilent Technologies) . *Ctr* serovar E and L2 were propagated by infection of HEp-2 cells [40] and pooled EBs were purified via a 30 % Gastrographin gradient.

DNA isolation from *Chlamydia*

Purified chlamydial EBs were pelleted by centrifugation at 15,000 rpm for 20 min (Biofuge primo R, Heraeus). The pellet was washed with HBSS and centrifuged again. After additional three washing steps, the pellet was resuspended in 20 µl HBSS and 20 µl proteinase K was added (20 mg/ml). After incubation for 1 h at 55 °C and 10 min at 100 °C, 210 µl HBSS and 250 µl phenol-chloroform were added. The sample was mixed vigorously and centrifuged at 15,000 rpm for 10 min. 200 µl were carefully removed (upper phase) and mixed with 20 µl 3 M sodium acetate (pH 5) and 200 µl isopropanol. The sample incubated for 30 min at - 80 °C and was centrifuged (after thawing) at 4 °C for 30 min and 15,000 rpm. Finally, the pellet was washed with 500 µl 70 % ethanol, centrifuged again, dried and resuspended in 10 µl $H_20$.

Expression and purification of protein

The expression plasmids for PmpG_29-673, PmpH_26-690 and PmpI_26-569 were transformed into *E. coli* BL21. One L LB medium containing the appropriate antibiotics was inoculated with an $OD_{600}$ of 0.1 and incubated while shaking at 37 °C until an OD of 0.7 was reached. Protein expression was subsequently induced by the addition of 1 ml of 1 M IPTG (isopropyl-β-D-thiogalactopyranoside). After 4 hours, the *E. coli* cells were pelleted for 10 min at 5,000 rpm (Avanti J-20, Beckman Coulter). The supernatant was discarded and the pellet resuspended in 20 ml lysis buffer (6 M guanidine/HCL, 20 mM Tris/HCL, 0.5 M NaCl, 1 mM β-mercaptoethanol). The cells were lysed overnight at 4° C on a rotating wheel. Next, the lysate was sonicated on ice twice for 30 seconds and then centrifuged for 1 h at 4 °C and 24,000 rpm (Avanti J-20, Beckman Coulter). The lysate was then transferred to a new 50 ml centrifuge tube and 1 ml Ni-NTA agarose (Qiagen) was added. This suspension was incubated under shaking for 3 h at room temperature and then transferred to a protein purification column (thermo scientific). The agarose was washed with 20 ml Washing buffer A, pH 8 (8 M urea, 0.1 M $NaH_2PO_4$, 10 mM Tris/HCl, 1 mM β-mercaptoethanol, 20 mM imidazole) and 20 ml Washing buffer B, pH 6.3 (8 M urea, 0.1 M $NaH_2PO_4$, 10 mM Tris/HCl, 1 mM β-mercaptoethanol 40 mM imidazole) and then eluted with Elution buffer pH 6.3 (8 M urea, 0.1 M $NaH_2PO_4$, 10 mM Tris/HCl, 1 mM β-mercaptoethanol, 500 mM imidazole). Finally, the protein concentration was determined by Bradford assay according to a standard protocol and the protein was checked for purity by SDS-PAGE followed by Coomassie staining.

Coomassie stained SDS-PAGE and immunoblot analysis

Unless otherwise stated, proteins for analysis by SDS-PAGE were always mixed in a ratio of 32.5 µl sample, 12.5 µl 4x protein blue marker (200 mM Tris/HCl, 8 % SDS, 20 % glycerol, 0.2 % bromophenol blue) and 5 µl 1 M DTT (dithiothreitol) and incubated at 100 °C for 10 min. The samples were then loaded onto a 10 % SDS gel and separated at 200 V for 80 min. For Coomassie staining, the gels were heated, washed in water for 10 min (3 times) and transferred to a Coomassie solution (0.008 % Coomassie G-250, 35 mM HCl). After reheating, the gels were incubated until bands became visible.
For immunodetection, SDS gels were first transferred to a polyvinylidene fluoride (PVDF) membrane, which was then incubated for 1 h by shaking in Blocking solution (3 % Milk powder, 0.05 % Tween 20 in PBS). Next, the membrane was incubated in Blocking solution containing primary antibody for 1 h, washed 3 times with PBS and incubated with an appropriate secondary antibody AP (alkaline phosphatase conjugated) for 1 h. After washing in PBS, the bands were visualized by incubation in Detection solution

(20 ml Detection buffer (0.1 M Tris/HCl pH 9.5, 0.1 M NaCl, 50 mM $MgCl_2$) + 66 µl 5-Brom-4-chlor-3-indoxylphosphat (BCIP) solution (0.5 g BCIP in 10 ml DMF) + 66 µl nitro blue tetrazolium (NBT) solution (0.5 g NBT in 10 ml 70 % DMF).

Protein binding assay

To test recombinant proteins for their binding ability to human cells, HEp-2 cells were seeded in well plates for 2 days at 37 °C and 6 % $CO_2$. The confluent cell layer was washed with HBSS and then overlaid with 250 µl of 200 µg/ml protein for different time periods (0 min, 1 min, 15 min, 30 min, 60 min). 10 µl protein solution mixed with 10 µl 1 M DTT, 25 µl protein blue marker and 55 µl $H_2O$ were used as an input sample. Cells of the time point "0 min" remained untreated in order to obtain information about the non-specific detection of the HIS antibody. At the time points, the protein solution was removed and the cells were washed 3 times with HBSS. The cells were overlaid with cell dissociation solution (Gibco) for 10 min at 37 °C and then transferred to a new Eppendorf reaction tube. After pelleting by centrifugation for 5 min at 1,000 × g (Biofuge Primo R, Heraeus), the pellet was resuspended in 97.5 µl HBSS, 37.5 µl protein blue marker and 15 µl 1 M DTT, incubated for 10 min at 100 °C and analyzed via SDS-PAGE and Western Blot.

Blue native Page

2 µg of renatured protein was mixed with 5 µl of 4 x Native PAGE™ Sample buffer and filled to 20 µl with $H_2O$. The XCell SureLock Mini-Cell and the Bis-Tris gel (containing a 3 - 12 % acrylamide gradient) were set up and prepared according to the manufacturer's instructions. The inside of the chamber was filled with native PAGE™ light blue buffer. After loading the gel, the outer area of the chamber was filled with native PAGE™ anode buffer. Electrophoresis was performed in a 4 °C room at 150 V (8 - 10 mA) for 60 min and then at 250 V (2 - 4 mA) for 90 min. The gel was removed from the chamber and Coomassie stained as previously described.

Oligomerization visualization using thioflavin T (ThT) fluorescence

To generate oligomer growth kinetics, the BMG ClarioStar plate reader was used with an absorbance of 445 nm and collected emission at 482 nm in 96-well low-binding half-area plates (Greiner) sealed by transparent polypropylene films. The samples contained 10 µM ThT in 50 mM Na-phosphate buffer, 50 mM NaCl, pH 7.4 . Identical samples were incubated shaking at 37°C. The samples were measured every 3 minutes without shaking.

Atomic force microscopy

25 µl of oligomerized protein were applied to freshly cleaved muscovite mica. After a 1-minute incubation at room temperature, the samples were washed 3 times with 100 µl dd$H_2O$ and then dried with a stream of $N_2$ gas. Images were taken in intermittent contact mode (AC mode) in a JPK Nano Wizard 3 atomic force microscope (JPK, Berlin) using a silicon cantilever with silicon tip (OMCLAC160TS-R3, Olympus) with a typical tip radius of 9 ± 2 nm, a force constant of 26 N / m and resonance frequency around 250 kHz and processed with Gwyddion (version 2.56). Over either amplitude images false color height images were superimposed using Gimp – GNU Image Manipulation Program.

APEX2 biotinylation assay

100 µl chlamydial pool was pelleted for 20 min at 15,000 rpm and 4 °C and then resuspended in 100 µl HBSS. After centrifugation, the pellet was resuspended in 200 µl 2 mM biotin phenol. After incubation at 37 °C for 30 min, 2 µl 100 mM $H_2O_2$ was added, gently swirled and incubated at room temperature for a further minute. To quench the reaction, 200 µl of Quenching-solution A (10 mM Trolox 20 mM sodium ascorbate) was added. After two further washing steps with 1 ml of Quenching-solution B (5 mM Trolox 10 mM sodium ascorbate) the pellet was resuspended in 500 µl Phopholysis buffer (150 mM NaCl, 20 mM Tris, 2 mM EDTA, 1 mM $Na_2VO_4$ 1 % Triton 1 % NP-40, 5 mM Trolox, 10 mM sodium ascorbate). After incubation at 4 °C for 30 minutes, 100 µl of streptavidin agarose was added and incubated overnight at 4 °C, while shaking. Biotinylated proteins were then purified using streptavidin beads. The beads were washed twice with 600 µl of Phopholysis buffer followed by 500 µl each of 1 M KCl, 0.1 M $Na_2CO_3$ and 2 M urea, 10 mM Tris pH 8. The beads were eluted by boiling them for 15 minutes in 50 µl protein blue marker with 5 µl 1 M DTT.

Detergent extraction assay

75 µl *Ctr* L2 wt or *Ctr* L2 transformants pool were pelleted by centrifugation at 15,000 rpm at 4 °C for 30 min (Biofuge primo R, Heraeus). The pellet was resuspended in 100 µl PBS. PBS or detergents (final concentration: 1 % Triton X-100, 2 % Sarcosyl, 1 % NP-40 and 50 mM DTT) were then added and incubated for 1 h at 37° C. During incubation, the samples were vortexed and ultrasonicated several times. The mixtures were centrifuged for 1 h at 4 °C and 100,000 g (Ultra Optima Max-E, Beckman). The supernatants (150 µl) were transferred to new reaction tubes and the pellets were completely resuspended in 150 µl PBS each. To all samples 57.7 µl protein blue marker and 23 µl 1 M DTT were added, resuspended and then heated at 100° C for 10 min. The samples were analyzed via Western Blot.

Infection and immunostaining

Semi-confluent HEp-2 cells were grown on glass coverslips. *Ctr* pool was diluted in cell culture media and layered on top the HEp-2 cells. After centrifugation at 2,800 rpm (Hettich™ ROTANTA 460 R) for 60 minutes, the supernatant was removed and replaced with cell culture media containing 1.2 µg/ml Cycloheximide. Subsequently the cells fixed with PFA (3 %), permeabilized with MeOH and further processed for immunofluorescence.

LC-MS Sample preparation

The wild-type *Ctr* L2 EB samples were centrifuged for 15 min at 16,000 × g before 10 µg supernatant per sample were loaded on a polyacrylamide gel (about 5 mm running distance) and the gel subjected to Coomassie Brilliant Blue staining. Purified proteins from Pmpl-APEX2 biotinylation experiments were as well shortly separated in a polyacrylamide gel and stained with Coomassie Brilliant Blue. Protein bands were cut out and processed as described [41]. Briefly, the isolated gel pieces were reduced (50 µl, 10 mM DTT), alkylated (50 µl, 50 mM iodoacetamide) and afterwards digested with trypsin (200 ng trypsin in 100 mM ammonium bicarbonate for wild-type Ctr L2 EB samples and 10 ng for samples from Pmpl-APEX2 biotinylation experiments). The peptides were resolved in 17 µl 0.1 % trifluoracetic acid and subjected to liquid chromatography.

LC-MS analysis

For the LC-MS analysis, a QExactive plus (Thermo Scientific, Bremen, Germany) mass spectrometer connected to an Ultimate 3,000 Rapid Separation liquid chromatography system (Dionex / Thermo Scientific, Idstein, Germany) equipped with an Acclaim PepMap 100 C18 column (75 µm inner diameter, 25 cm length, 2 µm particle size from Thermo Scientific, Bremen, Germany) was used essentially as described earlier [42]. The length of the isocratic LC gradient was 120 minutes (55 minutes kV for samples from Pmpl-APEX2 biotinylation experiments). The mass spectrometer was operating in positive mode and coupled with a nano electrospray ionization source. Capillary temperature was set to 250°C and source voltage to 1.5 kV (1.4 kV for samples from Pmpl-APEX2 biotinylation experiments). In the QExactive plus mass spectrometer for the survey scans a mass range from 200 to 2,000 m/z at a resolution of 140,000 was used. The automatic gain control was set to 3,000,000 and the maximum fill time was 50 ms. The 10 most intensive 2 and 3-fold charged peptide ions were isolated, fragmented by high-energy collision dissociation (HCD) and fragments analyzed at a resolution of 17,500.

Computational mass spectrometric data analysis

Peptides and proteins were identified and quantified using the MaxQuant environment (version 1.6.17.0, version 1.6.10.43 for samples from Pmpl-APEX2 biotinylation experiments, MPI for Biochemistry, Planegg, Germany), if not indicated otherwise with standard parameters. Searches were carried out using the *Chlamydia trachomatis* L2 (strain 434BuATCC VR-902B) UniProt proteome data base (UP000000795, downloaded 04/05/21) respectively *Chlamydia trachomatis* L2 UP000000583 downloaded at 11th September 2019 for samples from Pmpl-APEX2 biotinylation experiments and tryptic specificity (cleavage behind R and K) with a maximum of two missed cleavages sites. An initial search was performed with 20 ppm precursor mass tolerance and identified peptides were then used for recalibration using the 'software lock mass' feature of MaxQuant [43]. Afterward, a main search was conducted with a precursor mass tolerance of 4.5 ppm. The mass tolerance of fragment spectra was set to 20 ppm. Peptides and proteins were accepted at a false discovery rate of 1%. Label-free quantification [44] was enabled and based on unique and razor peptides. The minimal ratio count was set to two, peptides with variable modifications were included in the protein quantification; the 'match between runs' option was enabled. All identified proteins were reported for the wild-type Ctr L2 EB samples and only proteins identified with at least 2 peptides for Pmpl-APEX2 biotinylation samples.

**Results:**

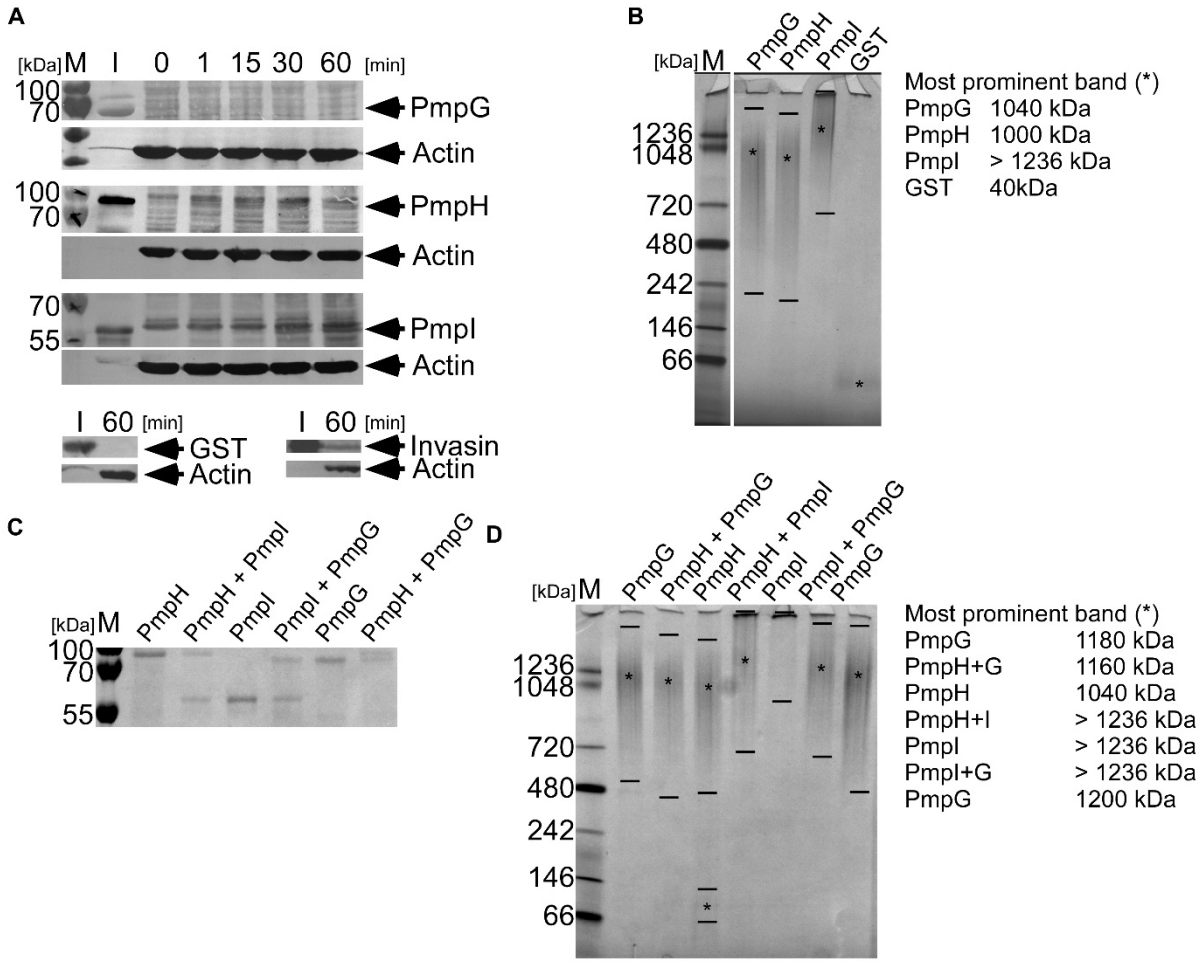


Figure 2: Recombinant full-length PmpG, PmpH and PmpI show adhesion and form homo- and heterooligomers.

**A.** HEp-2 cells were overlaid with recombinant PmpG, PmpH or PmpI (200 µg/ml) for different time spans. When the time points were reached, cells were washed, detached and analyzed via Western Blot. To visualize bound protein, membranes were treated with anti-His antibody or anti-actin antibody . The protein Invasin served as a positive control; GST as a negative control. **B.** For analysis of high molecular weight complexes, 2 µg of recombinant protein was separated on a Blue native PAGE and subsequently stained with Coomassie. [*] indicate the most prominent band. Horizontal black lines mark the boundary of the respective Pmp complex (one of two representative experiments shown). Main band and complex boundaries were identified using GelAnalyzer2010a [45]. **C.** To analyze the possible formation of heterologous complexes, 2 different denatured Pmps were mixed in equimolar amounts and dialyzed. The protein + protein mixtures were separated on a SDS gel and stained with Coomassie. **D.** Blue native Page of proteins renatured in C. . Renatured Pmp mixtures and their respective homomeric Pmps were loaded as indicated and separated by Blue native PAGE (one of two representative experiments shown). These complexes were analyzed using GelAnalyzer2010a as described in B. Input (I). Marker (M). Minute (min).

**Full-length Pmp fragments adhere to epithelial cells and are able to generate homomeric and heteromeric oligomers**

We have shown previously that motive-rich and motive-poor protein fragments of the passenger domain of PmpG, PmpH and PmpI form oligomeric complexes [17, 46]. We now wanted to test whether full-length passenger domain of those Pmp proteins would show similar behavior. While PmpG did not show binding to HEp-2 cells during the entire experiment, PmpH and PmpI over time adhered significantly to epithelial cells. PmpH adhesion started after 1 min of incubation and increased over time. PmpI adhesion was first visible at 15 min and became stronger over time (Figure 2 A). Recombinant invasin has been shown to adhere to HEp-2 cells and served as positive control [47, 48], while GST was the negative control.

Next, we determined the oligomerization state of recombinant renatured PmpG, PmpH and PmpI, by Blue native PAGE (Figure 2 B). All high molecular weight complexes generated by Pmps appeared as a smear that stretched over several hundred kDa. All tested Pmps showed an area of highest intensity (most prominent band) (Figure 2 B). In this way, PmpG showed complexes that stretched over a range of about 220 kDa to more than 1,236 kDa with a dominant band of 1,040 kDa. Complexes generated by PmpH were smaller ranging from 200 kDa to more than 1,236 kDa with a dominant band at 1,000 kDa. PmpI generated the largest high molecular weight complexes ranging from about 700 kDa up to the upper border of the gel and a dominant band of over 1,236 kDa. To investigate the generation of high molecular heteromeric complexes, different denatured Pmps were mixed in an equimolar ratio and then renatured (Figure 2 C). In all combinations, mixing 2 Pmps resulted in complexes with a molecular weight which was different from the complex sizes of the individual homomeric complexes (Figure 2 D). Interestingly, heteromeric complexes of PmpG and PmpH were smaller than the homomeric complex of PmpG and larger than the homomeric complex of PmpH. Heteromeric complexes containing PmpI were larger than the homomeric complexes generated from PmpG or PmpH but smaller than complexes of homomeric PmpI alone.

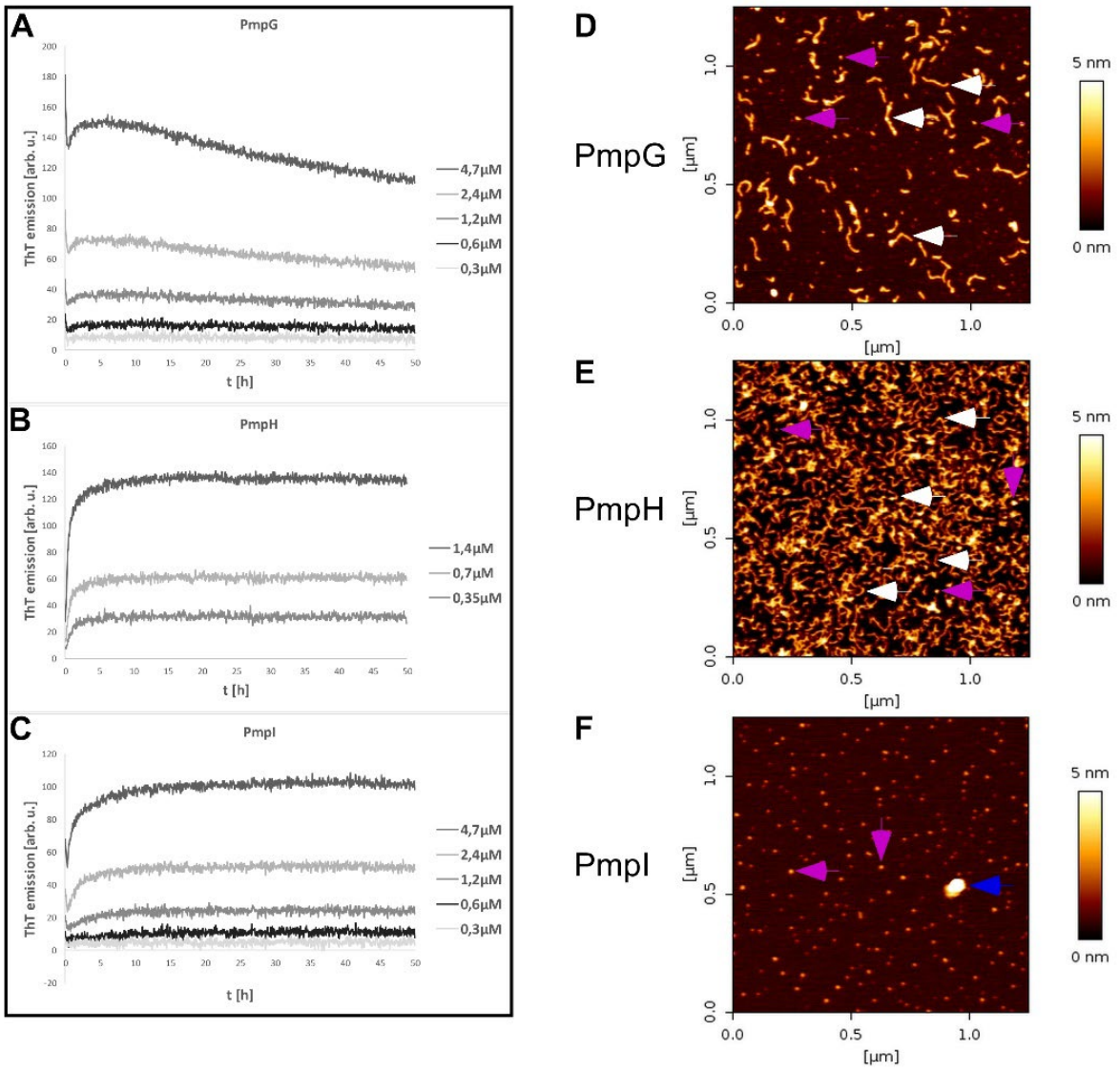


Figure 3: Growth kinetics of protofibrillar aggregates formed by monomeric PmpG (**A**), PmpH (**B**) and PmpI (**C**) visualized by ThT fluorescence and representative atomic force microscopy images (PmpG (**D**), PmpH (**E**) and PmpI (**F**)) of the corresponding complexes. Oligomerisation kinetics over a time span of 50 h of monomeric PmpG (**A**), PmpH (**B**) and PmpI (**C**). Representative atomic force microscopy images generated with protein samples taken at the end of the ThT assay. Purple arrows mark oligomeric structures, whereas white arrows point to protofibril structures. The blue arrow points to a large protein accumulation. Arb. u. = arbitrary unit

### Pmp full-length fragments exhibit lag-free amyloid-like formation kinetics

Previously, we had shown that protein fragments from *Cpn* Pmp21 and *Ctr* PmpA, PmpG, PmpD and PmpI form long rod-like particles ([17, 29]). Electron microscopy of these oligomers showed protofibril structures similar to amyloid-like proteins. ThT-assays of Pmp21 fragments confirmed these amyloid-like

structures [29]. We now tested whether the full-length PmpI passenger domain also formed highly fluorescent complexes with the benzothiazole dye.

PmpH started with a fluorescence of 28 which increased steadily and peaked at 141 at hour 18 (Figure 3 B). The emission remained stable and did only decrease slightly. PmpI showed similar results, starting with a fluorescence of 51 and peaking at 109 at hour 41, although the majority of oligomerisation was reached at about hour 20. Like PmpH, the emission remained stable until the end of the measurement period. (Figure 3 C). It was noticeable that PmpG did not start at a ThT emission close to 0 but almost at maximum emission at a fluorescence value of 132. The fluorescence of PmpG reached its peak at hour 6 with a value of 155, which decreased to an emission of 110 at 50 hours as the experiment progressed (Figure 3 A).

As expected, an increasing protein concentration resulted in an accelerated oligomerization kinetic, as for example doubling of the protein concentration led to a doubling in the final ThT emission (Figure 3 A – C). The ThT emission of PmpH (1.4 µM) started at 28 and increased within 16 h to a maximum of 140 (Figure 3 B). The emission remained stable and did only decrease slightly (131, 50 h). The ThT emission of PmpI (4.7 µM) started at approx. 55 and increased within 40 h to a maximum of 108 (Figure 3 C). Like PmpH, the emission remained stable until the end of the measurement period.

At the end of each experiment, samples were taken for subsequent analysis by atomic force microscopy. PmpG and PmpH appeared as oligomeric and protofibril-like structures with a curvilinear shape (Figure 3 D, E). In contrast to PmpG and PmpH, PmpI showed rather globular oligomers and a large protein accumulation (Figure 3 F).

Taken together, all tested full-length Pmps showed amyloid-like growth that resulted in oligomers (PmpG/H/I) and protofibrils (PmpG/H).

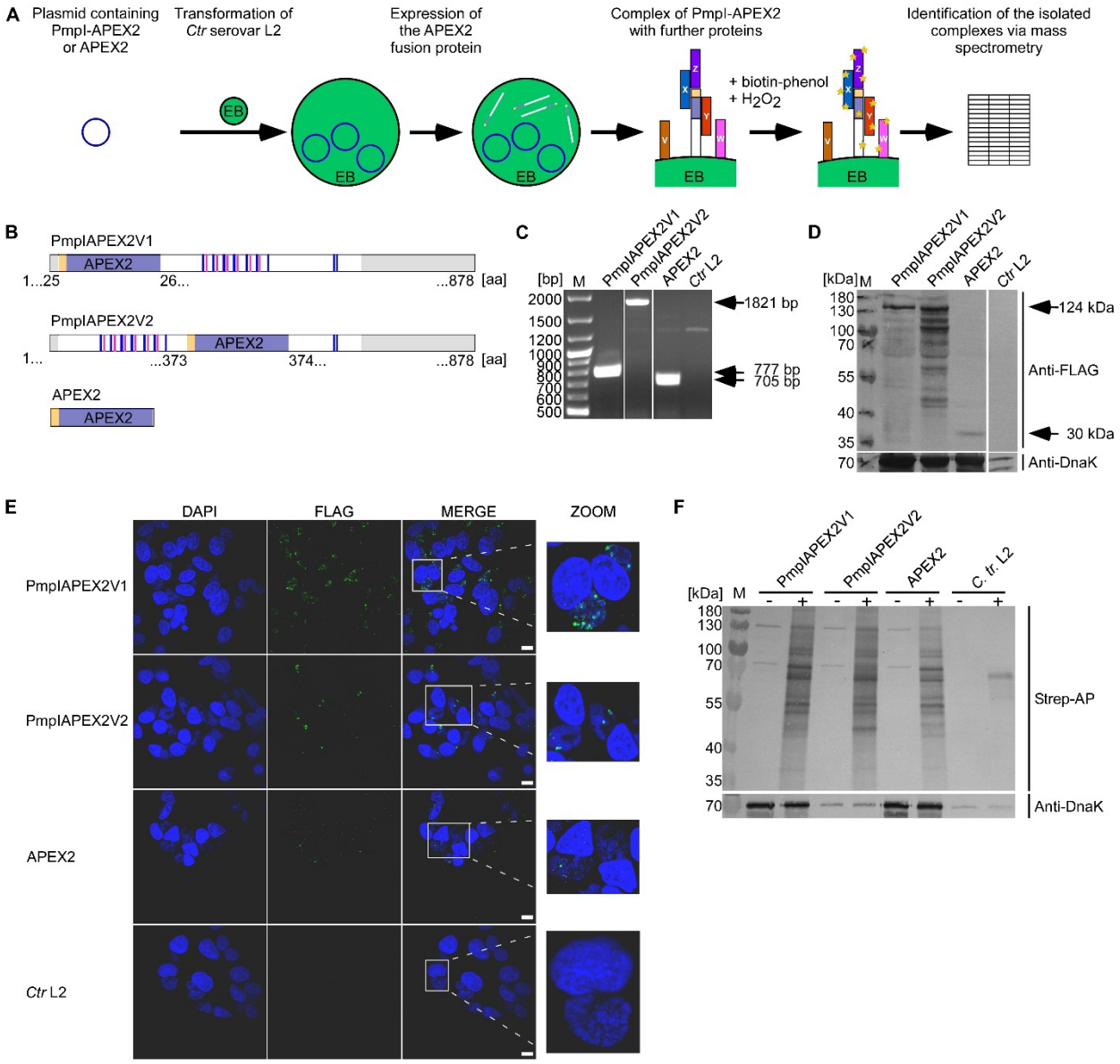


Figure 4: Proteomic labeling strategy of *Ctr* EB surface located PmpI

**A.** PmpI was genetically fused with APEX2, integrated in the plasmid pKM255 (expressed proteins shown in B) and constitutively expressed in *Chlamydia* by using the incD promoter. After the addition of biotin-phenol and $H_2O_2$ the PmpI-APEX2 fusion protein biotinylated proximal proteins (V, W, X, Y, Z). Next the chlamydial cell wall was solubilized and biotinylated proximity partners were isolated via streptavidin and analyzed via mass spectrometry. **B.** Schematic representation of cloned PmpI-APEX2 fusion proteins PmpIAPEX2V1 (APEX2 N-terminal), PmpIAPEX2V2 (APEX2 in central position) and APEX2 (no PmpI). N-terminal signal sequence (grey); central passage domain (white) ; C-terminal β-barrel domain (grey). FxxN motifs (blue). GGA (I, L, V) motifs (magenta) [27, 29]. 3x FLAG-tag (orange). The graphics were created with RStudio [32]. **C.** Isolated DNA from the *Ctr* L2 transformants were amplified with respective primers to proof the presents of the respective plasmids. Primers bound upstream of the signal sequence and at the downstream end of the *apex2* gene (PmpIAPEX2V1 product: 777 bp; PmpIAPEX2V2 product: 1821 bp; APEX2 product: 705 bp). The primers bound upstream of the inserted sequences (forwards-primer) and in the *apex2* gen (reverse-primer). **D.** 48 hpi infected cells were collected, samples prepared and loaded on a SDS-PAGE followed by Western Blot. For visualization of the APEX2 fusion proteins (PmpIAPEX2V1/PmpIAPEX2V2: 124 kDa, APEX2: 30 kDa), membranes were treated with anti-FLAG antibody or anti-DnaK antibody (loading control). **E.** HEp-2 cells infected with *Ctr* L2 transformants or *Ctr* L2 wt were fixed (17 hpi, -20 °C MeOH) and subsequent immunostained with anti-

FLAG antibody (green). DNA was stained with DAPI (blue). Individual cells with inclusions were shown enlarged (ZOOM). Size bar 10 µm. **F:** HEp-2 cells infected with *Ctr* L2 wt or *Ctr* L2 transformants were harvested (48 hpi) and purified. Subsequently, the biotinylation procedure was used and samples incubated without (-) and with (+) $H_2O_2$ and biotin-phenol. Samples were analyzed by SDS-PAGE and Western Blot followed by visualization via Strep-AP and Anti-DnaK antibody. Base pair (Bp). Kilodalton (kDa). Amino acids (aa). Marker (M).

**Development of a labelling system for the identification of proteins with close spatial proximity to PmpI**

The *in vitro* data strongly suggest that Pmp proteins form homo- and heterooligomers *in vitro.* In order to test for the spatial organization of Pmps *in vivo* at the EB surface, we used the APEX2 proximity system to identify the Pmp-specific EB-surface proteome.

In this method, a protein of interest is genetically fused with APEX2 and expressed in the target organism *Ctr* L2. The fusion protein localizes to its native subcellular position where it biotinylates (after the addition of biotin-phenol and $H_2O_2$) its neighbors (radius ≤ 20 nm). Biotinylated proteins are purified and identified by mass spectrometry. The PmpI protein was chosen due, to the previously described adhesion ability of smaller [13] but also larger fragments of the passenger domain as well as its ability to form large homomeric and heteromeric complexes (Figure 2). Since the impact of the position of the APEX2 protein inside the PmpI-APEX2 fusion protein on protein folding, function and localization was not known, two different fusion proteins were created: In PmpIAPEX2V1, APEX2 was positioned N-terminally directly after the signal sequence. In PmpIAPEX2V2, APEX2 was inserted at aa position 373 (Figure 4 B). APEX2 without PmpI served as a negative control, which should primarily localize in the cytosol. After transformation with the respective plasmids, *Ctr* L2 were propagated, isolated and their DNA extracted. Based on this DNA, PCRs were conducted to test for the presence of the correct plasmid (PmpIAPEX2V1 product: 777 bp; PmpIAPEX2V2 product: 1821 bp; APEX2 product: 705 bp). It was confirmed that all transformants contained the desired plasmid (Figure 4 C). To check for the expression of the fusion constructs, HEp-2 cells were infected with the *Ctr* transformants or *Ctr* L2 wt, and analyzed (Figure 4 D). For PmpIAPEX2V1 and PmpIAPEX2V2, distinct bands could be detected just above the 130 kDa marker band, which corresponds to the calculated MW of the fusion protein of 124 kDa. Both transformants showed additional bands below 124 kDa, which could be background generated by *Ctr* L2 and HEp-2. PmpIAPEX2V2 showed more degradation, giving it a much more diverse band pattern than PmpIAPEX2V1. In contrast, APEX2 showed a band of a size of about 37 kDa, which corresponds to the calculated MW of 30 kDa.

In general, cells infected with *Ctr* L2 PmpIAPEX2V1 showed more EBs emitting a FLAG signal with additionally higher intensity compared to cells infected with *Ctr* L2 PmpIAPEX2V2 or *Ctr* L2 APEX2. Finally, it was tested, if the APEX2 protein transformed in *Ctr* L2 was functional (Figure 4 F). 48 hpi *Ctr* L2

transformants and *Ctr* L2 wt were purified and used in the following biotinylation reaction. All chlamydial particles, which should be mostly EBs, were processed and analyzed by Western Blot. All EBs treated without $H_2O_2$ and biotin-phenol showed two distinct bands at 80 kDa and 140 kDa in contrast to *Ctr* L2 wt EBs that generated no band. Treated with $H_2O_2$ and biotin-phenol all transformants generated a diverse band pattern in contrast to *Ctr* L2 wt that only showed one band at 65 kDa. There were clear differences in the banding pattern between treated and untreated transformants, which in turn differ strongly from treated and untreated *Ctr* L2 wt. In summary, it could be clearly stated that the APEX2 expressed here was still functional.

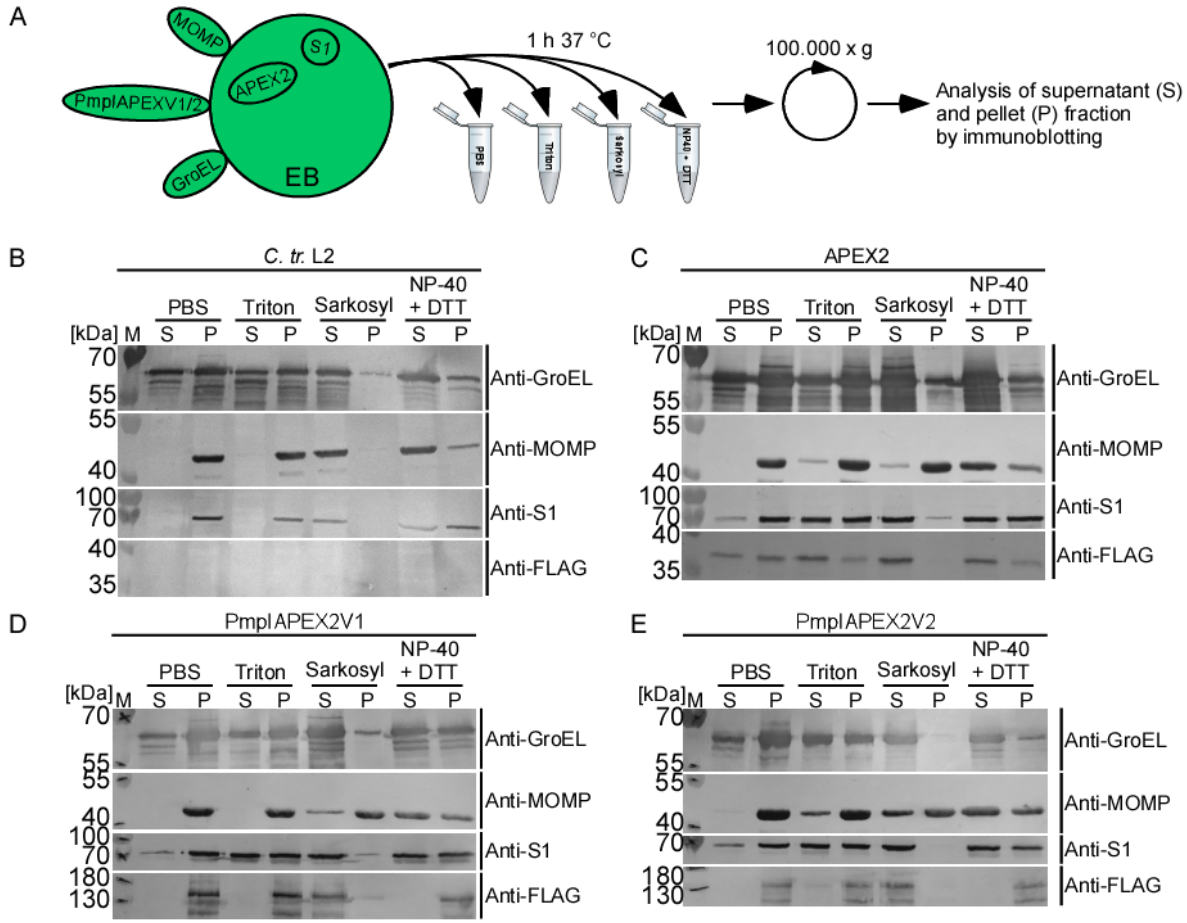


Figure 5: Localization studies of chlamydial proteins by detergent extractions

**A.** In detergent extraction studies *Ctr* L2 transformants or *Ctr* L2 wt EBs were incubated with PBS or the stated detergents ,separated by centrifugation into a pellet (P) and supernatant (S) fraction and analyzed via Western Blot. These studies were performed with pools of *Ctr* L2 wt (**B**), transformants expressing only APEX2 (**C**) and those expressing PmpIAPEX2V1 (**D**) or PmpIAPEX2V2 (**E**). The antibodies anti-GroEL1, anti-*Ctr* MOMP , anti-S1 and anti-FLAG were used for the detection of GroEL1 (EB surface localized), MOMP (major outer membrane protein), S1 (cytosolic localized protein) and FLAG-tagged fusion proteins. Kilodalton (kDa).

**PmpIAPEX2 fusion proteins localize to the surface of EBs**

In addition to the functionality of the APEX2 fusion proteins, it must be ensured that protein modifications, such as the integration of the APEX2 protein into PmpI, or an increased expression does not affect the native localization of PmpI to the surface of the EB. Therefore, extraction studies were performed in which EBs were treated with detergents of different potency. Depending on the detergent used, different proteins were solubilized from the EB. Centrifugation allowed separation into a supernatant fraction of solubilized proteins and a pellet fraction of undissolved proteins. The comparison of the proteins to be determined with proteins of known localization allowed an estimation of their localization.

MOMP is a major component of the chlamydial cell surface and part of the COMC [49]. PBS and the weak detergent Triton were incapable to extract MOMP out of the membrane of *Ctr* L2 wt EBs (Figure 5 B). Incubation with sarkosyl resulted in an almost complete extraction of MOMP into the supernatant. NP-40 + DTT was also able to extract most of the MOMP from the membrane. S1 is a cytosolic protein. Since treatment of Chlamydia with PBS or Triton leaves the membrane largely intact, no S1 was transferred into the supernatant from the *Ctr* L2 wt EBs, whereby it was found entirely in the pellet fraction. In contrast, treatment with sarkosyl or NP-40 + DTT led to a much stronger perforation of the membrane, whereby the S1 protein could be extracted completely (sarkosyl) or partially (NP-40 + DTT) in the supernatant fraction. Since it was the wild type, no fusion protein was detected by anti-FLAG.

In contrast to the wild type, in *Ctr* L2 transformed with the plasmid for the expression of APEX2 an extraction of S1 could already be observed in PBS and Triton (Figure 5 B, C). APEX2 showed an almost identical extraction pattern to intrachlamydial S1, confirming its desired cytosolic position (Figure 5 C).

There were no major differences in the extraction pattern of *Ctr* L2 expressing PmpIAPEX2V1 or PmpIAPEX2V2 (Figure 5 D, E). In both cases, treatment with PBS, Triton or NP-40 + DDT extracted only no to very small amounts (Triton, PmpIAPEX2V2) of fusion protein into the supernatant fraction. Only the strong detergent sarkosyl was able to transfer PmpIAPEX2V1 and PmpIAPEX2V2 almost completely into the supernatant fraction, further indicating its actual membrane localization.

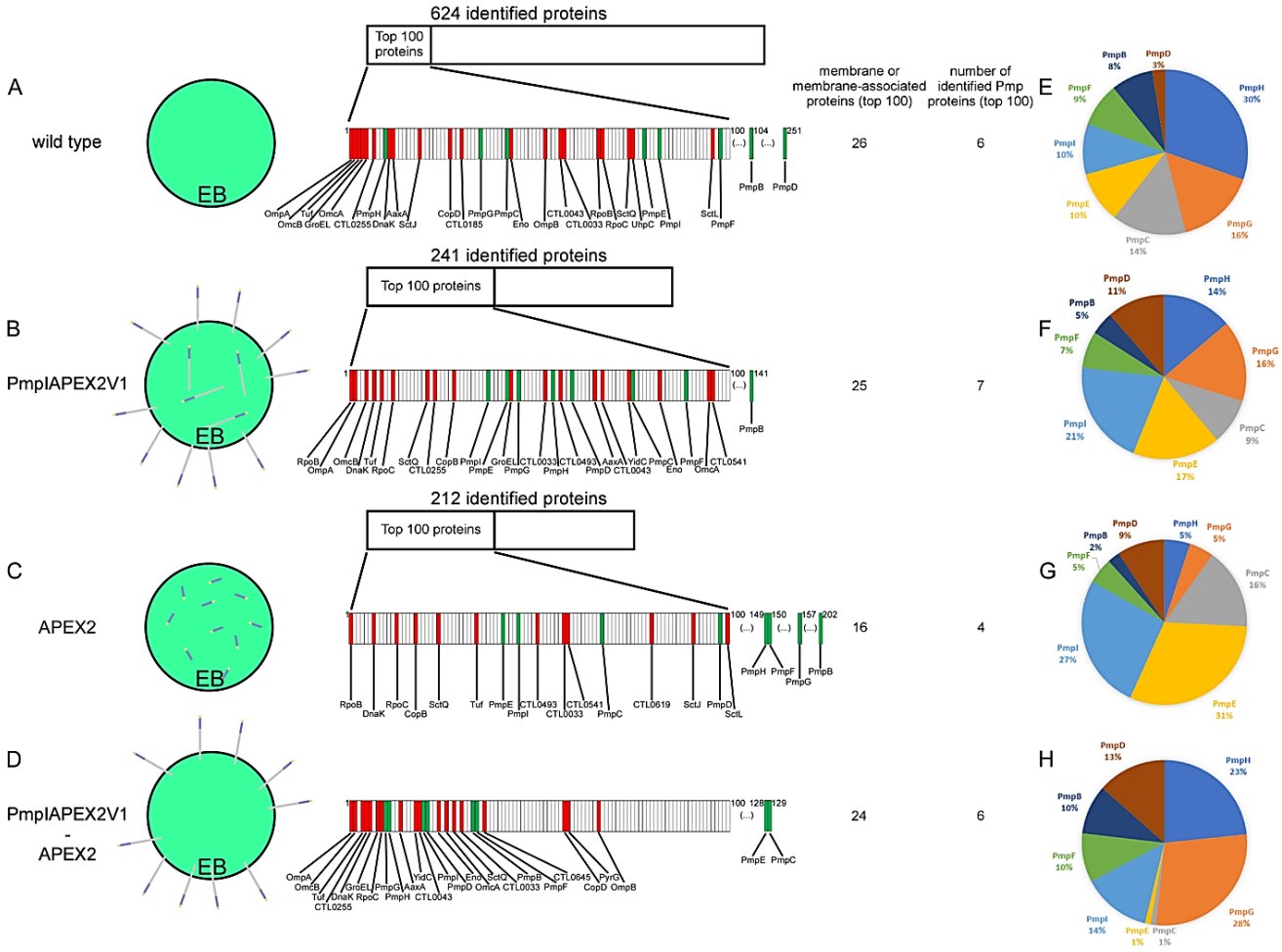


Figure 6: Nearest neighbor analysis for PmpIAPEX2

EBs were propagated, purified and prepared as earlier described. Proteins present were subsequently identified by mass spectrometry, sorted according to their quantity ( via their normalized intensity) and the proteins showing the top 100 mass spectrometric intensities were presented. Identified Pmp proteins outside the top 100 were additionally indicated to the right of the main graph with their corresponding ranking.

**A.** Untransformed *Ctr* L2 wild-type EBs were purified and examined for the native distribution of their proteins.

**B./C**. *Ctr* L2 transformed with the corresponding plasmid were propagated and purified. Next, proteins in proximity of the APEX2 fusion protein were labelled with biotin. Labeled proteins were isolated using streptavidin and analyzed.

**D.** Normalized intensities obtained in C were subtracted from B in order to obtain a resolved data set focusing primarily on membrane proteins. Membrane or membrane-associated proteins (red rectangles). Proteins are defined as membrane-associated if they localize to the inner membrane, periplasmic space or outer membrane. Identified Pmp proteins (green rectangles).

**E-H.** Percentage of Pmps found in A (E), B (F), C (G) and D (H). Here, 100 % corresponds to the total mass spectrometric intensities of all Pmps.

**PmpI interacts with other Pmp proteins on the surface of EBs**

Previous research and data generated here clearly show that Pmp proteins are present on the surface of Chlamydia, that recombinant Pmp generates high molecular complexes in the form of oligomers and protofibrils *in vitro* (Figure 3; [17, 29]), and further demonstrates that generated high molecular complexes can be both homomeric and heteromeric (Figure 2; [17]). To address the final question if one form of these complexes is actually present on the surface of Chlamydia or whether Pmps prefer to bind with certain proteins rather than others, both samples of complete wild-type *Ctr* L2 EBs and samples of streptavidin-purified samples of *Ctr* L2 PmpIAPEX2V1 and *Ctr* L2 APEX2 were analyzed and proteins identified. Identified meant that the normalized intensity of the protein produced a value in at least 2 out of 3 (Figure 6 A) or 3 out of 5 (Figure 6 B - C) replicates. These were ranked according to their quantitative amount (averaged normalized intensity). For comparison, untreated and untransformed wild-type *Ctr* L2 EBs were purified and subsequently analyzed by mass spectrometry. Due to the observed stronger degradation of PmpIAPEX2V2 (Figure 4 D) and the increased detection of PmpIAPEX2V1 in inclusions of infected cells (Figure 4 E), PmpIAPEX2V1 was used in the following analysis.

**Wild type**

A total of 624 different proteins were identified. Within the proteins showing the top 100 mass spectrometric intensities 26 membrane- or membrane-associated proteins, 7 type III secretion system-associated proteins and 6 Pmp proteins were identified. The top 5 proteins were the major outer membrane porin OmpA (position 1 (pos.1); 23.1 % of the total amount of protein detected) followed by the cysteine-rich outer membrane protein OmcB (pos. 2; 5.8 %), the elongation factor Tuf (pos. 3; 2.6 %), GroEL (pos. 4; 2.3 %) and the small cysteine-rich outer membrane protein OmcA (pos. 5; 2.1 %) making these 5 proteins alone account for 35.8 % of the total mass spectrometric intensities detected. Of these, OmpA, OmcB and OmcA were described as components of the COMC [49], whereas Tuf and GroEL were described as possible members that may be contaminants, although some of them have already been described as membrane-localizing and relevant for infection [49-52]. Within this study, the Pmp proteins had been of particular interest. 8 out of 9 could be detected in the analysis of wild-type *Ctr* L2 EBs. In descending order of spectrometric intensities, these were PmpH (pos. 10), PmpG (pos. 35), PmpC (pos. 42), PmpE (pos. 78), PmpI (pos. 82), PmpF (pos. 98), PmpB (pos. 104) and PmpD (pos. 251). Of these, PmpB and PmpD were no longer within the top 100 ranking. PmpA was not detected. Within the Pmps, PmpH accounted for the largest relative amount with 30 %, followed by PmpG (16 %) and PmpC (14 %; Figure 6 E). PmpE (10 %) and PmpI (10 %) were detected in similar amounts, followed by PmpF (9 %) and PmpB (8 %). PmpD accounted for the smallest proportion of detected Pmps with 3 % (Figure 6 E).

**APEX2**

In addition to untransformed *Ctr* L2 wt and transformants expressing PmpIAPEX2V1, a transformant was generated which exclusively expressed the APEX2 protein without PmpI. APEX2 should therefore primarily localize cytosolically, biotinylate cytosolic proteins and represent a negative control to PmpIAPEX2V1 (Figure 6 C). Within the top 100 proteins biotinylated by APEX2, 16 membrane or membrane-associated proteins, 6 proteins belonging to the type III secretion apparatus and 4 Pmp proteins were detected. The top 5 proteins were RpoB (pos. 1; 46 % of total detected averaged spectrometric intensity), the Metalloprotease-insulinase CTL0196 (pos. 2; 11 %), the putative exported protein CTL0809 (pos. 3; 4 %), RpsM (pos. 4; 2 %) and ClpP1 (pos. 5; 1 %). Within the top 100 ranking, only 4 Pmps could be found. These were PmpE (pos 41), PmpI (pos. 45), PmpC (pos. 67) and PmpD (pos. 98) followed by PmpH (pos. 149), PmpF (pos. 150), PmpG (pos. 157) and PmpB (pos. 202). This resulted in a ratio of PmpE (31 %), PmpI (27 %), PmpC (16 %), PmpD (9 %), PmpH (5 %), PmpG (5 %), PmpF (5 %) und PmpB (2 %). In accordance with the experimental setting, the most relevant proteins of the COMC, such as OmcA (pos. 204), OmcB (pos. 116), OmpA (pos. 232) and OmpB (pos. 139) were now detected at a much lower level, which again proved the functionality of this system. Other membrane proteins detected included GroEL (pos. 203), CTL0255 (pos. 146), AaxA (pos. 187) , CTL 0185 (pos. 164), and UhpC (pos. 39; Figure 6 C).

**PmpIAPEX2V1**

Among the top 100 proteins were 25 membrane- or membrane-associated proteins, 5 type III secretion system-associated proteins and 7 Pmp proteins. The top 5 proteins were the DNA-directed RNA polymerase subunit beta RpoB (pos. 1; 38 %) followed by OmpA (pos. 2; 10 %), CTL0196 (pos. 3;10 %), CTL0809 (pos. 4; 3 %) and OmcB (pos. 5; 3 %). Similar to GroEL or Tuf before, RpoB is a possible membrane-associated protein, as it was found in studies of the COMC [49, 50]. Considering that this was a search for the closest neighbors of the PmpI protein and that it was suspected that Pmps interact with themselves and other Pmps on the EB surface, it was not surprising that 7 of the total of 8 detected Pmps were now in the top 100. In descending order of intensity, these were PmpI (pos. 37), PmpE (pos. 42), PmpG (pos. 45), PmpH (pos. 54), PmpD (pos. 59), PmpC (pos. 75), PmpF (pos. 89) and PmpB (pos. 141). This resulted in a Pmp distribution of PmpI (21 %), PmpE (17%), PmpG (16%), PmpH (14%), PmpD (11%), PmpC (9 %), PmpF (7 %) and PmpB (5 %; Figure 6 F).

**PmpIAPEX2V1 minus APEX2**

It was possible that PmpIAPEX2V1 also biotinylated cytosolic proteins on its way to the membrane and that these were subsequently purified and analyzed (Figure 6 B). APEX2 biotinylated primarily cytosolic and some membrane proteins (Figure 6 C). To obtain a purified data set specialized for membrane and membrane-associated proteins, the normalized averaged intensities obtained from the APEX2 experiment were used and subtracted from the normalized averaged intensities of PmpIAPEX2V1. This was followed by a further ranking, which is shown in Figure 6 D. Within the top 100 were 24 membrane or membrane-associated proteins, 6 proteins related to the type III secretion system and 6 Pmps. It was noticeable that after the refinement of the data set, the majority of the membrane proteins showed a significant increase in ranking and thus there were already 21 membrane proteins in the top 35. Within the top 5 were the proteins OmpA (pos. 1; 47 %), OmcB (pos. 2; 13 %), CTL0196 (pos. 3; 6 %), Tuf (pos. 4; 4 %) and CTL0255 (pos. 5; 2 %). Other membrane proteins detected were GroEL (pos. 8), AaxA (pos. 14), YidC (pos. 18), OmcA (pos. 26), PyrG (pos. 58) and OmpB (pos. 66). GroEL, AaxA and OmpB remained roughly the same in their ranking while YidC and PyrG improved and OmcA decreased his rank. The 6 identifiable Pmps within the top 100 were PmpG (pos. 10), PmpH (pos. 11), PmpI (pos. 20), PmpD (pos. 21), PmpB (pos. 33) and PmpF (pos. 34) followed by PmpE (pos. 128) and PmpC (pos. 129) outside the top 100. Compared to wt, PmpD (pos. 251 (wt) -> 21), PmpB (pos. 104 (wt) -> 33), PmpF (pos. 98 (wt) -> 34), PmpI (pos. 82 (wt) -> 20) and PmpG (pos. 35 (wt) -> 10) were enriched, whereas PmpH (pos. 10 (wt) -> 11) remained roughly the same and PmpC (pos. 42 (wt) -> 129) and PmpE (pos. 78 (wt) -> 128) worsened in their ranking.

**Discussion:**

*Ctr* is a dangerous pathogen that even today cannot be effectively treated and therefore poses a constant threat to human health. Latest research showed the ability of small motif-rich and motif-poor Pmp fragments to oligomerize and generate homomeric and heteromeric high molecular weight complexes *in vitro* [17, 29]. Therefore, we first investigated the full-length protein fragments of PmpG (aa 29-673), PmpH (aa 26-690) and PmpI (aa 26-569).

Binding studies confirmed that PmpH and PmpI are able to bind to human cells. PmpG showed no visible binding in this experimental setting (Figure 2 A). This could mean that the binding of PmpG is weaker and therefore was not visible here. Indeed, other binding studies with an N-terminal part of the passenger domain in a comparable experimental setting showed no to hardly any binding of PmpG and also no infection-reducing effects when human cells were pretreated. In the stated study, PmpG was described together with PmpA as a protein with inconsistent and very little adhesion capacity [17]. In two other experimental settings in which yeast cells were presenting PmpG on their surface or latex beads coated with PmpG, binding to human cells was again observed [13]. It is possible that the agglomeration of PmpG on latex beads or presentation on yeast cells led to a stronger adhesive effect than soluble recombinant PmpG alone. It is unlikely that PmpG lost some of its binding strength after denaturing protein purification followed by renaturation, as PmpG-coated beads still adhered to cells [13]. In summary, it can be said that the experimental conditions under which PmpG is tested seems to have an important impact. Additionally, it is possible that PmpG could have further functions besides binding. It might be conceivable that PmpG has a supporting or stabilizing function in the formation of adhesive oligomers.

In our study, full-length protein fragments of PmpG, PmpH and PmpI generated high-molecular-weight protein complexes. Depending on the Pmp examined, homomeric complexes of a size of approx. 1,000 kDa (PmpH) to 1,300 kDa (PmpI) were generated (Figure 2 B). Mixtures of different Pmps resulted in heteromeric complexes, which localized in size between the respective homomeric complexes (Figure 2 D). Compared to previous research by Favaroni and Hegemann 2021, the homomeric complexes generated for both PmpG (approx. 900 kDa [17]) and PmpI (approx. 1,200 kDa [17]) here were only insignificant bigger, which means that in addition to the number of motifs, the size of the Pmp fragments used has no relevant influence on the final size of the oligomer possibly meaning that this size is optimal for its function or stability.

Past studies have shown that *Cpn* Pmp21_D-wt [29] and *Ctr* Pmp fragments [17] were capable of generating oligomeric structures that appeared as oligomers and protofibrils in electron microscopy.

In our study, similar to *Cpn* Pmp21_D-wt and other oligomeric proteins like Aβ [29], *Ctr* Pmp full-length proteins showed under *in vitro* conditions a lag-free concentration dependent increase in ThT signal over

time, which rapidly increased and reached a plateau demonstrating the oligomeric amyloid-like growth of a protein (Figure 3 A, B, C). Via AFM these samples appeared as oligomeric and protofibril-like structures for PmpG and PmpH, whereas PmpI showed oligomeric structures and large protein accumulations (Figure 3 D, E, F). Together with the data obtained here, it seems that all or a large number of Pmps form high molecular complexes in the form of oligomers of different sizes, independent of the chlamydial species considered, the number of motifs (if there are at least 2) or the size of the Pmp protein fragment. The ability to form oligomers seems to be of crucial importance for chlamydial infection. Indeed, Pmp21_D-wt oligomers have already been shown to have a stronger adhesion and infection-reducing effect than Pmp21_D-wt monomers or a Pmp21_D-mt mutant that was impaired in its ability to oligomerize [29]. Adhesion incompetent Pmps showed binding to human cells in heteromeric complexes with adhesion competent Pmps. In the same study, *in vitro* EM images of heteromeric complexes were displayed, which appeared as much longer protofibrils than their corresponding homomeric complexes [17]. It is unlikely that exactly such structures are present on EBs. Examination of chlamydial EBs for the polar distribution of the type III secretion system using cryo-electron tomography did not reveal any structures on the surface that might resemble protofibrils [53]. It is therefore more likely that smaller complexes such as homomeric or heteromeric oligomers are actually present. Various studies have already discovered a large number of functional oligomers, which were mostly described as supporting or stabilizing for biofilms, thus protecting the bacterium from external influences [54]. One protein repeatedly described in this context was the *E. coli* protein Curli. Comparable to Pmps, they generate high-molecular structures, long fibrils and are rich in β-sheets and lead to a fluorescence shift when mixed with thioflavin t [29, 55, 56]. They are also described with properties such as binding to surfaces, cell aggregation, biofilm formation, adhesion and invasion of host cells [56]. Strong interaction and binding between different Pmps and other membrane proteins could stabilize and strengthen the chlamydial membrane and thus provide an enhanced protection against harmful extracellular conditions. The binding of EBs to EBs to form EB clumps would also be conceivable. This would lead to a reduction in the attackable surface area exposed to the extracellular space. In addition, accumulation of EBs at one point of the host cell could promote an infection.

To tackle the challenging question of with whom Pmps bind on the surface of chlamydial EBs, we genetically fused PmpI with APEX2 and expressed it in the target organism *Ctr* L2. Untransformed *Ctr* L2 EBs served as the data set describing the wild-type situation.

Within the proteins showing the top 100 mass spectrometric intensities, about a quarter could be assigned to membrane or membrane-associated proteins. The 5 proteins showing the most mass spectrometric intensities were OmpA, OmcB, elongation factor Tuf, GroEL and OmcA (Figure 6 A) . This is comparable to

other studies such as Skipp *et al.* 2016 which also described OmpA, Tuf, GroEL and OmcB within their top 15 most abundant proteins [57]. Within our measurement, PmpH, PmpG, PmpC, PmpE, PmpI, PmpF, PmpB and PmpD were detected in decreasing amounts. PmpA could not be detected (Figure 6 E). Saka *et al.* 2011 investigated and compared the presence of chlamydial proteins between chlamydial RB and EB forms in *Ctr* L2. Comparable to them, similar relative amounts of PmpF, no PmpA and only small amounts of PmpD were detected in the EB form in our analyses [58]. This seems reasonable, since both PmpA (12 hpi) and PmpD (12 to 14 hpi) are expressed mostly in the RB form [24, 59]. In our study, PmpH and PmpC were detected in a more abundant relative amount, whereas the amounts of PmpG, PmpE and PmpB were lower. Interestingly, in our samples, PmpI accounted for 10 % of the Pmp amount, whereas none was detected in the aforementioned study.

Compared to the native distribution in wt, an isolation using PmpIAPEX2V1 resulted in a low enrichment of PmpF, a moderate enrichment of PmpI and PmpE as well as a strong enrichment of PmpD, whereas PmpG, PmpH and PmpC were depleted. An enrichment of PmpI was to be expected, as mass spectrometry did not distinguish between native PmpI and PmpIAPEX2V1. In addition, it was likely that PmpIAPEX2V1 also biotinylates itself and biotinylates bound native PmpI. The results indicate that PmpI probably prefers to bind to PmpB, PmpE and especially PmpD. Removal of cytosolic findings from the PmpIAPEX2V1 dataset resulted in a purified dataset in which 21 of the top 36 proteins were membrane- or membrane-associated proteins. Within this setting, almost all Pmps improved significantly in their ranking (PmpG, PmpI, PmpD, PmpB, PmpF) whereas most other membrane proteins (e.g. OmpA, OmcB, Tuf, CTL0255, GroEL) were again detected in a comparable initial position. The exception was YidC, which also improved its position in the ranking. This suggests that PmpI may primarily favor other Pmps or Pmp fragments as interaction partners, thus supporting the previously obtained in vitro data.

Interestingly, PmpD in particular has long been a protein of intense research. It is a membrane-associated protein that produces flower-like oligomeric structures on the surface of EBs [28]. Our results now suggest that there are also heteromeric PmpI-PmpD complexes on the surface of EBs. PmpD is of enormous importance for an infection. It is a highly conserved [30], a target of broadly cross-reactive neutralizing antibodies [60] and a PmpD null mutant showed greatly reduced infection on macaque eyes and cultured human cells [61]. Blue native PAGE of recombinant PmpI full length (without signal sequence and β-barrel) and PmpI-fragments demonstrated its strong oligomeric character. Complexes of PmpI and PmpD could lead to clusters with accumulated adhesive properties leading to an enhanced binding and infection.

In summary, PmpI is present on the surface of chlamydial EBs where it possibly binds and forms complexes with a variety of different Pmps as well as some membrane or membrane-associated proteins. This leads to a higher diversity of presented antigens on the chlamydial surface, which could provide a protective

function against the cells immune defense, as well as areas of increased adhesion on the EB surface, leading to increased infection. When critically analyzing these data, it must be borne in mind that the expression of Pmps can be influenced by the presence of antibiotics and that a minor influence cannot be ruled out here [30]. To verify these findings, future experiments will focus on determining the binding strength between PmpI and the different Pmps. Furthermore, additional Pmp-APEX2 transformants will further decipher the still incomplete picture of Pmp proteins, their binding partners and the appearance of the membrane landscape in general.

**References:**


1. Brunham, R.C. and J. Rey-Ladino, *Immunology of Chlamydia infection: implications for a Chlamydia trachomatis vaccine.* Nat Rev Immunol, 2005. **5**(2): p. 149-61.
2. Burton, M.J. and D.C. Mabey, *The global burden of trachoma: a review.* PLoS Negl Trop Dis, 2009. **3**(10): p. e460.
3. Potroz, M.G. and N.J. Cho, *Natural products for the treatment of trachoma and Chlamydia trachomatis.* Molecules, 2015. **20**(3): p. 4180-203.
4. Darville, T. and T.J. Hiltke, *Pathogenesis of genital tract disease due to Chlamydia trachomatis.* J Infect Dis, 2010. **201 Suppl 2**: p. S114-25.
5. Geisler, W.M., *Duration of untreated, uncomplicated Chlamydia trachomatis genital infection and factors associated with chlamydia resolution: a review of human studies.* J Infect Dis, 2010. **201 Suppl 2**: p. S104-13.
6. Newman, L., et al., *Global Estimates of the Prevalence and Incidence of Four Curable Sexually Transmitted Infections in 2012 Based on Systematic Review and Global Reporting.* PLoS One, 2015. **10**(12): p. e0143304.
7. Bastidas, R.J., et al., *Chlamydial intracellular survival strategies.* Cold Spring Harb Perspect Med, 2013. **3**(5): p. a010256.
8. Dautry-Varsat, A., A. Subtil, and T. Hackstadt, *Recent insights into the mechanisms of Chlamydia entry.* Cell Microbiol, 2005. **7**(12): p. 1714-22.
9. Elwell, C., K. Mirrashidi, and J. Engel, *Chlamydia cell biology and pathogenesis.* Nat Rev Microbiol, 2016. **14**(6): p. 385-400.
10. Ajonuma, L.C., et al., *CFTR is required for cellular entry and internalization of Chlamydia trachomatis.* Cell Biol Int, 2010. **34**(6): p. 593-600.
11. Stallmann, S. and J.H. Hegemann, *The Chlamydia trachomatis Ctad1 invasin exploits the human integrin beta1 receptor for host cell entry.* Cell Microbiol, 2016. **18**(5): p. 761-75.
12. Mamelak, D., et al., *Hsp70s contain a specific sulfogalactolipid binding site. Differential aglycone influence on sulfogalactosyl ceramide binding by recombinant prokaryotic and eukaryotic hsp70 family members.* Biochemistry, 2001. **40**(12): p. 3572-82.
13. Becker, E. and J.H. Hegemann, *All subtypes of the Pmp adhesin family are implicated in chlamydial virulence and show species-specific function.* Microbiologyopen, 2014. **3**(4): p. 544-56.
14. Gitsels, A., N. Sanders, and D. Vanrompay, *Chlamydial Infection From Outside to Inside.* Front Microbiol, 2019. **10**: p. 2329.
15. Fadel, S. and A. Eley, *Chlamydia trachomatis OmcB protein is a surface-exposed glycosaminoglycan-dependent adhesin.* J Med Microbiol, 2007. **56**(Pt 1): p. 15-22.
16. Grimwood, J. and R.S. Stephens, *Computational analysis of the polymorphic membrane protein superfamily of Chlamydia trachomatis and Chlamydia pneumoniae.* Microb Comp Genomics, 1999. **4**(3): p. 187-201.
17. Favaroni, A. and J.H. Hegemann, *Chlamydia trachomatis Polymorphic Membrane Proteins (Pmps) Form Functional Homomeric and Heteromeric Oligomers.* Front Microbiol, 2021. **12**: p. 709724.
18. Molleken, K., E. Becker, and J.H. Hegemann, *The Chlamydia pneumoniae invasin protein Pmp21 recruits the EGF receptor for host cell entry.* PLoS Pathog, 2013. **9**(4): p. e1003325.
19. Stephens, R.S., et al., *Genome sequence of an obligate intracellular pathogen of humans: Chlamydia trachomatis.* Science, 1998. **282**(5389): p. 754-9.
20. Rockey, D.D., J. Lenart, and R.S. Stephens, *Genome sequencing and our understanding of chlamydiae.* Infect Immun, 2000. **68**(10): p. 5473-9.
21. Vasilevsky, S., et al., *Chlamydial polymorphic membrane proteins: regulation, function and potential vaccine candidates.* Virulence, 2016. **7**(1): p. 11-22.

22. Lanfermann, C., et al., *Prophylactic Multi-Subunit Vaccine against Chlamydia trachomatis: In Vivo Evaluation in Mice.* Vaccines (Basel), 2021. **9**(6).
23. Longbottom, D., et al., *Molecular cloning and characterization of the genes coding for the highly immunogenic cluster of 90-kilodalton envelope proteins from the Chlamydia psittaci subtype that causes abortion in sheep.* Infect Immun, 1998. **66**(4): p. 1317-24.
24. Kiselev, A.O., et al., *Expression, processing, and localization of PmpD of Chlamydia trachomatis Serovar L2 during the chlamydial developmental cycle.* PLoS One, 2007. **2**(6): p. e568.
25. Wehrl, W., et al., *From the inside out--processing of the Chlamydial autotransporter PmpD and its role in bacterial adhesion and activation of human host cells.* Mol Microbiol, 2004. **51**(2): p. 319-34.
26. Tan, C., et al., *Variable expression of surface-exposed polymorphic membrane proteins in in vitro-grown Chlamydia trachomatis.* Cell Microbiol, 2010. **12**(2): p. 174-87.
27. Molleken, K., E. Schmidt, and J.H. Hegemann, *Members of the Pmp protein family of Chlamydia pneumoniae mediate adhesion to human cells via short repetitive peptide motifs.* Mol Microbiol, 2010. **78**(4): p. 1004-17.
28. Swanson, K.A., et al., *Chlamydia trachomatis polymorphic membrane protein D is an oligomeric autotransporter with a higher-order structure.* Infect Immun, 2009. **77**(1): p. 508-16.
29. Luczak, S.E., et al., *The Chlamydia pneumoniae Adhesin Pmp21 Forms Oligomers with Adhesive Properties.* J Biol Chem, 2016. **291**(43): p. 22806-22818.
30. Carrasco, J.A., et al., *Altered developmental expression of polymorphic membrane proteins in penicillin-stressed Chlamydia trachomatis.* Cell Microbiol, 2011. **13**(7): p. 1014-25.
31. Rhee, H.W., et al., *Proteomic mapping of mitochondria in living cells via spatially restricted enzymatic tagging.* Science, 2013. **339**(6125): p. 1328-1331.
32. Team, R., *RStudio: Integrated Development Environment for R*. 2021, RStudio, PBC. p. Used code by Fabienne Kocher.
33. Xu, J.B., M. McPartlon, and J. Li, *Improved protein structure prediction by deep learning irrespective of co-evolution information.* Nature Machine Intelligence, 2021.
34. Xu, J.B., *Distance-based protein folding powered by deep learning.* Proceedings of the National Academy of Sciences of the United States of America, 2019. **116**(34): p. 16856-16865.
35. Xu, J.B. and S. Wang, *Analysis of distance-based protein structure prediction by deep learning in CASP13.* Proteins-Structure Function and Bioinformatics, 2019. **87**(12): p. 1069-1081.
36. Wang, S., et al., *Accurate De Novo Prediction of Protein Contact Map by Ultra-Deep Learning Model.* Plos Computational Biology, 2017. **13**(1).
37. Wang, S., S.Q. Sun, and J.B. Xu, *Analysis of deep learning methods for blind protein contact prediction in CASP12.* Proteins-Structure Function and Bioinformatics, 2018. **86**: p. 67-77.
38. Wang, S., et al., *Folding Membrane Proteins by Deep Transfer Learning.* Cell Systems, 2017. **5**(3): p. 202-+.
39. Agaisse, H. and I. Derre, *A C. trachomatis cloning vector and the generation of C. trachomatis strains expressing fluorescent proteins under the control of a C. trachomatis promoter.* PLoS One, 2013. **8**(2): p. e57090.
40. Jantos, C.A., et al., *Antigenic and molecular analyses of different Chlamydia pneumoniae strains.* J Clin Microbiol, 1997. **35**(3): p. 620-3.
41. Poschmann, G., et al., *High-fat diet induced isoform changes of the Parkinson's disease protein DJ-1.* J Proteome Res, 2014. **13**(5): p. 2339-51.
42. Grube, L., et al., *Mining the Secretome of C2C12 Muscle Cells: Data Dependent Experimental Approach To Analyze Protein Secretion Using Label-Free Quantification and Peptide Based Analysis.* J Proteome Res, 2018. **17**(2): p. 879-890.
43. Cox, J. and M. Mann, *Quantitative, high-resolution proteomics for data-driven systems biology.* Annu Rev Biochem, 2011. **80**: p. 273-99.

44. Cox, J., et al., *Accurate proteome-wide label-free quantification by delayed normalization and maximal peptide ratio extraction, termed MaxLFQ.* Mol Cell Proteomics, 2014. **13**(9): p. 2513-26.
45. Istvan Lazar Jr., P.a.I.L.S., PhD, CSc *GelAnalyzer 2010a*.
46. Favaroni, A., *Role of adhesin proteins in Chlamydia infection*, in *Funktionelle Genomforschung der Mikroorganismen*. 2017, Heinrich-Heine-Universität Düsseldorf.
47. Dersch, P. and R.R. Isberg, *A region of the Yersinia pseudotuberculosis invasin protein enhances integrin-mediated uptake into mammalian cells and promotes self-association.* EMBO J, 1999. **18**(5): p. 1199-213.
48. Moelleken, K. and J.H. Hegemann, *The Chlamydia outer membrane protein OmcB is required for adhesion and exhibits biovar-specific differences in glycosaminoglycan binding.* Mol Microbiol, 2008. **67**(2): p. 403-19.
49. Liu, X., et al., *Identification of Chlamydia trachomatis outer membrane complex proteins by differential proteomics.* J Bacteriol, 2010. **192**(11): p. 2852-60.
50. Birkelund, S., et al., *Analysis of proteins in Chlamydia trachomatis L2 outer membrane complex, COMC.* FEMS Immunol Med Microbiol, 2009. **55**(2): p. 187-95.
51. Wuppermann, F.N., et al., *Chlamydia pneumoniae GroEL1 protein is cell surface associated and required for infection of HEp-2 cells.* J Bacteriol, 2008. **190**(10): p. 3757-67.
52. Longbottom, D., et al., *Proteomic characterisation of the Chlamydia abortus outer membrane complex (COMC) using combined rapid monolithic column liquid chromatography and fast MS/MS scanning.* PLoS One, 2019. **14**(10): p. e0224070.
53. Nans, A., H.R. Saibil, and R.D. Hayward, *Pathogen-host reorganization during Chlamydia invasion revealed by cryo-electron tomography.* Cell Microbiol, 2014. **16**(10): p. 1457-72.
54. Van Gerven, N., et al., *The Role of Functional Amyloids in Bacterial Virulence.* J Mol Biol, 2018. **430**(20): p. 3657-3684.
55. LeVine, H., 3rd, *Thioflavine T interaction with synthetic Alzheimer's disease beta-amyloid peptides: detection of amyloid aggregation in solution.* Protein Sci, 1993. **2**(3): p. 404-10.
56. Barnhart, M.M. and M.R. Chapman, *Curli biogenesis and function.* Annu Rev Microbiol, 2006. **60**: p. 131-47.
57. Skipp, P.J., et al., *Quantitative Proteomics of the Infectious and Replicative Forms of Chlamydia trachomatis.* PLoS One, 2016. **11**(2): p. e0149011.
58. Saka, H.A., et al., *Quantitative proteomics reveals metabolic and pathogenic properties of Chlamydia trachomatis developmental forms.* Mol Microbiol, 2011. **82**(5): p. 1185-203.
59. Nunes, A., et al., *Comparative expression profiling of the Chlamydia trachomatis pmp gene family for clinical and reference strains.* PLoS One, 2007. **2**(9): p. e878.
60. Crane, D.D., et al., *Chlamydia trachomatis polymorphic membrane protein D is a species-common pan-neutralizing antigen.* Proc Natl Acad Sci U S A, 2006. **103**(6): p. 1894-9.
61. Kari, L., et al., *Chlamydia trachomatis polymorphic membrane protein D is a virulence factor involved in early host-cell interactions.* Infect Immun, 2014. **82**(7): p. 2756-62.

# 3. Teil II Manuskript II

***Chlamydia pneumoniae* infection-mediating Pmp21 adhesin and Alzheimer's disease-related Aβ oligomers exhibit a common mode of binding cellular prion protein $PrP^C$**

Sebastian Wintgens, Filip Hasecke, Nadine Rösener, Wolfgang Hoyer, Johannes H. Hegemann

Erstautor
Beteiligungen:
Sebastian Wintgens: 55 %, Filip Hasecke 20 %, Nadine Rösener 15 %, Wolfgang Hoyer 5 %, Johannes H. Hegemann: 5 %

Sebastian Wintgens (SW) erstellte das gesamte Manuskript, wertete die Daten aus und erstellte alle Figuren und Figurlegenden (exklusive Figur 2). SW erbrachte die experimentellen Daten zu den Figuren 1, 3, 4, 5 und 6 (Figur 6 in Zusammenarbeit mit Dr. Nadine Rösener (NR)) sowie für die Abbildungen S1, S2, S3, S5 und S6.

Filip Hasecke (FH) erbrachte die experimentellen Daten zu Figur 2, wertete die dazu gehörigen Daten aus und erstellte Abbildung 2.

NR erbrachte die experimentellen Daten zu Figur 6 (Figur 6 in Zusammenarbeit mit SW) und Figur S4 und wertete die dazu gehörigen Daten aus.

Prof. Wolfgang Hoyer (WH) und Prof. Johannes H. Hegemann (JHH) übernahmen als korrespondierende Autoren Korrekturarbeiten am Manuskript und den Figuren. WH und JHH nahmen während der Entstehungsphase dieses Manuskripts als Betreuer der Doktorarbeit Einfluss auf das Experimentdesign und die Diskussion über die gesamte Laufzeit des Projekts.

Hiermit bestätige ich, dass diese Angaben korrekt sind.

Düsseldorf, den 30.05.2023

Sebastian Wintgens

## 3.1 Zusammenfassung

Chlamydien sind gramnegative, obligat intrazelluläre Bakterien, welche Menschen aber auch weitere Säugetiere, Vögel oder Reptilien befallen können. Neben dem Trachom auslösenden *C. trachomatis* ist *C. pneumoniae* das zweite wichtige Humanpathogen. Die typische Infektion erfolgt von Mensch zu Mensch durch Tröpfchen über den olfaktorischen Infektionsweg und führt zur Pneumonie. Zudem steht *C. pneumoniae* im Verdacht, in vielen weiteren chronischen Erkrankungen wie Asthma, Atherosklerose und der Alzheimer-Krankheit einen Einfluss auszuüben. Seit ca. 25 Jahren wird in vielen Studien ein möglicher kausaler Zusammenhang zwischen Alzheimer und einer Infektion mit *C. pneumoniae* untersucht. Nur wenige Untersuchungen beschrieben durch welchen Mechanismus eine chlamydiale Infektion zu Alzheimer führen könnte. Prominente und bereits lang erforschte Kandidaten für die Entstehung von Alzheimers sind Aβ-Oligomere und der PrP-Rezeptor. Wir zeigten in unserer Studie, dass *C. pneumoniae* Pmp21_D-wt (C-terminales Fragment von Pmp21_M) in einer vergleichbaren Kinetik zu Aβ hochmolekulare oligomere Strukturen generiert. Mittels Atomkraftmikroskopie visualisiertes Pmp21_D-wt erschien als Oligomer und Protofibril. Pmp21_D-wt Oligomere waren neben HEp-2 Zellen auch in der Lage, an nicht EGFR-exprimierenden CHO-K1 und Neuronen-ähnlichen SH-SY5Y zu binden. Interessanterweise war es möglich, in Pulldown-Experimenten natives PrP mithilfe von Pmp21_D-wt anzureichern. Diese Interaktion konnte durch abschließende Motiv-Studien auf bestimmte PrP-Domänen eingegrenzt werden, da Pmp21_D-wt Oligomere nur an PrP-Fragmente banden, welche Motive aufwiesen, welche auch schon für die Bindung mit Aβ oder α-Synuclein beschrieben wurden. Zusammenfassend unterstützen unsere Untersuchungen die Theorie, dass Chlamydien einen Einfluss auf die Pathogenese von Alzheimer haben könnte und zeigen erstmals eine Protein-Rezeptor-Bindung, die hierfür womöglich mitverantwortlich ist.

***Chlamydia pneumoniae* infection-mediating Pmp21 adhesins and Alzheimer's disease-related Aβ oligomers exhibit a common mode of binding cellular prion protein $PrP^C$**

Authors

Sebastian Wintgens[1], Filip Hasecke[2], Nadine S. Rösener[2], Wolfgang Hoyer[2,3], Johannes H. Hegemann[1]

[1] Institute of Functional Microbial Genomics, Heinrich-Heine-University Düsseldorf, 40204 Düsseldorf, Germany

[2] Institute of Physical Biology, Heinrich-Heine-University Düsseldorf, 40204 Düsseldorf, Germany

[3]Institute of Biological Information Processing (IBI-7) and JuStruct: Jülich Center for Structural Biology, Forschungszentrum Jülich, 52425 Jülich, Germany

**Abstract:**

*Chlamydia* are gram-negative, obligate intracellular pathogens that cause diverse infectious diseases. *C. pneumoniae* (*Cpn*) infection can lead to pneumonia, but may also exert an influence in chronic diseases including Alzheimer's disease (AD). A link between AD and *Cpn* infection has previously been supported, e.g., by detection of *Chlamydia* in AD-affected brain areas and by isolation of viable *Chlamydia* from AD brains. However, it remains elusive how a chlamydial infection could lead to AD. In AD pathogenesis, Aβ oligomers are suspected to cause receptor-mediated neurotoxicity upon binding to the cellular prion protein $PrP^C$. Here, we show that Pmp21_D, a fragment of the *Cpn* polymorphic membrane protein (Pmp) 21 that acts as an adhesin in infection, forms oligomers with morphologies and assembly kinetics comparable to those of Aβ protofibrils. Pmp21_D oligomers were able to bind to non-EGFR-expressing CHO-K1 cells as well as neuron-like SH-SY5Y cells, demonstrating that Pmp21_D has further cellular binding partners besides the previously identified EGFR and is in principal able to bind neuronal cells. *Cpn* elementary bodies colocalized with $PrP^C$ on HEp-2 cells, and endogenous $PrP^C$ directly interacted with adhering recombinant Pmp21_D in pull-down experiments, suggesting that $PrP^C$ is an additional receptor for Pmp21_D oligomers. Density gradient centrifugation showed that Pmp21_D oligomers and $PrP^C$ form large heteroassemblies, dependent on the same sites in the flexible PrP N-terminus as previously observed analogous assemblies of Aβ oligomers and $PrP^C$. In summary, our studies reveal a protein-receptor interaction that could be responsible for a potential role of *Chlamydia* in AD development.

**Introduction**

*Chlamydiae* are Gram-negative, obligate intracellular bacterial pathogens that infect a wide range of species, including humans, mammals and birds [1]. The two important human *Chlamydia* pathogens are *Chlamydia pneumoniae* (*Cpn*) and *C. trachomatis* (*Ctr*). *Ctr* causes trachoma, sexually transmitted diseases (STDs) and lymphogranuloma venereum (LGV) [2]. *Cpn* infects the upper and lower respiratory tract, and has been linked to lung cancer and a number of chronic diseases including asthma, arthritis, atherosclerosis, multiple sclerosis and Alzheimer's disease (AD) [1, 3-6]. The majority of the human population is exposed to *Cpn*, with antibody prevalences of 50 % by the age of 20 and 70 % to 80 % between the ages of 60-70 [4]. In general, chlamydial infections are treatable with antibiotics, but no vaccines are available so far. *Chlamydiae* exhibit a unique biphasic replication cycle. The infectious elementary body (EB) binds to the surface of a host cell via adhesins and invasins [7]. The EB is then taken up by endocytosis, forming a membrane-bound compartment termed the inclusion, in which it differentiates into the metabolically active, replicating and non-infectious reticulate body (RB). After several rounds of division, the RB differentiates back into the infectious EB form, which is released by cell lysis or extrusion [8, 9]. Under unfavorable growth conditions, *Chlamydiae* develop into an alternative replicative form called the aberrant body (AB), which is viable but non-cultivable and gives rise to a state known as "*Chlamydia* persistence". When conditions are again favorable, the AB reverts to an RB and normal replication ensues. *Chlamydia* persistence may represent the mechanism by which these organisms cause chronic inflammatory infections [10].

According to the WHO, Alzheimer's disease is the most common form of dementia (60-70 % of all cases) [11]. The disorder can be divided into the rare early-onset AD (EOAD; approximately 5 % of AD cases; < 65 years of age) and the typical late-onset AD (LOAD; > 65 years of age) [12]. LOAD is caused by a complex combination of genetic and environmental factors, which may involve infectious co-factors [13-15]. Core features of AD pathology are extracellular amyloid plaques, resulting from the accumulation of amyloid beta (Aβ) peptides, and neurofibrillary tangles (NFTs) consisting of intracellular Tau fibrils, which impair neuronal function and ultimately result in neurodegeneration [16].

Within the amyloidogenic pathway, cleavage of the naturally occurring amyloid precursor protein (APP) by β- and γ-secretases gives rise to 39- to 42-aa Aβ peptides, which can subsequently generate Aβ aggregates like oligomers, protofibrils and insoluble fibrils [17, 18]. The physiological roles of APP and its Aβ cleavage products are not fully understood [19]. Likewise, the toxic effects of Aβ cleavage products are diverse. Some studies have proposed an interplay between Aβ oligomers and lipid rafts [20-22] – receptor-rich areas in which high concentrations of Aβ oligomers could interfere with signal transduction [21].

Indeed, binding of Aβ oligomers to the N-methyl-D-aspartic acid receptor (NMDAR), the α-amino-3-hydroxy-5-methyl-4-isoxazolepropionate (AMPA) receptor and the α7 nicotinic cholinergic receptor (α7nAChR) leads to enhanced uptake of Aβ oligomers via endocytic mechanisms that result in damage to intracellular systems [23, 24].

An important amyloid peptide receptor is the prion protein (PrP), which has a high affinity for Aβ oligomers [25]. Native cellular PrP ($PrP^C$) is a glycosylphosphatidylinositol-anchored (GPI-anchored) membrane protein located in lipid rafts on the outer surface of the plasma membrane of neurons and other cells. At present its physiological functions are poorly understood; however, $PrP^C$ might be involved in functions such as neurite outgrowth, apoptosis control (anti-apoptotic during oxidative stress-induced cell death, pro-apoptotic during ER stress), synaptic plasticity, learning and memory, $Cu^{2+}$ binding, and/or myelin maintenance [26, 27]. In its pathogenic, alternatively folded scrapie form $PrP^{Sc}$, it is postulated to form amyloid fibrils [28-31]. Indeed, $PrP^{Sc}$ is able to convert normally folded $PrP^C$ into $PrP^{Sc}$ [32] that can aggregate and cause neuronal cell death [33]. Diseases associated with $PrP^{Sc}$ include Creutzfeldt-Jakob disease in humans as well as bovine spongiform encephalopathy in cattle [30]. Intriguingly, $PrP^C$ has been described as a receptor for oligomeric forms of Aβ [34].

Binding of Aβ oligomers to $PrP^C$ leads to recruitment of the metabotropic glutamate receptor 5 (mGluR5), a transmembrane protein located in postsynaptic densities; it in turn activates the protein kinase Fyn, which triggers calcium accumulation and phosphorylation of eukaryotic elongation factor 2 (eEF2), leading to loss of neuronal plasticity [35, 36]. Moreover, activated Fyn phosphorylates the NR2B subunit of NMDAR, resulting in the degradation of this receptor [35]. Furthermore, activated Fyn inhibits long-term potentiation (LTP) [34], and causes loss of synapses [37, 38], dendritic spine turnover *in vivo* [39] and memory impairment, as well as cognitive deficits [40, 41]. Finally, activated Fyn induces hyper-phosphorylation of Tau, an axonal microtubule-associated protein, which results in NFT formation, with fatal consequences for neurons. These findings delineate an Aβ oligomer-induced signal transduction pathway that requires $PrP^C$ and Fyn, and disrupts synaptic function, with deleterious consequences in patients with Alzheimer's disease [42].

In light of the multifactorial nature of AD, infections might also play a role in its pathogenesis. Available data suggest that viruses, bacteria and unicellular parasites may be associated with cognitive decline. Microbes may either directly induce formation of AD-like pathology in the brain, or act indirectly to over-stimulate the immune system, leading to a hyperinflammatory response that may exacerbate neurodegenerative changes [43, 44]. In the last two decades, a link between AD and infection with *Cpn* has become increasingly plausible. In the first publication linking *Chlamydia* to AD, brain samples from

Alzheimer's patients were shown to be significantly more often PCR positive for the presence of chlamydial 16S rRNA and the *ompA* gene than were samples from a control group [45]. In addition, immunohistochemical staining showed that *Cpn* colocalized with amyloid plaques and NFTs, the two pathological hallmarks of AD [46]. Interestingly, infection of human astrocytoma cells with *Cpn* upregulated several genes connected with lipid homeostasis, neuroinflammation, APP processing and microtubule function, and shifted APP processing even more to the pro-amyloidogenic pathway [3]. How *Cpn* enters the brain has not been intensively investigated. Possible routes are direct entry into the central nervous system following infection of the olfactory system [47, 48] or transport of infected monocytes across the blood-brain barrier [49-51].

Polymorphic membrane proteins (Pmps) are a family of chlamydial surface proteins that mediate EB adhesion to host cells. The number of Pmps is species-dependent, with nine members in *Ctr* (PmpA-PmpI) and 21 members in *Cpn* (Pmp1-Pmp21) [52]. Pmp proteins possess an N-terminal sec-signal sequence, a central passenger domain (PD) and a C-terminal β-barrel, all of which are features typical of autotransporters [53]. Moreover, all Pmps harbor multiple repeats of GGA(I/L/V) and FxxN peptide motifs that are relevant for function, adhesion and oligomerization [52, 54, 55]. The PDs of all nine *Ctr* and several of the *Cpn* Pmps are exposed on the surface of the EB, and most of them are proteolytically processed [52, 56-60]. The Pmp characterized in most detail is *Cpn* Pmp21. Pmp21 has multiple adhesive domains and was identified as an invasin that interacts with the epidermal growth factor receptor (EGFR) of the host [61]. Pmp21 is localized on the surface of EBs where it occurs in variously processed forms (N-M-C-Pmp21, N-M-Pmp21, N-Pmp21, M-Pmp21 and C-Pmp21) [55, 59, 62, 63]. Mutation studies revealed that at least two FxxN motifs or one GGA(I/L/V) and one FxxN motif are necessary for Pmp21 adhesion, oligomerization and EGFR binding [54, 55]. For *Ctr*, a new study has also found evidence for homo- and hetero-oligomerization of different Pmp proteins [64].

In relation to a possible link between AD and *Cpn* infection, we have previously shown that a fragment of *Cpn* Pmp21, Pmp21_D (Figure 1A), forms adhesive oligomers with structural characteristics that are very similar to those of protofibrillar Aβ oligomers [54]. Here, we show that the oligomerization kinetics of *Cpn* Pmp21_D resemble those found for dimAβ (Figure 1B), an artificial Aβ dimer that facilitates the separate analysis of protofibril versus fibril formation [65]. These data suggest that Pmp21_D oligomerization occurs by a nucleation-free mechanism similar to that described for the formation of Aβ protofibrils, but not Aβ fibrils. Importantly, incubation of human epithelial cells with dimAβ oligomers reduces subsequent *Cpn* infection, possibly by competition for common cell-surface receptors. In short-term infection experiments, *Cpn* EBs and the $PrP^C$ colocalize, suggesting that EBs adhere to $PrP^C$. Moreover, a deletion analysis of $PrP^C$ revealed a specific interaction of Pmp21_D oligomers with the intrinsically disordered N-terminus of PrP,

which is also required for the binding of Aβ oligomers. Thus, Pmp21 could potentially contribute to the generation of AD by engaging in receptor interactions similar to those of Aβ oligomers.

**Methods**:

Bacterial strains and cell culture

*E. coli* XL1-Blue (Stratagene) was used for plasmid amplification and *E. coli* Origami (Novagen) for protein expression. The *C. pneumoniae* strain GiD [66] was propagated in HEp-2 cells (ATCC: CCL-23) in the presence of 1.2 µg/ml cycloheximide (*Chlamydia* culture medium); EBs were purified by using a 30 % gastrographin gradient (Schering).

HEp-2 (ATCC Nr.: CCL-23), CHO-K1 (ATCC Nr.: CCL-61) and SH-SY5Y (ATCC Nr.: CRL-2266) cells were cultured in Dulbecco's modified Eagle medium (DMEM) GlutaMax (Gibco Life Technologies). The medium was supplemented with 10 % fetal calf serum (FCS), non-essential amino acids, vitamins, amphotericin B (2.5 µg/ml) and gentamicin (50 µg/ml). To induce neural differentiation of SH-SY5Y cells, the cultivation surface (glass slides in 24-well plates or directly in 24-well plates) was coated with poly-L-lysine according to the manufacturer's instructions. After seeding the cells in full medium, they were allowed to adhere overnight. On the following day, the medium was removed and replaced with full medium containing 10 µM retinoic acid (Sigma-Aldrich). Five days later, the medium was removed and replaced by medium lacking FCS and antibiotics, but containing 50 ng/ml brain-derived human neurotrophic factor (BDNF; Sigma-Aldrich). After three days, the cells were differentiated and could be maintained in complete medium without BDNF.

Expression and purification of recombinant Pmp21 protein fragments.

The plasmids for the expression of N-terminal $HIS_6$-tagged Pmp21_D-wt and Pmp21_D-mt [55] were transferred into the *E. coli* strain Origami for expression. Typically, for protein expression, 1 L of LB medium with the necessary selection marker (here: ampicillin 50 µg/ml) was inoculated with an $OD_{600}$ of 0.1 and incubated with shaking (140 rpm) at 37 °C until an $OD_{600}$ of 0.7 to 1 was reached. Then, protein expression was induced by adding isopropyl-β-D-thiogalactopyranoside (IPTG) at a final concentration of 1 mM IPTG. After 4 h of expression, the *E. coli* suspension was harvested at 5,000 rpm (Avanti J-20, Beckman Coulter) for 10 min. For protein purification under denaturing conditions, the pellet was first resuspended in 20 ml of lysis buffer (6 M guanidinium chloride, 20 mM Tris/HCl, 0.5 M NaCl, 1 mM β-mercaptoethanol) and incubated overnight at 4 °C on a rotating wheel. On the next day, the suspension was sonicated twice on ice for 30 sec each and centrifuged at 24,000 rpm and 4 °C (Avanti J-20, Beckman Coulter). After equilibration with lysis buffer, the lysate was loaded onto a HisTrap™ HP and washed with 20 ml each of washing buffer A pH 8 (8 M urea, 0.1 M $NaH_2PO_4$, 10 mM Tris/HCl, 1 mM β-mercaptoethanol, 20 mM imidazole) and 20 ml washing buffer B pH 6.3 ( 8 M urea, 0.1 M $NaH_2PO_4$, 10 mM Tris/HCl, 1 mM β-

mercaptoethanol, 40 mM imidazole). The protein was eluted with elution buffer pH 6.3 (8 M urea, 0.1 M $NaH_2PO_4$, 10 mM Tris/HCl, 1 mM β-mercaptoethanol, 500 mM imidazole). Protein concentration was determined by the Bradford assay according to a standard protocol. Protein purity was checked by Coomassie stained SDS-PAGE and Western blot. Depending on the experimental requirements, the protein solution was transferred into a dialysis tube (VISKING dialysis tubing, SERVA) and renatured at 4 °C in 1 l of PBS pH 7.4 or 30 mM Tris/HCl pH 7.4. The dialysis buffer was changed twice within 48 h. The purified protein was stored at 4 °C. For the preparation and usage of Pmp21_D-wt oligomers for density-gradient ultracentrifugation, Pmp21_D-wt protein was oligomerized for at least 72 h at 37 °C.

Purification of recombinant PrP

Expression and purification of recombinant full-length PrP and its fragments was performed as described previously (see [67] for PrP(23−230), PrP(23−144), PrP(90−230), and PrP(121−230) and [68] for PrP(23-111), respectively). PrP(23−111Δ41−94) was obtained as a synthetic peptide from peptides&elephants, and dissolved in Milli-Q water to a stock concentration of ~250 µM.

Infection-blocking experiment

The assay was performed as described in [69]. A confluent HEp-2 cell layer ($1 \times 10^6$ cells per well on a coverslip (12 mm diameter)) was washed once with Hanks' balanced salt solution (HBSS). Then 250 µl of 50 µg/ml dimAβ or Pmp21_D-wt in cell culture medium was added and the cells were incubated for 2 h at 37 °C and 6 % $CO_2$. PBS in cell culture medium was used as a negative control. Gradient-purified chlamydial EBs were then added to the protein solution (multiplicity of infection (MOI): 20) by swirling and without centrifugation, and incubated again for 2 h at 37 °C and 6 % $CO_2$. The solution was removed and replaced with 1 ml of *Chlamydia* culture medium. After 48 h at 37 °C in the presence of 6 % $CO_2$, the infected cells were fixed and permeabilized with 96 % methanol for 10 min, washed with PBS, and either stored at 4 °C or stained for direct immunofluorescence with a *Chlamydia*-specific antibody (Pathfinder; Bio-Rad). Inclusion bodies were quantified by counting 20 fields of view each. The result is reported as a percentage relative to the PBS-treated negative control.

Adhesion studies

Confluent layers of HEp-2, CHO-K1 or differentiated SH-SY5Y cells in 24-well plates were washed with cold HBSS. Subsequently, 260 µl of a 100 µg/ml solution of Pmp21_D-wt was prepared in cell culture medium. A 10-µl sample was taken for further analysis (input sample for Western blot) and mixed with 10 µl of 1 M dithiothreitol (DTT), 25 µl of 4× protein blue marker (200 mM Tris/HCl, 8 % SDS, 20 % glycerol, 0.2 % bromophenol blue) and 55 µl of PBS, and incubated at 100 °C for 10 min. Cells were exposed to the protein solution for different times (0 min (untreated), 1 min, 15 min, 30 min, 60 min) at 37 °C and 6 % $CO_2$, and then washed three times with HBSS. Cells were detached by incubation with 200 µl of cell-dissociation solution (Cell Dissociation Solution Non-enzymatic 1 x, Sigma-Aldrich; 10 min, 37 °C), transferred to a reaction tube, and pelleted by centrifugation for 5 min at 1,000 × g (Heraeus Biofuge Primo R). The cell dissociation solution was then removed and the pellet was resuspended in 97.5 µl PBS, 37.5 µl protein blue marker and 15 µl DTT. After incubation for 10 min at 100 °C, all samples were analyzed on Western blots.

Pull-down of native PrP using Pmp21_D-wt

Three confluent wells (6-well plate) containing HEp-2 or CHO-K1 cells were covered with 1.5 ml of 200 µg/ml recombinant Pmp21_D-wt in 30 mM Tris/HCl and incubated for 1 h at 37 °C. The protein solution was removed and the cells were gently washed 3 times each with 1 ml 30 mM Tris/HCl pH 7.4. Cells in each well were resuspended in 330 µl of phospho-lysis buffer (150 mM NaCl, 2 mM EDTA, 1 % Triton X100, 20 mM Tris pH 6.9, 1 mM $NaVO_4$, 1 % NP40) with protease inhibitor (1:100 dilution), combined in a 2-ml Eppendorf reaction tube, and sonicated on ice for 10 s with an ultrasonic rod (10 % power). After centrifugation at 10,000 × g for 10 min, the supernatant was transferred to a new reaction tube, and an input sample (65 µl supernatant + 25 µl 4 × protein blue marker + 10 µl 1 M DTT incubated at 100 °C for 10 min) was collected. Then 100 µl of Ni-NTA agarose was added to the lysate, mixed, and incubated for 1 h at 4 °C while swirling. Next, the sample was transferred to a SnapSpin column and centrifuged at 2,000 rpm for 2 min. The agarose was washed twice with 600 µl each of 30 mM Tris/HCl, 20 mM imidazole and 30 mM Tris/HCl, 40 mM imidazole. From each washing step, a sample of 65 µl was taken and processed like the input sample. The elution of Pmp21_D-wt and bound native PrP was performed by incubating the agarose in 100 µl 30 mM Tris/HCl 500 mM imidazole for 5 min, followed by centrifugation for 2 min at 8,000 rpm. Then 38.5 µl of protein blue marker and 15.4 µl of 1 M DTT were added to the eluate, incubated at 100 °C for 10 min, and analyzed by SDS PAGE and Western blot. The relative protein amounts on the

blots were determined using the software GelAnalyzer [70]. “Elution” values represent the amount of the relevant protein relative to that in the input lane.

Density gradient (ultra-)centrifugation (DGC)

*Sample preparation*: 10 µM of Pmp21_D-wt oligomers were co-incubated with 10 µM of PrP(23−144), PrP(23−230), PrP(23−111), PrP(90−230), PrP(121−230) or PrP(23−111Δ41−94) in 30 mM Tris/HCl (pH 7.4) for 1.5 h at room temperature. The numbers in brackets (PrP(XXX-XXX)) indicate amino acid positions. Alternatively, 15 µM dimAβ oligomers were co-incubated with 10 µM of either Pmp21_D-wt oligomers, PrP(23−230) or PrP(121−230) in 30 mM Tris/HCl (pH 7.4) for 1.5 h at room temperature. To analyze a sample containing 10 µM of Pmp21_D-wt oligomers, 15 µM dimAβ oligomers and 10 µM PrP(23-230) in 30 mM Tris/HCl, pH 7.4, both oligomer types were combined before PrP(23-230) was added and the sample was incubated for 1.5 h at room temperature. Pmp21_D-wt oligomers alone (10 µM), dimAβ oligomers alone (15 µM) or PrP(23−144) alone (10 µM) were used as controls. The final volume of each sample was 100 µl.

DGC: The method used is based on the QIAD protocol [71]. Each 100-µl sample was layered onto a buffered (30 mM Tris/HCl, pH 7.4) discontinuous sucrose gradient in an 11 mm × 34 mm centrifuge tube (for volumes and concentrations of the sucrose see ref. [67]). Centrifugation was carried out in an Optima MAX-XP ultracentrifuge (Beckman Coulter) equipped with a TLS-55 swing-out rotor (Beckman Coulter) for 3 h at 259,000 × g and 4 °C. Each gradient was fractionated manually from top to bottom into 13 142-µl fractions and the remaining volume was diluted with 80 µl of buffer (fraction 14).

Preparation of monomeric dimAβ for ThT kinetic analysis

DimAβ was recombinantly produced and prepared for kinetic analysis as previously described [65]. Briefly, lyophilized protein was dissolved in 6 M guanidinium chloride, 50 mM sodium-phosphate buffer (pH 7.4). To obtain monomeric dimAβ, size-exclusion chromatography was performed on a Superdex 75 increase column (GE Healthcare) equilibrated with 35 mM $Na_2HPO_4$, 50 mM NaCl, 5 mM NaOH (pH 11). The high pH was necessary to stabilize the monomeric state of dimAβ. Levels of dimAβ was determined based on UV absorption at 280 nm using the extinction coefficient 2,980 $M^{-1}cm^{-1}$. Immediately prior to the start of the ThT kinetics experiments the pH was adjusted using 1.5 % vol 1 M $NaH_2PO_4$, yielding 50 mM Na-phosphate, 50 mM NaCl (pH 7.4), as the final buffer composition. Monomeric peptide was processed on ice until the very start of the kinetic experiment.

CD spectroscopy

Far-UV CD spectra of Pmp21_D-wt and dimAβ were measured on a JASCO J-815 spectropolarimeter at a protein concentration of 0.2 mg/mL, corresponding to 8.5 µM Pmp21_D-wt or 20 µM dimAβ, in 1 mm Suprasil Quarz cuvettes (Hellma). In order to obtain a spectrum of monomeric dimAβ, its rapid oligomerization was prevented by measuring at 4 °C. All other spectra were recorded at 20 °C. Spectra of monomeric states of proteins were recorded immediately after elution of the monomer fraction from SEC. Spectra of the oligomeric states of proteins were recorded after elution of the monomer fraction from SEC and subsequent quiescent incubation for 100 h (Pmp21_D) or 24 h (dimAβ) in 50 mM Na-phosphate, 50 mM NaCl (pH 7.4). The oligomeric states of the samples were confirmed by AFM.

Amyloid formation assays using Thioflavin T (ThT) fluorescence

Measurements of growth kinetics were performed using a BMG ClarioStar plate reader with ThT excitation at 445 nm and emission collected at 482 nm in 96-well, low-binding, half-area plates (Greiner) which were sealed with transparent polypropylene films. Samples contained 10 µM ThT in 50 mM Na-phosphate buffer, 50 mM NaCl, pH7.4. Typically, three identical 100-µL samples were incubated at 37 °C. Measurements were taken every 3 min without shaking in between.

Atomic force microscopy (AFM)

To image protein assemblies, 25-µl aliquots of the samples were deposited on freshly cleaved muscovite mica slides. After 1 min of incubation at room temperature, samples were washed three times with 100 µl dd$H_2O$, and subsequently dried under $N_2$ gas. Imaging was performed in intermittent-contact mode (AC mode) in a JPK Nano Wizard 3 atomic-force microscope (JPK, Berlin) using a silicon cantilever with silicon tip (OMCLAC160TS-R3, Olympus) with a typical tip radius of 9 ± 2 nm, a force constant of 26 N/m and resonance frequency around 250 kHz. The images were processed using Gwyddion (version 2.56). False-color height images were superimposed over either amplitude images or phase images using Gimp (GNU Image Manipulation Program).

Data analysis of ThT kinetics

The polymerisation kinetics of Pmp21D and the first phase of the biphasic growth kinetics of dimAβ were fit to a superposition of a one-step oligomerization reaction $nM \rightarrow M_n$. The mass concentration of oligomers, $M_{gO/CF}$ , evolves in time according to the following expression [65]:

$$M_{gO/CF}(t) = M_0 - [M_0^{1-n} + (n-1)nkt]^{1/(1-n)} \quad \text{(Eqn. 1)}$$

with $M_0$ being the total protein concentration, k the oligomerization rate constant, and n the oligomer size or reaction order. Global fits to the concentration-dependent oligomer/protofibril formation data were performed with n and k as shared fit parameters. For both fits, the proportionality constant relating M(t) to ThT fluorescence intensity was treated as a fit parameter with an individual value for every sample.

Progeny experiment

A glass slide bearing a confluent layer of HEp-2 cells ($1 \times 10^6$ cells per well on a coverslip (12 mm diameter), control infection) and two glass slides bearing differentiated SH-SY5Y cells were infected with suspensions of *Chlamydia pneumoniae* (MOI: 2) in medium via centrifugation (1 h, 3,000 rpm, (ROTANTA 460R, Hettich)). The solution was then removed and replaced by 1 ml of *Chlamydia* culture medium. To control for successful infection, one slide of each cell line was fixed and permeabilized with methanol 48 h post infection (hpi), followed by staining with Pathfinder and DAPI. At 72 hpi, the second slide bearing infected SH-SY5Y cells was washed once with 1 ml $H_2O$ and any chlamydial progeny present were harvested by water lysis for 20 min in 200 µl $H_2O$, diluted 1/5 and 1/25 in total of 200 µl medium and used to infect HEp-2 cells (via centrifugation). At 48 hpi, cells were fixed. After staining with Pathfinder, inclusions in 20 visual fields each from three independent control and progeny infections (1/5 and 1/25) were counted, averaged, and compared to the control infection.

Coomassie stained SDS-PAGE and immunoblot analysis

Unless otherwise indicated, samples obtained from assays or elutions were mixed with the appropriate amounts of 4× protein blue marker (200 mM Tris/HCl, 8 % SDS, 20 % glycerol, 0.2 % bromophenol blue) and 5 µl of 1 M DTT, and incubated at 100 °C for 10 min. Subsequently, samples were loaded onto a 10 % or 15 % SDS gel and electrophoretically fractionated at 200 V for 80 min. Prior to Coomassie staining, the gel was washed three times in hot water and then transferred to a Coomassie solution (0.008 % Coomassie G-250, 35 mM HCl), heated again and shaken until protein bands were visible. For western blot and

immunodetection, the proteins on the unstained SDS gel were transferred to a polyvinylidene fluoride (PVDF) membrane. After incubation for 1 h in blocking solution (3 % milk powder, 0.05 % Tween 20 in TBS), the membranes were treated with primary anti-HIS antibody (mouse) 1:2,500 (Qiagen), anti-EGFR antibody (rabbit) 1:2,000 (Thermo Fisher Scientific), anti-PrP antibody (mouse) 1:1,000 (SAF 32; bertin-bioreagent) or anti-Actin (mouse) 1:2,500 (Sigma) for 1 h at RT, washed three times with TBS and then treated with secondary anti-mouse or anti-rabbit antibody coupled to alkaline phosphatase (AP) 1:30,000 (Sigma) for 1 h. After washing with TBS, the protein bands were visualized by incubation in detection solution (20 ml detection buffer (0.1 M Tris/HCl pH 9.5, 0.1 M NaCl, 50 mM $MgCl_2$) + 66 µl 5-brom-4-chlor-3-indoxylphosphate (BCIP) solution (0.5 g BCIP in 10 ml DMF) + 66 µl nitroblue tetrazolium (NBT) solution (0.5 g NBT in 10 ml 70% DMF). DGC fractions were analyzed by SDS-PAGE and subsequent silver staining. For this purpose, a sample of each fraction was diluted 1:1 in sample buffer (12 % glycerol, 4 % SDS, 50 mM Tris/HCl, pH 7.4, 2 % β-mercaptoethanol). For analysis, 15 % Tris/glycine gels capped by a 7 % stacking gel prepared according to standard protocols were used and loaded with 15 µl of each fraction. SDS-PAGE was performed at a constant voltage of 140 V and gels were silver stained according to a protocol based on Heukeshoven and Dernick [72].

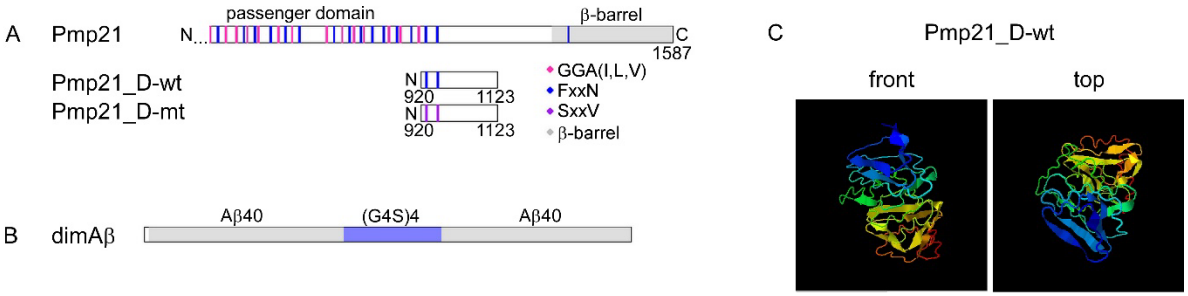


Figure 1: **A.** Schematic representation of full-length Pmp21 (Pmp21) and its fragments Pmp21_D-wt and Pmp21_D-mt. Pmp21 contains an N-terminal signal sequence (not shown), a central passenger domain containing GGA(I,L,V) (magenta) and FxxN (blue) motives, and a C-terminal β-barrel domain [55]. Pmp21_D-wt is a wild-type fragment of Pmp21 with adhesive properties [55]. In Pmp21_D-mt, the two FxxN motives have been replaced by SxxV motives, resulting in the complete loss of adhesive capacity and a weakend ability to form oligomers [54]. **B.** Schematic representation of dimAβ, which is comprised of two copies of Aβ40 that are connected by a 20-aa glycine-serine linker ((G4S)4) [65]. The graphics (A, B) were created with RStudio [73]. **C.** The structure of Pmp21_D-wt as predicted by I-Tasser (C-scores: Pmp21_D-wt (-3.05)). A C-score is usually in a range of -5 to 3, and the higher the score, the higher the confidence in the model [74].

## Results

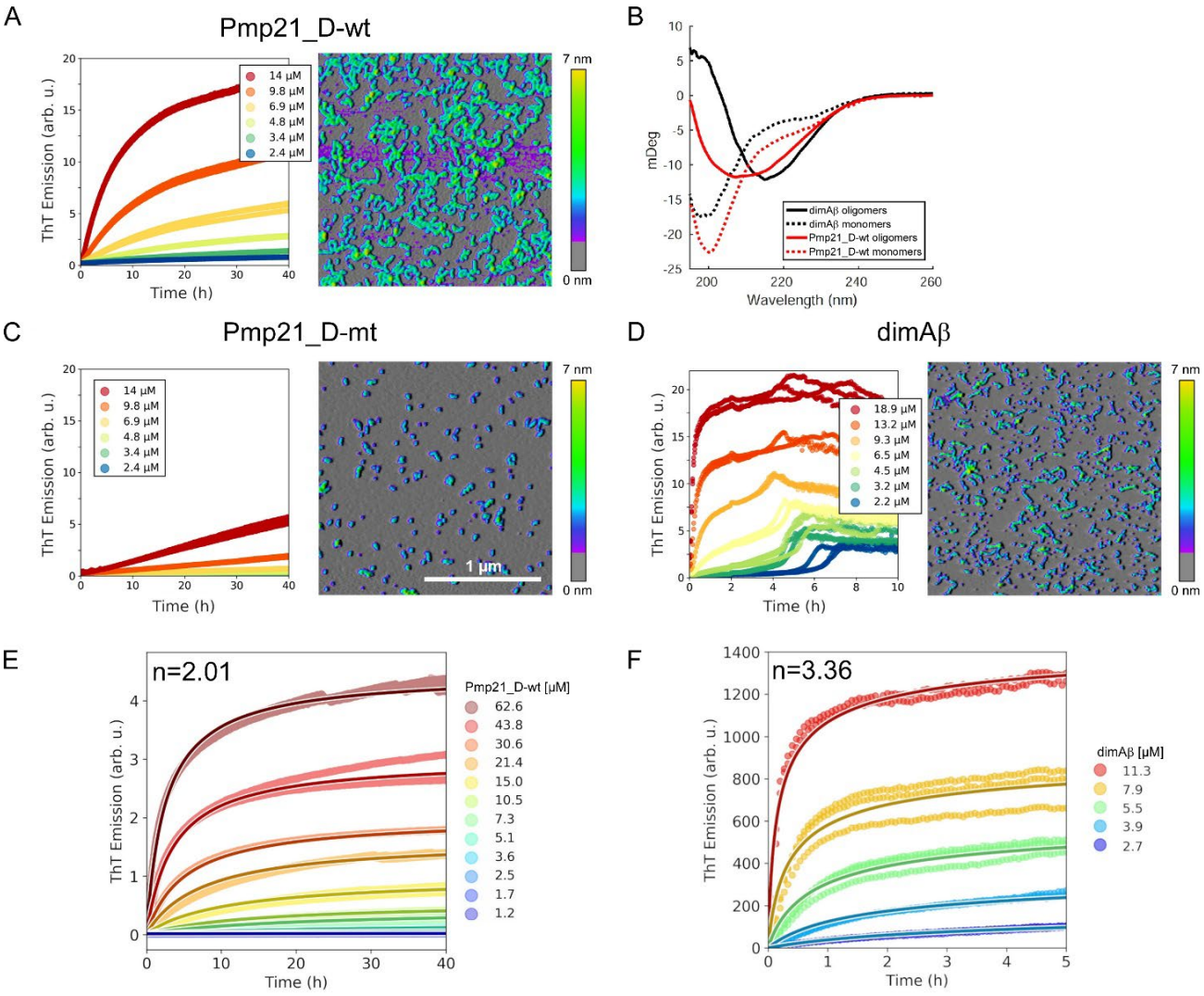


Figure 2: Kinetics of formation of protofibrillar aggregates formed by Pmp21_D-wt and dimAβ.

**A-F.** Concentration-dependent assembly time traces for Pmp21_D-wt (**A**,**E**), Pmp21_D-mt (**C**) and dimAβ (**D**,**F**) monitored by ThT fluorescence and representative atomic force microscopy (AFM) images of the corresponding assemblies. The AFM image of dimAβ shown in (**D**) is a representative sample (10 µM) taken during the initial assembly phase. Global fits to concentration-dependent time traces of Pmp21_D-wt assembly (**E**) and the initial phase of dimAβ assembly (**F**) based on a one-step oligomerization model (see Methods: Eqn. 1) [65] yielded reaction orders of 2.01 (**E**) and 3.36 (**F**), respectively. (**B**) Far-UV CD spectra of Pmp21_D-wt (red) and dimAβ (black) before (dashed lines) and after (solid lines) oligomer formation at a protein concentration of 0.2 mg/mL (corresponding to 8.5 µM Pmp21_D-wt or 20 µM dimAβ).

**Pmp21_D-wt oligomers and Aβ protofibrils exhibit similar lag-free formation kinetics**

We reported previously that Pmp21_D-wt forms oligomers with shapes similar to those of Aβ protofibrils [54]. Protofibrils are a specific type of Aβ assemblies with curvilinear shapes that result from "beads-on-a-string" accretion of spherical oligomers [65, 75-79]. The analysis of protein aggregation kinetics provides insight into the molecular mechanism of aggregation and can inform on the individual steps of the assembly reactions. For example, kinetic analysis demonstrated that Aβ protofibrils are not intermediates on the pathway to Aβ amyloid fibrils but represent an alternative, metastable aggregation product. Here, we compared the kinetics of Pmp21_D-wt oligomerization with those of Aβ assembly, in order to test if the mechanism of Pmp21_D-wt oligomerization might be related to that Aβ protofibril formation. We used the dye Thioflavin T (ThT) as a probe that shows increased fluorescence in the presence of both metastable oligomers and amyloid fibrils.

Incubation of monomeric Pmp21_D-wt at 37 °C resulted in a lag-free increase in ThT signal, which eventually saturated (Figure 2A, E). Samples obtained from this assay were examined by AFM and showed curvilinear assemblies with heights of about 4 nm (Figure 2A, right). CD spectroscopy indicated that the Pmp21_D-wt monomer is intrinsically disordered (Figure 2B), although structure prediction by I-Tasser proposes a β-helix fold (Figure 1C). Upon oligomerization, the random coil signal of the monomer was partially lost and a CD signal characteristic for β-sheet secondary structure emerged (Figure 2B). The negative control Pmp21_D-mt is a genetic mutation in which the two FxxN motifs have been replaced by two SxxN (Figure 1A). As expected, it showed only low ThT fluorescence and a strongly reduced number of oligomers of a height of approx. 1.5 - 4 nm (Figure 2C).

To facilitate the investigation of Aβ protofibril formation, we have previously introduced dimAβ, a dimeric Aβ variant in which two Aβ40 units are linked together in one polypeptide chain by a flexible glycine-serine linker (Figure 1B) [65]. The linkage of two Aβ units increases local Aβ concentration, which in turn sharpens the distinction between the kinetics of metastable oligomer formation and amyloid fibril formation [65].

Like Aβ40 and Aβ42, dimAβ exhibits biphasic assembly kinetics (Figure 2D) under conditions that favor oligomerization [65, 80, 81]. The first kinetic phase corresponds to oligomerization into protofibrillar oligomers. In contrast to amyloid fibril formation, this phase occurs without a lag, indicating that no nucleation step is involved in this oligomerization reaction. AFM images of the species formed during the first kinetic phase showed spherical and curvilinear aggregates with heights of approximately 3.5-4.5 nm (Figure 2D, right). As in the case of Pmp21_D-wt, formation of dimAβ oligomers resulted in the loss of random coils and gain of β-sheet secondary structure according to CD spectroscopy (Figure 2B). The second kinetic phase of dimAβ assembly, which is discernible as a second increase in ThT fluorescence, reflects amyloid fibril formation [65] (Figure 2D). The lag-time of this second phase can be attributed to

the primary and secondary nucleation steps that are prerequisites of nucleated polymerization of Aβ amyloid fibrils.

Upon comparing the assembly kinetics of Pmp21_D-wt (Figure 2A, E) with those of dimAβ (Figure 2D, F), we find that the timecourse of Pmp21_D-wt assembly is similar to that of the first kinetic phase of dimAβ assembly, i.e., formation of protofibrillar oligomers. In both cases, there is a lag-free increase in ThT fluorescence intensity which approaches a concentration-dependent steady state. The similarity of the formation kinetics is in line with the similar morphologies of the assemblies (Figure 2A, D), and suggests that these structures form through related mechanisms.

As we have shown previously, the concentration-dependent kinetics of dimAβ oligomerization can be fit to an $n^{th}$-order oligomerization reaction, $n\mathrm{M} \rightarrow \mathrm{M}_n$, with a global rate constant for all concentrations, yielding a high reaction order of $n = 3.3 \pm 0.2$ (Figure 2F) [65]. The high reaction order is evident in the raw data, which shows that a modest increase in protein concentration results in a dramatic acceleration of dimAβ oligomerization (Figure 2F). Considering that one dimAβ molecule contains two Aβ units, the reaction order of 3.3 suggests a size of six to seven Aβ units for the rate-limiting oligomer subunit. Pmp21_D-wt assembly can also be fit to the $n^{th}$-order oligomerization model (Figure 2E), again indicating that Pmp21_D-wt oligomers and dimAβ oligomers form through related mechanisms. In the case of Pmp21_D-wt, however, the reaction order is lower, with a value of ~2.0, which implies that initial dimerization of Pmp21_D-wt molecules is the rate-determining step in oligomer formation. In conclusion, the kinetic data suggest that Pmp21_D oligomerization occurs by a mechanism analogous to Aβ protofibril formation, with a lower number of Pmp21_D molecules sufficient to drive oligomer formation compared to Aβ.

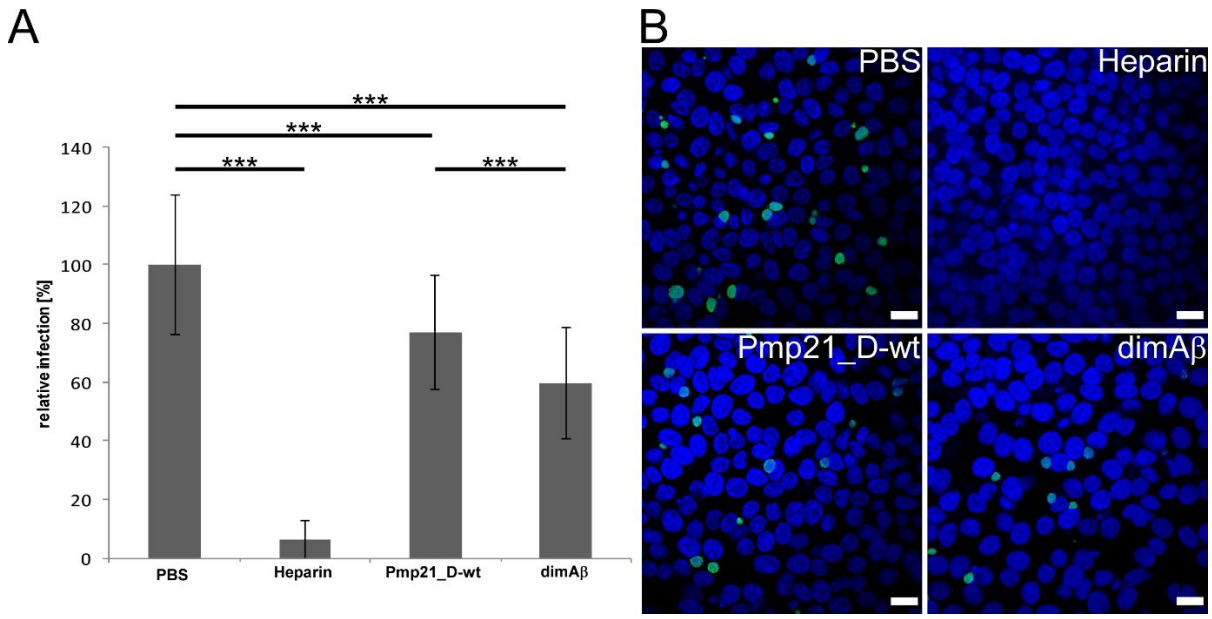


Figure 3: dimAβ, like Pmp21_D-wt, is able to reduce subsequent infection with *Cpn* after incubation with HEp-2 cells.

**A.** HEp-2 cells were pre-incubated with PBS, heparin, 50 µg/ml Pmp21_D-wt oligomers or 50 µg/ml dimAβ oligomers. They were then infected with *Chlamydia pneumoniae* (MOI: 20) and fixed 48 h post infection. After staining with *Chlamydia*-specific antibody (Pathfinder; green) and DAPI (blue; **B**), inclusions of 20 visual fields each from three independent infections were counted, averaged, and shown in relation to untreated cells (PBS). Data shown are means +/- S.D. Statistical significance was assessed with Student's t test (*, *P* = 0.05; **, *P* = 0.01; ***, *P* = 0.001; n.s. = not significant). Scale bars, 20 µm.

**Oligomeric dimAβ targets receptors that are relevant for *Chlamydia* infection.**

Viable *Chlamydia* have been found in brain areas of Alzheimer-diseased patients [82] and could have a direct effect on the development of AD [47], for example by promoting the pro-amyloidogenic pathway of APP processing [3]. Our experiments have so far demonstrated that Pmp21_D-wt and dimAβ form protofibrillar oligomers of similar shape and size with similar kinetics (Figure 2), suggesting that *Chlamydia* adhesins can adopt structures that are related to those of neurotoxic Aβ oligomers. To determine whether receptors implicated in the toxic activity of Aβ oligomers in AD play a role in chlamydial infection, we tested whether the presence of recombinant oligomeric dimAβ interferes with the establishment of a subsequent chlamydial infection. In this infection-blocking experiment, HEp-2 cells were first pretreated with recombinant Pmp21_D-wt or recombinant dimAβ oligomers, and then infected with *C. pneumoniae* (MOI: 20; Figure 3B). Pretreatment of HEp-2 cells with the positive control (heparin) reduced subsequent infection by approximately 94 %, compared to the negative control PBS (Figure 3A) [83]. Incubation of HEp-2 cells with Pmp21_D-wt oligomers diminished the subsequent *Cpn* infection by 23 %. Intriguingly, pretreatment with dimAβ oligomers reduced infection by approximately 40 %. Indeed, Aβ oligomers are

known to interact with and activate the epidermal growth factor receptor (EGFR) [84]. Thus, the infection-blocking capacity of dimAβ oligomers suggests that ,like Pmp21, they bind to EGFR or even more infection relevant receptors.

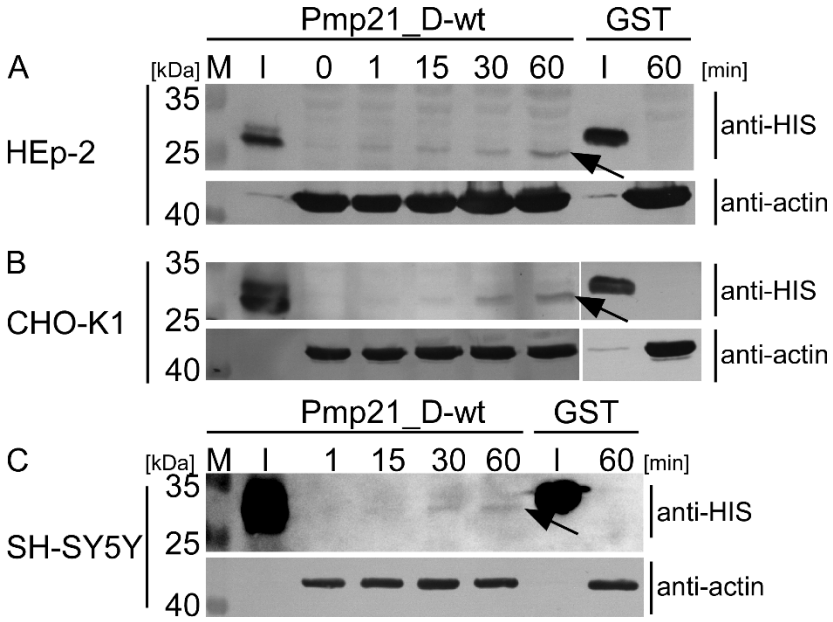


Figure 4: Recombinant Pmp21_D-wt oligomers bind to both EGFR- and non-EGFR-expressing mammalian cells.

HEp-2 (**A**), CHO-K1 (**B**), and SH-SY5Y (**C**) cells in 24-well plates were incubated with 100 µg/ml Pmp21_D-wt oligomers or GST (negative control; a cytosolic protein with no adhesive properties) for the indicated times (0 min, 1 min, 30 min or 60 min) at 37 °C. "0 min" refers to cells incubated with medium only. At the indicated time points, cells were harvested, mixed with sample buffer and analyzed by SDS-PAGE and on Western blots. For visualization, membranes were treated with anti-HIS (1:2,500, mouse) or anti-actin (1:2,500, mouse), followed by anti-mouse IgG-alkaline phosphatase antibody (1:30,000). Pmp21_D-wt is labelled with black arrows. Abbreviations used are: kilodalton (kDa), input (I), marker (M), minute (min).

**Recombinant Pmp21 adheres to EGFR-expressing and non-expressing mammalian cells**

*C. pneumoniae* Pmp21 is an adhesin and invasin that binds to EGFR of human cells [54, 61]. In order to test whether there are further receptors for Pmp21_D-wt, protein-binding studies were performed with recombinant Pmp21_D-wt oligomers on different EGFR-positive and -negative cell lines. In the positive control, binding of Pmp21_D-wt to human epithelial HEp-2 cells was first detected after 1 min and increased further until the 60-min time point, as previously described [54]. The epithelial cell line CHO-K1 (Chinese hamster ovary cells) does not express EGFR (Figure S 1) [85]. Interestingly, binding of Pmp21_D-wt to CHO-K1 cells was detectable after 15 min and increased in intensity over time. Finally, we tested whether Pmp21_D-wt binds to the differentiated neuroblastoma cell line SH-SY5Y, which is often used to study Parkinson's disease and AD's disease [86, 87]. Binding to SH-SY5Y cells was first detectable at 30 min

and had increased by the 60-min time point. In contrast, the negative control (recombinant GST) neither bound to HEp-2, CHO-K1 nor differentiated SH-SY5Y cells during the course of the experiment. These data support the hypothesis that Pmp21_D-wt has at least one more cellular binding partner besides EGFR and furthermore show that Pmp21_D-wt can, in principle, bind to neuronal cells.

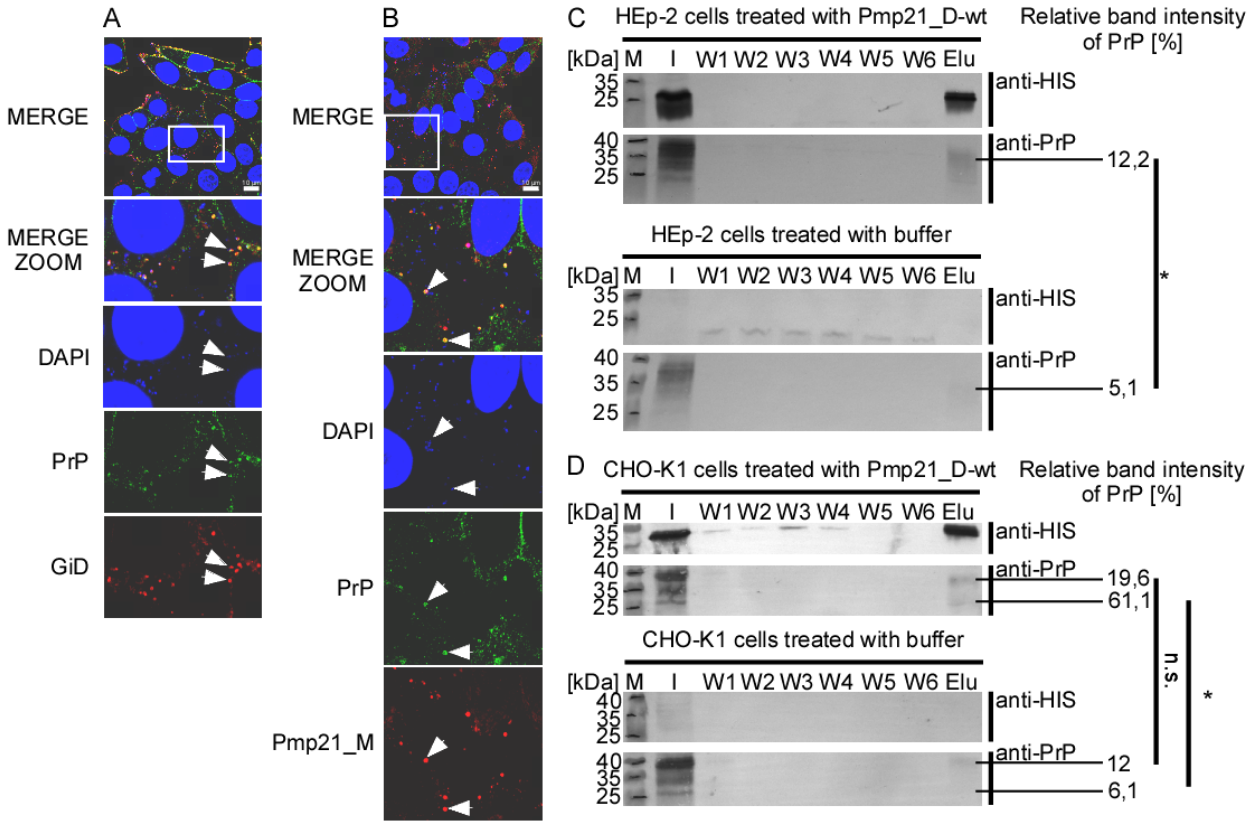


Figure 5: *Chlamydia pneumoniae* EBs colocalize with endogenous PrP on HEp-2 cells, which can be enriched with recombinant Pmp21_D-wt

**A. B.** Infection of HEp-2 cells with *Chlamydia pneumoniae* (MOI: 5). After 15 min of infection, cells were fixed (3 % paraformaldehyde (PFA)), permeabilized (MeOH) and immunostained with primary antibodies directed against either PrP (1:200, mouse; **A. B.**), GiD (1:40, rabbit); **A**) or Pmp21_M (1:25, rabbit; **B**)). Depending on the primary antibody, anti-mouse Alexa Fluor 488 (green) or anti-rabbit Alexa Fluor 594 (red) served as the secondary antibody. DAPI/DNA (blue). The area in the white box is shown at higher magnification in the inset. Arrows (white) indicate examples of colocalization between *Cpn* EBs and PrP. Scale bars, 10 µm. **C. D.** HEp-2 and CHO-K1 cells were incubated with Pmp21_D-wt or buffer (30 mM Tris pH 7.4). After cell lysis, native PrP bound to Pmp21_D-wt was enriched via affinity chromatography on Ni-NTA agarose. Samples were fractionated by SDS-PAGE and analyzed on Western blots. For visualization, membranes were treated with α-HIS (1:2,500, mouse) or anti-PrP (1:1,000, mouse) followed by anti-mouse IgG-alkaline phosphatase antibody (1:30,000). Band intensity was measured using the software GelAnalyzer2010a [70]. Numbers [%] represent the relative band intensity relative to the input. In every case, the data are derived from three independent experiments and blots. Abbreviations used are: Input (I), wash fractions (W1-W6), elution (Elu), kilodalton (kDa), marker (M).

### The human prion protein $PrP^C$ is an interaction partner for Pmp21_D-wt and is recruited to invading *Cpn* EBs

Since our data on the one hand suggest the presence of additional host-cell receptors (apart from EGFR) for Pmp21 (Figure 4B), and imply that Pmp21_D-wt can give rise to oligomeric and curvilinear protofibrils very similar to those formed by the amyloid dimAβ peptide (Figure 2), we tested whether the prion protein

(PrP) – which shows a particularly high binding capacity for Aβ oligomers [88-90] – serves as an additional Pmp21 interaction partner.

To determine whether there is a link between PrP and chlamydial infection, HEp-2 cells were infected with *Cpn* for 15 min. Interestingly, immunofluorescence microscopy indicated that chlamydial EB signals were indeed associated with PrP signals (Figure 5A, B). Next, we directly tested for interaction between oligomeric Pmp21_D-wt and the endogenous PrP receptor. On immunoblots, endogenous human PrP protein separates into three major bands, which are thought to represent the diglycosylated (38 kDa), the monoglycosylated (33 kDa) and the unglycosylated (26 kDa) isoforms of PrP, respectively [91]. HEp-2 cells were incubated with recombinant His-tagged Pmp21_D-wt and a direct interaction was probed by pulldown experiments. In the affinity-enriched Pmp21_D-wt fraction, significant amounts of PrP could also be detected (12.2 % of total input) (Figure 5C), while the buffer-treated control cells only contained 5.1 %, indicating a significantly Pmp21-mediated enrichment of PrP. Similarly, in Pmp21 pulldown experiments using CHO-K1 cells, the 26-kDa PrP was found to be significantly enriched in the elution fraction (61.1 % of input) compared to the buffer control experiment (6.1 % of input) (Figure 5D). The 38-kDa PrP protein was also enriched in the Pmp21 pulldown experiment (19.6 % of input versus 12 % without Pmp21). In conclusion, cellular PrP is associated with invading infectious chlamydial EBs during *Cpn* infection, and Pmp21_D-wt directly interacts with endogenous PrP.

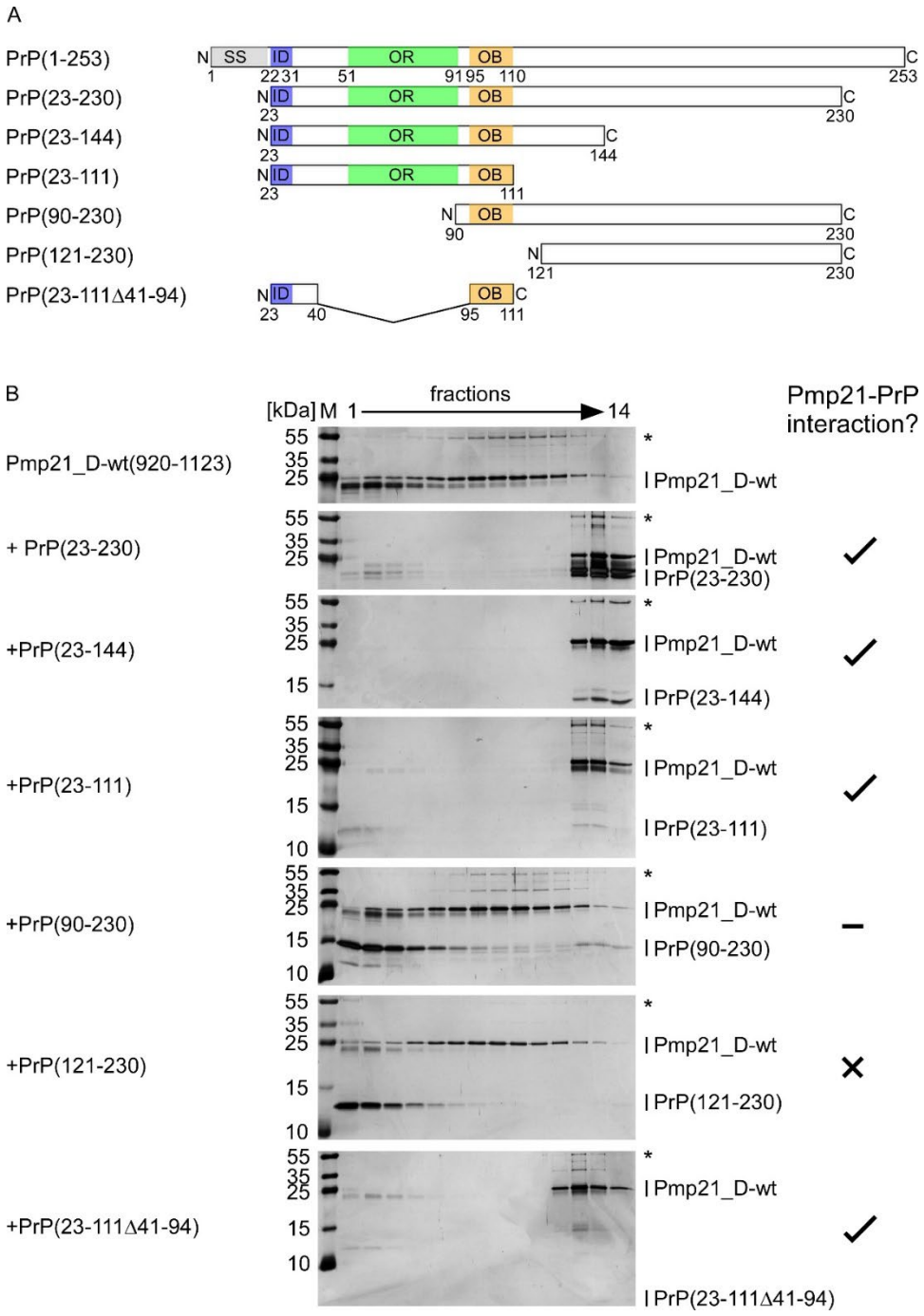


Figure 6: Interaction of Pmp21_D-wt with PrP variants

**A.** Graphical representations of the full-length PrP protein (PrP(1-253)) and its variants analyzed by sucrose-density-gradient ultracentrifugation (DGC). The ID domain (blue) is responsible for interdomain interactions [92], cell adhesion [93] and localization to lipid rafts [94]. OR (green) is the octarepeat region, and the OB region (orange) is important for binding of Aβ and α-synuclein oligomers. The graphic was created with RStudio [73]. **B.** Interaction of Pmp21_D-wt oligomers with the indicated fragments of PrP. Pmp21_D-wt oligomers (10 µM) were coincubated with of different PrP fragments in 30 mM Tris/HCl, pH 7.4 for 1.5 h at room temperature and then separated by DGC. 14 fractions were then collected from top to bottom and analyzed by silver-stained Tris/glycine SDS-PAGE. Monomeric proteins were found primarily in the top fractions, oligomeric proteins in the middle fractions and high-molecular-weight complexes in the heavy bottom fractions (right). Due to its small molecular

size, PrP(23-111Δ41-94) is only slightly visible in the gel (bottom figure). * indicate SDS-resistant Pmp21_D-wt dimers. Interaction is indicated by ✓ (interaction), - (weak interaction) or x (no visible interaction).

**PrP$^c$ protein domains required for binding of Aβ and Pmp21_D are conserved**

To further analyze the interaction between PrP and Pmp21_D-wt, and identify the PrP domain(s) involved, various fragments of soluble human PrP (Figure 6A) were incubated with Pmp21_D-wt oligomers and analyzed by sucrose-density-gradient centrifugation (DGC). The OB domain is known to be essential for the binding of Aβ (1-42) oligomers [68] and the formation of large hetero-assemblies [67, 68]. This was also the case for the dimAβ construct used in this study, which formed hetero-assemblies with full-length PrP(23-230), but not with the N-terminally truncated PrP(121-230) construct (Figure S 4).

We analyzed Pmp21_D-wt oligomers by separating the protein mixtures according to size by DGC (Figure 6B). The Pmp21_D-wt oligomers themselves showed a broad distribution and were found in fractions 1 to 14, with the highest concentrations occurring in fractions 6 to 11. A degraded Pmp21_D-wt fragment (seen below the full-length protein in Figure 6B) was mainly found in fractions 1 to 3. Interestingly, incubation of Pmp21_D-wt oligomers with PrP(23-230) and the N-terminal fragments PrP(23-144) or PrP(23-111) resulted in a massive shift of the Pmp21_D-wt protein bands to higher fraction numbers (11-14), containing complexes of higher molecular weights. The corresponding PrP fragments were also found in fractions 11 to 14. It has previously been shown that the soluble PrP protein itself is found mainly in the low-molecular-weight fractions 1 to 3 [67]. These data therefore indicate that the ID-, OR- and OD-harboring PrP fragments formed large, heteroassemblies with oligomeric Pmp21_D-wt. In contrast, analysis of the C-terminal PrP(90-230) fragment (harboring only the OD domain) with Pmp21_D-wt revealed very little complex formation, with only a small amount of Pmp21 and PrP protein being found in the high-molecular-weight fractions 12 to 14. The additional N-terminal deletion variant PrP(121-230), which lacks the OB domain, shows no capacity for complex formation with Pmp21_D-wt oligomers at all. Previous work had shown that the ID domain in combination with the OB domain binds to Aβ(1-42) oligomers [95]. Thus, we tested the corresponding PrP fusion construct PrP(23-111Δ41-94) for its capacity to interact with Pmp21_D-wt oligomers, and found that the two proteins formed high-molecular-weight complexes that appeared in fractions 11 to 14 (Fig. 6B).

In conclusion, Pmp21_D-wt oligomers can form heterogeneous aggregates with PrP, similar to those found for Aβ(1-42) oligomers [67, 68]. The PrP deletion study reveals that the ID and OB domains within the flexible PrP N-terminus are essential for the formation of these heteromeric complexes. The interaction of Pmp21_D-wt oligomers with the N-terminal PrP(23-111) fragment harboring ID and OB domains was also confirmed in a pulldown experiment, while the C-terminal PrP fragment PrP(121-230) showed very little interaction (Figure S 5).

**Discussion**

*Chlamydia pneumoniae* infects the upper and lower respiratory tract [4]. The infectious EBs bind to the host cell epithelia via specific adhesins and invasins [96], among which the family of Pmp proteins are essential [55, 97]. Central to Pmp function are multiple FxxN and GGA(I,L,V) peptide motifs within the central passenger domain, with at least two motifs being required for successful binding to the host receptor [55]. It has been shown that Pmp21 binds to and activates the EGFR, inducing its own uptake and therefore acting both as an adhesin and invasin [61]. Pmp proteins from *Ctr* and from *Cpn* form homo- and hetero-oligomers and at least two FxxN motifs are necessary for effective folding, oligomerization and adhesive properties [54, 64]. Infections with *Cpn* are suspected to play a role in the development of Alzheimer's disease [3].

AD is a neurodegenerative brain disease and the most common cause of dementia worldwide. AD is a multifactorial condition that is influenced by genetic and environmental factors, very likely including infections by a number of pathogenic microbes, with several viruses and the intracellularly replicating bacterium *Cpn* being the most prominent ones [45, 98-100]. Over the past 25 years, experimental evidence for a direct association between a *Cpn* infection and AD has accumulated [45-47, 82, 101]. However, direct molecular evidence for such an association has been lacking.

Initially, we provided evidence that a fragment of the *Cpn* adhesin and invasin Pmp21, Pmp21-D, formed oligomers and protofibrils comparable to Aβ [54]. In this study, we determined the oligomerization kinetics of monomeric Pmp21_D-wt, its point-mutated version Pmp21_D-mt and dimAβ, purified by size-exclusion chromatography. As expected from previous work [54], Pmp21_D-wt showed a concentration-dependent oligomerization rate, which was significantly faster than that of the negative control Pmp21_D-mt. This was confirmed by AFM, which revealed the formation of significantly more, and considerably larger, oligomers and protofibrils in the case of Pmp21_D-wt (Figure 2A, C, D). Interestingly, assembly kinetics of Pmp21_D-wt and the first oligomerization phase of dimAβ were almost identical. Both demonstrated a lag-free increase in their ThT signals, as well as yielding curvilinear aggregates (Figure 2A, D, E, F). In addition, CD spectroscopy showed for both proteins a spectrum indicative of intrinsic disorder in the monomeric state and a signal corresponding to β-sheet secondary structure in their oligomeric form (Fig. 2 B). Finally, the oligomerization kinetics of both proteins could be fitted to an $n^{th}$-order oligomerization model. All these similarities point to a common mechanism of oligomer formation. Aβ is generated by the cleavage of the amyloid precursor protein (APP), mediated by β- and γ-secretases and resulting in 36- to 43-amino-acids long Aβ peptides, with molecular weights of around 4.5 kDa, which include the amyloidogenic species Aβ40, Aβ42 and Aβ43 [102]. The protofibrillar

Aβ oligomers thought to be the main neurotoxic species are heterogeneous in size, spanning a range of approx. 50 to 1,500 kDa [75-78, 103]. Interestingly, Pmp21_D-wt, as well as *Ctr* Pmp fragments, have been shown to form oligomeric structures in the range of approx. 600 to over 1,300 kDa [64]. Owing to the large size of the Pmp fragments, Pmp oligomers may consist of approx. 12 (100 kDa, PmpD fragment) to over 50 (25 kDa, PmpA fragment) monomers [64]. Thus, neither Pmp nor Aβ segments adopt one particular dominant oligomeric entity, but form a broad spectrum of differently sized oligomers.

Recent research suggests that Pmp full-length and processed forms could form homo- and hetero-oligomeric structures on the EB surface that exhibit adhesive properties [64]. *Cpn* Pmp21 and its *Ctr* homolog PmpD localize to the chlamydial cell surface, where they undergo extensive processing [56, 57, 59, 104]. Thus, it is possible that processed Pmp fragments that lack the outer membrane attachment β-barrel-domain detach from the chlamydial cell surface and together with, or in addition to, other Pmp fragments [64] or other chlamydial proteins, form soluble homo- and hetero-oligomeric structures. Pmps are essential proteins in chlamydial infection [55, 61]. These soluble oligomeric structures could represent a further defense mechanism of *Chlamydiae*, in which soluble homomeric or heteromeric oligomers act as "dummy EBs" to counteract part of the immune response by binding antibodies directed against EBs. Moreover, the soluble oligomers could bind again to EBs (demonstrated in [64]), leading to an enhanced concentration of adhesins possibly enhancing adhesion, or bind to additional human receptors and induce yet unknown effects.

The similarities between the biophysical properties of Aβ and Pmp oligomers prompted us to test whether dimAβ oligomers had any effects on chlamydial infection. Pre-treatment of cells with dimAβ oligomers resulted in a reduction of the subsequent infection by approx. 40 % (Fig. 3). This suggests that Pmp21 and Aβ bind to at least one common receptor. This is consistent with studies showing that Aβ is able to bind to a wide range of cell-surface receptors, including EphB2, TNF-R1, RAGE1, the NMDA receptor, $PrP^C$ and the EGFR [84, 105-107]. Binding (and hence blocking) of the EGFR by oligomerized dimAβ would consequently result in reduced binding of proteins such as Pmp21 and thus in an attenuated infection. Indeed, Aβ peptides have long been associated with anti-microbial activity, and are thought to serve as a defensive component of innate immunity [108, 109]. Individuals are at great risk of being infected by *Cpn* throughout their live. By the age of 20 years, about 50 % of individuals have antibodies against *Cpn*, and the incidence rises to 80 % in people aged 60-70 years [4]. It is therefore plausible that, in response to early and recurring chlamydial infections, Aβ formation could be stimulated as a form of immune defense and thus, in addition to its infection-inhibiting effect, could contribute to the development of AD.

Our studies have demonstrated that recombinant oligomeric Pmp21_D-wt binds to EGFR-expressing HEp-2 and differentiated SH-SY5Y cells, as well as to non-EGFR-expressing CHO-K1 cells (Figure 4). The ability

of *Cpn* to infect neuronal cells seems reasonable and necessary in the context of findings of viable *Cpn* in brain biopsies [45, 101]. In addition, several studies show that *Cpn* are able to infect neuronal cells [110-112]. Whether neuronal cells are typical hosts, which have received less attention so far, or whether they play only a secondary role has not yet been widely investigated. However, poor replication ability in SH-SY5Y cells, at least in the sense of proliferation of chlamydial material (Figure S 6), points to the latter. Additionally, we found evidence for binding of Pmp21_D-wt to non-EGFR-expressing CHO-K1 cells pointing to additional receptors. A larger number of possible binding partners for Pmp21 on the human cellular surface could increase the chance of binding to a host cell, increase the diversity of signaling and thus increase the probability of a successful infection.

Based on the structural and functional similarities between dimAβ and Pmp21_D-wt identified so far, we tested $PrP^C$ (described as one of the receptors for Aβ [34]) as a possible further human interaction partner for Pmp21_D-wt. Short-term infection experiments showed distinct colocalization between $PrP^C$ and chlamydial EBs at 15 min post infection (Figure 5A, B). This indicates that chlamydial EBs might use $PrP^C$ during the entry process. Pull-down experiments in which native $PrP^C$ could be enriched by interaction with Pmp21_D-wt suggest that Pmp21 may be one of the chlamydial surface proteins that can bind to $PrP^C$ (Figure 5C, D). This is the first evidence for a potential function of $PrP^C$ in microbial infections. The interaction could be advantageous for *Cpn*, as binding of the human HS-1-associated protein X-1 (HAX-1) to $PrP^C$ can mediate anti-apoptotic activity [113]. If binding of Pmp21 oligomers also has such an effect, a subsequent infection would benefit as a result.

The assumption that Pmp21 oligomers binds to $PrP^C$ is strengthened by the results of the DGC, in which binding of Pmp21_D-wt oligomers to specific $PrP^C$ domains such as ID and OB could be shown (Figure 6); these same domains have already described as important binding sites for oligomeric Aβ [67]. Upon binding, $PrP^C$ and Pmp21_D-wt oligomers form high molecular weight assemblies. This mode of interaction was previously observed for $PrP^C$ with Aβ oligomers or α-synuclein oligomers [67, 68, 114]. The interaction is dependent on multivalent interactions of oligomers with the flexible PrP N-terminus, which might modulate the receptor distribution at the cell membrane [68]. Furthermore, co-incubation of dimAβ oligomers with Pmp21_D-wt oligomers did not result in the formation of large structures (Figure S 4). Addition of PrP(23-230) to both premixed oligomers results in a shift of all proteins to high-molecular-weight fractions, indicating that PrP can co-assemble with Pmp21_D-wt oligomers and Aβ oligomers. Initial protein binding studies in which cells were pre-treated with PrP-specific antibodies (SAF32, CD230) failed to prevent subsequent binding of recombinant Pmp21_D-wt oligomers (Figure S 2). This may be due to the limitations of the available antibodies, which do not recognize the N-terminal end that is particularly important for the binding properties of $PrP^C$. Alternatively, it may indicate the existence of further

important receptors for Pmp21_D-wt oligomers. This may also explain why pre-treatment of cells with CD230 also had no effect on infectivity (Figure S 3). Future neutralization experiments should therefore be repeated with an N-terminal-specific PrP antibody.

In this study, we were able to show that there are significant similarities between oligomeric Pmp21_D-wt and dimAβ. Their oligomerization kinetics indicate that they make use of very similar assembly mechanisms. Moreover, oligomers and protofibrils showed very similar sizes and structures as analyzed by AFM. Preincubation of human cells with dimAβ reduced subsequent infectivity by *Cpn*. Pmp21_D-wt not only bound to EGFR, but also to specific binding domains of $PrP^C$. All of the players involved in this study play a role in the development of AD [38, 42, 115, 116]. We therefore propose that Pmp21 may initiate or contribute to the development of AD through two different mechanisms.

In an ordinary infection, *Cpn* enters the body via the olfactory system and subsequently infects the lung tissue. Within this process, they possibly enter the brain via infection of the olfactory bulbs that connect the oral cavity with the brain and subsequently lead to infections in other regions such as caudate, putamen and piriform cortex [47, 48]. In addition, it has already been shown that *Cpn* are able to infect macrophages respectively monocytes and resist in their persistent form within those cells, digestion for up to three days. This would allow transport through the blood system and penetration of the blood-brain barrier [49-51]. In the brain, EBs can bind to neuronal cells by either surface-attached Pmps, processed Pmp fragments (and further adhesins) binding to EGFR, the $PrP^C$ and other unknown receptors to infect them. If *Cpn* are a potential causer or contributor for the development of AD, it is either due to the infection of neuronal cells or a matter of signaling events mediated by Pmp21-$PrP^C$ interaction.

In the first scenario, Pmp21 fragments without β-barrel – and likely also fragments of the other Pmps on the EB cell surface – detach from the chlamydial surface and oligomerize. Pmp oligomers (and possibly also oligomers anchored on the EB surface) bind to the cell surface receptor $PrP^C$ and by analogy to oligomeric Aβ trigger a toxic signaling pathway [36] in which the Pmp21-$PrP^C$ complex leads to phosphorylation of FYN via mGluR5, and ultimately to synaptic toxicity and neuronal dysfunction (Figure 7).

In the second scenario, soluble oligomers could induce an inflammation in the infected brain areas, which would lead to an increased production of Aβ peptides as a defense response [108, 109]. It has already been shown that *Cpn* Pmp20 and Pmp21 are able to trigger a dose-dependent inflammatory response in human endothelial cells through the production of the inflammatory mediators interleukin (IL)-6, IL-8 and monocyte chemoattractant protein-1 (MCP-1) and activation of the NF-κB pathway [117]. Studies have shown that strong activation of the NF-κB pathway increases the likelihood of developing AD, while suppression of this pathway reduces the likelihood of AD development [118].

Pmps are multifunctional proteins. Recently, it has been suggested that Pmps, in addition to acting as adhesins and invasins, may also provide protection against the host immune response. Due to the high number of single Pmp proteins, combined with processed Pmp forms and the ability to interact with each other, generate an enormous antigenic variation on the surface of the EB that *Chlamydiae* could use as a decoy against the host immune response [64]. Additionally, it is conceivable that Pmp oligomers, as a local enrichment of infection-relevant antigen, could act as "dummy EBs" and bind antibodies of the immune response.

In conclusion, this study provides the first molecular evidence for a direct role of a *Chlamydia pneumoniae* infection in the mechanisms of AD development. The strong similarities between the biophysical properties of the chlamydial adhesin Pmp21 and the Aβ peptide and the binding properties of both proteins to the cellular co-receptor $PrP^C$ provide evidence for a role of the chlamydial Pmp proteins in AD development.

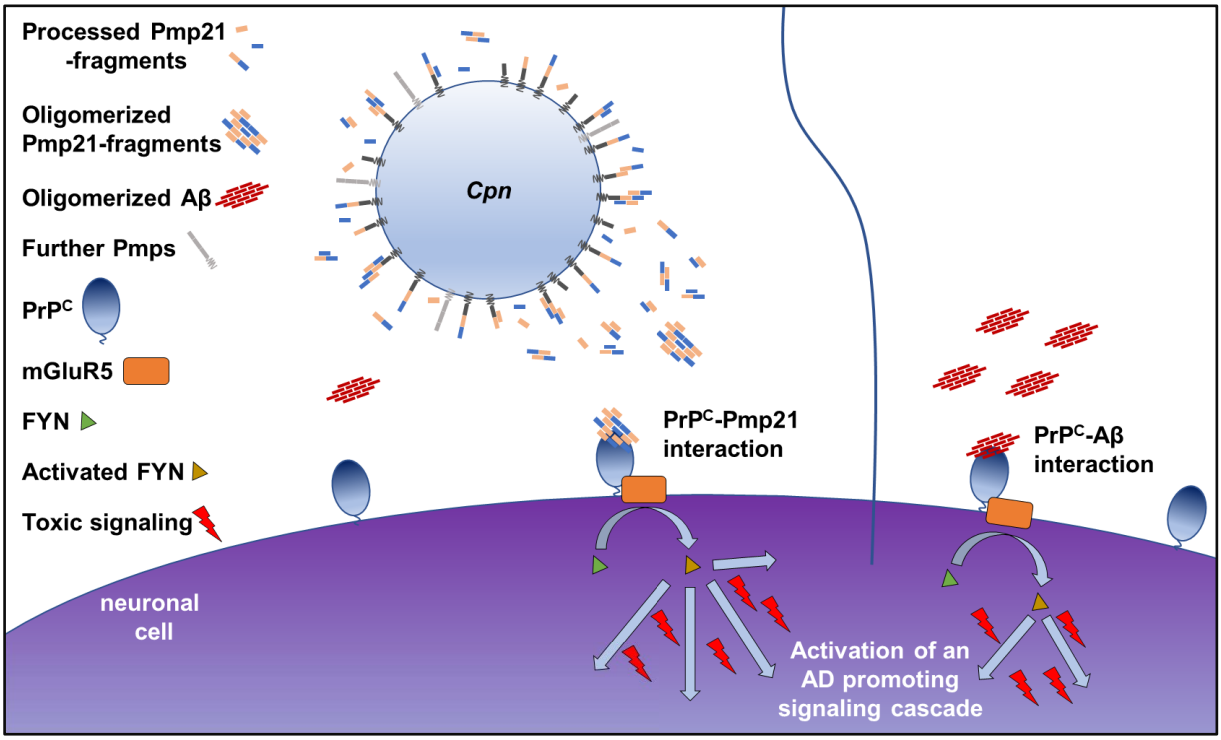


Figure 7: Hypothetical model. Soluble Pmp21 oligomers lead to an AD promoting signaling cascade.
During chlamydial infection, infectious *Chlamydiae* enter the host brain [45, 46]. On the surface of the chlamydium are a number of different adhesins, including the Pmp family, that facilitate adhesion and subsequent invasion into the host cell [52, 54, 55]. Pmps are anchored to the surface via their C-terminal β-barrel. They are subject to strong processing and can detach from the surface as Pmp fragments (without β-barrel), bind to other Pmp proteins/fragments and subsequently generate homomeric and heteromeric oligomeres [52, 56-60, 64]. Comparable to oligomeric Aβ, Pmp21 oligomers bind to $PrP^C$ in addition to the previously published EGFR [61] and consequently trigger activation of FYN via mGluR5, which subsequently leads to an AD-promoting signaling cascade.

## Supplements

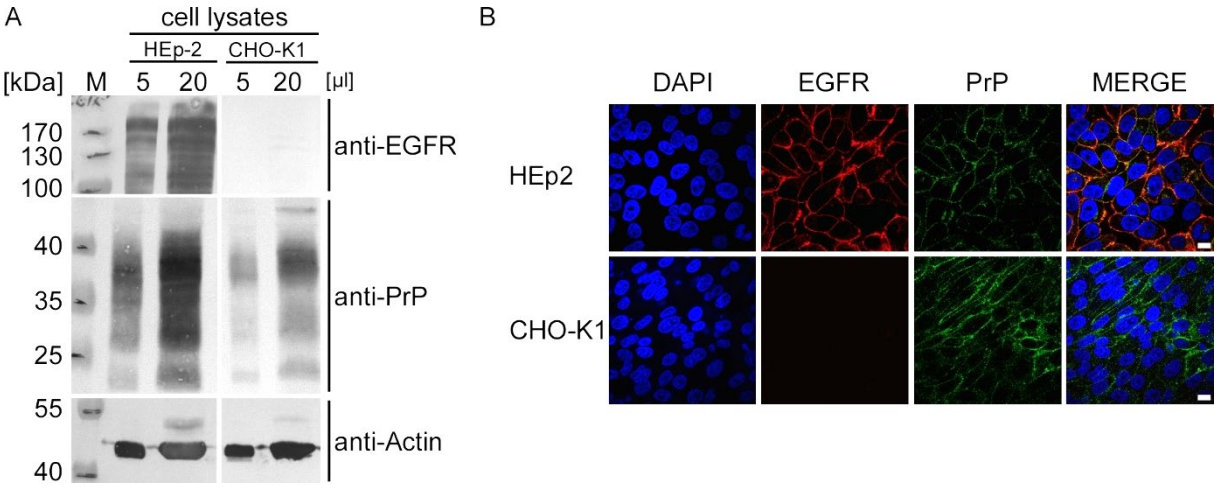


Figure S 1: Expression of EGFR and PrP in HEp-2 and CHO-K1 cells.

A. HEp-2 and CHO-K1 cells were lysed with phospho-lysis buffer and the processed samples were analyzed by SDS-PAGE and Western blot. Anti-EGFR (1:2,000, rabbit), anti-PrP (1:1,000, mouse) and anti-actin were used as primary antibodies. Depending on the primary antibody, anti-mouse IgG-alkaline phosphatase antibody (1:30,000) or anti-rabbit IgG-alkaline phosphatase antibody (1:30,000) served as the secondary antibody. B. HEp-2 and CHO-K1 cells were grown, fixed (3% PFA), permeabilized (MeOH) and immunostained with appropriate primary antibodies (EGFR 1:400, rabbit; PrP 1:200, mouse). Depending on the primary antibody, anti-mouse Alexa Fluor 488 (green) or anti-rabbit Alexa Fluor 594 (red) served as the secondary antibody. DAPI/DNA (blue). Scale bar 10 µm.

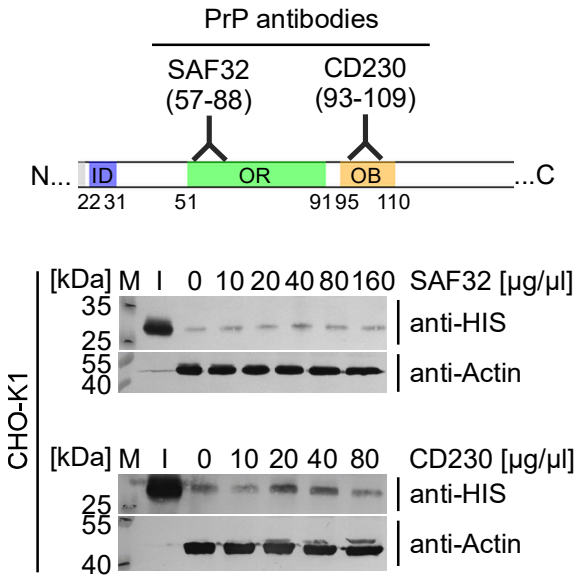


Figure S 2: Pre-incubation with PrP antibodies has no effect on subsequent adhesion of Pmp21_D-wt to CHO-K1 cells.

CHO-K1 cells were confluently seeded on 24-well plates. The medium was then removed and replaced with medium containing the indicated concentrations of SAF32 or CD230 (clone 6D11, Biolegend). After 2 h, Pmp21_D-wt was added to the medium at a final concentration of 200 ug/ml. As in a standard adhesion assay, cells were subsequently washed, detached, and bound protein was analyzed via SDS-PAGE and Western blot. The graphic was created with RStudio [73].

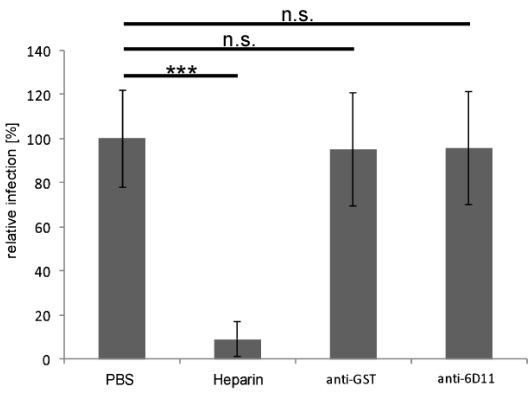


Figure S 3: Pre-incubation of HEp-2 cells with antibodies against PrP (CD230) does not inhibit subsequent infection with *Chlamydia pneumoniae*
HEp-2 cells were pre-incubated with either PBS, 1.25 µg/ml heparin, 20 µg/ml anti-CD230 (antibody 6D11), or 20 µg/ml anti-GST. They were then infected with *Chlamydia pneumoniae* (MOI: 20) and fixed after 48 h. After staining with *Chlamydia*-specific antibody (Pathfinder), inclusions of 20 visual fields each from 3 independent infections were counted, averaged, and results are shown in relation to untreated cells (PBS). Data shown are the means +/- S.D. Statistical significance was assessed with Student's t test (*, p = 0.05; **, p = 0.01; ***, p = 0.001; n.s. = not significant).

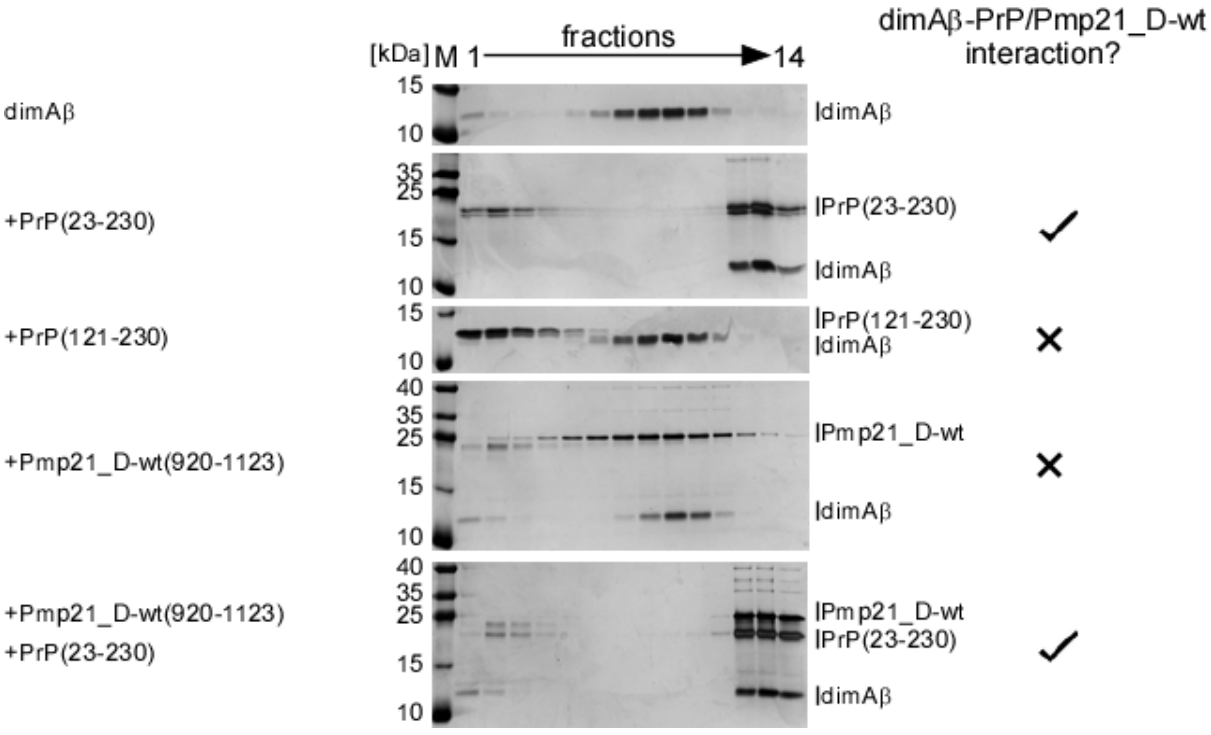


Figure S 4: Heteroassembly formation of dimAβ and huPrP fragments and Pmp21_D-wt
dimAβ and different huPrP fragments or/and Pmp21_D-wt were mixed, incubated together, and fractionated by sucrose-density-gradient ultracentrifugation (DGC). Fractions were then collected from top to bottom and analyzed by silver-stained Tris/glycerol SDS-PAGE. Monomeric proteins were found primarily in the initial fractions, oligomeric proteins in the middle fractions and high molecular weight complexes in the bottom fractions (right).

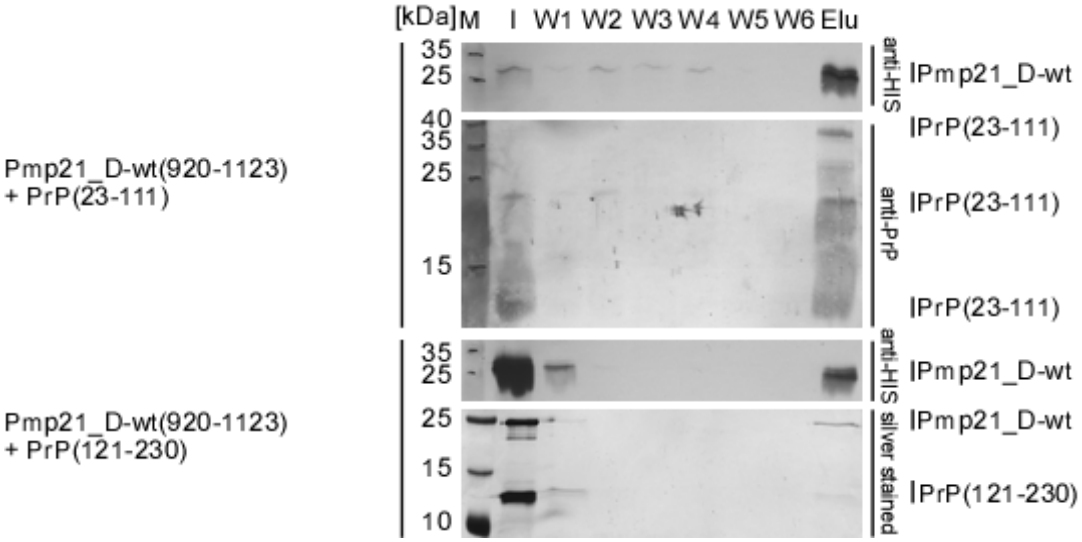


Figure S 5: Recombinant Pmp21_D-wt interacts with the N-terminal portion of PrP in pulldown assays.

Pmp21_D-wt oligomers and the indicated PrP fragments were mixed at a concentration of 10 µM and incubated together exactly as for DGC. Subsequently, pulldown assays were performed with Ni-NTA agarose to enrich for Pmp21 and its bound PrP interaction partner. After sample preparation, SDS-PAGE and Western blotting, membranes were treated with α-HIS (1:2,500, mouse) or anti-PrP (1:1,000, mouse) followed by an anti-mouse IgG-alkaline phosphatase antibody (1:30,000). Since no antibody was available for the detection of PrP(121-230), the SDS gel was silver stained. Input (I). Wash fractions (W1-W6). Elution (Elu). Kilodalton (kDa). Marker (M)

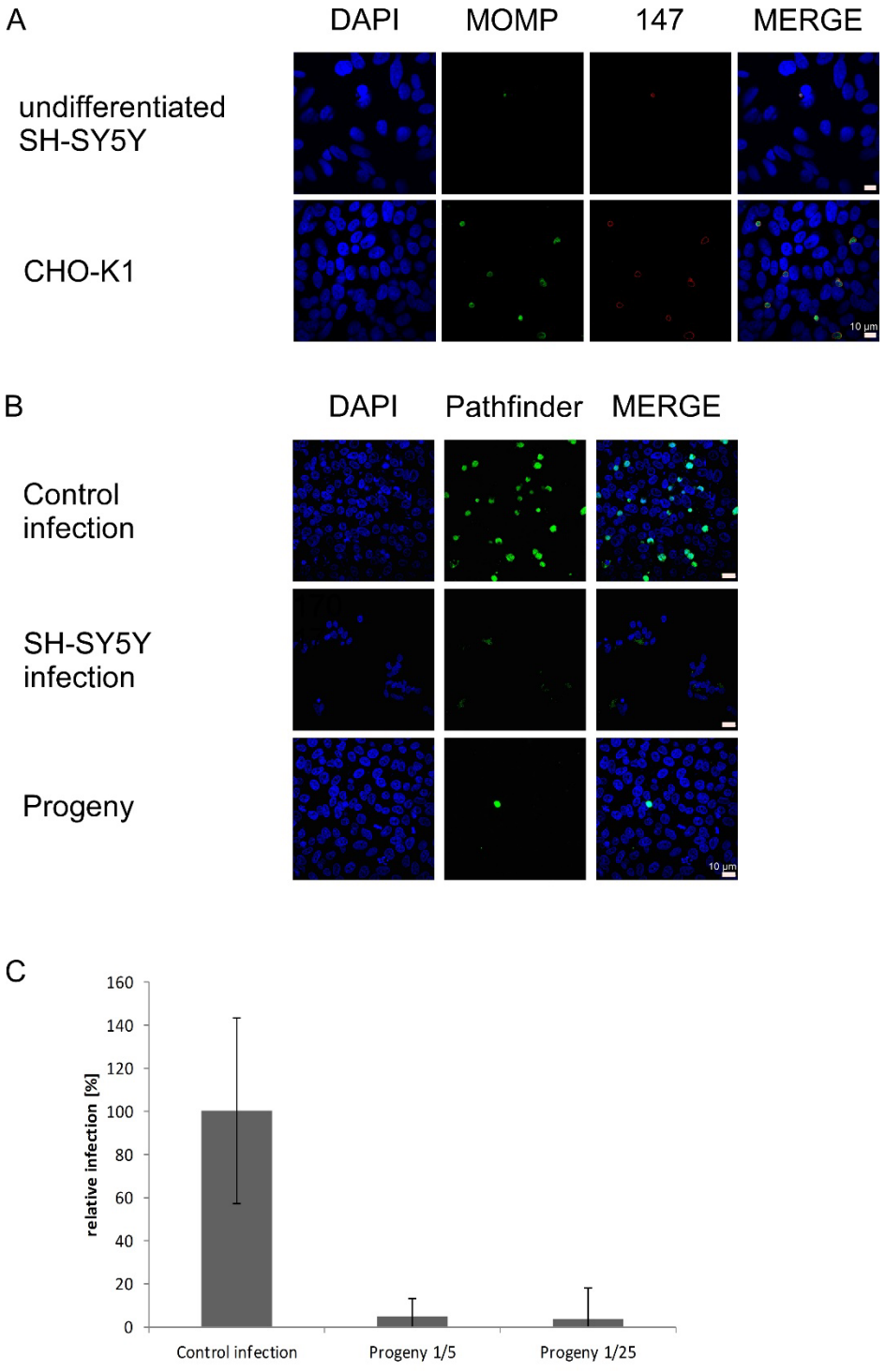


Figure S 6

A. Undifferentiated SH-SY5Y and CHO-K1 cells were infected with *Chlamydia pneumoniae* (MOI: 4). At 48 hpi they were fixed (PFA 3%), permeabilized (MeOH) and stained with an antibody against the major outer membrane protein MOMP (mouse, 1:100), and anti-147[?] (rabbit, 1:50). Depending on the primary antibody, anti-mouse Alexa Fluor 488 (green) or anti-rabbit Alexa Fluor 594 (red) served as secondary antibody. DAPI/DNA (blue). Scale bar 10 µm

B and C. To determine whether chlamydial infection of SH-SY5Y results in EBs that are viable and capable of initiating a new infection, a progeny assay was performed. For this, a glass slide bearing confluent HEp2 cells (control infection) and two glass slides bearing differentiated SH-SY5Y cells were infected with *Chlamydia pneumoniae* (MOI 2). To control for successful infection, one HEp-2 slide and SH-SY5Y slide was fixed and permeabilized with methanol at 48 hpi, and stained with Pathfinder and DAPI. B. Rows 1 (control infection) and 2 (SH-SY5Y infection). The third glass slide bearing infected SH-SY5Y cells was harvested by water lysis at 72 h, diluted 1/5 and 1/25 in medium and these samples were used to infect HEp2 cells, which were then fixed at 48 hpi. After staining with *Chlamydia*-specific antibody (Pathfinder), inclusions of 20 visual fields each from three independent control infections and two progeny infections (1/5 and 1/25) were counted, averaged, and shown in relation to the control infection. DAPI/DNA (blue), Pathfinder/Inclusions (green). Scale bar 10 µm.

## References


1. Bachmann, N.L., A. Polkinghorne, and P. Timms, *Chlamydia genomics: providing novel insights into chlamydial biology.* Trends Microbiol, 2014. **22**(8): p. 464-72.
2. Ceovic, R. and S.J. Gulin, *Lymphogranuloma venereum: diagnostic and treatment challenges.* Infect Drug Resist, 2015. **8**: p. 39-47.
3. Al-Atrache, Z., et al., *Astrocytes infected with Chlamydia pneumoniae demonstrate altered expression and activity of secretases involved in the generation of beta-amyloid found in Alzheimer disease.* BMC Neurosci, 2019. **20**(1): p. 6.
4. Kuo, C.C., et al., *Chlamydia pneumoniae (TWAR).* Clin Microbiol Rev, 1995. **8**(4): p. 451-61.
5. Wang, C., N. Zhang, and L. Gao, *Association between Chlamydia pneumoniae infection and lung cancer: a meta-analysis.* Transl Cancer Res, 2019. **8**(8): p. 2813-2819.
6. Littman, A.J., L.A. Jackson, and T.L. Vaughan, *Chlamydia pneumoniae and lung cancer: epidemiologic evidence.* Cancer Epidemiol Biomarkers Prev, 2005. **14**(4): p. 773-8.
7. Tan, M., J. Hegemann, and C. Suetterlin, *Chlamydia Biology: From Genome to Disease*. 2020, Norfolk, UK: Caister Academic Press. 570.
8. Bastidas, R.J., et al., *Chlamydial intracellular survival strategies.* Cold Spring Harb Perspect Med, 2013. **3**(5): p. a010256.
9. Dautry-Varsat, A., A. Subtil, and T. Hackstadt, *Recent insights into the mechanisms of Chlamydia entry.* Cell Microbiol, 2005. **7**(12): p. 1714-22.
10. Panzetta, M.E., R.H. Valdivia, and H.A. Saka, *Chlamydia Persistence: A Survival Strategy to Evade Antimicrobial Effects in-vitro and in-vivo.* Front Microbiol, 2018. **9**: p. 3101.
11. *Dementia*. 2021 [cited 2022 03.31.2022].
12. Mendez, M.F., *Early-Onset Alzheimer Disease.* Neurol Clin, 2017. **35**(2): p. 263-281.
13. Bertram, L., C.M. Lill, and R.E. Tanzi, *The genetics of Alzheimer disease: back to the future.* Neuron, 2010. **68**(2): p. 270-81.
14. Panza, F., et al., *Time to test antibacterial therapy in Alzheimer's disease.* Brain, 2019. **142**(10): p. 2905-2929.
15. Sochocka, M., K. Zwolinska, and J. Leszek, *The Infectious Etiology of Alzheimer's Disease.* Curr Neuropharmacol, 2017. **15**(7): p. 996-1009.
16. Lane, C.A., J. Hardy, and J.M. Schott, *Alzheimer's disease.* Eur J Neurol, 2018. **25**(1): p. 59-70.
17. Muller, U.C., T. Deller, and M. Korte, *Not just amyloid: physiological functions of the amyloid precursor protein family.* Nat Rev Neurosci, 2017. **18**(5): p. 281-298.
18. Reiss, A.B., et al., *Amyloid toxicity in Alzheimer's disease.* Rev Neurosci, 2018. **29**(6): p. 613-627.
19. Gabriele, R.M.C., et al., *Knockdown of Amyloid Precursor Protein: Biological Consequences and Clinical Opportunities.* Front Neurosci, 2022. **16**: p. 835645.
20. Sciacca, M.F., et al., *Two-step mechanism of membrane disruption by Abeta through membrane fragmentation and pore formation.* Biophys J, 2012. **103**(4): p. 702-10.
21. Kawarabayashi, T., et al., *Dimeric amyloid beta protein rapidly accumulates in lipid rafts followed by apolipoprotein E and phosphorylated tau accumulation in the Tg2576 mouse model of Alzheimer's disease.* J Neurosci, 2004. **24**(15): p. 3801-9.
22. Hong, S., et al., *Soluble Abeta oligomers are rapidly sequestered from brain ISF in vivo and bind GM1 ganglioside on cellular membranes.* Neuron, 2014. **82**(2): p. 308-19.
23. Lai, A.Y. and J. McLaurin, *Mechanisms of amyloid-Beta Peptide uptake by neurons: the role of lipid rafts and lipid raft-associated proteins.* Int J Alzheimers Dis, 2010. **2011**: p. 548380.
24. Lee, S.J., et al., *Towards an understanding of amyloid-beta oligomers: characterization, toxicity mechanisms, and inhibitors.* Chem Soc Rev, 2017. **46**(2): p. 310-323.
25. Mroczko, B., et al., *Cellular Receptors of Amyloid beta Oligomers (AbetaOs) in Alzheimer's Disease.* Int J Mol Sci, 2018. **19**(7).

26. Miranzadeh Mahabadi, H. and C. Taghibiglou, *Cellular Prion Protein (PrPc): Putative Interacting Partners and Consequences of the Interaction.* Int J Mol Sci, 2020. **21**(19).
27. Bremer, J., et al., *Axonal prion protein is required for peripheral myelin maintenance.* Nat Neurosci, 2010. **13**(3): p. 310-8.
28. Wang, L.Q., et al., *Cryo-EM structure of an amyloid fibril formed by full-length human prion protein.* Nat Struct Mol Biol, 2020. **27**(6): p. 598-602.
29. Glynn, C., et al., *Cryo-EM structure of a human prion fibril with a hydrophobic, protease-resistant core.* Nat Struct Mol Biol, 2020. **27**(5): p. 417-423.
30. Wille, H. and J.R. Requena, *The Structure of PrP(Sc) Prions.* Pathogens, 2018. **7**(1).
31. Kraus, A., et al., *High-resolution structure and strain comparison of infectious mammalian prions.* Mol Cell, 2021. **81**(21): p. 4540-4551 e6.
32. Horwich, A.L. and J.S. Weissman, *Deadly conformations--protein misfolding in prion disease.* Cell, 1997. **89**(4): p. 499-510.
33. Ugalde, C.L., et al., *Pathogenic mechanisms of prion protein, amyloid-beta and alpha-synuclein misfolding: the prion concept and neurotoxicity of protein oligomers.* J Neurochem, 2016. **139**(2): p. 162-180.
34. Lauren, J., et al., *Cellular prion protein mediates impairment of synaptic plasticity by amyloid-beta oligomers.* Nature, 2009. **457**(7233): p. 1128-32.
35. Kong, C., et al., *Binding between Prion Protein and Abeta Oligomers Contributes to the Pathogenesis of Alzheimer's Disease.* Virol Sin, 2019. **34**(5): p. 475-488.
36. Brody, A.H. and S.M. Strittmatter, *Synaptotoxic Signaling by Amyloid Beta Oligomers in Alzheimer's Disease Through Prion Protein and mGluR5.* Adv Pharmacol, 2018. **82**: p. 293-323.
37. Bate, C. and A. Williams, *Amyloid-beta-induced synapse damage is mediated via cross-linkage of cellular prion proteins.* J Biol Chem, 2011. **286**(44): p. 37955-37963.
38. Kudo, W., et al., *Cellular prion protein is essential for oligomeric amyloid-beta-induced neuronal cell death.* Hum Mol Genet, 2012. **21**(5): p. 1138-44.
39. Heiss, J.K., et al., *Early Activation of Experience-Independent Dendritic Spine Turnover in a Mouse Model of Alzheimer's Disease.* Cereb Cortex, 2017. **27**(7): p. 3660-3674.
40. Chung, E., et al., *Anti-PrPC monoclonal antibody infusion as a novel treatment for cognitive deficits in an Alzheimer's disease model mouse.* BMC Neurosci, 2010. **11**: p. 130.
41. Gimbel, D.A., et al., *Memory impairment in transgenic Alzheimer mice requires cellular prion protein.* J Neurosci, 2010. **30**(18): p. 6367-74.
42. Um, J.W., et al., *Alzheimer amyloid-beta oligomer bound to postsynaptic prion protein activates Fyn to impair neurons.* Nat Neurosci, 2012. **15**(9): p. 1227-35.
43. Piekut, T., et al., *Infectious agents and Alzheimer's disease.* J Integr Neurosci, 2022. **21**(2): p. 73.
44. Li, F., M. Hearn, and L.E. Bennett, *The role of microbial infection in the pathogenesis of Alzheimer's disease and the opportunity for protection by anti-microbial peptides.* Crit Rev Microbiol, 2021. **47**(2): p. 240-253.
45. Balin, B.J., et al., *Identification and localization of Chlamydia pneumoniae in the Alzheimer's brain.* Med Microbiol Immunol, 1998. **187**(1): p. 23-42.
46. Gerard, H.C., et al., *Chlamydophila (Chlamydia) pneumoniae in the Alzheimer's brain.* FEMS Immunol Med Microbiol, 2006. **48**(3): p. 355-66.
47. Little, C.S., et al., *Chlamydia pneumoniae induces Alzheimer-like amyloid plaques in brains of BALB/c mice.* Neurobiol Aging, 2004. **25**(4): p. 419-29.
48. Little, C.S., et al., *Age alterations in extent and severity of experimental intranasal infection with Chlamydophila pneumoniae in BALB/c mice.* Infect Immun, 2005. **73**(3): p. 1723-34.
49. Gieffers, J., et al., *Chlamydia pneumoniae infection in circulating human monocytes is refractory to antibiotic treatment.* Circulation, 2001. **103**(3): p. 351-6.
50. Gieffers, J., et al., *Phagocytes transmit Chlamydia pneumoniae from the lungs to the vasculature.* Eur Respir J, 2004. **23**(4): p. 506-10.
51. MacIntyre, A., et al., *Chlamydia pneumoniae infection promotes the transmigration of monocytes through human brain endothelial cells.* J Neurosci Res, 2003. **71**(5): p. 740-50.
52. Grimwood, J. and R.S. Stephens, *Computational analysis of the polymorphic membrane protein superfamily of Chlamydia trachomatis and Chlamydia pneumoniae.* Microb Comp Genomics, 1999. **4**(3): p. 187-201.
53. Henderson, I.R. and A.C. Lam, *Polymorphic proteins of Chlamydia spp.--autotransporters beyond the Proteobacteria.* Trends Microbiol, 2001. **9**(12): p. 573-8.
54. Luczak, S.E., et al., *The Chlamydia pneumoniae Adhesin Pmp21 Forms Oligomers with Adhesive Properties.* J Biol Chem, 2016. **291**(43): p. 22806-22818.
55. Molleken, K., E. Schmidt, and J.H. Hegemann, *Members of the Pmp protein family of Chlamydia pneumoniae mediate adhesion to human cells via short repetitive peptide motifs.* Mol Microbiol, 2010. **78**(4): p. 1004-17.

56. Swanson, K.A., et al., *Chlamydia trachomatis polymorphic membrane protein D is an oligomeric autotransporter with a higher-order structure.* Infect Immun, 2009. **77**(1): p. 508-16.
57. Kiselev, A.O., et al., *Expression, processing, and localization of PmpD of Chlamydia trachomatis Serovar L2 during the chlamydial developmental cycle.* PLoS One, 2007. **2**(6): p. e568.
58. Tan, C., et al., *Variable expression of surface-exposed polymorphic membrane proteins in in vitro-grown Chlamydia trachomatis.* Cell Microbiol, 2010. **12**(2): p. 174-87.
59. Wehrl, W., et al., *From the inside out--processing of the Chlamydial autotransporter PmpD and its role in bacterial adhesion and activation of human host cells.* Mol Microbiol, 2004. **51**(2): p. 319-34.
60. Montigiani, S., et al., *Genomic approach for analysis of surface proteins in Chlamydia pneumoniae.* Infect Immun, 2002. **70**(1): p. 368-79.
61. Molleken, K., E. Becker, and J.H. Hegemann, *The Chlamydia pneumoniae invasin protein Pmp21 recruits the EGF receptor for host cell entry.* PLoS Pathog, 2013. **9**(4): p. e1003325.
62. Vandahl, B.B., et al., *The expression, processing and localization of polymorphic membrane proteins in Chlamydia pneumoniae strain CWL029.* BMC Microbiol, 2002. **2**: p. 36.
63. Grimwood, J., L. Olinger, and R.S. Stephens, *Expression of Chlamydia pneumoniae polymorphic membrane protein family genes.* Infect Immun, 2001. **69**(4): p. 2383-9.
64. Favaroni, A. and J.H. Hegemann, *Chlamydia trachomatis Polymorphic Membrane Proteins (Pmps) Form Functional Homomeric and Heteromeric Oligomers.* Front Microbiol, 2021. **12**: p. 709724.
65. Hasecke, F., et al., *Origin of metastable oligomers and their effects on amyloid fibril self-assembly.* Chem Sci, 2018. **9**(27): p. 5937-5948.
66. Jantos, C.A., et al., *Antigenic and molecular analyses of different Chlamydia pneumoniae strains.* J Clin Microbiol, 1997. **35**(3): p. 620-3.
67. Rosener, N.S., et al., *A d-enantiomeric peptide interferes with heteroassociation of amyloid-beta oligomers and prion protein.* J Biol Chem, 2018. **293**(41): p. 15748-15764.
68. Rosener, N.S., et al., *Clustering of human prion protein and alpha-synuclein oligomers requires the prion protein N-terminus.* Commun Biol, 2020. **3**(1): p. 365.
69. Moelleken, K. and J.H. Hegemann, *The Chlamydia outer membrane protein OmcB is required for adhesion and exhibits biovar-specific differences in glycosaminoglycan binding.* Mol Microbiol, 2008. **67**(2): p. 403-19.
70. Istvan Lazar Jr., P.a.I.L.S., PhD, CSc *GelAnalyzer 2010a*.
71. Brener, O., et al., *QIAD assay for quantitating a compound's efficacy in elimination of toxic Abeta oligomers.* Sci Rep, 2015. **5**: p. 13222.
72. Heukeshoven, J. and R. Dernick, *Improved silver staining procedure for fast staining in PhastSystem Development Unit. I. Staining of sodium dodecyl sulfate gels.* Electrophoresis, 1988. **9**(1): p. 28-32.
73. Team, R., *RStudio: Integrated Development Environment for R*. 2021, RStudio, PBC. p. Used code by Fabienne Kocher.
74. Zhang, Y., *I-TASSER server for protein 3D structure prediction.* BMC Bioinformatics, 2008. **9**: p. 40.
75. Ono, K. and M. Tsuji, *Protofibrils of Amyloid-beta are Important Targets of a Disease-Modifying Approach for Alzheimer's Disease.* Int J Mol Sci, 2020. **21**(3).
76. Chromy, B.A., et al., *Self-assembly of Abeta(1-42) into globular neurotoxins.* Biochemistry, 2003. **42**(44): p. 12749-60.
77. Jan, A., D.M. Hartley, and H.A. Lashuel, *Preparation and characterization of toxic Abeta aggregates for structural and functional studies in Alzheimer's disease research.* Nat Protoc, 2010. **5**(6): p. 1186-209.
78. Walsh, D.M., et al., *Amyloid beta-protein fibrillogenesis. Detection of a protofibrillar intermediate.* J Biol Chem, 1997. **272**(35): p. 22364-72.
79. Walsh, D.M., et al., *Amyloid beta-protein fibrillogenesis. Structure and biological activity of protofibrillar intermediates.* J Biol Chem, 1999. **274**(36): p. 25945-52.
80. Hasecke, F., et al., *Protofibril-Fibril Interactions Inhibit Amyloid Fibril Assembly by Obstructing Secondary Nucleation.* Angew Chem Int Ed Engl, 2021. **60**(6): p. 3016-3021.
81. Schutzmann, M.P., et al., *Endo-lysosomal Abeta concentration and pH trigger formation of Abeta oligomers that potently induce Tau missorting.* Nat Commun, 2021. **12**(1): p. 4634.
82. Hammond, C.J., et al., *Immunohistological detection of Chlamydia pneumoniae in the Alzheimer's disease brain.* BMC Neurosci, 2010. **11**: p. 121.
83. Wuppermann, F.N., J.H. Hegemann, and C.A. Jantos, *Heparan sulfate-like glycosaminoglycan is a cellular receptor for Chlamydia pneumoniae.* J Infect Dis, 2001. **184**(2): p. 181-7.
84. Wang, L., et al., *Epidermal growth factor receptor is a preferred target for treating amyloid-beta-induced memory loss.* Proc Natl Acad Sci U S A, 2012. **109**(41): p. 16743-8.
85. Nogami, M., et al., *Requirement of autophosphorylated tyrosine 992 of EGF receptor and its docking protein phospholipase C gamma 1 for membrane ruffle formation.* FEBS Lett, 2003. **536**(1-3): p. 71-6.
86. Xicoy, H., B. Wieringa, and G.J. Martens, *The SH-SY5Y cell line in Parkinson's disease research: a systematic review.* Mol Neurodegener, 2017. **12**(1): p. 10.

87. de Medeiros, L.M., et al., *Cholinergic Differentiation of Human Neuroblastoma SH-SY5Y Cell Line and Its Potential Use as an In vitro Model for Alzheimer's Disease Studies.* Mol Neurobiol, 2019. **56**(11): p. 7355-7367.
88. Beraldo, F.H., et al., *Regulation of Amyloid beta Oligomer Binding to Neurons and Neurotoxicity by the Prion Protein-mGluR5 Complex.* J Biol Chem, 2016. **291**(42): p. 21945-21955.
89. Aimi, T., et al., *Dextran sulfate sodium inhibits amyloid-beta oligomer binding to cellular prion protein.* J Neurochem, 2015. **134**(4): p. 611-7.
90. Nygaard, H.B., *Targeting Fyn Kinase in Alzheimer's Disease.* Biol Psychiatry, 2018. **83**(4): p. 369-376.
91. Pan, T., et al., *Heterogeneity of normal prion protein in two- dimensional immunoblot: presence of various glycosylated and truncated forms.* J Neurochem, 2002. **81**(5): p. 1092-101.
92. McDonald, A.J., et al., *Altered Domain Structure of the Prion Protein Caused by Cu(2+) Binding and Functionally Relevant Mutations: Analysis by Cross-Linking, MS/MS, and NMR.* Structure, 2019. **27**(6): p. 907-922 e5.
93. Schmitt-Ulms, G., et al., *Binding of neural cell adhesion molecules (N-CAMs) to the cellular prion protein.* J Mol Biol, 2001. **314**(5): p. 1209-25.
94. Taylor, D.R., I.J. Whitehouse, and N.M. Hooper, *Glypican-1 mediates both prion protein lipid raft association and disease isoform formation.* PLoS Pathog, 2009. **5**(11): p. e1000666.
95. Rösener, N., *Functional and structural characterization of the Aß-PrP interaction*. 2019, Heinrich-Heine-Universität Düsseldorf: Universität- und Landesbibliothek.
96. Elwell, C., K. Mirrashidi, and J. Engel, *Chlamydia cell biology and pathogenesis.* Nat Rev Microbiol, 2016. **14**(6): p. 385-400.
97. Becker, E. and J.H. Hegemann, *All subtypes of the Pmp adhesin family are implicated in chlamydial virulence and show species-specific function.* Microbiologyopen, 2014. **3**(4): p. 544-56.
98. Pogo, B.G., J. Casals, and T.S. Elizan, *A study of viral genomes and antigens in brains of patients with Alzheimer's disease.* Brain, 1987. **110 ( Pt 4)**: p. 907-15.
99. Friedland, R.P., C. May, and J. Dahlberg, *The viral hypothesis of Alzheimer's disease. Absence of antibodies to lentiviruses.* Arch Neurol, 1990. **47**(2): p. 177-8.
100. Itzhaki, R.F., et al., *Herpes simplex virus type 1 in brain and risk of Alzheimer's disease.* Lancet, 1997. **349**(9047): p. 241-4.
101. Balin, B.J., et al., *Chlamydia pneumoniae: An Etiologic Agent for Late-Onset Dementia.* Front Aging Neurosci, 2018. **10**: p. 302.
102. Chuang, E., et al., *Amyloid assembly and disassembly.* J Cell Sci, 2018. **131**(8).
103. Sehlin, D., et al., *Large aggregates are the major soluble Abeta species in AD brain fractionated with density gradient ultracentrifugation.* PLoS One, 2012. **7**(2): p. e32014.
104. Kiselev, A.O., M.C. Skinner, and M.F. Lampe, *Analysis of pmpD expression and PmpD post-translational processing during the life cycle of Chlamydia trachomatis serovars A, D, and L2.* PLoS One, 2009. **4**(4): p. e5191.
105. Leissring, M.A., et al., *Enhanced proteolysis of beta-amyloid in APP transgenic mice prevents plaque formation, secondary pathology, and premature death.* Neuron, 2003. **40**(6): p. 1087-93.
106. Du, Y., et al., *alpha2-Macroglobulin as a beta-amyloid peptide-binding plasma protein.* J Neurochem, 1997. **69**(1): p. 299-305.
107. Carson, J.A. and A.J. Turner, *Beta-amyloid catabolism: roles for neprilysin (NEP) and other metallopeptidases?* J Neurochem, 2002. **81**(1): p. 1-8.
108. Soscia, S.J., et al., *The Alzheimer's disease-associated amyloid beta-protein is an antimicrobial peptide.* PLoS One, 2010. **5**(3): p. e9505.
109. De Chiara, G., et al., *Infectious agents and neurodegeneration.* Mol Neurobiol, 2012. **46**(3): p. 614-38.
110. Ikejima, H., H. Friedman, and Y. Yamamoto, *Chlamydia pneumoniae infection of microglial cells in vitro: a model of microbial infection for neurological disease.* J Med Microbiol, 2006. **55**(Pt 7): p. 947-952.
111. Appelt, D.M., et al., *Inhibition of apoptosis in neuronal cells infected with Chlamydophila (Chlamydia) pneumoniae.* BMC Neurosci, 2008. **9**: p. 13.
112. Boelen, E., et al., *Chlamydia pneumoniae infection of brain cells: an in vitro study.* Neurobiol Aging, 2007. **28**(4): p. 524-32.
113. Jing, Y.Y., et al., *A novel PrP partner HS-1 associated protein X-1 (HAX-1) protected the cultured cells against the challenge of H(2)O(2).* J Mol Neurosci, 2011. **45**(2): p. 216-28.
114. Konig, A.S., et al., *Structural details of amyloid beta oligomers in complex with human prion protein as revealed by solid-state MAS NMR spectroscopy.* J Biol Chem, 2021. **296**: p. 100499.
115. Vojtechova, I., et al., *Infectious origin of Alzheimer's disease: Amyloid beta as a component of brain antimicrobial immunity.* PLoS Pathog, 2022. **18**(11): p. e1010929.
116. Tiwari, S., et al., *Alzheimer's disease: pathogenesis, diagnostics, and therapeutics.* Int J Nanomedicine, 2019. **14**: p. 5541-5554.

117. Niessner, A., et al., *Polymorphic membrane protein (PMP) 20 and PMP 21 of Chlamydia pneumoniae induce proinflammatory mediators in human endothelial cells in vitro by activation of the nuclear factor-kappaB pathway.* J Infect Dis, 2003. **188**(1): p. 108-13.
118. Jones, S.V. and I. Kounatidis, *Nuclear Factor-Kappa B and Alzheimer Disease, Unifying Genetic and Environmental Risk Factors from Cell to Humans.* Front Immunol, 2017. **8**: p. 1805.

# 4. Teil III Manuskript III

**Prophylactic Multi-Subunit Vaccine against *Chlamydia trachomatis*: In Vivo Evaluation in Mice**

Christian Lanfermann, Sebastian Wintgens, Thomas Ebensen, Martin Kohn, Robert Laudeley, Kai Schulze, Claudia Rheinheimer, Johannes H. Hegemann, Carlos Alberto Guzmán and Andreas Klos

Zweitautor
Beteiligungen:
Christian Lanfermann: 25 %, Sebastian Wintgens: 15 %, Thomas Ebensen: 15 %, Martin Kohn: 10 %, Robert Laudeley: 5 %, Kai Schulze: 5 %, Claudia Rheinheimer: 5 %, Johannes H. Hegemann: 5 %, Carlos Alberto Guzmán: 5 %, Andreas Klos: 10 %

Sebastian Wintgens (SW) klonierte alle Plasmide, welche zur Expression der Pmp-Proteine notwendig waren. SW etablierte ein Expressions- und Aufreinigungssystem für alle verwendeten Pmp-Proteine und stellte vielfach die Pmps sowie Ctad1 in einem rekombinanten Expressionsystem in *E. coli* Origami oder *E. coli* BL21 her. Exprimierte Proteine wurden von SW aufgereinigt, von Endotoxinen befreit, stetig über Coomassie gefärbte SDS-PAGEs und Blots auf ihre Qualität kontrolliert, Degradation bestimmt, bei - 80 °C gelagert und zum Kooperationspartner AG Klos gesendet. Das Manuskript (insbesondere Einleitung sowie Material und Methoden) wurden von SW mitbearbeitet. Tabelle 1, Tabelle 2, Figur S1 und Schema 1 wurden von SW erstellt.

Hiermit bestätige ich, dass diese Angaben korrekt sind.

Düsseldorf, den 30.05.2023

Sebastian Wintgens

## 4.1 Zusammenfassung

*Chlamydia trachomatis* ist das am häufigsten sexuell übertragbare pathogene Bakterium. Urogenitale Serovare dieses intrazellulären Erregers führen zu Urethritis und Zervizitis. Aufsteigende Infektionen führen zu entzündlichen Beckenerkrankungen, Salpingitis und Oophoritis. Eine von 200 urogenitalen Infektionen führt zur Eileiterunfruchtbarkeit. Die Serovare A - C verursachen ein Trachom, welches in Erblindung resultieren kann. Die Serovare D - K führen zu urogenitalen Infektionen. Es besteht ein dringender Bedarf an einem Impfstoff. Wir haben einen neuen Fünf-Komponenten-Subunit-Impfstoff in einem Mausmodell mit Impfung und Lungeninfektion charakterisiert. Vier rekombinante Mitglieder der Pmp-Familie und Ctad1 aus *C. trachomatis* Serovar E, die alle an der Adhäsion und Bindung von Chlamydien-Elementarkörpern an Wirtszellen beteiligt sind, wurden mit dem mukosalen Adjuvans zyklisches Diadenosinmonophosphat kombiniert. Die intranasale Anwendung führte zu einem hohen Grad an serovarübergreifendem Schutz gegen urogenitale und okuläre Stämme von *C. trachomatis*, der mindestens fünf Monate anhielt. Kritische Bewertungsparameter waren das Körpergewicht, der klinische Score, die Chlamydienlast, ein Granulozytenmarker und die Zytokine IFN- /TNF- im Lungenhomogenat. Impfstoff-Antigen-spezifische Antikörper und eine gemischte Th1/Th2/Th17 T-Zell-Antwort mit multifunktionalen CD4+ und CD8+ T-Zellen korrelieren mit dem Schutz. Der Serumtransfer schützte die Empfänger jedoch nicht, was darauf schließen lässt, dass zirkulierende Antikörper nur eine untergeordnete Rolle in der Infektionsabwehr spielen. Langfristig könnte unser neuer Impfstoff dazu beitragen, die gefürchteten Folgen von *C. trachomatis*-Infektionen beim Menschen zu verhindern.

vaccines

MDPI

*Article*

# Prophylactic Multi-Subunit Vaccine against *Chlamydia trachomatis:* In Vivo Evaluation in Mice

**Christian Lanfermann [1], Sebastian Wintgens [2,†], Thomas Ebensen [3,†], Martin Kohn [1], Robert Laudeley [1], Kai Schulze [3], Claudia Rheinheimer [1], Johannes H. Hegemann [2,‡], Carlos Alberto Guzmán [3,‡] and Andreas Klos [1,*]**

1 Institute of Medical Microbiology and Hospital Epidemiology, Medical School Hannover, 30625 Hannover, Germany; Lanfermann.Christian@mh-hannover.de (C.L.); Kohn.Martin@mh-hannover.de (M.K.); Laudeley.Robert@mh-hannover.de (R.L.); Rheinheimer.Claudia@mh-hannover.de (C.R.)
2 Institute of Functional Microbial Genomics, Heinrich-Heine-University Düsseldorf, 40225 Düsseldorf, Germany; Sebastian.Wintgens@uni-duesseldorf.de (S.W.); Johannes.Hegemann@hhu.de (J.H.H.)
3 Department of Vaccinology and Applied Microbiology, Helmholtz Centre for Infection Research, 38124 Braunschweig, Germany; Thomas.Ebensen@helmholtz-hzi.de (T.E.); Kai.Schulze@helmholtz-hzi.de (K.S.); CarlosAlberto.Guzman@helmholtz-hzi.de (C.A.G.)
* Correspondence: Klos.Andreas@mh-hannover.de
† These authors equally contributed to this work.
‡ These authors equally contributed to this work.

**Abstract:** *Chlamydia trachomatis* is the most frequent sexually-transmitted disease-causing bacterium. Urogenital serovars of this intracellular pathogen lead to urethritis and cervicitis. Ascending infections result in pelvic inflammatory disease, salpingitis, and oophoritis. One of 200 urogenital infections leads to tubal infertility. Serovars A–C cause trachoma with visual impairment. There is an urgent need for a vaccine. We characterized a new five-component subunit vaccine in a mouse vaccination-lung challenge infection model. Four recombinant Pmp family-members and Ctad1 from *C. trachomatis* serovar E, all of which participate in adhesion and binding of chlamydial elementary bodies to host cells, were combined with the mucosal adjuvant cyclic-di-adenosine monophosphate. Intranasal application led to a high degree of cross-serovar protection against urogenital and ocular strains of *C. trachomatis*, which lasted at least five months. Critical evaluated parameters were body weight, clinical score, chlamydial load, a granulocyte marker and the cytokines IFN-γ/TNF-α in lung homogenate. Vaccine antigen-specific antibodies and a mixed Th1/Th2/Th17 T cell response with multi-functional $CD4^+$ and $CD8^+$ T cells correlate with protection. However, serum-transfer did not protect the recipients suggesting that circulating antibodies play only a minor role. In the long run, our new vaccine might help to prevent the feared consequences of human *C. trachomatis* infections.

**Keywords:** *Chlamydia trachomatis*; vaccine; mouse model; lung infection; immune response; polymorphic membrane proteins; Pmp; Ctad1; c-di-AMP; sexually-transmitted disease



**Citation:** Lanfermann, C.; Wintgens, S.; Ebensen, T.; Kohn, M.; Laudeley, R.; Schulze, K.; Rheinheimer, C.; Hegemann, J.H.; Guzmán, C.A.; Klos, A. Prophylactic Multi-Subunit Vaccine against *Chlamydia trachomatis:* In Vivo Evaluation in Mice. *Vaccines* **2021**, *9*, 609. https://doi.org/10.3390/vaccines9060609

Academic Editor: Vasso Apostolopoulos

Received: 3 May 2021
Accepted: 3 June 2021
Published: 6 June 2021



## 1. Introduction

*Chlamydiae* are Gram-negative, intracellular bacteria with a unique reproductive cycle: infective elementary bodies (EBs) induce their uptake into mucosal cells where they remain in inclusions [1]. In this niche, they transform to metabolically active reticulate bodies and divide until hundreds of new infectious EBs are produced and released. In humans and animals, *Chlamydiae* cause infections of the urogenital, respiratory and gastrointestinal tract, and the eye.

### 1.1. *Chlamydia trachomatis* and Diseases Caused by This Intracellular Bacterium

*Chlamydia trachomatis* (C.tr.) has 19 serovars based on the major outer membrane protein (MOMP), and over 60 genotypes [2]. Serovars D-K representing the genital tract and L1-L3 representing the lymphogranuloma venereum (LGV) biovar of C.tr. lead to

infections of urethra or cervix uteri. With an estimated prevalence of 4.2% in 14- to 49-year-old men and women worldwide, C.tr. is the most frequently reported bacterium causing a sexually-transmitted disease (STD). According to WHO, there were 124 million new cases in 2016 [3].

PCR studies suggest that 4.4% of sexually active 17-year-old female teenagers and 4.5% of all 18- to 19-year-old women in Germany are latently infected with C.tr. [4]. Acute genital C.tr. infections lead to few physical complaints, in particular in women. Hence, most infections remain initially unrecognized and untreated. Partially due to different serovars, C.tr. can repetitively infect the same person (reviewed in Phillips et al. [5]). It can ascend to the upper genital tract resulting in inflammation of the fallopian tubes or ovaries, or in other painful and difficult to treat pelvic inflammatory diseases. Ectopic pregnancy is one of the feared sequelae of chlamydial tissue damage [6]. More important, it has been estimated that 1 out of 200 urogenital infections leads to permanent tubal infertility [7]. Additionally, there is a relevant financial burden for society caused by often unsuccessful therapeutic attempts to later satisfy the wish to have children. Pregnant women can transmit C.tr. to newborns in the birth canal leading to conjunctivitis and pneumonia, which do not readily respond to therapy [8].

In particular men, mostly with a certain genetic background, can suffer from reactive arthritis [9]. In this rheumatic disease, persistent viable C.tr. with reduced metabolism are detectable in the synovia of the affected joints for up to several years. Additionally, there is an ongoing discussion about a potential link between C.tr. infections and urogenital tumors [10].

In developing countries, this STD is even more frequent. Under these circumstances, routine PCR screenings of young women in order to manage the disease and to avoid its sequelae is impracticable. Even in industrialized countries, only screening for C.tr.-DNA during pregnancy has been successful [11]. Attempts to change human risk behavior and to decrease infection rates by information campaigns and by providing for all woman $\leq$25 years the opportunity for an annual PCR screening paid by the health insurance remained ineffective.

The serovars A–C forming the trachoma biovar of C.tr. are responsible for this neglected tropical disease [12,13]: According to the WHO Global Health Observatory 2019, trachoma remains a public health problem in 43 countries [14]. It is responsible for partial or total visual impairment of 1.8 million people. In 2017, 83.5 million people received antibiotics for trachoma, and 231,000 people received surgery for its late blinding stage, trachomatous trichiasis. Originally, the WHO aimed to eliminate trachoma by 2020. Apparently, with the so far applied SAFE Strategy (Surgery, Antibiotics, Facial cleanliness, Environmental improvement) alone, it will be impossible to achieve this ambitious, but highly unrealistic aim, even in the coming years.

Obviously, there is an urgent need to develop a vaccine against C.tr. that prevents urogenital infection with its sequelae, in particular female infertility, and, additionally, one preventing trachoma. However, there is still no such vaccine available.

### *1.2. Former Attempts to Develop a Vaccine against Chlamydia trachomatis*

According to the review "Seventy Years of Chlamydia Vaccine Research-Limitations of the Past and Directions for the Future" by Phillips et al., 78 studies have been performed with C.tr. between 1949 and 2017 [5]. Its main conclusion is that " ... no single antigen type or target, adjuvant, or route of administration has been established as a clear front-runner for effective vaccination." [5]. Unfortunately, most attempts of vaccine development have been unsuccessful, either due to missing (cross-serovar) protection or even due to increased immunopathology during a subsequent chlamydial infection (reviewed in: [15–19]). An extensive presentation or discussion of all these vaccine candidates goes beyond the scope of the manuscript, thus, we focused our analysis on the most successful or, in regard to this project, most relevant vaccination studies.

In several clinical trachoma studies with live or inactivated EBs of C.tr., transient reduction of the disease and a reduced bacterial load occurred. However, discouraging studies led to the conclusion that this type of vaccination "might lead to a more severe disease upon challenge with a heterologous serovar", and that the protection achieved is only short-lived and possibly serovar or serogroup specific (as reviewed in [19]). Presently, it is under investigation whether or not attenuated C.tr. isolates, such as the plasmid-deficient derivative of a C.tr. D strain, which is protective against genital tract infections of Rhesus macaques [20], can be used in humans (reviewed in [19]). However, there are safety concerns and challenges attached to the manufacturing of a whole cell Chlamydia vaccine according to industrial good manufacturing practice standards [20,21].

Thus, many researchers have shifted their efforts to potential C.tr. subunit vaccines. As reviewed in [19], the majority of them are directed against surface exposed antigens such as purified native nMOMP or recombinant rMOMP or polymorphic membrane proteins (rPmp's), but others also targeted intracellular antigens, such as plasmid-encoded glycoprotein 3 or chlamydial protease-like activity factor.

Several investigations concern the nine Pmp's A to I that form the largest protein family in C.tr. [22]—with four of them being part of the multi-subunit vaccine used in the present study. These proteins of ~100 to 150 kDa share autotransporter characteristics with a short N-terminal Sec signal sequence (24 to 50 amino acids, aa), a large passenger domain (PD, ~650 to 1200 aa), and a C-terminal β-barrel (~300 aa) for outer membrane translocation. Evidence suggests that Pmp proteins form functional homomeric oligomers [23]. Pmp's from C.tr. act as adhesins and are essential for infection [24]. Indeed, a C.tr. mutant strain harboring a *pmpD* null mutant shows reduced attachment to epithelial cells in vitro and in a non-human primate macaque model of ocular infection a 13-fold reduced chlamydial burden in comparison to the wild-type strain [25]. Pmp21, the C. *pneumoniae* homolog of the C.tr. PmpD, has been shown to be an adhesin and invasin, which is binding to and activating the epidermal growth factor (EGF) receptor as part of the EB internalization process [26].

Antibodies to PmpD neutralize all C.tr. serovars in vitro, and PmpD as antigen leads to protection in various animal systems [27]. Vaccination of mice with short PD protein fragments from PmpE, F, G, and H from C. *muridarum* combined with DDA/MPL as adjuvant confers protection against C. *muridarum* after vaginal challenge [28]. Moreover, PmpE, F, G, and H fragments plus MOMP from C.tr. D protect against a C.tr. challenge infection in mice [29]. Based on the high protein identity between C.tr. serovars and C. *muridarum*, short protein fragments from the PD from all nine C.tr. serovar E Pmp's were tested in mice using subcutaneous (s.c.) application and CpG-1826 and Montanide ISA 720 VG as adjuvants. Indeed, this results in limited cross-species protection against a subsequent C. *muridarum* infection [30]. A PD fragment from PmpC from C.tr. B applied by s.c. and intramuscular (i.m.) route also cross-protects against a challenge with C. *caviae* in the guinea pig [31]. Similarly, partial cross-protection was observed for a PmpA PD fragment from C.tr. E plus CpG-ODN 1826 adjuvant against a subsequent *C. muridarum* infection. Yet, here, adjuvant-induced immunopathology upon challenge of the genital tract was reported [32]. Thus, Pmp proteins can protect against a C.tr. infection and show even partial cross-species protection. However, limited success or immunopathology has been often an issue.

### *1.3. Selection of Chlamydial Antigens, the Adjuvant and the Test System for Our New Vaccine*

We selected for our new five-component subunit vaccine (5cVAC) five promising candidate antigens from C.tr. serovar E in their recombinant, purified form (see Table 1). Four antigens are members of the Pmp adhesin protein family. The fifth antigen is Ctad1, a novel adhesin which exploits as invasin the human integrin β1 receptor [33]. So far, it has not been tested as a vaccine antigen.

**Table 1.** Identities (%) among species and serovars of the complete proteins (Cp) and protein fragments (Pf) which were used as antigens in the vaccine. Depicted are also the protein fragments of *Chlamydia trachomatis* (C.tr.) serovar E/DK20 used for vaccination (in amino acids, aa). Identities are given in relation to those (versus, vs) of C.tr. D/UW3/CX, A/HAR-13, L2 LGV II 434, and *C. muridarum* (C.mu.). The strain names of the different serovars from which this information is derived are included in the column titles of Table 2.

| | C.tr. E/DK20 Pf Antigen | C.tr. E Cp vs. C.tr. D Cp | C.tr. E Pf vs. C.tr. D Pf | C.tr. E Cp vs. C.tr. A Cp | C.tr. E Pf vs. C.tr. A Pf | C.tr. E Cp vs. C.tr. L2 Cp | C.tr. E Pf vs. C.tr. L2 Pf | C.tr. E Cp vs. C.mu. Cp | C.tr. E Pf vs. C.mu. Pf |
|---|---|---|---|---|---|---|---|---|---|
| PmpA | 53aa-665aa | 99.8% | 99.7% | 99.8% | 99.8% | 100.0% | 100.0% | 76.8% | 81.2% |
| PmpD | 34aa-619aa | 99.1% | 99.5% | 99.0% | 99.5% | 99.4% | 99.7% | 71.7% | 68.6% |
| PmpG | 29aa-673aa | 99.4% | 99.5% | 99.9% | 99.7% | 97.5% | 97.7% | 72.8% | 67.2% |
| PmpH | 26aa-690aa | 99.7% | 99.6% | 94.7% | 92.5% | 94.7% | 92.9% | 75.4% | 69.1% |
| Ctad1 | 1aa-433aa | 100.0% | 100.0% | 98.6% | 98.6% | 98.4% | 98.4% | 82.0% | 82.0% |

The plethora of former vaccination studies showed also that not only the antigens but also adjuvant and route of application are critical for the success, as recently reviewed [34,35]. Although still a controversial issue, most experts speculate that a protective vaccine against Chlamydia might require a combined humoral and cellular immune response [19].

Cyclic-di-adenosine monophosphate (c-di-AMP) is a second messenger in prokaryotes that exhibits strong immune modulatory properties. It was selected as adjuvant because it can stimulate antigen-specific antibody and Th1/Th2/Th17 T cell responses, as well as CD8 cytotoxic T lymphocytes by promotion of cross-presentation. Moreover, c-di-AMP is suitable for mucosal and systemic application, and, when administered by the mucosal route, leads to mucosal responses at local and distant mucosal territories. The c-di-AMP also promotes a self-limited immune activation, which is restricted to the administration site, resulting in an enhanced safety profile [36–39].

Finally, it is not clear which surrogate marker of the immune response could actually best replace observable protection. Selecting only immune-dominant components for the vaccine without verification of the protective potential carries the risk to choose a non-protective or to reject erroneously an essential one. Hence, instead of using immunological surrogate markers only suggesting protection, we determined efficacy directly, i.e., the protection achieved by the adjuvanted vaccine in our relatively fast-to-perform and highly quantifiable mouse vaccination-lung challenge C.tr. infection model [40]. We have already used this model for successful identification of a member of a new class of C.tr.-directed antibiotics [41]. With its short challenge phase of only 7 days, we have a suitable screening method at our disposal, where one can easily quantify the main defining parameters of protection.

The purpose of this study was to identify by broad analysis a useful combination of adjuvant and antigens, which successfully targets several serovars of the human pathogen C.tr. in lung infection. We wanted to evaluate the protection achieved after vaccination by two different application routes, and to get insights in the induced humoral and cellular immune responses in the lung infection model. Thereby, we wanted to lay the foundation for confirmatory future studies challenging vaccinated mice with C.tr. by the transcervical-intrauterine route and determining achieved protection in regard to chlamydia-induced tissue-reorganization or infertility.

Indeed, after mucosal application, our new multi-subunit vaccine led in the lung infection model to a high degree of protection against C.tr. E, and cross-serovar protection against serovar D from the urogenital, L2 from the lymphogranuloma and serovar A from the trachoma biovar. Moreover, we found long-lasting 5cVAC-specific antibodies and, most likely, in our case functionally more important, T cell responses in the vaccinated animals.

## 2. Materials and Methods

### *2.1. Chlamydial Strains and Their Growth in Cell Culture*

For the mouse vaccination-lung challenge infection experiments, the following strains of different C.tr. serovars were propagated in baby hamster kidney 21 cells (BHK-21, ATCC: CCL-10) as previously described [40]: the genital serovars E, strain DK20 (Origin: Institute of Ophthalmology, London), D, strain UW3/CX (ATCC: VR-885), and L2, strain LGV II 434 (ATCC: VR-902B), as well as the ocular C.tr. serovar A, strain HAR-13 (ATCC: VR-571B; a kind gift of S. Birkelund, Aarhus, Denmark).

Inclusion-forming units (IFU) of the stock-solutions were assessed by repetitive titration using cervix epithelial HeLa-T cells, kindly provided by R. Heilbronn, Berlin, Germany [42]. For negative controls, i.e., 'mock' infection, BHK-21 cells were identically processed as our chlamydial stock preparations, however, without the addition of any bacteria. All chlamydial and the mock preparations were Mycoplasma-free tested by PCR.

### *2.2. Preparation and Purification of the Recombinant Antigens PmpA, PmpD, PmpG, PmpH, and Ctad1 Derived from C.tr. Serovar E/DK20*

In most experiments, combined with an adjuvant (see below), an equimolar mix of the following five purified, recombinant antigens derived from serovar E of C.tr. was applied (5cVAC): PmpA, PmpD, PmpG, PmpH, and Ctad1.

Our 5cVAC antigen composition consists of PD protein fragments from PmpA, D, G, and H. We succeeded in producing full-length PD fragments from PmpA (protein fragment aa 53 to 665), PmpG (aa 29 to 637), and PmpH (aa 26 to 690), while for PmpD only the first half of the large PD (aa 34 to 619) could be generated in sufficient amounts. Full-length Ctad1 (aa 1 to aa 433) is the fifth component of 5cVAC. All recombinant antigens are derived from serovar E of C.tr. One experiment was performed with 2cVAC, i.e., an equimolar mix of the two antigens PmpD and Ctad1, only. See Table 2 for protein IDs and lengths of the complete proteins (aa) of the five antigens of 5cVAC from *C. trachomatis* E/DK20, and their homologous proteins in C.tr. D, A, L2, and *C. muridarum*.

Gene fragments encoding PDs of the four Pmps were PCR-amplified from genomic DNA of C.tr. serovar E strain DK20 and were cloned into the single-cut expression vector pKM32 via homologous in vivo recombination in yeast strain CEN.PK 2-1C [43]. Subsequently, the resulting plasmids were amplified in *E. coli* strain XL1 blue and verified via control restriction enzyme digests followed by gel electrophoresis and sequencing. Next, the four *pmp* containing plasmids as well as pST42 (carrying *ctad1*; [33]) were transformed into our expression strains *E. coli* BL21 (Pmp's) and *E. coli* Origami (Ctad1).

Protein expression was induced in liquid culture (usually 1000 mL) using 1 mM IPTG for 4 h at 37 °C. Cells were collected by centrifugation (5000 rpm). Pelleted cells were lysed under denaturing conditions using a lysis buffer (6 M guanidine-HCl/20 mM Tris HCl/0.5 M NaCl/1 mM β-mercaptoethanol) overnight at 4 °C. On the following day, the lysate was sonicated on ice for 1 min. Insoluble debris was removed by centrifugation at 24,000 rpm for 1 h. Recombinant proteins were subsequently purified by affinity chromatography under denaturing conditions.

Soluble fractions containing N-terminal (Pmp's) or C-terminal (Ctad1) His-tagged proteins were loaded onto HiTrap chelating HP columns (GE Healthcare). Bound His-tagged proteins were sequentially washed with buffer B (8 M urea/0.1 M $NaH_2PO_4$/10 mM Tris HCl/1 mM β-mercaptoethanol (not for Ctad1)/20 mM imidazole; pH 8), and buffer C (8 M urea/0.1 M $NaH_2PO_4$/10 mM Tris/HCl/1 mM β-mercaptoethanol (not for Ctad1)/40 mM imidazole; pH 6.3). Proteins were eluted with 8 M urea/0.1 M $NaH_2PO_4$/10 mM Tris/HCl/1 mM β-mercaptoethanol (not for Ctad1)/500 mM imidazole (pH 6.3). For renaturation, eluted proteins (PmpG, PmpH, PmpD, Ctad1) were dialyzed three times against PBS (pH 7.4) at 4 °C over two nights. As this procedure caused PmpA to precipitate, PmpA was renatured using Amicon centrifugation. In this process, 1 mL of elution fraction was mixed with 10 mL of PBS + 200 mM arginine, loaded onto an Amicon® Ultra-15 Centrifugal Filter unit and centrifuged at 4 °C as recommended by the manufacturer, until the volume was

reduced to 1 mL. This step was repeated once. At last, endotoxin was reduced by the use of endotoxin removal columns (ToxinEraser Endotoxin Removal Kit). Coomassie-stained SDS-Page and Western blot of the purified recombinant antigens used in the vaccine formulation are depicted in Supplement Figure S1. The concentration of each recombinant protein was determined via Bradford assay and adjusted to a minimum of 700–1000 µg/mL.

**Table 2.** Protein ID (NCBI) and lengths of complete proteins in amino acids (aa) of the five antigens of 5cVAC which are derived from *C. trachomatis* E, and their homologous proteins in C.tr. A, D, L2, and *C. muridarum*. The strain names of the different serovars from which this information is derived are included in the column titles. Source NCBI: National Center for Biotechnology Information (NCBI) [44].

| Pmp's | C.tr. E E/DK20 | C.tr. *D* *UW3/CX* | C.tr. A A/HAR-13 | C.tr. LGV L2/434/Bu | *C. muridarum* Nigg 2 MCR |
|---|---|---|---|---|---|
| **A** | WP_009872639.1 (975aa) | WP_010725190.1 (975aa) | WP_009871764.1 (975aa) | WP_009872639.1 (975aa) | WP_010231239.1 (976aa) |
| **D** | WP_009872948.1 (1530aa) | WP_010725352.1 (1531aa) | WP_011324878.1 (1531aa) | WP_009873422.1 (1530aa) | WP_010229791.1 (1520aa) |
| **G** | WP_014541208.1 (1013aa) | WP_010725377.1 (1013aa) | WP_011324914.1 (1013aa) | WP_009873478.1 (1012aa) | WP_010229977.1 (986aa) |
| **H** | WP_014541209.1 (1014aa) | WP_010725378.1 (1016aa) | WP_011324915.1 (1018aa) | WP_009873479.1 (1006aa) | WP_010229979.1 (980aa) |
| **Ctad1** | WP_010724985.1 (433aa) | WP_010724985.1 (433aa) | WP_011324521.1 (433aa) | AGJ64368.2 (477aa) | AID37821.1 (446aa) |

### *2.3. Immunoblotting and Coomassie-Staining*

SDS-PAGE and immunoblotting were performed as described previously [45]. Recombinant proteins were detected with monoclonal anti-His (Qiagen, Hilden, Germany) antibodies and visualized with AP-conjugated antibody (Sigma, Munich, Germany). Gels were stained with Coomassie Brilliant Blue G250 (Serva, Heidelberg, Germany) (Supplement Figure S1).

### *2.4. Preparation of the c-di-AMP-Adjuvanted Vaccine Directly before Application to Mice*

In all mouse vaccination experiments (i.e., with 5cVAC and 2cVAC), a final volume of 30 µL containing $3.95 \times 10^{-11}$ mol of each LPS-reduced/free antigen (summing up to approximately 12.5 µg protein for 5cVAC in total) and 10 µg of the adjuvant c-di-AMP was administered to the mice. For the experiment with 2cVAC, $3.95 \times 10^{-11}$ mol of PmpD and Ctad1 were administered with the identical amount of c-di-AMP in the identical total volume. Under sterile conditions and on ice, the vaccine components were mixed and vortexed thoroughly. For dilution PBS/L-arginin 200 mM was used. Aliquots of the prepared stock solutions of 5cVAC and 2cVAC were stored at −80 °C.

According to the total amount needed on the day of vaccination, several aliquots of the antigen mix were thawed and pooled. Directly before application the adjuvant c-di-AMP in $H_2O$ was added 1 in 30. This solution was kept on ice until application. Corresponding to that, as negative controls, 1 µL c-di-AMP (without antigens) in 30 µL buffer, or 30 µL buffer alone, respectively, were administered per mouse.

### *2.5. Three Experimental Setups of the Mouse Vaccination-Chlamydia Trachomatis Lung Challenge Infection Model: Short-Term, Serum-Transfer, and Long-Term Protection*

The phase of vaccination with adjuvanted 5cVAC (or 2cVAC) was identical in all three experimental setups (Figure 1a–c). The hormonal cycle of seven-week-old female C57BL/6J mice was synchronized by intraperitoneal (i.p.) application of 2.5 mg medroxyprogesterone acetate in 200 µL 0.9% NaCl, in order to diminish hormone dependent variations, and additionally to facilitate comparison with results of a potential urogenital infection model in the future. To induce protection, the mice were vaccinated three times with 30 µL of

c-di-AMP-adjuvanted 5cVAC, or the adjuvant c-di-AMP alone, or buffer, respectively, at day 7, 21, and 28. Vaccination was usually performed by the intranasal (i.n.) route. This application route was also selected since it has been demonstrated that it triggers similar local immune responses in both, the respiratory and the urogenital tracts [46,47].

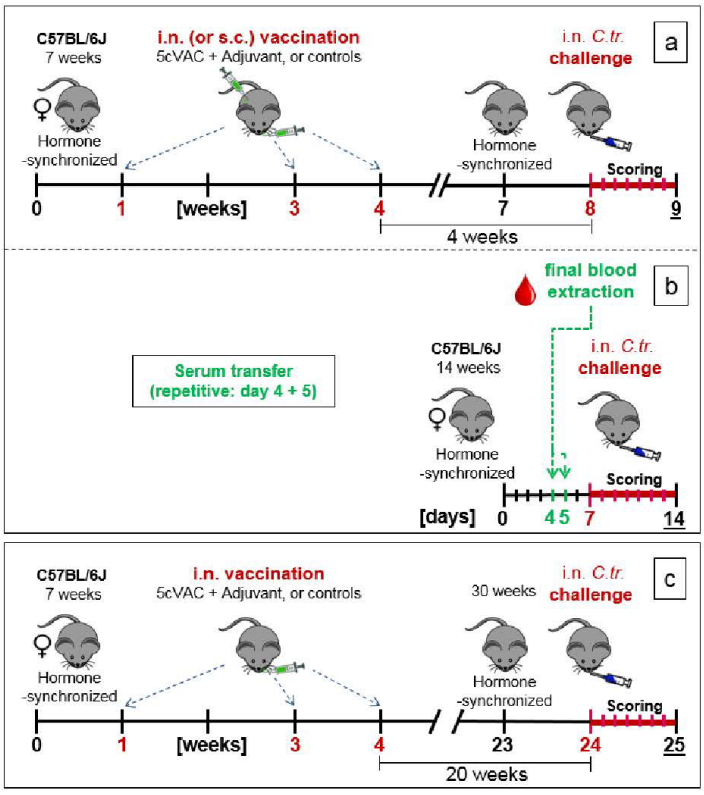


**Figure 1.** Experimental setup of the three vaccination trials using the *Chlamydia trachomatis* lung challenge infection models: short-term (**a**), serum transfer-short-term (**b**), and long-term protection (**c**). Experimental setup of short-term protection model (**a**) 1, 3, and 4 weeks after hormone-induced synchronization, eight-week-old female C57BL/6J mice were repetitively treated with an identical volume of c-di-AMP-adjuvanted antigens, or adjuvant, or buffer, respectively. The administered 5cVAC contains an equimolar mix of 5 (and 2cVAC of 2) recombinant antigens derived from serovar E of *C. trachomatis* (C.tr. E). Four weeks after the last booster vaccination, the 15-week-old hormone-synchronized mice were i.n. challenge-infected with different strains/serovars. Under close monitoring and using humane endpoint defining criteria, body weight and clinical score were determined daily. On day 7 of challenge infection, all mice were painlessly sacrificed for further analysis of their blood and lung tissue. Serum transfer-short-term protection model (**b**) four weeks after administration of the third dose of adjuvanted 5cVAC or adjuvant, or buffer, respectively, serum of healthy donor mice was collected by heart puncture. The pooled sera were transferred to 14- to 15-week-old healthy, hormone-synchronized female mice. Then, lung challenge infection was performed with the identical amount of C.tr. E as used in (**a**). Long-term protection (**c**) vaccination with adjuvanted 5cVAC was conducted as described in (**a**). However, the period between the last i.n. administration of the vaccine and challenge infection with C.tr. E was prolonged from 4 to 20 weeks, and a smaller amount of C.tr. E was applied to the then older and more sensitive mice.

In a few experiments, the adjuvanted 5cVAC was applied not by i.n. but alternatively parenterally by s.c. route (as indicated in the corresponding figure).

(a) Short-term protection model (Figure 1a): in week 7 of the experiment, the cycle of the female mice was hormone-synchronized again. In week 8, i.e., 4 weeks after the last booster vaccination, the 15-week-old mice were challenged by i.n. application of Chlamydia differently pretreated animals per group for the C.tr. E, D, and L2, and mice per group for C.tr. A, respectively). One group of animals received mock material instead of Chlamydia (usually $n = 8$, only in one experiment (as indicated) $n = 4$).

Preliminary i.n. titration-experiments had been performed to identify the optimal amount of the different C.tr. serovars for the main experiments (Supplement Figures S2 and S3). In the lung-pneumonia model this can be done by daily observation of body weight, clinical score, and survival, i.e., time until the humane endpoint (see Supplement Table S1) is reached, and the mice have to be sacrificed painlessly. In order to observe vaccine-induced protection with high sensitivity, C.tr. infected mice had to exhibit a severe, but still tolerable course of infection. Chlamydial infections lead to a protracted course of disease, and therefore, they usually recover even when the body weight is reduced by >20%. Hence, our permit from the corresponding authorities allows even then (under close supervision) continuation of observation. Yet, we had to avoid transient weight loss of >25–30%, and the survival rate should remain in the range of 90%. In any case, most animals had to reach the end of the observation period for the intended analysis of their blood and lung tissue. When we originally established this mouse model for C.tr. [40], we had seen that a time frame of 7 days is optimal. During the following days, most infected and severely sick C57BL/6J mice recover little by little (see also Supplement Figures S2 and S4) until infectious Chlamydia are no longer detectable in lung homogenate after 2–3 weeks [40]. Notably, if longer observation periods were chosen, some mice would stay ill and would prematurely reach the humane endpoint due to exhaustion. To induce a similar severity of resulting pneumonia, according to the pre-tests (Supplement Figures S2 and S3), different amounts of inclusion forming units (IFU) of the genital serovars E, D, L2 and the ocular serovar A of C.tr. per mouse had to be used: $1.3 \times 10^6$ for serovar E, $2 \times 10^6$ for D, $4 \times 10^5$ for L2, and $4 \times 10^6$ for A.

(b) Serum transfer-short-term protection model (Figure 1b): We wanted to clarify to which extent antibodies that are circulating in murine blood after vaccination with c-di-AMP-adjuvanted 5cVAC are actually conferring protection against C.tr. E. Four weeks after the last i.n. or s.c. application of the vaccine, or buffer, or c-di-AMP alone, respectively, i.e., exactly at the time point when the challenge infection was normally performed, the mice were sacrificed and their blood was collected by heart puncture. The sera of the four differently treated groups of animals ($n = 10$–$14$ per group) were pooled and 170 µL were transferred twice intravenously (i.v.) to non-vaccinated 14- to 15-week-old healthy animals ($n = 5$–$7$ per group) on days 4 and 5 after their hormone-synchronization. C.tr.-specific antibodies were determined in the four donor pool sera as well as in the sera of the individual recipient animals. For that purpose, small blood samples were collected on the day between serum-transfer and i.n. C.tr. E-challenge infection. One week after hormone-treatment and two days after the last serum-transfer, i.n. challenge infection was conducted with $1.3 \times 10^6$ IFU of C.tr. E, i.e., exactly like in the short-term protection model.

(c) Long-term protection model (Figure 1c): To determine the long-term protection achieved, mice that had been vaccinated i.n. with c-di-AMP-adjuvanted 5cVAC in week 1, 3, and 4, as described above, were hormone-synchronized again in week 23. Twenty weeks after the last booster vaccination, the mice were challenged i.n. with C.tr. E. According to preliminary titration experiments (Supplement Figure S4), 31-week-old mice react more sensitive to chlamydial infection, independent of body weight or vaccination. Thus, a more than three-times lower IFU ($4 \times 10^5$) of C.tr. E

had to be administered for challenge in this setting. Otherwise, a relevant portion of the older non-vaccinated, infected mice would not have achieved the desired seven-day-observation period after challenge infection, thereby reducing the group size of this essential control group.

The exact number of mice per group for each experiment is depicted in Supplement Tables S2 and S3, and summed up as a range in each legend. For both, i.n. application of the vaccine and i.n. C.tr. challenge, mice were anesthetized by i.p. injection of 0.1 mL anesthetic solution (100 mg/kg BW Anesketin, 4 mg/kg Rompun in 0.9% NaCl) per 10 g body weight.

The observation period after chlamydial challenge infection was seven days in all three related models. In order to reduce variation within experiments with a specific serovar as much as possible, mice of the vaccinated and the non-vaccinated control groups were housed in mixed cages and handled in parallel. The depicted results usually combine data obtained in two or three (and four for the long-term experiment) staggered, otherwise identical experiments. Mice were monitored closely and assessed daily using humane end-point defining criteria. On the last day of challenge infection and developing pneumonia, all mice were painlessly sacrificed for further analysis of their lung (and partially also their spleen) as well as their blood which was drawn by heart-puncture.

### *2.6. Clinical Scoring*

The clinical score was recorded daily after challenge infection. It is based on pilo-erection, body posture, locomotion, breathing, dehydration, attention/curiosity and secretion from nose and eyes (for details see Supplement Table S1).

### *2.7. Determination of Bacterial Load in Mouse Lung Homogenate by Flow Cytometry*

Homogenates from the right lung lobes were harvested as described elsewhere [48]. The determination of the different C.tr. strains in the cryopreserved homogenate was performed by flow cytometry as previously described by us for *C. psittaci* [49]. In brief, cryopreserved lung homogenates were thawed 15 min on ice. The samples were vortexed for 3 min and centrifuged for 15 min, 500× *g*, 4 °C. HeLA–Cells were infected with the serial diluted supernatant and cultured for 16–20 h. For staining of intracellular Chlamydia and the cells, Pathfinder® (Fluorescein-conjugated murine monoclonal antibody to chlamydial LPS; 0.1% Evans Blue; Bio-Rad, Hercules, CA, USA) in PBA-S (PBS supplemented with 0.25% BSA, 0.5% saponin for permeabilization) was used. To calculate bacterial content (IFU) in the samples with lung homogenate, as internal standard, a dilution series of the corresponding Chlamydia stock preparation with known concentration was analyzed in parallel.

### *2.8. Determination of TNF-α and IFN-γ and Myeloperoxidase Levels in Lung Homogenate*

Concentration of the key cytokines TNF-α and IFN-γ and the granulocyte marker myeloperoxidase (MPO) were determined in the mouse lung homogenate by ELISA according to the manufacturers protocol (TNF-α: ELISA MAX™ Deluxe Set Mouse TNF-α, BioLegend, 430904; IFN-γ: ELISA MAX™ Deluxe Set Mouse IFN-γ, BioLegend, 430804; MPO: MPO, Mouse, ELISA kit, Hycult Biotech, HK210-02). Absorbance was measured at 450 nm/540 nm (Synergy HTC Multi-Mode Reader Biotec® plate reader).

### *2.9. ELISAs for Circulating 5cVAC-Specific IgA/M/G and IgG Subtypes in Blood*

The levels of 5cVAC-specific Igs were determined by ELISA (modified from a recently described Ig-ELISA using homogenate of *C. psittaci* as antigen [49]) in mouse EDTA-plasma or serum, as indicated in the graphs. Polystyrene microtiter plates were pre-coated at 4 °C for 16 h with 100 µL of 1 µg/mL equimolar 5cVAC antigen mix per well in PBS, or the equimolar amount of only one of the recombinant antigens, as indicated in the graphs, respectively. Non-specific binding-sites were blocked by PBS containing 1% BSA and 5% sucrose.

After washing the pre-coated plate, a serial dilution of high-titer standard plasma (see below) or pre-diluted plasma or serum samples were added for 1.5 h at 37 °C. The specimens were collected before and/or 7 days after challenge infection, as indicated. Only a small amount of blood can be drawn (according to local authorities and GV-SOLAS) from animals a few days before infection. Thus, based on a pilot test (data not shown), all respective EDTA-plasma samples were diluted 1:316 and higher for determination of antigen-specific IgA and IgM, or 1:3160 and higher for quantification of antigen-specific IgG, respectively. For the analysis of blood obtained by heart puncture from sacrificed mice at the end of the seven-day observation period, less limiting serum or even pool serum could be analyzed at a lower dilution.

After washing, the following biotinylated secondary antibodies were applied: IgA-rat anti-mouse (α-chain), HRP, AK-Online, ABIN135043, 1:5000; IgM-rat-anti-mouse, HRP, BD Biosciences, 550588, 1:1000; total IgG-F(ab')2 goat anti-mouse IgG, HRPO, Dianova, 115-036-062, 1:10,000; $IgG_1$-rat-anti-mouse, HRP BD Biosciences, 559626, 1:1000; $IgG_{2a}$-rat-anti-mouse, HRP, BD Biosciences, 553391, 1:1000; $IgG_{2b}$-goat anti-mouse, HRP, Invitrogen M32407, 1:2000. Next, 10 µg/mL streptavidin conjugated HRP (Jackson Immuno Research, 016-030-084) was used. Plates were washed again and incubated with substrate buffer (90 mM Na-acetate, 90 mM citric acid, 100 µg/mL TMB, 0.0045% $H_2O_2$) at RT in the dark. After 20 min, the enzymatic reaction was stopped and photometric absorbance was determined at 450 nm/540 nm (Synergy HTC Multi-Mode Reader Biotec® plate reader).

Arbitrary units (U) were calculated for each Ig-class in relation to a standard, serial diluted high-titer pool plasma. The standard plasma (stored in frozen aliquots) had been collected from mice after vaccination with adjuvanted 5cVAC and subsequent challenge with C.tr. E. Arbitrary units were determined by the inverse function of the four parametric logistic equation, using iterative curve fitting of the standard curve (GraphPad Prism, GraphPad Software, San Diego, CA, USA).

### *2.10. Functional Analysis of Mouse Splenocytes: Proliferation, ELISpot, Flow Cytometry*

For the determination of cellular proliferation, ELISpot assay and multifunctional flow cytometric analysis of T cells, the spleens of mice (pretreated with adjuvanted 5cVAC, or adjuvants, or buffer, respectively) were aseptically removed. For further analysis, cell suspensions of spleens of each mouse were freshly prepared and erythrocytes were lysed.

#### 2.10.1. Measurement of Cellular Proliferation

The splenocytes were cultured in the presence of different concentrations of 5cVAC antigen (0.5–10 µg/mL) or buffer as negative control, as indicated. Positive controls received 5 µg/mL concanavalin A. The ability of immune cells derived from spleen to proliferate upon restimulation with 5cVAC as well as their cytokine profile were measured 96 h post restimulation. The proliferative activity was determined by the incorporation of [$^3$H]-thymidine (CPM). Beta-emission was measured using a scintillation counter (Wallac 1450, Micro-Trilux).

#### 2.10.2. ELISpot Assay

The number of antigen-specific cytokine-producing splenocytes was determined using an ELISpot assay as previously described [50]. 96-well plates (BD Pharmingen, San Diego, California) were coated with anti-IFN-γ, anti-IL-2, anti-IL-4, or anti-IL-17 antibodies overnight at 4 °C. Then, plates were washed once with culture medium (RPMI, 10% FCS, PenStrep, L-glutamine, and β-mercaptoethanol), and cells were seeded in culture medium with or without 5cVAC (1 µg/mL). Plates were incubated 24 h for IFN-γ and 48 h for the other cytokines. Then, cells were removed and the plates processed according to manufacturer's instructions. Colored spots were counted with an ELISpot reader (CTL-Europe GmbH) and analyzed using the ImmunoSpot image analyzer software v3.2. In order to determine the number of cytokine-secreting cells in the spleen, murine IFN-γ, IL-2, IL-4, and IL-17 ELISpot kits (BD Pharmingen) were used according to the manufacturer's

instructions. Colored spots were counted with an ELISpot reader (C.T.L.) and analyzed using the ImmunoSpot image analyzer software v3.2.

2.10.3. Flow Cytometric Determination of Multifunctional T Cells

Splenocytes ($2 \times 10^7$ cells per mL) were incubated (37 °C, 5% $CO_2$) in RPMI containing the 5cVAC antigen or buffer to determine the basal cytokine production. Viable singlet leukocytes were gated for $CD3^+$, $CD4^+$, $CD8^+$ and subsequently analyzed for the expression of intracellular IL-2, IL-4, IL-10, IL-17, TNF-α, and IFN-γ as previously described in Landi et al. [37].

*2.11. Group Sizes and Statistical Analysis*

In the majority of cases, logarithmic transformation of parametric data was performed in order to accomplish Gaussian distribution. For statistical analysis, the following tests have been used: two-way ANOVA with Bonferroni post-test for comparison of body weight and Kruskal–Wallis test with Dunn's multiple comparison post-test (≥3 groups) or Mann–Whitney *t*-test (2 groups) for the clinical score. For bacterial load, MPO, IFN-γ, and TNF-α, one-way ANOVA with Bonferroni's multiple comparison were used. For cellular proliferation, ELISpot and multifunctional T cell analysis, the statistical significance of the differences observed between the different experimental groups was analyzed using two-way ANOVA followed by Tukey's multiple comparisons test. Statistics were calculated using the GraphPad Prism software version 5.02 (and 8.4.0 for data obtained on splenocytes) for Windows, GraphPad Software, San Diego, CA, USA. Differences were considered significant at $p < 0.05$ or lower. If not indicated otherwise, *–**** indicate statistical significances between the 5cVAC group and the buffer control group with $p < 0.05$, <0.01, and <0.001, $p < 0.0001$, respectively.

## 3. Results

*3.1. Intranasal Vaccination with the c-di-AMP-Adjuvanted 5cVAC-Formulation Improves Loss of Body Weight and Clinical Score in Lung Challenge Infection with Serovar E, D, L2, or A of C. Trachomatis*

Female eight-week-old C57BL/6J mice received c-di-AMP-adjuvanted 5cVAC three times within three weeks via the i.n. route (Figure 1a: short-term protection model). As negative controls, animals were pretreated in parallel with the adjuvant alone, or buffer. Four weeks after the last booster vaccination, the 15-week-old animals were infected i.n. with $1.3 \times 10^6$ IFU of C.tr. E, or with serovars D, L2 and A, respectively. To induce with these serovars a similar severity of the resulting lung disease, different amounts (IFU) in the range from $4 \times 10^5$ to $4 \times 10^6$ IFU had to be used (see also Section 2). Some control mice received Chlamydia-free mock material instead.

During 7 days of C.tr. E challenge infection, body weight (%) (Figure 2a1) and clinical score (Figure 2a2) were assessed daily. Intriguingly, with a delay of 2–3 days, there was a drastic improvement in body weight and clinical score in i.n. vaccinated mice demonstrating strong vaccine-induced protection. Moreover, according to this course of the disease-characterizing parameters, the vaccinated animals exhibited similar cross-serovar protection against the genital C.tr. serovars D and L2, as well as the ocular serovar A (Figure 2b1–d2).

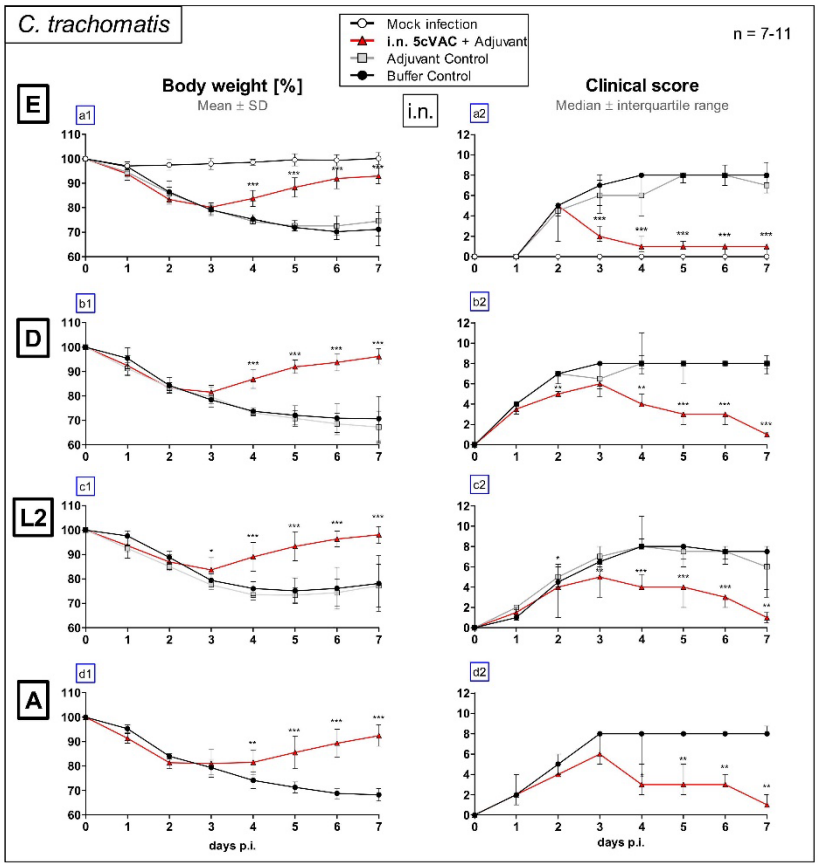


**Figure 2.** Loss of body weight and clinical score in lung challenge infection with *C. trachomatis* serovar E, D, L2, or A (marked by boxed letters to the left) after i.n. vaccination with c-di-AMP-adjuvanted 5cVAC. In the short-term protection model (see Section 2 and Figure 1a), mice were either pre-treated with c-di-AMP-adjuvanted 5cVAC, the adjuvant alone, or buffer, as indicated. $N$ = 7–11 differently pretreated animals per group for the C.tr. genital serovars E, D, and L2, and 7 mice per group for C.tr. A, respectively, were infected i.n. with the different serovars, or mock-infected ($n$ = 8). Day 0 post infection (p.i.) in this graph corresponds to week 8 in Figure 1a. During the following seven days, body weight (%) (left panels (**a1**–**d1**), mean ± standard deviation) and clinical score (right panels (**a2**–**d2**), median ± interquartile range) were assessed daily. The performed statistical analysis is described in Section 2. *,**,*** indicate statistical significances between the 5cVAC group (red) and the buffer control group (black) with $p < 0.05$, <0.01, and <0.001, respectively. The exact size of each group can be found in Supplement Table S2.

### 3.2. *Intranasal Vaccination with c-di-AMP-Adjuvanted 5cVAC Improves Bacterial Clearance and Leads to Decreased Levels of the Granulocyte Marker MPO in the Lung after Challenge Infection with four Different Serovars of C. trachomatis*

On day 7 after challenge infection with the four different C.tr. serovars E, D, L2, or A, respectively, the i.n. vaccinated mice as well as the animals of the two control groups were sacrificed to determine the amount of viable, infectious Chlamydia (IFU) and the level of the granulocyte marker MPO in their lung homogenate (Figure 3). After challenge with C.tr. E, the chlamydial load in the lung of i.n. vaccinated mice was approximately

100-fold lower as compared to both non-vaccinated control groups. Remarkably, a drastic reduction of the bacterial load could be seen after challenge infection with serovar D and A. The difference of vaccinated to (buffer) control mice was still significant after challenge with serovar L2, but less striking (Figure 3a1–d1). The level of the granulocyte marker MPO in lung homogenate was also lower in vaccinated mice after challenge infection with C.tr. E, D, and A (Figure 3a2,b2,d2), suggesting diminished granulocyte driven inflammation. The improved clearance of Chlamydia from the lung and the lower level of the granulocyte marker after i.n. application indicate not only that this form of repetitive mucosal application of c-di-AMP-adjuvanted 5cVAC protects against C.tr. E, but also that this vaccine induces cross protection against three additional, different serovars.

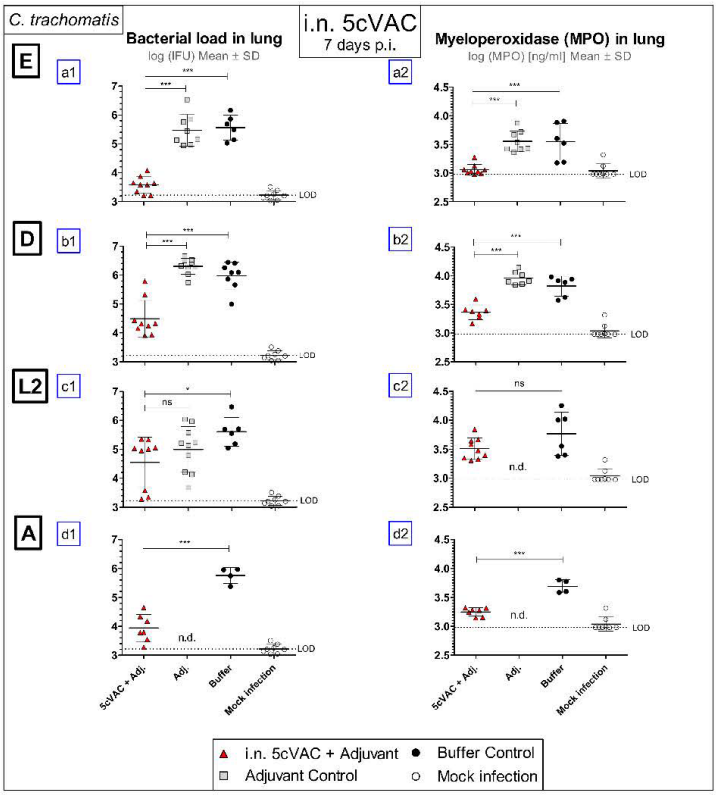


**Figure 3.** Bacterial load and granulocyte marker MPO in the mouse lung on day 7 of challenge infection with various serovars of *C. trachomatis* after i.n. vaccination with adjuvanted 5cVAC. In the short-term protection model (Figure 1a), mice were either pre-treated with c-di-AMP-adjuvanted 5cVAC, the adjuvant alone, or buffer, as indicated. The mice were challenged with C.tr. serovar E, D, L2, or A (marked by boxed letters to the left) to check for cross-serovar protection (**a1**–**d1**, **a2**–**d2**). On day 7 of chlamydial challenge (i.e., week 8 in Figure 1a), the amount of viable, infectious Chlamydia (left panels, mean ± standard deviation of log10 (IFU)) and the level of MPO (right panels, mean ± standard deviation of log10)) were determined in lung homogenate of the pretreated animals surviving that period ($n$ = 6–10 per group for serovar E, D and L2, $n$ = 4–7 for serovar A—as indicated by the number of symbols in the figure). Mock infection: n = 8. LOD = limit of detection; n.d. = not determined; ns = not significant. The performed statistical analysis is described in Section 2. * and *** indicate statistical significances with $p < 0.05$ and <0.001, respectively. The exact size of each group can be found in Supplement Table S2.

### *3.3. Intranasal Vaccination with Adjuvanted 5cVAC Leads to Decreased Levels of the Key Cytokines TNF-α and IFN-γ in Lung Homogenate after Challenge Infection with Different Serovars of C. trachomatis*

As part of the innate immune response against the intracellular pathogen, the cytokines TNF-α and IFN-γ are elevated in Chlamydia-infected lungs [40]. Thus, on day 7 of challenge infection with the four different C.tr. serovars, the levels of these two cytokines were determined (Figure 4a1–d1,a2–d2) in the lung homogenate of vaccinated and non-vaccinated control mice. Depending on i.n. vaccination with adjuvanted 5cVAC, lower levels of the two key cytokines were present after challenge infection.

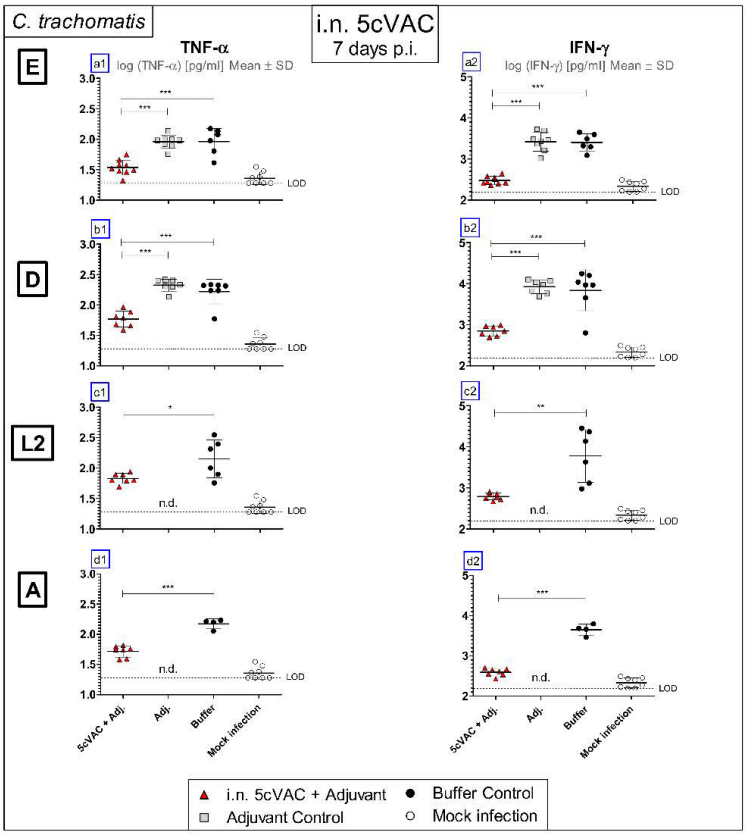


**Figure 4.** TNF-α and IFN-γ in lung homogenate on day 7 of challenge infection with various serovars of *C. trachomatis* (marked by boxed letters to the left) in the short-term protection model after i.n. vaccination with adjuvanted 5cVAC. Mice were either pre-treated with c-di-AMP-adjuvanted 5cVAC, c-di-AMP alone, or buffer, as indicated. The mice were challenged with C.tr. serovar E, D, L2, or A to check for cross-serovar protection (**a1**–**d1**,**a2**–**d2**). On day 7 of chlamydial challenge, TNF-α (left panels, mean ± standard deviation of log10) and IFN-γ (right panels, mean ± standard deviation of log10) were determined in lung homogenate of the differentially pretreated mice surviving that period ($n$ = 6–9 per group for serovar E, D and L2, $n$ = 4–7 for serovar A – as indicated by the number of symbols in the figure). Mock infection: $n$ = 8. LOD = limit of detection, n.d. = not determined. The performed statistical analysis is described in Section 2. *,**,*** indicate statistical significances with $p < 0.05$, <0.01, and <0.001, respectively. The exact size of each group can be found in Supplement Table S2.

### *3.4. After Challenge Infection with Serovar E of C. trachomatis, s.c. Vaccination with c-di-AMP-Adjuvanted 5cVAC Does Not Lead to Relevant Protection in Regard to Body Weight, Clinical Score, Bacterial Load, the Levels of the Granulocyte Marker MPO, TNF-α or IFN-γ in Lung Homogenate*

In contrast to the positive findings obtained after i.n. application of c-di-AMP-adjuvanted 5cVAC, s.c. vaccination had, even after challenge with the serovar E C.tr. strain that is closest related to the vaccine, no effect on the elevated clinical score, and only on day 7 a minimal ameliorating effect on weight loss (Figure 5a,b). Moreover, s.c. vaccination did not have any positive effect on the amount of viable C. tr. E or the elevated level of the granulocyte marker MPO in the lung (Figure 5c,d). In addition, we could not detect decreased levels of TNF-α or IFN-γ caused by s.c. vaccination (Figure 5e,f). These findings prove the importance of the i.n. route of 5cVAC application.

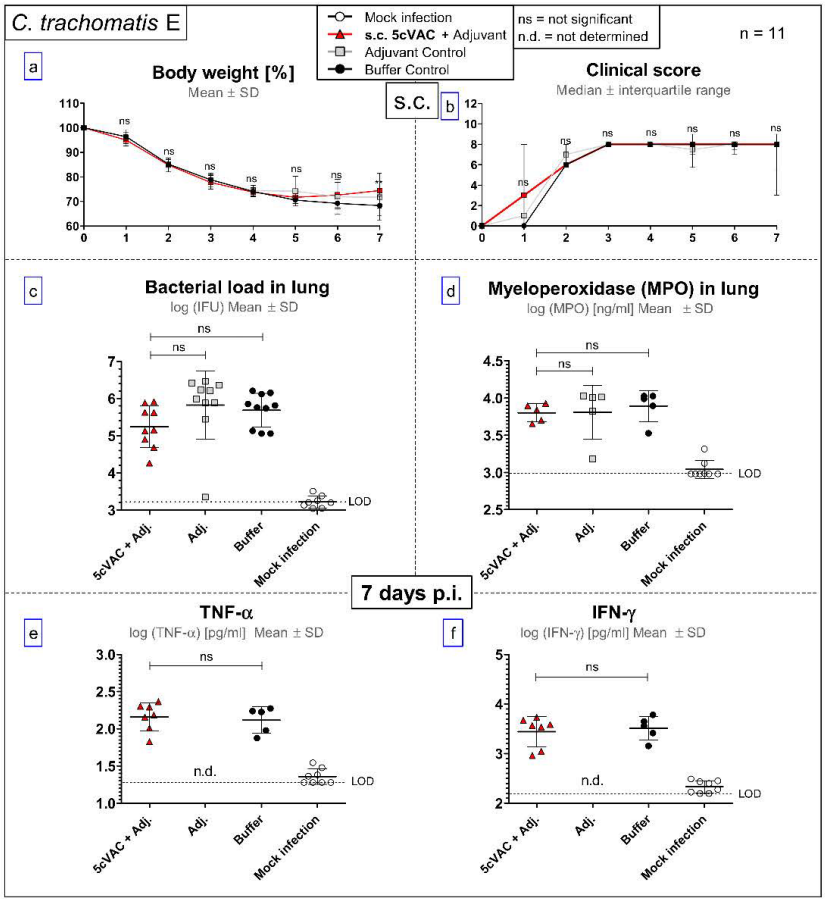


**Figure 5.** Body weight, clinical score, bacterial load, granulocyte marker MPO, TNF-α, and IFN-γ in lung challenge infection with *C. trachomatis* E in the short-term protection model after s.c. vaccination with c-di-AMP-adjuvanted 5cVAC. In this short-term protection experiment (see Figure 1a), adjuvanted 5cVAC was applied by the s.c. route. Animals pretreated with adjuvant, or buffer, respectively, served as negative controls. Per group, $n = 11$ differently pretreated 15-week-old animals were infected i.n. with the usual amount of C.tr. E ($1.3 \times 10^6$ IFU), the serovar the antigens in 5cVAC are derived from. On each of the following days, body weight ((**a**), in % as mean ± standard deviation)

and clinical score ((**b**), median ± interquartile range) were assessed. On day 7 after i.n. challenge infection, the surviving animals (also indicated by the number of symbols in the figure) were sacrificed for determination of the amount of viable, infectious Chlamydia ((**c**), mean ± standard deviation of log10 (IFU); $n$ = 9–10), and the levels (mean ± standard deviation of log10) of MPO ((**d**); $n$ = 5), TNF-α ((**e**); $n$ = 5–7) and IFN-γ ((**f**); $n$ = 5–7) in the lung homogenate. Mock infection: $n$ = 8. LOD = limit of detection; n.d. = not determined, ns = not significant. The performed statistical analysis is described in Section 2. ** indicates statistical significance with $p < 0.01$. The exact size of each group can be found in Supplement Table S2.

### *3.5. IgA, IgM, and Total IgG antibody Response Profiles towards the Adjuvanted 5cVAC Antigen-Mix or the Single Vaccine Components in Blood of Five Mice after Vaccination with 5cVAC, Seven Days before or after C.tr. E Challenge, Respectively*

To get an impression of individual humoral immune responses against the five different antigens, plasma of the first five mice which were vaccinated i.n. with 5cVAC was analyzed 7 days before and 7 days after C.tr. E challenge infection (Figure 6). Due to limited blood volume which can be drawn from mice during an ongoing experiment and the broad analysis performed with each sample (18 ELISAs for three types of Igs with six different antigens), the plasma had to be pre-diluted to 1:316 for antigen-specific IgA and IgM, or 1:3160 for IgG, respectively. Elevated levels [U] of IgA or IgM correspond in this experimental setup to titers of 1:300 to 3000, and elevated units of IgG to titers of 1:3000 to 30,000, or higher (data not shown, see also Figure 7). All negative controls with plasma of individual non-vaccinated C.tr. E-challenged or non-challenged mice remained below <1 U (data not shown).

To overcome the limiting amount of plasma of individual animals and to be able to detect also potentially lower antigen-specific IgG levels (at least in the larger amount of blood obtained by heart puncture seven days after infection) the sera of $n$ = 9 vaccinated, challenged and euthanized mice were pooled. This larger volume of pool serum could be analyzed with less diluted samples, i.e., starting a dilution curve (now also) for IgG already at 1:316 (Figure 7).

The specific humoral responses against the five recombinant antigens varied steeply between the individual mice, in particular for IgM. The level of vaccine-induced circulating anti-5cVAC-IgG in the five analyzed mice was in a rather similar order (with a discrepancy of ± 50% maximal) before and after challenge infection. The highest reliable antibody responses in the samples of the individual mice (Figure 6) and in the pool plasma (Figure 7) were obtained against the antigens PmpD and Ctad1, and partially also against PmpH. The pool serum of vaccinated and challenged mice remained positive against the 5cVAC mix (and above the OD value of the negative control) at a dilution of approximately 1:100,000 or higher (Figure 7). Within the sensitivity of the assays, (almost) no antibodies against PmpA could be detected.

Most likely, due to limited sensitivity of an ELISA utilizing homogenate of Chlamydia-infected cells, we could not verify directly the presence of antibodies raised by adjuvanted 5cVAC against 'endogenous' chlamydial antigens (data not shown). However, the IgA and IgG responses against the recombinant antigens seven days after challenge infection were mostly higher (or equal) to those found in the same animal directly before challenge infection (Figure 6). That indicates that the recombinant proteins of 5cVAC had indeed primed the immune system for the corresponding endogenous chlamydial proteins.

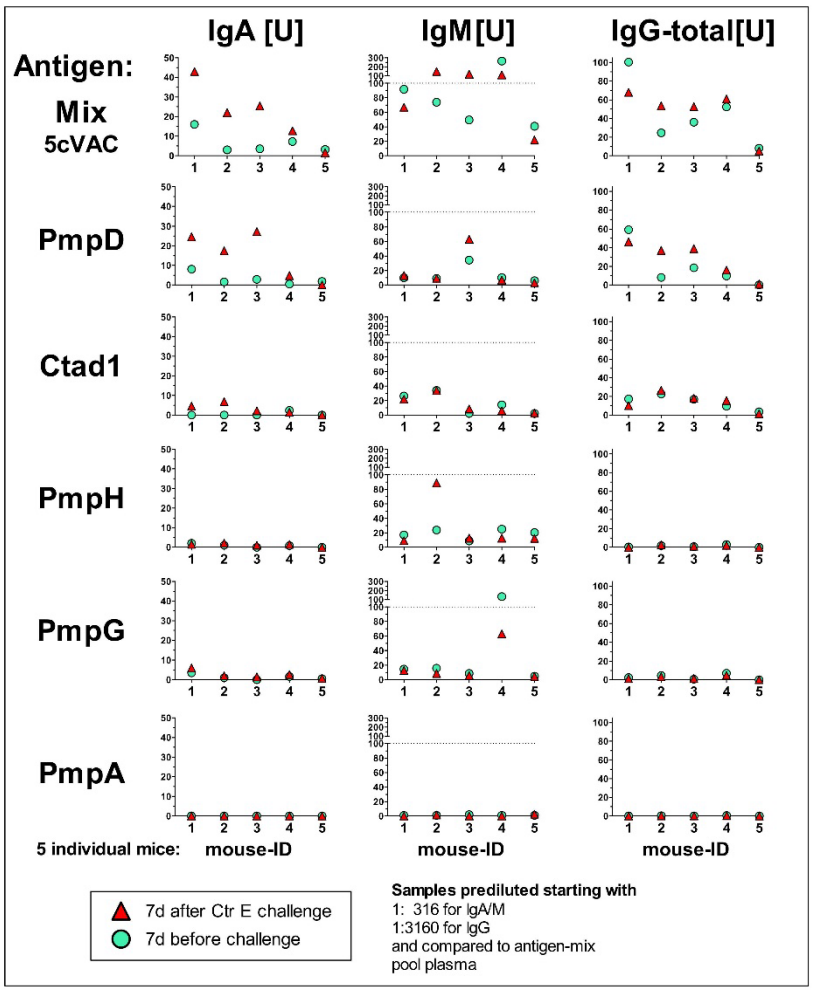


**Figure 6.** Antibody response profiles towards the 5cVAC-mix or its five components in mouse plasma of five individual mice, seven days before or after *C. trachomatis* E challenge. ELISAs detecting IgA (**left**), IgM (**middle**), and total IgG (**right**) directed against the 5cVAC antigen-mix or the single vaccine components (in the indicated rows) were performed with plasma from individual i.n. 5cVAC-vaccinated mice obtained in the short-term protection model seven days before (green circles) and after (red triangles) C.tr. E ($1.3 \times 10^6$ IFU) infection. To permit direct comparison of the results, arbitrary units of the different Ig's [U] were calculated in relation to a standard curve based on pool plasma obtained after 5cVAC application and C.tr. E challenge. The samples had to be prediluted to 1:316 for IgA/M and 1:3160 for IgG, respectively. All corresponding negative controls with plasma of individual non-vaccinated C.tr. E-challenged or non-challenged mice remained below <1 U (data not shown).

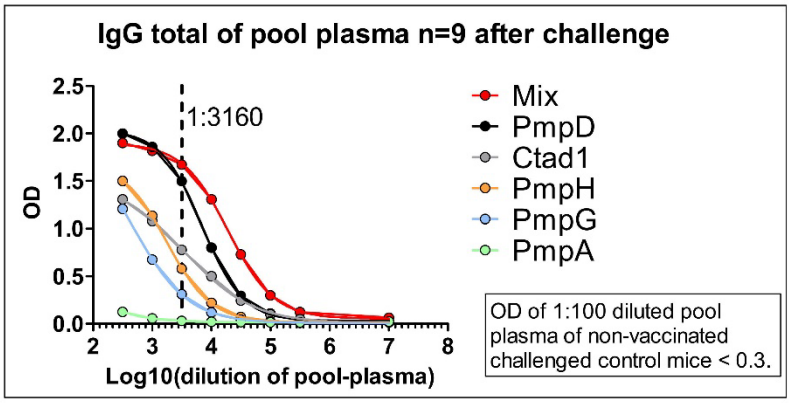


**Figure 7.** 5cVAC-specific IgG-antibodies in pool-plasma obtained from mice vaccinated i.n. with adjuvanted-antigen seven days after challenge infection with *C. trachomatis* E. The amount of IgG directed against the 5cVAC-mix or the individual recombinant antigens, respectively, was determined in pool plasma of $n = 9$ 5cVAC-vaccinated and C.tr. E-challenged mice. Due to the larger available volume, dilution could already start at 1:316, and thus, lower antigen-specific IgG-responses are detectable, here. The vertical broken line at 1:3160 indicates the lowest dilution used before in total-IgG analysis of five individual mice (Figure 6). Pool plasma of non-vaccinated control mice that were challenged i.n. for seven days with C.tr. E served as negative control; even just 1:100 diluted, its OD depending on total IgG against the 5cVAC mix remained <0.3 (data not shown).

### *3.6. Intranasal Vaccination with c-di-AMP-Adjuvanted Two-Component 2cVAC Is Still Effective against C.tr. E, but with A Smaller Degree of Protection as Compared to 5cVAC*

After vaccination with 5cVAC, PmpD and Ctad1 were the two antigens that led to the most robust specific IgA and IgG response (Figures 6 and 7). Therefore, they were selected for a vaccination experiment applying i.n. an equimolar mix of these two proteins, only (2cVAC). Compared to non-vaccinated control mice, starting on the fourth day of C.tr. E challenge infection, pretreatment with 2cVAC resulted in similar regain in body weight as with 5cVAC in a former, otherwise identical experiment (Figure 8a). However, the decrease in the clinical score was less pronounced after vaccination with adjuvanted 2cVAC.

On days 5 and 6 p.i., the clinical score of 2cVAC-pretreated mice was smaller than that of mice which had only received buffer or adjuvant, but higher than that of 5cVAC-pretreated animals (Figure 8b). In accordance with that, the amount of infectious Chlamydia in the lung of 2cVAC-treated mice was lower than in the negative controls, but higher than in the 5cVAC-pretreated animals (Figure 8c). Moreover, the levels of MPO and IFN-γ in the lung homogenate of 2cVAC-vaccinated mice were lower than those of non-vaccinated mice. In contrast to 5cVAC-pretreated mice, there was only a similar trend for TNF-α (Figure 8d–f). Thus, the two-component vaccine 2cVAC was still effective against C.tr. E, but achieved a smaller degree of protection as compared to 5cVAC.

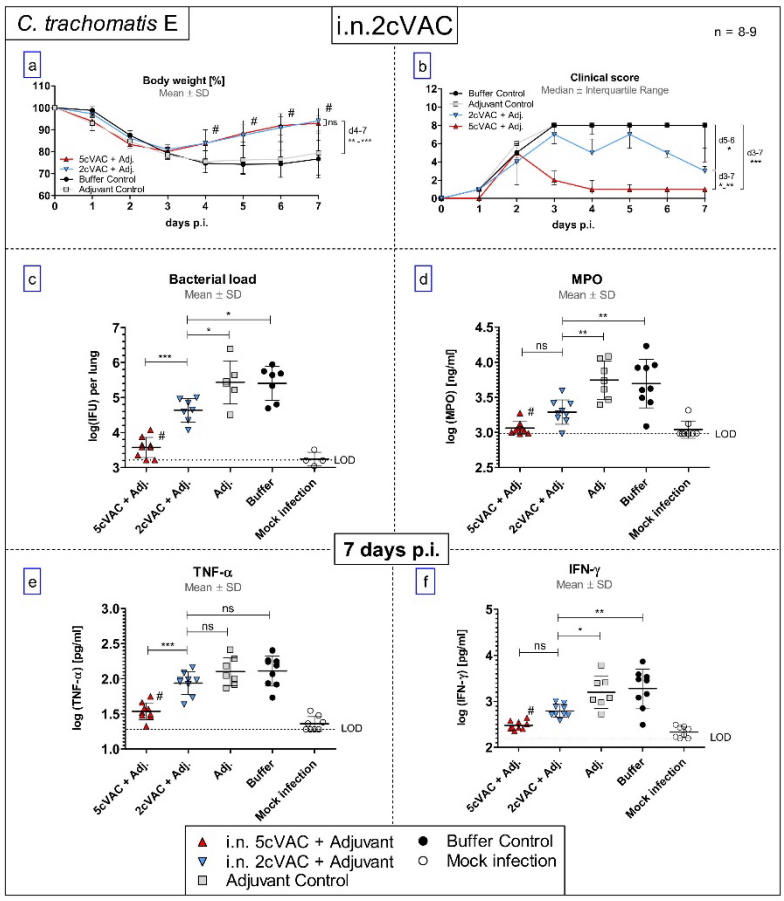


**Figure 8.** Body weight, clinical score, bacterial load, granulocyte marker MPO, TNF-α, and IFN-γ in lung challenge infection with *C. trachomatis* E in the short-term protection model after i.n. vaccination with c-di-AMP-adjuvanted two-component 2cVAC. In this modified short-term protection model (see Figure 1a), vaccinated mice received only two of the five components contained in 5cVAC (2cVAC: PmpD and Ctad1) plus c-di-AMP by the i.n. route (blue triangles). Animals pretreated with adjuvant, or buffer, respectively, served as negative controls. Per group, $n$ = 8–9 differently pretreated 15-week-old animals were infected i.n. with 1.3 × $10^6$ IFU of C.tr. E. On each of the following days, body weight ((**a**), in % as mean ± standard deviation) and clinical score ((**b**), median ± interquartile range) were assessed. On day 7 after i.n. challenge infection, the surviving animals (also indicated by the number of symbols in the figure) were sacrificed for determination of the amount of viable, infectious Chlamydia ((**c**), mean ± standard deviation of log10 (IFU); $n$ = 6–9), and the levels (mean ± standard deviation of log10; $n$ = 7–9) of MPO (**d**), TNF-α (**e**), and IFN-γ (**f**) in the lung homogenate. Mock infection: $n$ = 4 for bacterial load, $n$ = 8 for other parameters. For better comparability, data obtained in a previous, otherwise identical experiment with i.n. 5cVAC pretreatment are also depicted (red triangles). LOD = limit of detection; ns = not significant. The performed statistical analysis is described in Section 2. *,**,*** indicate statistical significances with $p < 0.05$, <0.01, and <0.001, respectively. Statistical significance ($p < 0.05$) between the 5cVAC and the adjuvant/buffer control groups is marked with # in the panels (**a**,**c**,**d**–**f**). The exact size of each group can be found in Supplement Table S2.

### *3.7. Serum-Transfer Demonstrates That Circulating Antibodies Raised by c-di-AMP-Adjuvanted 5cVAC Alone Are Not Protective against C. trachomatis E Lung Infection*

To clarify the protective potential of circulating antibodies which are induced by c-di-AMP-adjuvanted 5cVAC after i.n. or s.c. application of the vaccine, respectively, a serum-transfer from vaccinated or non-vaccinated control mice to naïve mice was conducted (Figures 1b, 9 and 10). Two days later, the recipient mice were challenged i.n. with C.tr. E. Moreover, anti-5cVAC antibodies were determined in the transferred pool plasma from the donors as well as in the sera of the individual recipient mice before infection (Figure 9).

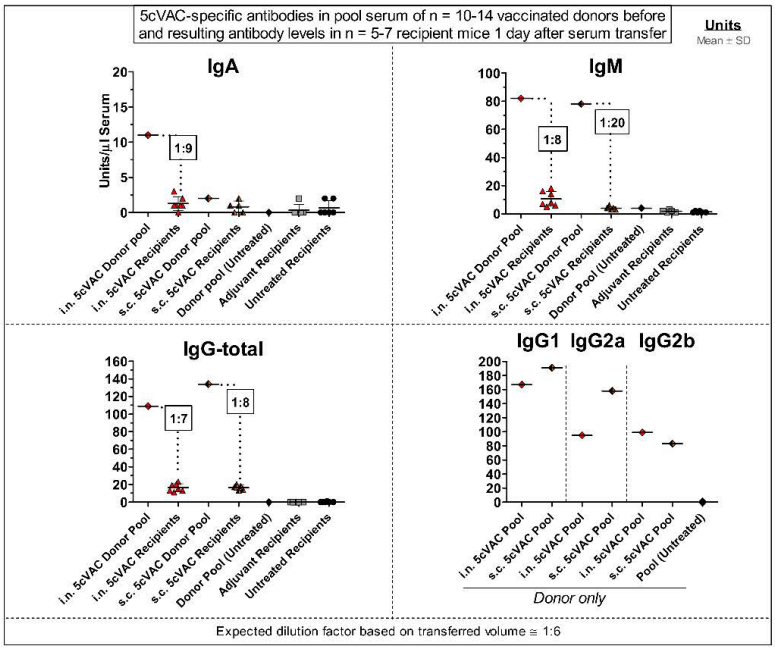


**Figure 9.** Specific IgA, IgM, total-IgG, and IgG-subtypes in transferred donor pool sera from differentially vaccinated non-infected mice and resulting Ig-levels in healthy recipient mice (before i.n. challenge with *C. trachomatis* E). Hormone-synchronized, non-vaccinated, 15-week-old C57BL/6J ($n$ = 5–7 per group) received i.v. pool sera (of 10–14 animals per group) that had been vaccinated i.n. or s.c. with c-di-AMP-adjuvanted 5cVAC (see also Figure 1b). Alternatively, they received pool sera of mice that had been pretreated with c-di-AMP alone (adjuvant recipients), or that were not pretreated at all (untreated recipients). One day after serum administration, a small amount of blood was collected from each recipient to determine resulting individual antibody levels in comparison to the Ig levels found in the corresponding transferred pool serum. The boxes in the graph show the calculated factors of dilution of the 5cVAC-specific antibodies. Anti-5cVAC IgA, IgM, total IgG, as well as $IgG_1$, $IgG_{2a}$, and $IgG_{2b}$ were determined as arbitrary units (U) in the transferred pool sera. The IgG-subtypes were only determined in the pool sera from the donors. In this context, "Pool (Untreated)" represents the results combined from the various negative controls. The size of each group can be found in Supplement Table S3.

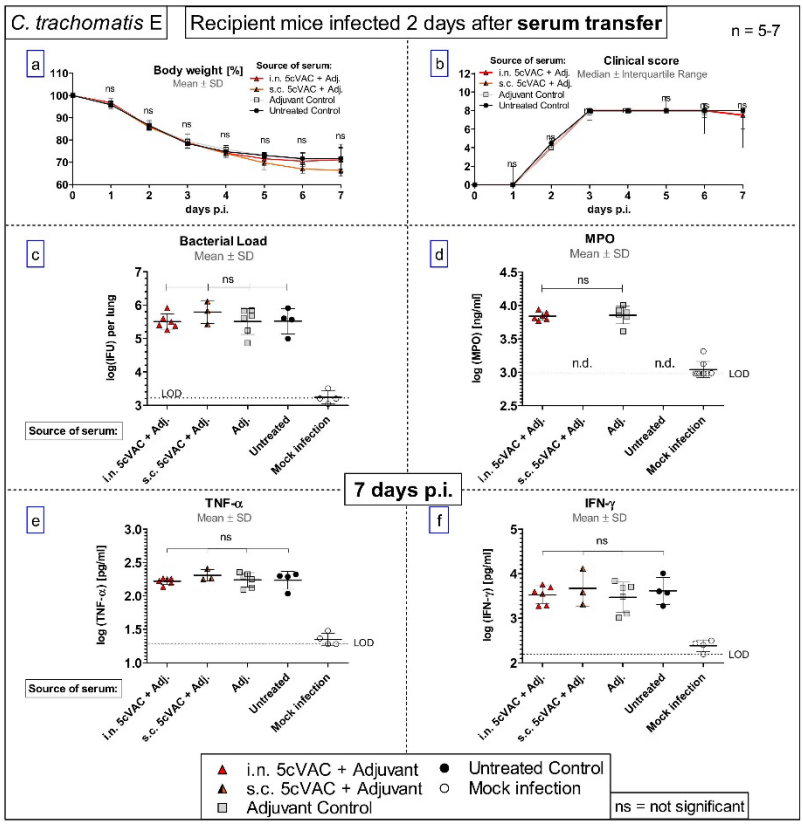


**Figure 10.** Body weight, clinical score, bacterial load, granulocyte marker MPO, TNF-α, and IFN-γ in recipients of transferred pool sera from vaccinated healthy mice, after i.n. challenge infection with *C. trachomatis* E. Hormone-synchronized, non-vaccinated, 15-week-old C57BL/6J ($n$ = 5–7 per group) received i.v. pool sera of 10–14 animals (per group) that had been vaccinated i.n. or s.c. with c-di-AMP-adjuvanted 5cVAC. Other recipients received pool sera of mice that had been pretreated with c-di-AMP alone (Adj.; adjuvant recipients), or that were not pretreated at all (Untreated; untreated recipients). Two days after serum-transfer, the recipients were challenged i.n. with $1.3 \times 10^6$ IFU of C.tr. E (see also Figure 1b). Afterwards, body weight ((**a**), in % as mean ± standard deviation) and clinical score ((**b**), median ± interquartile range) were assessed daily. On the seventh day of challenge infection, the animals were sacrificed for determination of the bacterial load of infectious Chlamydia ((**c**), mean ± standard deviation of log10(IFU); $n$ = 3–6) and of the levels (mean ± standard deviation of log10) of MPO ((**d**); $n$ = 6), TNF-α ((**e**); $n$ = 3–6) and IFN-γ ((f); $n$ = 3–6) in lung homogenate. Mock infection: usually $n$ = 4; $n$ = 8 for MPO. LOD = limit of detection; n.d. = not determined; ns = not significant. The performed statistical analysis is described in Materials and Methods. The exact size of each group can be found in Supplement Table S3.

Similar amounts of 5cVAC-specific IgM, and total IgG antibodies were present in the pool sera of donor mice that had been vaccinated i.n. or s.c., respectively. Moreover, independently of the route of 5cVAC-application, specific antibodies of the $IgG_1$, $IgG_{2a}$ and $IgG_{2b}$ subclass were also detectable in the two pool sera. Thereby, 5cVAC-specific $IgG_{2a}$ seemed to be slightly less elevated in the serum obtained after i.n. vaccination; whereas $IgG_1$- and $IgG_{2b}$-levels appeared to be similarly high (Figure 9). As expected, 5cVAC-specific IgA antibodies were only present in the transferred pool serum of donor

mice that had been vaccinated by the i.n. route, i.e., via the mucosa (Figure 9, upper left panel). Remarkably, after C.tr. E challenge infection of the serum-recipients, the comparison of body weight, clinical sore, chlamydial load in the lung, MPO, TNF-α, or IFN-γ (Figure 10a–f) between the different groups did not show any significant effect caused by the transferred two 5cVAC-specific hyper-immune antisera-irrespective of whether these sera were raised by i.n. or by s.c. application of the vaccine.

### *3.8. Results of the Long-Term Protection Study*

Following the long-term protection model, five months after the last i.n. booster vaccination, hormone-synchronized female mice differently pretreated with either c-di-AMP-adjuvanted 5cVAC, or adjuvant, or buffer alone, were challenged with $4 \times 10^5$ of C.tr. E.

#### 3.8.1. Diminished Weight Loss, Clinical Score, and Higher Bacterial Clearance from the Lung

The daily-assessed body weight (%) (Figure 11a) and the clinical score (Figure 11b) showed an improved course of disease of the i.n. 5cVAC-vaccinated mice, starting from day 4 or 5 after challenge infection. Corresponding to that, five months after the last i.n. application of adjuvanted 5cVAC, the bacterial load in lung homogenate was significantly smaller 7 days after C.tr. E challenge infection as compared to control mice that had been pretreated with c-di-AMP only, or buffer (Figure 11c). No significant decrease of MPO, TNF-α, or IFN-γ occurred due to vaccination (Figure 11d–f). Nevertheless, these results clearly indicate that i.n. vaccination with c-di-AMP-adjuvanted 5cVAC leads in mice to a certain degree of long-term protection against C.tr.

#### 3.8.2. Vaccine-Specific Humoral Immune Responses in Blood and Cellular Responses in the Spleen Five Months after the Last Intranasal Booster Vaccination with c-di-AMP-Adjuvanted 5cVAC

To gain insight into vaccine-induced specific immune responses in our long-term protection model (Figure 1c), 5cVAC-induced antibody (Figure 12) and cellular (Figure 13) responses were analyzed five months after the last i.n. applications of the adjuvanted vaccine without (i.e., one day before) or seven days after a C.tr. E lung challenge infection, respectively. In this experimental setting, all mice were euthanized on the day of the collection of serum and splenocytes.

Even after that relatively long period, we could still detect 5cVAC-specific IgA, IgM and IgG as well as $IgG_1$, $IgG_{2a}$ and $IgG_{2b}$ in blood obtained slightly ahead as well as after challenge infection, although with rather wide variations from mouse to mouse (Figure 12a,b). As expected, without challenge infection, the antibody levels of mice vaccinated i.n. were much lower after four additional months as compared to those determined in pool serum obtained four weeks after the last booster vaccination (Figure 9).

Moreover, splenocytes of vaccinated and control mice from the long-term experiment, harvested either without or seven days after a C.tr. E challenge infection, proliferated in a dose-dependent manner after incubation with 5cVAC. The dose–response curve of splenocytes from vaccinated mice was shifted to lower antigen concentrations in comparison to that of splenocytes from control mice pretreated with adjuvant alone, or buffer (Figure 13a,b).

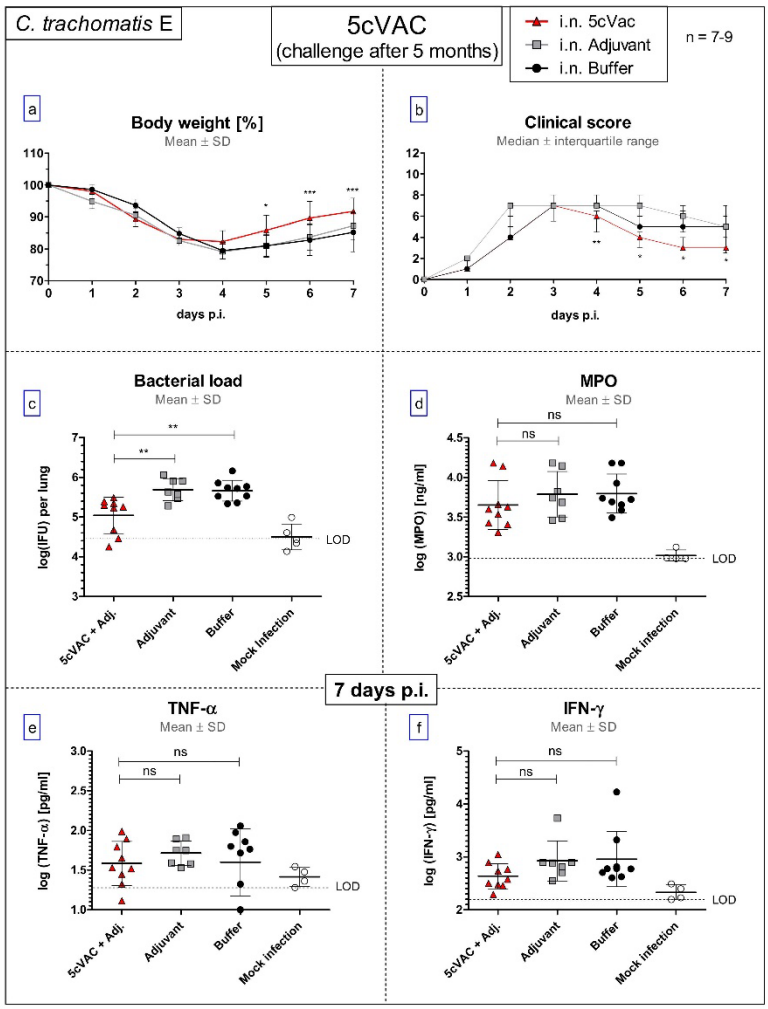


**Figure 11.** Body weight, clinical score, bacterial load, granulocyte marker MPO, TNF-α, and IFN-γ in lung challenge infection with *C. trachomatis* E in the long-term protection model five months after i.n. vaccination with adjuvanted 5cVAC. Twenty weeks after the last i.n. booster vaccination, $n$ = 7–9 hormone-synchronized female mice differently pretreated either with c-di-AMP-adjuvanted 5cVAC, or c-di-AMP or buffer, were challenged with $4 \times 10^5$ IFU of C.tr. E (see also Figure 1c) and analyzed. Body weight ((**a**), in % as mean ± standard deviation) and clinical score ((**b**), median ± interquartile range) were assessed daily. On day 7 after challenge infection, the animals were sacrificed for determination of the bacterial load, i.e., the amount of viable, infectious Chlamydia ((**c**), mean ± standard deviation of log10(IFU)), and the levels (mean ± standard deviation of log10) of MPO (**d**), TNF-α (**e**) and IFN-γ (**f**) in the lung homogenate. Mock infection: $n$ = 4–5. LOD = limit of detection, ns = not significant. The performed statistical analysis is described in Section 2. *,**,*** indicate statistical significances with $p < 0.05$, <0.01, and <0.001, respectively. The exact size of each group can be found in Supplement Table S3.

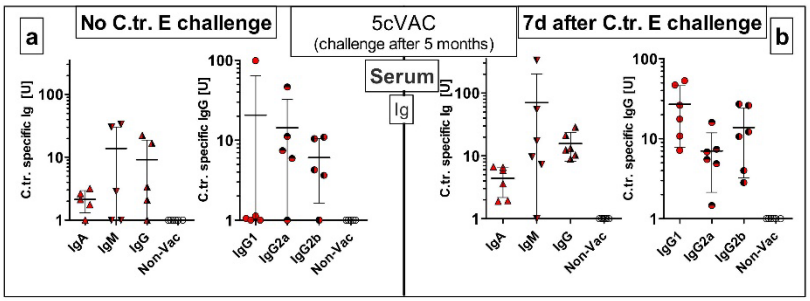


**Figure 12.** Antigen-specific humoral responses in mice 5 months after the last i.n. booster vaccinations with c-di-AMP-adjuvanted 5cVAC. 5cVAC-specific circulating Ig's were determined in serum 20 weeks after the last i.n. application of the c-di-AMP-adjuvanted vaccine, without (left side) and seven days after challenge infection with $4 \times 10^5$ IFU of C.tr. E (right side). 5cVAC-specific IgA, IgM, IgG as well as $IgG_1$, $IgG_{2a}$, and $IgG_{2b}$ were still detectable in most mice ($n$ = 5–7 per group) without (**a**) as well as after challenge (**b**). In control mice (that received only c-di-AMP or buffer), no 5cVAC-specific antibodies could be detected (<1 U). The exact size of each group can be found in Supplement Table S3.

ELISpot-analysis of the splenocytes demonstrated a 5cVAC-dependent release of IFN-γ, IL-2, IL-4, and IL-17 after restimulation (Figure 13c,d). For unknown reasons, the background release of IL-17 caused by adjuvant or buffer was relatively high in the splenocytes of mice that were not challenge infected. Nevertheless, the number of IL-17 positive spots was significantly higher after re-stimulation with 5cVAC (Figure 13c). The determined number of spot forming units was similar or higher 7 days after C.tr. E challenge infection (Figure 13d); the number of IFN-γ, IL-2, IL-4, and in particular IL-17 producing splenocytes from mice that had been vaccinated i.n. with c-di-AMP-adjuvanted 5cVAC increased drastically due to re-stimulation with 5cVAC. In spleens of the control mice, such IL-2, IL-4, and IL-17 producing cells were almost absent. Most likely, due to the ongoing challenge infection, there was only a slightly higher background in IFN-γ spot forming units (yet, with a three-times higher response of splenocytes from vaccinated mice).

Therefore, we determined only from splenocytes of challenged mice double or triple positive $CD4^+$ or $CD8^+$ T cells by FACS-analysis (Figure 13e,f). Indeed, only after re-stimulation with 5cVAC, similar elevated numbers of (IFN-γ/TNF-α/IL-2)-triple-positive, (IFN-γ/TNF-α)-double-positive, to a smaller extend also (IFN-γ/IL-2)-double-positive, and IFN-γ-single-positive $CD4^+$ T cells could be detected (Figure 13e). Moreover, there was also an increase in mainly (IFN-γ/TNF-α) and partially also (IFN-γ/IL-2)-double positive $CD8^+$ T cells from vaccinated mice after re-stimulation with 5cVAC. That did not occur in T cells from control mice (Figure 13f).

These findings show that vaccination with c-di-AMP-adjuvanted 5cVAC causes long-lasting antigen-specific antibody as well as T cell responses, which correlate with protection against C.tr.

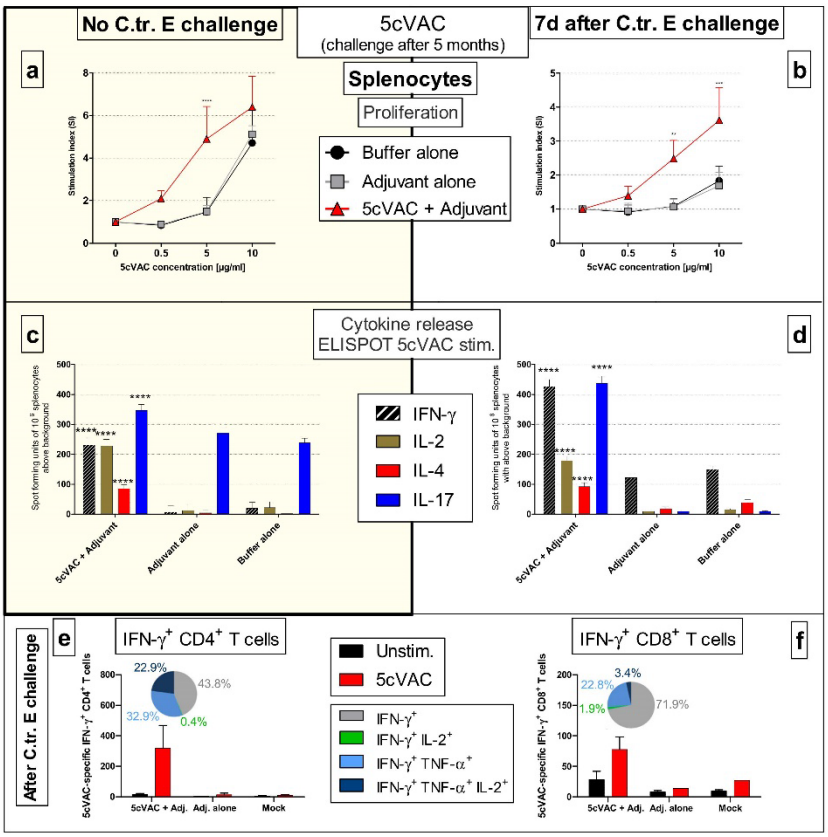


**Figure 13.** Antigen-specific cellular responses in mice, 5 months after the last i.n. booster vaccinations with adjuvanted 5cVAC. 5cVAC-induced cellular responses in the spleen were analyzed 20 weeks after the last i.n. application of the c-di-AMP-adjuvanted vaccine, without (**a**,**c**) and seven days after challenge infection with $4 \times 10^5$ IFU of C.tr. E (**b**,**d**–**f**). Mice that received only c-di-AMP or buffer served as negative controls. Proliferation of splenocytes from vaccinated and control mice without (**a**) and after (**b**) challenge was determined in response to increasing concentrations of 5cVAC. The depicted stimulation indexes (SI) are the ratio of [3H]-thymidine uptake of stimulated versus non-stimulated samples. (**c**,**d**) show the dependence of the number of (ELI)Spots of IFN-γ, IL-2, IL-4, and IL-17-producing 5cVAC-restimulated cells (per $10^6$ spleen cells after subtraction of background values of unstimulated cells) on vaccination with adjuvanted 5cVAC. The results presented come from cells of $n = 5$ vaccinated and 6 non-vaccinated (buffer- or adjuvant-treated) healthy (**a**,**c**), or $n = 7$ vaccinated and 10 non-vaccinated (buffer- or adjuvant-treated) infected mice (**b**,**d**). Flow cytometric identification of multifunctional 5cVAC-restimulated $CD4^+$ (**e**) and $CD8^+$ (**f**) T cells was performed in $n = 4$ vaccinated and 4 non-vaccinated mice after challenge infection. The pie charts depict the proportion of single (light grey), double (green and light blue), and triple (dark blue) cytokine producers. The bar chart indicates the frequency (mean ± SD) of single (IFN-γ), double ($IFN\text{-}\gamma^+/TNF\text{-}\alpha^+$, $IFN\text{-}\gamma^+/IL\text{-}2^+$) and triple ($IFN\text{-}\gamma^+/TNF\text{-}\alpha^+/IL\text{-}2^+$) Th1 cytokine-producing multifunctional $CD4^+$ and $CD8^+$ T cells. The number of unstimulated cells was subtracted from the respective number of stimulated samples. The performed statistical analysis is described in Section 2. For statistical analysis of the cellular responses, differences from the 5cVAC restimulated versus non-stimulated splenocytes are shown by **,***,****: ** $p < 0.01$, *** $p < 0.001$ or **** $p < 0.0001$). The exact size of each group can be found in Supplement Table S3.

## 4. Discussion

The vaginal mouse infection model with the strict mouse pathogen C. *muridarum* leads to histopathological changes of the upper genital tract and infertility, and is thus, rather close to the human disease the vaccine is intended for. However, with an observation period of up to nine weeks post (challenge) infection, it is rather lengthy. In addition, vaginal application of human C.tr. strains does not cause ascending genital infection with the complications feared in women, but only vaginal shedding for several weeks. Transcervical-intrauterine application of C.tr. as performed by others [21], is technically demanding and only partially physiological. Of course, these urogenital models are nevertheless extremely valuable in C.tr. vaccine research.

Usually, C.tr. can cause pneumonia in human newborns only [8]. Nevertheless, for practical reasons, as demonstrated here, our mouse C.tr. lung infection model [40,41] complements, and in some regards even surpasses the valuable confirmatory urogenital model with all its pros and cons, as a relatively fast and highly quantifiable screening method. Moreover, we had to consider that the identities of the recombinant antigens derived from C.tr. E are, compared to other C.tr. serovars, lower for C. *muridarum* (67–82%; Table 1). Therefore, we chose a model which does not depend on this mouse pathogen and an uncertain degree of cross species protection of 5cVAC. In this work, the C.tr. pneumonia model was also instrumental to determine in detail the efficacy of our new adjuvanted vaccine candidate against various serovars (i.e., broadness of the elicited response and potential universal character of the vaccine candidate), to compare the five (5cVAC) with a two component (2cVAC) vaccine, to address long-term protection, and to characterize vaccine-induced specific humoral and cellular immune responses.

An ideal vaccine should increase the chances of cross-protection between various C.tr. serovars in respiratory and genital (and even ocular) infection. Additionally, it should diminish the risk of escape mutants of the bacterium under selective pressure of population-wide vaccination. Hence, a multi-subunit vaccine, which combines several essential targets, appeared highly advantageous.

The rational for selection of the five chlamydial antigens of C.tr. serovar E contained in 5cVAC was additionally the following: (a) as described above, literature and our own data [23,24,30,32] indicate Pmp's as promising antigens; (b) these proteins as well as Ctad1 are located on the surface of infectious EBs [33,51]; (c) they are participating in adhesion and binding of C.tr. E to the host cell [24,33], yet, the functional importance of these surface proteins for binding might vary depending on serovar, infected host cell type or tissue; and (d) there is high sequence identity between the Pmp and Ctad1 proteins across C.tr. serovars (E versus L2 or A: 92–100%), while it is lower to other species (C.tr. E versus C. *muridarum*: 67–82%), thus increasing chances for broad cross-serovar protection (see also Table 1). If the humoral response played a role in 5cVAC-induced protection, it seemed likely that induced antibodies bound to several of these antigens on the surface of EBs might neutralize chlamydial binding and diminish infection to the highest extent. With that said, of course, one could not be sure how far specific cellular immune responses might be alternatively or additionally relevant in vaccine-induced defense against the intracellular pathogen after its uptake, and whether antibodies might represent a minor contributor or just a correlate of protection, as our passive serum transfer studies seem to suggest (see below).

Intranasal application of c-di-AMP-adjuvanted 5cVAC was highly protective against C.tr. serovar E: After lung challenge infection, compared to controls the bacterial load was reduced by 2 log10 levels. Loss of body weight and clinical score, as well as the levels of the granulocyte marker MPO and the cytokines IFN-$\gamma$ and TNF-$\alpha$ in the lung were significantly diminished. The degree of determined protection and the kinetics were similar as observed in a C.tr. E/C.tr. E reinfection experiment under similar conditions (unpublished data). Vaccinated as well as re-infected mice become sick for 3 to 4 days after i.n. challenge before they recover within a few days. The similar course suggests maximal achievable protection by our new vaccine. Importantly, after i.n. application of

adjuvanted 5cVAC, effective cross-protection developed against serovars D and L2, and even the ocular serovar A indicating a broad vaccine-induced protection across various C.tr. serovars. The significantly more favorable development of body weight and clinical score and the diminished chlamydial load in lung compared to control mice prove that vaccine-induced protection against C.tr. lasts at least five months. Remaining protection seems to be lower five months after the last i.n. booster application with adjuvanted 5cVAC. Thus, for instance, there were no 5cVAC-dependent changes in the level of MPO, IFN-γ or TNF-α in lung homogenate, and the bacterial load decreased only by approximately 80% as compared to 99%. Yet, a direct comparison of the results achieved in this long-term protection experiment with those achieved in the short-term protection experiment is only possible to a limited extent, because the amount of C.tr. E in the challenge infections was different. It had to be reduced by a factor of >3 in the 31-week-old, more sensitive mice (see also M&M and Supplement Figure S4). In this regard, it is critical to consider the normal life-span of mice, the age of the mice included in this experiment at the time of the challenge, and the potential effects of an ongoing immune senescence process.

The results of our Ig-ELISAs were highly suggestive for a functional significance of circulating antigen-specific antibodies induced after i.n. 5cVAC application. The highest reliable (of the rather heterogeneous) antibody responses in 5cVAC i.n. treated mice were obtained against the antigens PmpD and Ctad1, and partially also against PmpH.

Adjuvanted 2cVAC—i.e., an equimolar mix of recombinant PmpD and Ctad1—was still effective against C.tr. E. Yet, according to the clinical score as well as chlamydial clearance and MPO, IFN-γ, and TNF-α in the lung homogenate, 2cVAC was less effective than 5cVAC. One can draw the conclusions (a) that PmpD and/or Ctad1 are highly protective and (b) that at least one of the other three antigens contained in 5cVAC is additionally inducing protection, emphasizing the importance of a multi-subunit vaccine. That is of even more concern, as one cannot exclude that the success of the vaccine-induced defense might also depend on the respective C.tr. serovar and the infected organ. Furthermore, a multi-subunit vaccine reduces the risk of immune escape resulting from either pathogen evolution or vaccination-derived selective pressure.

This risk might be much higher in case of a 'single-antigen' MOMP-based vaccine. In C.tr. vaccination studies, MOMP plays a prominent role [6,16,19]. According to the overview by Phillips et al. from 2019 [5]: "To date, the MOMP has emerged as the most suitable substitute for whole cell targets and its delivery as a combined systemic and mucosal vaccine is most effective." Yet, as reviewed in [19], MOMP induces C.tr. serovar- or at least serogroup-specific responses. Furthermore, against *C. muridarum*, nMOMP purified (in small amounts) from the chlamydial EBs was more protective than purified recombinant rMOMP [52–54]-limiting for practical reasons its use as vaccine. Presently, the most suitable and promising substitute for a chlamydial whole cell target is probably a complex recombinant protein vaccine combining the variable domain VD4 and surrounding constant immunogenic regions of MOMP from different serovars, in order to cover the most frequent ones, combining s.c. and i.n. administration [55]. A promising phase-1-clinical trial has been recently finished [56]. However, without loss of function the MOMP gene *ompA* can mutate and is subject to immune selective pressure and recombination, as demonstrated by the existing various C.tr. genotypes and serovars [57]. The identification of a novel, hybrid C.tr. genomic mosaic L2b/D-Da strain causing an outbreak of LGV indicates also this ability of C.tr. for genetic variation [58]. Population-wide vaccination with parts of MOMP—if successful—might raise such pressure leading to the selection of existing C.tr. serovars that are not targeted by the vaccine, and of new C.tr. MOMP mutants or variants who escape the defense caused by vaccine-induced antibodies or T cells.

Interestingly, after vaccination with shorter recombinant fragments from all nine C.tr. E Pmps combined with CpG-1826 and Montanide ISA 720 as adjuvants by 2× the i.m. plus 1× the s.c. route, BALB/c mice vaccinated with PmpC, G, or H were best protected against an i.n. *C. muridarum* challenge infection [30]. In that quite different experimental setting, the IgG serum titer against PmpG was the highest, PmpH was on the third position,

PmpD on the fifth and PmpA second to last. Thus, in that [30] and our study, only the low humoral responses to PmpA are in total accordance.

It is important to note, however, that high immunogenicity or immuno-dominance of an antigen does not mean that it must participate in the observed defense. Antibodies might be just a 'biomarker' correlating with protection rather than a main effector mechanism for the immune protection achieved. In fact, after vaccination with adjuvanted 5cVAC, circulating antibodies play, if at all, only a minor role, as most convincingly demonstrated by absent protection against C.tr. E after transfer of hyper-immune serum.

The rather similar measured values of 5cVAC-specific antibodies in the blood of individual recipients (collected on the day between serum-transfer and i.n. C.tr. E-challenge infection) within each treatment group demonstrate the reliable performance of the serum transfer experiment. The amount of C.tr.-specific antibodies in the recipients was approximately 10% (1:7 to 1:20) of the amount found in the administered pool serum. The measured factors are pretty close to the predicted dilution factor of approximately 1:6. This prediction takes into account only the addition of the known volume of transferred serum ($2 \times 170$ µL) to the naïve recipient's (according to body weight) estimated total blood volume, but e.g., not redistribution into other body fluids. Serum transfer did not lead to any protection in the recipients. Thus, approximately 1:10-diluted vaccine-induced circulating antibodies alone are not protective against C.tr. E.

This view is further supported by negative preliminary results obtained in a flow cytometric neutralization assay with HeLa or Syrian hamster kidney (HaK) cells after preincubation of EBs from C.tr. E with the hyper-immune serum (data not shown). Delayed improvement of body weight and clinical score after an unchanged onset of disease argue also against a main protective role of antibodies because one might expect that, if neutralizing EBs, they would prevent host cell infection and thus, already affect the start of challenge infection. Finally, in the plasma of the fifth of the individually analyzed animals, 5cVAC-specific IgA, IgM or IgG were hardly detectable after vaccination. Yet, an approximately 50-fold (compared to the mean of other mice smaller) decrease of the bacterial load still occurred (data not shown). Of course, one cannot completely exclude that small amounts of circulating antibodies below the detection limit of our Ig-ELISA were already interfering in infection of this mouse.

Subcutaneous application of c-di-AMP-adjuvanted 5cVAC was not protective in C.tr. E challenge. Only the i.n., i.e., mucosal application of our new vaccine protected against chlamydial lung infection. Our findings comparing the antibody responses after vaccination by the two different routes exclude that smaller amounts of circulating 5cVAC-specific IgM, IgG or $IgG_1$, $IgG_{2a}$, and $IgG_{2b}$ are responsible for that. However, our results—in particular those of the serum-transfer experiment—do not rule out augmentation of T cell responses by circulating antibodies, or a critical role of mucosal, secretory IgA.

In a C.tr. study of Stary et al. [21], mice were vaccinated with UV-inactivated EBs alone or with commonly used adjuvants. Surprisingly, more Chlamydia were found after genital challenge infection in the uterus of vaccinated animals as compared to controls. Most likely, tolerance was induced by regulatory T cells-explaining negative outcomes of trials based on whole cell EBs in the 1960s. In parallel, UV-inactivated EBs covalently linked to a potent TLR7/8 agonist and complexed with nano charge-switching synthetic adjuvant particles were also applied. Intriguingly, similar to our new vaccine, s.c. vaccination was not protective. However, genital as well as i.n. application resulted via mucosal cross-protection in a decreased chlamydial load in that organ. After mucosal application of the adjuvanted vaccine, $CD4^+$ effector T cells migrate to the uterus and establish tissue-resident memory cells. These cells are reactivated upon genital challenge triggering migration of circulating memory T cells into the infected organ. In a recall response, they release cytokines for pathogen clearance, thereby blocking infection at an early stage. According to the Stary study, both migration waves are required for optimal defense against Chlamydia. In contrast to oral vaccination, i.n. vaccination leads to efficient responses not only to local nasopharynx- and bronchus-associated lymphoid tissue (NALT/BALT), but also at distant mucosal ter-

ritories, such as in vaginal secretions of the genitourinary tract [59]. Moreover, mucosal sites function as a common system-wide organ, which act as an interface between the physical environment and the host mucosal defenses [60]. On this background [21,58,59], one can draw the conclusions that adjuvant and route of application play critical roles for the success of a vaccine against the primarily mucosa-infecting Chlamydia. Furthermore, a similar immunological mechanism as described above might also be involved in our case. Thus, one can speculate that after i.n. application cross-mucosal protection including the urogenital tract might also be achieved with 5cVAC, if combined with the right adjuvant.

It seems reasonable to speculate that 5cVAC-induced cellular immune responses of $CD4^+$, $CD8^+$, memory, tissue-resident, regulatory, and other T cell subsets, might be more important than antibodies for the observed success of i.n. vaccination. An unambiguous clarification of this issue is beyond the scope of this work and will need to be solved by further studies. However, both the IgG subtypes of the raised antigen-specific antibodies in plasma or serum and the ELISpot-analysis of splenocytes after restimulation with 5cVAC strongly suggest the induction of a mixed Th1/Th2/Th17 immune response. The remarkably high stimulation of antigen-specific $CD4^+$ T cells still 5 months after i.n. vaccination underscores the potency of c-di-AMP as mucosal adjuvant.

In addition to buffer, i.n. application of c-di-AMP alone was included as negative control in most experiments, to rule out any potential short-term protective effect as a result of c-di-AMP-mediated immune stimulation. As expected, it did not have any effect, as demonstrated in the short-term protection model for C.tr. E or D on body weight, clinical score (Figure 2a1–b2), bacterial load and MPO (Figure 3a1–b2), or TNF-α and IFN-γ (Figure 4a1–b2). The adjuvant did also not modify the same parameters in the 2cVAC short-term experiment (Figure 8a–f) and the long-term experiment (Figure 11) using C.tr. E for challenge. In addition, there was also no visible effect of the adjuvant alone in non-vaccinated mice on the levels of antigen-specific antibodies (Figure 9) or the responses of their splenocytes (Figure 13). Based on these multiple identical results and for practical reasons, the adjuvant control (in addition to the buffer control) was not included in the analysis of the observed protective effect of adjuvanted 5cVAC in challenge infection with C.tr. A in the short-term model (Figure 2d1,d2, Figure 3d1,d2 and Figure 4d1,d2), and partially also with C.tr. L2 (Figure 4c1,c2). However, it seems highly unlikely, that a non-specific effect of c-di-AMP alone should only take place after challenge infection with serovars, other than D or E.

The adjuvancity of c-di-AMP is explained by the stimulation of STING (stimulator of interferon genes), which in turn leads to a signal transduction cascade promoting expression of type I interferons and TNF-α. The proof of concept for vaccine candidates against several other pathogens (e.g., influenza virus, hepatitis viruses, *Trypanosoma cruzi*, *Streptococcus pyogenes*, etc.) causing mucosal and non-mucosal infections has been already provided in different experimental animal models [36–39] and some of them are currently going into clinical development. Most likely due to incorporation of c-di-AMP in the i.n. 5cVAC vaccine, strength and quality of the antigen-specific $CD4^+$ and $CD8^+$ T cell responses were also augmented here, as indicated by the presence of bi- and trifunctional $CD4^+$ and $CD8^+$ T cells. These cytokine producers were dominated by cells double positive for IFN-γ and TNF-α, which is in agreement with other studies using c-di-AMP as adjuvant. Such multifunctional $CD4^+$ T cells have been demonstrated to be important during C.tr. infection, e.g., in pigs. Käser and co-workers revealed that C.tr. infections result in the induction of $CD4^+$ T cells that are either IFN-γ-single, or (IFN-γ/TNF-α)-double cytokine-producing T-helper 1 cells [61]. Interestingly, IL-17-producing $CD4^+$ T cells were rare or completely absent. One might expect that several overlapping and difficult to dissect cellular or humoral immune mechanisms might contribute to 5cVAC-induced protection against C.tr.

Taken together, we obtained in mice with our new adjuvanted multi-subunit vaccine highly promising results in lung C.tr. challenge infection, and gained insights into the vaccine-induced immune response. The three main reasons of our success might be: (A)

we used in 5cVAC longer protein fragments of the extracellular Pmp PDs than others combining them with full length Ctad1 as antigens; (B) with c-di-AMP, a different mucosal adjuvant was chosen, which primarily stimulates dendritic cells and has been shown to be capable of promoting both, humoral and broad cellular immune responses [59,62]; and (C) the adjuvanted protective vaccine was administered i.n., i.e., to the mucosa.

Nevertheless, there is still a long way to go. (1) The composition and ration of the subunits should be optimized. (2) Our results suggest that 5cVAC-induced protection diminishes five months after the third application of the adjuvanted vaccine. We want to investigate how far the mode and timing of application influences duration of protection, e.g., combining mucosal and non-mucosal application of 5cVAC, or using an additional booster application. (3) It is likely, that c-di-AMP-adjuvanted 5cVAC is also protective in genital mouse infection, and that this protection includes several C.tr. serovars. Based on our results, the next major step in the development of our vaccine will be to switch to a urogenital mouse model. Now, that we know that effective cross-serovar protection is inducible with i.n. adjuvanted 5cVAC, it will be critical to assess how far mucosal cross-protection is achievable in the urogenital tract after i.n. application of 5cVAC, as described for other antigens [21]. With c-di-AMP as adjuvant, this might actually be the case, as demonstrated already for other pathogens. So far at least, c-di-AMP lived up to most of our expectations, e.g., the induction 5cVAC-specific antibody and mixed Th1/Th2/Th17 T cell responses, as well as CD8 cytotoxic T cells, and relevant induced protection [36–39]. Intranasal or sublingual administration should be able to promote such responses in the genitourinary tracts, as previously demonstrated for HIV and HSV antigens (unpublished data), however, vaginal administration of adjuvanted 5cVAC might be also a feasible alternative. With such experiments in mind, we will check before, how far i.n. adjuvanted 5cVAC cross-protects against C. *muridarum* in mouse lung infection. In any case, we can use transcervical-intrauterine application of C.tr. to investigate in longer lasting, but more focused experiments vaccine-induced protection in the urogenital tract. (4) Our observation of the induced immune response in the lung infection model as well as the analytic transfer experiment of serum (with circulating antibodies) provide insight into 5cVAC-induced immune responses. On that basis, one can develop hypotheses about the nature of induced protection. Yet, future experiments are also required to confirm the presumed protective immune mechanisms by challenge of 5cVAC-vaccinated mice who exhibit defects in parts of their immune system—e.g., K/O mice without functional B cells and antibodies including IgA, or by challenge infections of vaccinated $CD8^+$ or $CD4^+$ T cell-depleted animals. However, the fact that deficits in the B cell compartment can also affect cellular immunity [63], might render final analysis difficult.

## 5. Conclusions

Our results show that repetitive i.n. vaccination with 5cVAC - consisting of 4 recombinant Pmp proteins and Ctad1 derived from C.tr. E combined with the adjuvant c-di-AMP - protects mice efficiently against an experimental lung challenge infection with C. tr. E. Moreover, cross-serovar protection was induced as demonstrated for 2 additional urogenital and 1 trachoma serovar. Experiment using 2cVAC showed that at least one of the two contained antigens (PmpD and Ctad1) and at least one of the three not-contained antigens (PmpA, PmpG, and PmpH) is inducing protection. This result emphasizes the importance of a multi-subunit vaccine. In addition, such a vaccine should be less prone for selection of immuno-evasive C.tr. mutants. Protection, although probably weakened, was still detectable 5 months after the last i.n. application of 5cVAC. The importance of mucosal application is indicated by the lack of protection observed after s.c. application of our vaccine. High, but varying amounts of antigen-specific IgA, IgM, and IgG are induced by i.n. vaccination. Yet, serum-transfer experiments suggest that circulating antibodies play a minor role in vaccine-induced protection. Most likely, the observed antigen-specific T cell responses are functionally more important in case of our vaccine. While still subject to optimization and testing in mouse urogenital and other animal models, the results

obtained here are highly promising. We hope that, in the long run, our new vaccine might help to prevent the feared consequences of human C.tr. urogenital infections, in particular infertility, as well as blindness due to trachoma.

## 6. Patents

A patent application for the c-di-AMP-adjuvanted vaccine 5cVAC naming A.K., R.L., J.H.H., S.W., T.E., and C.A.G. as inventors has been filed (EP2115349.6; not published, yet). C.A.G. and T.E. are named as inventors in patents covering the use of c-di-AMP as vaccine adjuvant (PCT/EP 2006010693), as well as neonatal adjuvant (EP 19193982).

**Supplementary Materials:** The following are available online at https://www.mdpi.com/article/10.3390/vaccines9060609/s1, Table S1: Clinical scoring (mouse pneumonia)., Table S2: Mouse group sizes per experiment and C.tr. serovar of Figures 2–8, Table S3: Mouse group sizes per experiment and C.tr. serovar of Figures 9–13, Figure S1: Recombinant proteins used in the 2cVAC and 5cVAC vaccine formulation., Figure S2: Body weight and clinical score p.i. of an orientating i.n. C.tr. titration experiment for identification of the optimal amount of each serovar using 14- to 15-week-old female, hormone-synchronized mice., Figure S3: Kaplan-Meier-Plot (survival) of an orientating i.n. C.tr. titration experiment for identification of the optimal amount of each serovar using 14- to 15-week-old female, hormonesynchronized mice., Figure S4: Body weight, clinical score, and Kaplan-Meier-Plot (survival) of an orientating i.n. C.tr. titration experiment for identification of the optimal amount of serovar E using 31-week-old female, hormone-synchronized mice.

**Author Contributions:** In alphabetic order of the initials: A.K., C.A.G., C.L., C.R., J.H.H., K.S., M.K., R.L., S.W., and T.E. Conceptualization: A.K. (animal model), J.H.H. (chlamydial antigens), and C.A.G. (adjuvant, immunization strategy, and T cell immune monitoring); Methodology, R.L., C.L. (animal model), and S.W. (antigens); Formal/statistical analysis, C.L., K.S., and T.E.; Investigation, C.L., M.K., R.L., C.R., K.S., T.E., and S.W.; Writing—original draft preparation, A.K., C.L., and T.E.; Writing—review and editing, A.K., J.H.H., C.A.G., T.E., and C.L.; Visualization, C.L., K.S., and T.E.; Supervision, A.K., J.H.H., and C.A.G.; Funding acquisition, A.K., J.H.H., and C.A.G. All authors have read and agreed to the published version of the manuscript.

**Funding:** The experiments performed in the mouse model and the analysis of the obtained tissue and blood samples were mainly funded by MHH-LOM of the research group Klos. Christian Lanfermann and Martin Kohn were partially funded by the ZIB PhD program from the Hannover Medical School. The HZI research was partially funded by grants from the European Community's Horizon 2020 grant agreement no. 730964 (TRANSVAC2), and the Helmholtz Association (HAI-IDR). The funders had no role in the design of the study; in the collection, analyses, or interpretation of data; in the writing of the manuscript, or in the decision to publish the results. S.W. was a scholarship holder of the Graduate School 'Molecules of Infection (MOI III)' funded by the Jürgen Manchot Foundation.

**Institutional Review Board Statement:** All animal experiments were approved by the Lower Saxony state government and the corresponding authorities of the LAVES (33.12-42502-04-17/2589: Development of a vaccine against *Chlamydia trachomatis* in a mouse lung infection model). They were performed in accordance with the law of animal welfare used for experiments (TierSchVersV), with the German regulations of the GV-SOLAS for the protection of animal life and the FELASA. Chlamydial infections lead to a protracted and delayed course of disease. For that reason, Chlamydia-infected mice can adapt to and tolerate weight loss relatively well. They usually recover even when the body weight is reduced by >20%. For these reasons, our permit allows continuation of the experiment under close supervision. Studies involving humans: not applicable.

**Informed Consent Statement:** Not applicable.

**Data Availability Statement:** The raw data supporting the conclusions of this article will be made available by the authors, without undue reservation.

**Acknowledgments:** We are particularly grateful to Elena Reinhard for her technical help and Blair Prochnow for his critical reading of the manuscript.

**Conflicts of Interest:** A patent application for the c-di-AMP-adjuvanted vaccine 5cVAC naming A.K., R.L., J.H.H., S.W., T.E., and C.A.G. as inventors has been filed (EP2115349.6; not published yet). C.A.G. and T.E. are named as inventors in patents covering the use of c-di-AMP as vaccine adjuvant (PCT/EP 2006010693) and neonatal adjuvant (EP 19193982). Beside this, the authors declare no conflict of interest.

## References


1. Bastidas, R.J.; Elwell, C.A.; Engel, J.N.; Valdivia, R.H. Chlamydial intracellular survival strategies. *Cold Spring Harb. Perspect. Med.* **2013**, *3*, a010256. [CrossRef] [PubMed]
2. Smelov, V.; Vrbanac, A.; van Ess, E.F.; Noz, M.P.; Wan, R.; Eklund, C.; Morgan, T.; Shrier, L.A.; Sanders, B.; Dillner, J.; et al. Chlamydia trachomatis Strain Types Have Diversified Regionally and Globally with Evidence for Recombination across Geographic Divides. *Front. Microbiol.* **2017**, *8*, 2195. [CrossRef] [PubMed]
3. Rowley, J.; Hoorn, S. Vander; Korenromp, E.; Low, N.; Unemo, M.; Abu-Raddad, L.J.; Chico, R.M.; Smolak, A.; Newman, L.; Gottlieb, S.; et al. Chlamydia, gonorrhoea, trichomoniasis and syphilis: Global prevalence and incidence estimates, 2016. *Bull. World Health Organ.* **2019**, *97*, 548. [CrossRef] [PubMed]
4. Seedat, J.; Marcus, U.; Fehrmann, S.; Paape, C.; Petschelt, J. Robert Koch-Institut, Epidemiologisches Bulletin 46/2013. 2013. Available online: www.rki.de/epidbull (accessed on 15 May 2021).
5. Phillips, S.; Quigley, B.L.; Timms, P. Seventy years of Chlamydia vaccine research - Limitations of the past and directions for the future. *Front. Microbiol.* **2019**, *10*, 70. [CrossRef] [PubMed]
6. Brunham, R.C.; Rey-Ladino, J. Immunology of Chlamydia infection: Implications for a Chlamydia trachomatis vaccine. *Nat. Rev. Immunol.* **2005**, *5*, 149–161. [CrossRef] [PubMed]
7. Hoenderboom, B.M.; Van Benthem, B.H.B.; Van Bergen, J.E.A.M.; Dukers-Muijrers, N.H.T.M.; Götz, H.M.; Hoebe, C.J.P.A.; Hogewoning, A.A.; Land, J.A.; Van Der Sande, M.A.B.; Morré, S.A.; et al. Relation between Chlamydia trachomatis infection and pelvic inflammatory disease, ectopic pregnancy and tubal factor infertility in a Dutch cohort of women previously tested for chlamydia in a chlamydia screening trial. *Sex. Transm. Infect.* **2019**, *95*, 300–306. [CrossRef] [PubMed]
8. Darville, T. Chlamydia trachomatis infections in neonates and young children. *Semin. Pediatr. Infect. Dis.* **2005**, *16*, 235–244. [CrossRef]
9. Gaston, J.S.H. Immunological basis of chlamydia induced reactive arthritis. *Sex. Transm. Infect.* **2000**, *76*, 156–161. [CrossRef]
10. Schlott, T.; Eiffert, H.; Bohne, W.; Landgrebe, J.; Brunner, E.; Spielbauer, B.; Knight, B. Chlamydia trachomatis modulates expression of tumor suppressor gene caveolin-1 and oncogene C-myc in the transformation zone of non-neoplastic cervical tissue. *Gynecol. Oncol.* **2005**, *98*, 409–419. [CrossRef]
11. Sethi, S.; Roy, A.; Garg, S.; Sree Venkatesan, L.; Bagga, R. Detection of Chlamydia trachomatis infections by polymerase chain reaction in asymptomatic pregnant women with special reference to the utility of the pooling of urine specimens. *Indian J. Med. Res. Suppl.* **2017**, *146*, 59–63. [CrossRef]
12. Faris, R.; Andersen, S.E.; McCullough, A.; Gourronc, F.; Klingelhutz, A.J.; Weber, M.M. Chlamydia trachomatis Serovars Drive Differential Production of Proinflammatory Cytokines and Chemokines Depending on the Type of Cell Infected. *Front. Cell. Infect. Microbiol.* **2019**, *9*, 399. [CrossRef]
13. Lesiak-Markowicz, I.; Schötta, A.M.; Stockinger, H.; Stanek, G.; Markowicz, M. Chlamydia trachomatis serovars in urogenital and ocular samples collected 2014–2017 from Austrian patients. *Sci. Rep.* **2019**, *9*, 18327. [CrossRef]
14. World Health Organization Status of elimination of trachoma as a public health problem. Available online: https://apps.who.int/neglected_diseases/ntddata/trachoma/trachoma.html (accessed on 15 January 2021).
15. Brunham, R.C.; Rappuoli, R. Chlamydia trachomatis control requires a vaccine. *Vaccine* **2013**, *31*, 1892–1897. [CrossRef]
16. De La Maza, L.M.; Zhong, G.; Brunham, R.C. Update on Chlamydia trachomatis vaccinology. *Clin. Vaccine Immunol.* **2017**, *24*, e00543-16. [CrossRef]
17. Gottlieb, S.L.; Johnston, C. Future prospects for new vaccines against sexually transmitted infections. *Curr. Opin. Infect. Dis.* **2017**, *30*, 77–86. [CrossRef]
18. Poston, T.B.; Gottlieb, S.L.; Darville, T. Status of vaccine research and development of vaccines for Chlamydia trachomatis infection. *Vaccine* **2019**, *37*, 7289–7294. [CrossRef]
19. De La Maza, L.M.; Pal, S.; Olsen, A.E.; Follmann, F. Chlamydia Vaccines. In *Chlamydia Biology—From Genome to Disease*; Tan M, J.H., Hegemann, S.C., Eds.; Caister Academic Press: Norfolk, UK, 2020.
20. Qu, Y.; Frazer, L.C.; O'Connell, C.M.; Tarantal, A.F.; Andrews, C.W.; O'Connor, S.L.; Russell, A.N.; Sullivan, J.E.; Poston, T.B.; Vallejo, A.N.; et al. Comparable Genital Tract Infection, Pathology, and Immunity in Rhesus Macaques Inoculated with Wild-Type or Plasmid-Deficient Chlamydia trachomatis Serovar D. *Infect. Immun.* **2015**, *83*, 4056–4067. [CrossRef]
21. Stary, G.; Olive, A.; Radovic-Moreno, A.F.; Gondek, D.; Alvarez, D.; Basto, P.A.; Perro, M.; Vrbanac, V.D.; Tager, A.M.; Shi, J.; et al. A mucosal vaccine against Chlamydia trachomatis generates two waves of protective memory T cells. *Science* **2015**, *348*, aaa8205. [CrossRef]
22. Grimwood, J.; Stephens, R.S. Computational analysis of the polymorphic membrane protein superfamily of Chlamydia trachomatis and Chlamydia pneumoniae. *Microb. Comp. Genom.* **1999**, *4*, 187–201. [CrossRef]

23. Luczak, S.E.T.; Smits, S.H.J.; Decker, C.; Nagel-Steger, L.; Schmitt, L.; Hegemann, J.H. The Chlamydia Pneumoniae Adhesin Pmp21 forms oligomers with adhesive properties. *J. Biol. Chem.* **2016**, *291*, 22806–22818. [CrossRef]
24. Becker, E.; Hegemann, J.H. All subtypes of the Pmp adhesin family are implicated in chlamydial virulence and show species-specific function. *Microbiologyopen* **2014**, *3*, 544–556. [CrossRef] [PubMed]
25. Kari, L.; Southern, T.R.; Downey, C.J.; Watkins, H.S.; Randall, L.B.; Taylor, L.D.; Sturdevant, G.L.; Whitmire, W.M.; Caldwell, H.D. Chlamydia trachomatis polymorphic membrane protein D is a virulence factor involved in early host-cell interactions. *Infect. Immun.* **2014**, *82*, 2756–2762. [CrossRef]
26. Mölleken, K.; Becker, E.; Hegemann, J.H. The Chlamydia pneumoniae Invasin Protein Pmp21 Recruits the EGF Receptor for Host Cell Entry. *PLoS Pathog.* **2013**, *9*, e1003325. [CrossRef] [PubMed]
27. Crane, D.D.; Carlson, J.H.; Fischer, E.R.; Bavoil, P.; Hsia, R.C.; Tan, C.; Kuo, C.C.; Caldwell, H.D. Chlamydia tracomatis polymorphic membrane protein D is a species-common pan-neutralizing antigen. *Proc. Natl. Acad. Sci. USA* **2006**, *103*, 1894–1899. [CrossRef] [PubMed]
28. Yu, H.; Karunakaran, K.P.; Jiang, X.; Shen, C.; Andersen, P.; Brunham, R.C. Chlamydia muridarum T cell antigens and adjuvants that induce protective immunity in mice. *Infect. Immun.* **2012**, *80*, 1510–1518. [CrossRef] [PubMed]
29. Karunakaran, K.P.; Yu, H.; Jiang, X.; Chan, Q.; Moon, K.M.; Foster, L.J.; Brunham, R.C. Outer membrane proteins preferentially load MHC class II peptides: Implications for a Chlamydia trachomatis T cell vaccine. *Vaccine* **2015**, *33*, 2159–2166. [CrossRef] [PubMed]
30. Pal, S.; Favaroni, A.; Tifrea, D.F.; Hanisch, P.T.; Luczak, S.E.T.; Hegemann, J.H.; de la Maza, L.M. Comparison of the nine polymorphic membrane proteins of Chlamydia trachomatis for their ability to induce protective immune responses in mice against a C. muridarum challenge. *Vaccine* **2017**, *35*, 2543–2549. [CrossRef] [PubMed]
31. Inic-Kanada, A.; Stojanovic, M.; Schlacher, S.; Stein, E.; Belij-Rammerstorfer, S.; Marinkovic, E.; Lukic, I.; Montanaro, J.; Schuerer, N.; Bintner, N.; et al. Delivery of a chlamydial adhesin N-PmpC subunit vaccine to the ocular mucosa using particulate carriers. *PLoS ONE* **2015**, *10*, e144380. [CrossRef] [PubMed]
32. Müller, T.; Becker, E.; Stallmann, S.; Waldhuber, A.; Römmler-Dreher, F.; Albrecht, S.; Mohr, F.; Hegemann, J.H.; Miethke, T. Vaccination with the polymorphic membrane protein A reduces Chlamydia muridarum induced genital tract pathology. *Vaccine* **2017**, *35*, 2801–2810. [CrossRef] [PubMed]
33. Stallmann, S.; Hegemann, J.H. The Chlamydia trachomatis Ctad1 invasin exploits the human integrin β1 receptor for host cell entry. *Cell. Microbiol.* **2016**, *18*, 761–775. [CrossRef]
34. Uddowla, S.; Freytag, L.C.; Clements, J.D. Effect of adjuvants and route of immunizations on the immune response to recombinant plague antigens. *Vaccine* **2007**, *25*, 7984–7993. [CrossRef]
35. Durando, P.; Iudici, R.; Alicino, C.; Alberti, M.; de Florentis, D.; Ansaldi, F.; Icardi, G. Adjuvants and alternative routes of administration towards the development of the ideal influenza vaccine. *Hum. Vaccin.* **2011**, *7*, 29–40. [CrossRef]
36. Ebensen, T.; Debarry, J.; Pedersen, G.K.; Blazejewska, P.; Weissmann, S.; Schulze, K.; McCullough, K.C.; Cox, R.J.; Guzmán, C.A. Mucosal administration of cycle-di-nucleotide-adjuvanted virosomes efficiently induces protection against influenza H5N1 in mice. *Front. Immunol.* **2017**, *8*, 1223. [CrossRef]
37. Landi, A.; Law, J.; Hockman, D.; Logan, M.; Crawford, K.; Chen, C.; Kundu, J.; Ebensen, T.; Guzman, C.A.; Deschatelets, L.; et al. Superior immunogenicity of HCV envelope glycoproteins when adjuvanted with cyclic-di-AMP, a STING activator or archaeosomes. *Vaccine* **2017**, *35*, 6949–6956. [CrossRef]
38. Lirussi, D.; Ebensen, T.; Schulze, K.; Trittel, S.; Duran, V.; Liebich, I.; Kalinke, U.; Guzmán, C.A. Type I IFN and not TNF, is Essential for Cyclic Di-nucleotide-elicited CTL by a Cytosolic Cross-presentation Pathway. *EBioMedicine* **2017**, *22*, 100–111. [CrossRef]
39. Sanchez Alberti, A.; Bivona, A.E.; Cerny, N.; Schulze, K.; Weißmann, S.; Ebensen, T.; Morales, C.; Padilla, A.M.; Cazorla, S.I.; Tarleton, R.L.; et al. Engineered trivalent immunogen adjuvanted with a sting agonist confers protection against trypanosoma cruzi infection. *npj Vaccines* **2017**, *2*, 9. [CrossRef]
40. Dutow, P.; Wask, L.; Bothe, M.; Fehlhaber, B.; Laudeley, R.; Rheinheimer, C.; Yang, Z.; Zhong, G.; Glage, S.; Klos, A. An optimized, fast-to-perform mouse lung infection model with the human pathogen Chlamydia trachomatis for in vivo screening of antibiotics, vaccine candidates and modified host-pathogen interactions. *Pathog. Dis.* **2016**, *74*. [CrossRef]
41. Rother, M.; Gonzalez, E.; Teixeira da Costa, A.R.; Wask, L.; Gravenstein, I.; Pardo, M.; Pietzke, M.; Gurumurthy, R.K.; Angermann, J.; Laudeley, R.; et al. Combined Human Genome-wide RNAi and Metabolite Analyses Identify IMPDH as a Host-Directed Target against Chlamydia Infection. *Cell Host Microbe* **2018**, *23*, 661–671. [CrossRef]
42. Sommer, K.; Njau, F.; Wittkop, U.; Thalmann, J.; Bartling, G.; Wagner, A.; Klos, A. Identification of high- and low-virulent strains of Chlamydia pneumoniae by their characterization in a mouse pneumonia model. *FEMS Immunol. Med. Microbiol.* **2009**, *55*, 206–214. [CrossRef]
43. Mölleken, K.; Schmidt, E.; Hegemann, J.H. Members of the Pmp protein family of Chlamydia pneumoniae mediate adhesion to human cells via short repetitive peptide motifs. *Mol. Microbiol.* **2010**, *78*, 1004–1017. [CrossRef]
44. Bethesda (MD): National Library of Medicine (US), National Center for Biotechnology Information. Available online: https://www.ncbi.nlm.nih.gov/ (accessed on 11 March 2021).
45. Sambrook, J.; Maniatis, T. *Molecular Cloning: A Laboratory Manual*; Cold Spring Harbor Laboratory Press: New York, NY, USA, 1989.

46. Gherardi, M.M.; Pérez-Jiménez, E.; Nájera, J.L.; Esteban, M. Induction of HIV Immunity in the Genital Tract After Intranasal Delivery of a MVA Vector: Enhanced Immunogenicity After DNA Prime-Modified Vaccinia Virus Ankara Boost Immunization Schedule. *J. Immunol.* **2004**, *172*, 6209–6220. [CrossRef] [PubMed]
47. Plante, M.; Jerse, A.; Hamel, J.; Couture, F.; Rioux, C.R.; Brodeur, B.R.; Martin, D. Intranasal Immunization with Gonococcal Outer Membrane Preparations Reduces the Duration of Vaginal Colonization of Mice by *Neisseria gonorrhoeae*. *J. Infect. Dis.* **2000**, *182*, 848–855. [CrossRef] [PubMed]
48. Bode, J.; Dutow, P.; Sommer, K.; Janik, K.; Glage, S.; Tümmler, B.; Munder, A.; Laudeley, R.; Sachse, K.W.; Klos, A. A New Role of the Complement System: C3 Provides Protection in a Mouse Model of Lung Infection with Intracellular Chlamydia psittaci. *PLoS ONE* **2012**, *7*, e50327. [CrossRef] [PubMed]
49. Kohn, M.; Lanfermann, C.; Laudeley, R.; Glage, S.; Rheinheimer, C.; Klos, A. Complement and Chlamydia psittaci: Non-myeloid derived C3 predominantly induces protective adaptive immune responses in mouse lung infection. *Front. Immunol.* **2021**, *12*, 485. [CrossRef]
50. Schulze, K.; Ebensen, T.; Chandrudu, S.; Skwarczynski, M.; Toth, I.; Olive, C.; Guzman, C.A. Bivalent mucosal peptide vaccines administered using the LCP carrier system stimulate protective immune responses against Streptococcus pyogenes infection. *Nanomed. Nanotechnol. Biol. Med.* **2017**, *13*, 2463–2474. [CrossRef]
51. Tan, C.; Hsia, R. ching; Shou, H.; Carrasco, J.A.; Rank, R.G.; Bavoil, P.M. Variable expression of surface-exposed polymorphic membrane proteins in in vitro-grown Chlamydia trachomatis. *Cell. Microbiol.* **2010**, *12*, 174–187. [CrossRef]
52. Pal, S.; Theodor, I.; Peterson, E.M.; De la Maza, L.M. Immunization with the Chlamydia trachomatis mouse pneumonitis major outer membrane protein can elicit a protective immune response against a genital challenge. *Infect. Immun.* **2001**, *69*, 6240–6247. [CrossRef]
53. Pal, S.; Peterson, E.M.; De La Maza, L.M. Vaccination with the chlamydia trachomatis major outer membrane protein can elicit an immune response as protective as that resulting from inoculation with live bacteria. *Infect. Immun.* **2005**, *73*, 8153–8160. [CrossRef]
54. Pal, S.; Tatarenkova, O.V.; de la Maza, L.M. A vaccine formulated with the major outer membrane protein can protect C3H/HeN, a highly susceptible strain of mice, from a *Chlamydia muridarum* genital challenge. *Immunology* **2015**, *146*, 432–443. [CrossRef]
55. Wern, J.E.; Sorensen, M.R.; Olsen, A.W.; Andersen, P.; Follmann, F. Simultaneous subcutaneous and intranasal administration of a CAF01-adjuvanted Chlamydia vaccine elicits elevated IgA and protective Th1/Th17 responses in the genital tract. *Front. Immunol.* **2017**, *8*, 569. [CrossRef]
56. Abraham, S.; Juel, H.B.; Bang, P.; Cheeseman, H.M.; Dohn, R.B.; Cole, T.; Kristiansen, M.P.; Korsholm, K.S.; Lewis, D.; Olsen, A.W.; et al. Safety and immunogenicity of the chlamydia vaccine candidate CTH522 adjuvanted with CAF01 liposomes or aluminium hydroxide: A first-in-human, randomised, double-blind, placebo-controlled, phase 1 trial. *Lancet Infect. Dis.* **2019**, *19*, 1091–1100. [CrossRef]
57. Joseph, S.J.; Didelot, X.; Rothschild, J.; De Vries, H.J.C.; Morré, S.A.; Read, T.D.; Dean, D. Population genomics of chlamydia trachomatis: Insights on drift, selection, recombination, and population structure. *Mol. Biol. Evol.* **2012**, *29*, 3933–3946. [CrossRef]
58. Borges, V.; Cordeiro, D.; Salas, A.I.; Lodhia, Z.; Correia, C.; Isidro, J.; Fernandes, C.; Rodrigues, A.M.; Azevedo, J.; Alves, J.; et al. Chlamydia trachomatis: When the virulence-associated genome backbone imports a prevalence-associated major antigen signature. *Microb. Genom.* **2019**, *5*, e000313. [CrossRef]
59. Ebensen, T.; Libanova, R.; Schulze, K.; Yevsa, T.; Morr, M.; Guzmán, C.A. Bis-(3′,5′)-cyclic dimeric adenosine monophosphate: Strong Th1/Th2/Th17 promoting mucosal adjuvant. *Vaccine* **2011**, *29*, 5210–5220. [CrossRef]
60. Gill, N.; Wlodarska, M.; Finlay, B.B. The future of mucosal immunology: Studying an integrated system-wide organ. *Nat. Immunol.* **2010**, *11*, 558–560. [CrossRef]
61. Käser, T.; Pasternak, J.A.; Delgado-Ortega, M.; Hamonic, G.; Lai, K.; Erickson, J.; Walker, S.; Dillon, J.R.; Gerdts, V.; Meurens, F. Chlamydia suis and Chlamydia trachomatis induce multifunctional CD4 T cells in pigs. *Vaccine* **2017**, *35*, 91–100. [CrossRef]
62. Ebensen, T.; Schulze, K.; Riese, P.; Link, C.; Morr, M.; Guzmán, C.A. The bacterial second messenger cyclic diGMP exhibits potent adjuvant properties. *Vaccine* **2007**, *25*, 1464–1469. [CrossRef]
63. Crooke, S.N.; Ovsyannikova, I.G.; Poland, G.A.; Kennedy, R.B. Immunosenescence and human vaccine immune responses. *Immun. Ageing* **2019**, *16*, 25. [CrossRef]

# 5. Teil IV Abschließende Diskussion

Essentieller und grundlegender Schritt im Infektionszyklus von Chlamydien ist die Bindung des EBs an die Wirtszelle. Diese Bindung erfolgt mithilfe von auf der Oberfläche lokalisierten Adhäsinen. Trotz vieler Fortschritte in den letzten Jahren ist die Oberfläche chlamydialer EBs, die darauf präsentierten Proteine, die Form ihres Auftretens, ihre genaue Funktion und eventuelle Bindepartner bis heute nur unvollständig verstanden. Bisher konnten einige Adhäsine für *C. pneumoniae* und *C. trachomatis* identifiziert werden. *C. pneumoniae* und *C. trachomatis* verwenden OmcB, welches an HS-GAGs bindet, und Proteine der Pmp-Familie. Bekanntes Beispiel ist das *C. pneumoniae* spezifische Pmp21, welches durch seine Bindung an den EGFR, diesen aktiviert und zur Aufnahme des EBs in die Zelle beiträgt. Ein weiteres Adhäsin von großem Interesse ist das *C. pneumoniae* spezifische LipP (vgl. 1.4). Aufgrund ihrer Wichtigkeit im Infektionsprozess sind Adhäsine der Pmp-Familie ideale Impfstoffkandidaten und von großem wissenschaftlichen Interesse.

## 5.1 Pmps favorisieren Proteine der Pmp-Familie als Interaktionspartner auf der chlamydialen Oberfläche

Im ersten Manuskript wurde demonstriert, dass Pmp-Volllänge-Fragmente (ohne die C-terminale β-Fass-Domäne) von PmpG, PmpH und PmpI aus *C. trachomatis* in der Lage sind Oligomere zu generieren, welche in unterschiedlich starkem Maß eine Bindung an HEp-2 Zellen vermitteln. Hierbei zeigten PmpH und PmpI eine stärkere Bindung als PmpG. Zudem führte die Kombination von rekombinanten PmpG + PmpH, PmpG + PmpI und PmpH + PmpI zu der Entstehung von heteromeren Oligomeren, welche eine andere Größe als die jeweiligen homomeren Oligomere zeigten. In diesem kombinierten Zustand waren keine homomeren Komplexe zu beobachten, was darauf hindeutet, dass die heteromere Form womöglich bevorzugt wird.
In einer Studie, welche den Zusammenhang zwischen der Anzahl vorhandener FxxN und GGA (I, L, V) -Motive in einem Pmp-Proteinfragment und dessen Eigenschaften untersuchte, zeigten auch dort beschriebene kurze Pmp-Fragmente vergleichbare Resultate [278]. Sowohl die Kombination von Fragmenten aus PmpA + PmpG als auch PmpA + PmpI resultierte in heteromeren Oligomeren. Übrig gebliebene homomere Oligomere aus PmpA waren im „Blue Native“-Gel kaum bis nicht zu erkennen [278]. Aufgrund von möglichen Überlagerungen der gebildeten Oligomergrößen (z.B. PmpA Homo-Oligomere: ca. 800 - 1700 kDa; PmpA + PmpI Hetero-Oligomere: ca. 800 - 1400 kDa) müssen die Daten allerdings mit

Vorbehalt interpretiert werden. Interessanterweise waren bindungsschwache Proteine wie PmpA in einem heteromeren Komplex mit adhäsionskompetentem PmpI in der Lage an HEp2-Zellen zu binden [278]. Paes *et al*. 2018 zeigten, dass bei einer Aufreinigung von einem 65 kDa PmpD-Fragment ein Gemisch aus oligomeren Spezies unterschiedlicher Größe und nur eine geringe Menge an monomeren PmpD von einer Nickel-Affinitätschromatographie-Säule eluiert was darauf hindeutet, dass Pmps den Oligomer-Zustand bevorzugen [277]. Daten von Luczak *et al.* 2016 demonstrierten anhand von *C. pneumoniae* Pmp21-Fragmenten, dass Pmp21_D in seiner oligomerisierten Form signifikant stärker an HEp-2 Zellen bindet als in seiner Monomer-Form [275].

Zusammenfassend zeigen diese Daten, dass Pmp Proteine die Fähigkeit besitzen, Oligomere zu generieren. Die oligomeren Formen könnten wichtige Funktionen innerhalb der Infektion übernehmen. Möglicherweise erzeugt die Akkumulation von mehreren Pmp-Proteinen im Homo- oder Hetero-Oligomer eine verstärkte Bindung an den Wirt. Darüber hinaus könnte die große Zahl möglicher unterschiedlicher heteromerer Pmp Oligomere für die Immunabwehr relevant sein.

Auf ThT-Fluoreszenz basierende Assays demonstrierten, dass die Wachstums-Kinetik von oligomerisierenden PmpG, PmpH und PmpI Proteinen einen verzögerungsfreien, konzentrationsabhängigen Anstieg des ThT-Signals aufweist und damit Amyloid-ähnliches Wachstum eines Proteins zeigt. In der Amyloid-Forschung wird der Farbstoff Thioflavin T (ThT) eingesetzt. Bindung an Amyloid-Strukturen resultiert in einer verstärkten ThT-Fluoreszenz und erlaubt auf diese Weise die Erzeugung einer Amyloidgenerierungs-Kinetik [412]. Mittels Atomkraftmikroskopie visualisierte Proben von oligomerisierten Protein erschienen als punktartige Oligomere (PmpG, PmpH, PmpI) oder kurze gerade bis kurvenförmige Protofibrillen (PmpG, PmpH).

Vergleichbares konnte auch in Arbeiten von Luczak *et al.* 2016 und Favaroni *et al.* 2021 gezeigt werden. Sowohl oligomerisiertes *C. pneumoniae* Pmp21_D als auch Fragmente von *C. trachomatis* PmpA, PmpG, PmpD und PmpI erschienen, analysiert mittels Transmissionselektronenmikroskopie (TEM), als Oligomere oder kurze Protofibrillen [275, 278]. Heteromere Komplexe (z. B. PmpA + PmpG) resultierten in signifikant längeren Protofibrillen [278].

Wie in 1.9.2 erläutert gibt es neben den pathologischen Amyloid-Proteinen eine Vielzahl funktioneller Oligomere bzw. amyloider Proteinstrukturen, welche einen positiven physiologischen Effekt ausüben können. Bei Bakterien üben sie meistens einen unterstützenden und stabilisierenden Effekt auf Biofilme aus und schützen so vor äußeren Einflüssen [413]. Eines der bestuntersuchten Proteine ist das *E. coli* Membranprotein Curli. Ähnlich zu chlamydialen Pmps ist es reich an β-Faltblatt Strukturen. Zudem führt die Bindung von Curli an Thioflavin T zu einem Fluoreszenz-Shift, welches eines der Kennzeichen für Amyloide darstellt [275, 327, 414]. Curli werden Eigenschaften wie die Bindung an Oberflächen,

Zellaggregation und Biofilmbildung zugeschrieben. Zusätzlich vermittelt Curli Adhäsion, ist als wichtig für die Invasion von Wirtszellen beschrieben und ist Auslöser von Entzündungsreaktionen [327]. Es wäre vorstellbar, dass Pmp-Homo-Oligomere und Hetero-Oligomere, vergleichbar zu Strukturen von Curli, über ihre Amyloid-artigen Strukturen eine verstärkte Adhäsion und Internalisierung sowie Interaktion mit der Wirtszelle vermitteln [327]. Obwohl rekombinantes Pmp-Protein *in vitro* Protofibrillen generiert, ist das Vorliegen von protofibrillären oder Fibrillen-artigen Strukturen auf EBs bislang nicht geklärt. Bei Untersuchungen zur Verteilung der Typ-III-Sekretionssystemes auf der Zelloberfläche chlamydialer EBs mittels Kryo-Elektronentomographie konnten keine Fibrillen-artigen Strukturen detektiert werden [415]. Für die Funktionsfähigkeit des *Candida albicans* Adhäsins Als5 ist dessen amyloidähnliche Proteinaggregation notwendig [416]. Lösliche Formen von Als5 generieren Amyloidfibrillen. Auf der Zelloberfläche verankertes Als5 Protein bildet hingegen Adhäsin-Flächen, so genannte „patches“ [416]. Es ist möglich, dass es sich bei Pmps vergleichbar verhält und eine Proteinansammlung in „patches“ in verstärkter Adhäsion resultiert. Womöglich erlauben Pmp-Oligomere auch die Nutzung von Biofilmen anderer Pathogene. So zeigten Sapi *et al.* 2019, dass *Borrelia burgdorferi* in der Lage ist, Biofilme in Borrelien-infizierten menschlichen Hautläsionen zu generieren, welche zu 84 % auch positiv für chlamydiale Antigene und DNA von *C. pneumoniae* und *C. trachomatis* waren. Chlamydien und Borrelien formten im Zentrum des Biofilms eine gut organisierte, gemischte Struktur [417]. Warum Chlamydien in den Biofilmen von Hautläsionen lokalisieren, welche konkreten Vorteile für eine Infektion bestehen könnten und welche molekularbiologischen Zusammenhänge hier bestehen, blieb allerdings unbeantwortet.

Bei Verwendung, des auf räumlicher Nähe basierenden, APEX2-Makierungssystems wird das zu untersuchende Protein zunächst genetisch mit einer modifizierten Ascorbatperoxidase (APEX2) fusioniert. APEX2 markiert im Folgenden das native proteinöse Umwelt in einem Radius von ca. 20 nm mit Biotin. Markierte Proteine werden isoliert und analysiert. In Manuskript 1 wurde ein PmpIAPEX2-Fusionsprotein konstruiert, welches auf die chlamydiale EB-Oberfläche lokalisierte und anschließend Proteine in räumlicher Nähe markierte. Mittels PmpIAPEX2 markierte Proteine wurden isoliert, massenspektrometrisch analysiert und nach ihrem Vorkommen in einem Ranking angeordnet. Die Analysen ergaben eine Anreicherung verschiedener Proteine der Pmp-Familie (PmpD, PmpG, PmpI, PmpB und PmpF) sowie dem Protein YidC und Proteinen des Typ-III-Sekretionssystems. Die Anreicherung der Pmps deutet auf eine mögliche Interaktion zwischen PmpI und zuvor genannten, angereicherten Pmps auf der EB Zelloberfläche hin. PmpD zeigte die stärkste Anreicherung. PmpD ist das *C. pneumoniae* Pmp21 Homolog in *C. trachomatis*. Es ist Fokus intensiver Forschungen und wurde via Transmissionselektronenmikroskopie als blumenartige oligomere Struktur auf der Oberfläche von EBs

beobachtet [276]. Es ist zudem hoch konserviert [257] und wird als ein Pan-neutralisierendes Antigen beschrieben [272]. Infektionsstudien mit einer PmpD-Null Mutante resultierten in einer stark reduzierten Infektion von Makaken Augen und kultivierten menschlichen Zellen, was die Bedeutung innerhalb der Infektion weiter unterstreicht [271]. Der Umstand, dass in dem hier verwendeten experimentellen Setting neben Pmps auch andere Proteine angereichert werden konnten, könnte darauf hinweisen, dass PmpI (und womöglich weitere Pmps) mit anderen Membran- oder Membran-assoziierten Proteinen interagieren.

Zusammenfassend lässt sich feststellen, dass PmpI ein Adhäsin ist, dessen Bindung an HEp-2 Zellen anhand von rekombinanten Protein und PmpI präsentierenden Hefe-Zellen demonstriert werden konnte [93, 278]. Vorbehandlung von HEp-2 Zellen mit PmpI reduziert eine darauffolgende Infektion und unterstreicht damit seine Wichtigkeit im Adhäsionsprozess [93, 278]. PmpI interagiert *in vitro* sowohl als kurzes [278] wie auch als langes Fragment (mit vollständiger Passagierdomäne) mit sich selbst und weiteren Pmp-Proteinen und erzeugt auf diese Weise homomere und heteromere Oligomere. Die vorliegenden Daten unterstreichen, dass neben den bisher gezeigten *in vitro* Interaktionen PmpI womöglich auch *in vivo* an andere Pmps auf der Oberfläche von EBs bindet. Hierbei zeigt es eine Bevorzugung bestimmter Proteine wie PmpD. Mögliche Auswirkungen dieser Interaktion sind die Entstehung heteromerer Strukturen, sowie eine Akkumulation von adhäsivem Protein mit einer verstärkten Bindung und damit Infektion als möglicher Folge. Interaktionen zwischen Pmp und nicht-Pmp Proteinen könnte zudem eine verstärkte Vernetzung der EB-Oberfläche und damit eine größere Stabilität der chlamydialen Umhüllung erzeugen.

Ob die räumliche Nähe beschriebener Proteine auf direkter, indirekter oder keiner Interaktion beruht, ist ungeklärt und muss in zukünftigen Untersuchungen wie z.B. mit Pulldown-Experimenten oder FRET weiter entschlüsselt werden. Bisherige Untersuchungen und Ähnlichkeiten innerhalb der Pmp-Familie legen nahe, dass die hier dargestellten Resultate auf andere Pmps neben PmpI übertragbar sind, bedürfen aber weiteren Untersuchungen sowie Weiterverwendung des APEX2-Systems mit anderen Pmps wie PmpD (besonders starke Anreicherung durch PmpI) und PmpC (keine Anreicherung) .

## 5.2 *C. pneumoniae* Pmp21 und Aβ-Oligomere weisen einen ähnlichen Bindungsmodus für das zelluläre Prion Protein $PrP^C$ auf

Vor mehr als 20 Jahren entstand die Theorie, dass eine chlamydiale Infektion einen Zusammenhang mit der Alzheimererkrankung haben könnte (vgl. 1.9.5) [45, 363]. Es folgten einige Studien die diesen Verdacht bestärkten [363, 397, 399, 418]. Trotz all dieser Hinweise gibt es nur wenige Untersuchungen, welche eine

direkte Kausalität zwischen einer chlamydialen Erkrankung und der Entstehung von Alzheimer zeigen konnten.

In Manuskript II konnte gezeigt werden, dass Pmp21_D (C-terminales Fragment der Pmp21-Passagierdomäne) amyloidartige Oligomere erzeugt, welche in ihrer Entstehungs-Kinetik, in ihrem Erscheinungsbild als Oligomer und Protofibril und im CD-Spektrum sehr große Ähnlichkeiten zum Aβ-Peptid und seiner Amyloidgenerierung aufwiesen. Diese Ähnlichkeiten deuten darauf hin, dass Pmp21 und Aβ einen gemeinsamen Mechanismus der Oligomergenerierung verwenden könnten. Innerhalb des amyloiden Weges der APP-Prozessierung entstehen Aβ-Peptide mit einer Größe von 36 bis 43 Aminosäuren und einem Molekulargewicht von etwa 4,5 kDa. Diese beinhalten die amyloidogenen Spezies Aβ40, Aβ42 und Aβ43 [312]. Neurotoxische protofibrilläre Aβ-Oligomere sind in ihrer Größe heterogen und umfassen einen Molekulargewichtsbereich von ca. 50 bis 1500 kDa. Interessanterweise lässt sich bei Pmps womöglich ein ähnliches Verhalten in Bezug zu Größe und Oligomerisierung beobachten. Bisher untersuchte Pmp-Fragmente wie Pmp21_D (vgl. Manuskript II und [275]) als auch *C. trachomatis* Pmp-Fragmente (vgl. Manuskript I und [278]) generieren oligomere Strukturen einer Größe von 600 bis 1300 kDa. In Abhängigkeit vom untersuchten Pmp-Fragments ist es vorstellbar, dass Pmp-Oligomere daher aus ca. 12 (100 kDa, PmpD Fragment) bis über 50 Monomeren (25 kDa, PmpA Fragment) bestehen [278]. Zusammenfassend bilden weder Pmps noch Aβ eine bestimmte dominante oligomere Form, sondern ein breites Spektrum von Oligomeren unterschiedlicher Größe.

Pmps befinden sich auf der chlamydialen Oberfläche, wo sie Prozessierungsprozessen unterliegen (vgl. 1.7.4). Es ist vorstellbar, dass aus diesen Prozessen entstandene Pmp-Fragmente erneut an EB-Oberflächen verankerte Pmps binden und so Pmp-„patches“ oder auch homomere und heteromere Oligomere Strukturen generieren, welche womöglich in zuvor genannten Effekten wie verstärkter Adhäsion oder „Immune-Escape“ ([278]) resultieren würden. Die in Manuskript I beschriebene Präferenz von PmpI, primär in der räumlichen Nähe weiterer Pmps (PmpD, PmpG, PmpI, PmpB und PmpF) zu lokalisieren, unterstützt diese Vermutung. Des Weiteren wäre es vorstellbar, dass prozessierte Pmp-Fragmente (ohne β-Fass) sich von der chlamydialen Oberfläche lösen und zusammen mit oder zusätzlich zu anderen Pmp-Proteinen lösliche oligomere Strukturen bilden. Pmps haben wesentliche Funktionen in Adhäsion und Infektion. Lösliche Komplexe aus Antigenen, wie den Pmp Proteinen könnten, nach der Zelllyse am Ende des Infektionszyklus freigesetzt werden, Antikörper des Immunsystems binden und so als „Dummy“-EBs wirken und damit den zuvor beschriebenen „Immun-Escape“-Mechanismus ergänzen.

Interessanterweise resultierte eine Vorinkubation von HEp-2 Zellen mit dimAβ (zwei Kopien von Aβ40, die durch einen Glycin-Serin-Linker verbunden sind) in einer reduzierten Folgeinfektion mit *C. pneumoniae* und demonstrierte damit, dass Aβ infektionsrelevante Rezeptoren blockiert. Dieses Resultat ist auf

mehrfache Weise vorstellbar, da bereits viele Untersuchungen eine breite Rezeptornutzung (unter anderem den $PrP^C$ und EGFR) durch Aβ beschreiben [419-422]. Im Zuge dessen würde eine Bindung durch dimAβ an den EGFR folglich zu einer reduzierten Bindung von auf dem EB lokalisierten Pmp21 und damit zu einer abgeschwächten Infektion als Folge führen. Zudem steht Aβ im Verdacht antimikrobielle Aktivität auszuüben und als defensive Komponente der angeborenen Immunität zu dienen [392]. So resultierte die Inkubation unterschiedlicher Aβ Peptide mit acht von zwölf Pathogenen zu einem reduzierten Wachstum [392]. Dies würde darauf hindeuten, dass neben einem Binden an den EGFR der HEp-2 Zellen auch das noch im Medium vorhandene Peptid und dessen Interaktion mit den EBs zu einer reduzierten Folgeinfektion beitragen könnte.

Bindestudien an nicht EGFR-exprimierenden CHO-Zellen in Manuskript II zeigten, dass die Bindung von Pmp21 nicht ausschließlich an den EGFR stattfindet. Basierend auf den bisher identifizierten strukturellen und funktionellen Ähnlichkeiten zwischen dimAβ und Pmp21_D und der Tatsache, dass $PrP^C$ einer der wichtigsten Rezeptoren für Aβ darstellt [423, 424], wurde der $PrP^C$ als weiterer humaner Rezeptor für Pmp21 getestet. Kurzzeit-Infektionsexperimente demonstrierten eine Kolokalisation von humanem $PrP^C$-Signal und chlamydialen EBs auf der Oberfläche von HEp-2 Zellen. In Pulldown-Experimenten konnte zelluläres $PrP^C$ mithilfe von Pmp21_D angereichert werden. Final demonstrierten Versuche mittels Dichtegradientenzentrifugation, dass oligomeres Pmp21_D nur in Präsenz spezifischer $PrP^C$-Domänen wie ID und OB (beschrieben als notwendige Domänen für die Bindung mit Aβ [425]) eine Bindung mit $PrP^C$ eingehen kann.

Es ist vorstellbar, dass eine Bindung von Pmp21_D Oligomeren an den $PrP^C$, vergleichbar zu Aβ Oligomeren, eine Signalkaskade auslöst, in welcher als Folge das Transmembranprotein metabotrope Glutamatrezeptor 5 (mGluR5) rekrutiert wird und dieser die Proteinkinase Fyn aktiviert. Aktiviertes Fyn resultiert unter anderem in Kalziumakkumulation, Phosphorylierung des eukaryotischen Elongationsfaktors 2 (eEF2) und damit zum Verlust neuronaler Plastizität, Hemmung der Langzeitpotenzierung (LTP), Synapsenverlust sowie Gedächtnisstörungen und kognitiven Defiziten [426-432]. Zudem induziert aktiviertes Fyn die Hyperphosphorylierung von Tau und damit die Entstehung von neurofibrillären „Tangles“ (NFTs), einem Hauptkennzeichen der Alzheimer-Pathogenese [386, 387, 424].

Die Bindungen von oligomeren Proteinen wie Aβ und α-Synuklein an den $PrP^c$-Rezeptor sind zwei der Protein-Rezeptorinteraktionen, für welche ein neurotoxischer Effekt nachgewiesen werden konnte [429, 433].

Auf Grundlage dieser Analysen ist es vorstellbar, dass Chlamydien auf 2 Wegen zur Entstehung der Alzheimererkrankung beitragen könnten.

**I.** Chlamydien gelangen (i) durch Infektion über das olfaktorische System [399, 434], (ii) Infektion großer Nervenbahnen [435] oder (iii) durch das Durchschreiten der Blut-Hirn-Schranke mittels infizierter Monozyten in das Gehirn [436-438]. Es ist vorstellbar, dass sich Pmp21 - und vielleicht auch weitere Pmp-Fragmente - von der EB-Oberfläche ablösen und Homo- und Hetero-Oligomere generieren. Alternativ oder zusätzlich lösen sich Homo- und Hetero-Oligomere direkt von der EB-Oberfläche. Die Folge sind Entzündungen in entsprechenden Hirnarealen. Studien zeigen, dass *C. pneumoniae* Pmp20 und Pmp21 dosisabhängige Entzündungsreaktionen in menschlichen Endothelzellen durch die Produktion der Entzündungsmediatoren Interleukin (IL)-6, IL-8 und Monozyten-Chemoattraktant-Protein-1 (MCP-1) durch Aktivierung des NF-kappaB-Signalweges auslösen [448]. Als möglicher Abwehrmechanismus könnte in Folge vermehrt Aβ generiert werden [392]. Experimente, in denen die Vorbehandlung von Humanzellen mit dimAβ und die anschließende Zugabe von EBs zu einer reduzierten Folgeinfektion durch *C. pneumoniae* führten, deuten auf eine Abwehrfunktion durch Aβ hin (siehe Manuskript II). Eine wachsende Menge an Publikationen legt nahe, dass die Produktion von Aβ und in Folge die Entstehung von Oligomeren und Fibrillen, Bestandteil der angeborenen Immunität im Gehirn darstellen [395, 439, 440]. Bakterien können durch Aβ verklumpen und eingeschlossen werden, wodurch Replikation, Verbreitung und Zelleintritt reduziert werden könnte [392, 440, 441]. In einigen Fällen konnte eine stärkere bakterizide Wirkung von Aβ im Vergleich zum menschlichen antimikrobiellen Peptid LL-37 beobachtet werden [392, 440]. Womöglich bilden Aβ-Peptide ringförmige Protofibrillen, welche als Poren in der Membran das Austreten von Membraninhalten ermöglichen [442]. Es ist vorstellbar, dass bei einer Infektion durch *C. pneumoniae* im Gehirn Aβ produziert und in Folge das EB umhüllt und alternativ auch mit weiteren EBs agglutiniert. Mögliche Folge könnte, durch das Abschirmen chlamydialer Adhäsine, eine reduzierte oder ausbleibende Bindung an Humanzellen darstellen. Die Agglutinierung von EBs könnte eine Infektion reduzieren und eine Vernichtung durch Mikroglia erleichtern. Ob Aβ an EBs bindet, Aβ direkte toxische Effekte auf EBs ausübt oder primär EBs und damit dessen Adhäsine abschirmt ist bisher unbekannt und Ziel zukünftiger Forschung.

Eine verstärkte Produktion von Aβ als Verteidigungsreaktion auf wiederkehrende Infektionen im Gehirn durch *C. pneumoniae* und weiteren Pathogenen könnte darauf schließen lassen, dass Alzheimer ein unbeabsichtigter Kollateralschaden der Immunverteidigung darstellt. Mit zunehmendem Alter nimmt die Leistungsfähigkeit des Immunsystems ab. Gleichzeitig nimmt die Wahrscheinlichkeit für eine *C. pneumoniae* Infektion zu [44]. In Folge häufen sich womöglich Infektionsereignisse im Gehirn und verursachen Entzündungszustände, welche länger andauern und chronisch werden können. Als Folge dieser Entzündungszustände wird über einen längeren Zeitraum das Hirngewebe geschädigt und vermehrt Aβ produziert. Eine anhaltende Überproduktion von Aβ könnte die Wahrscheinlichkeit Alzheimer zu

erzeugen erhöhen. Unterstützt wird diese Hypothese durch Untersuchungen, welche demonstrierten, dass eine Hochregelung des NF-kappaB-Signalweges zu einer erhöhten Wahrscheinlichkeit an Alzheimer zu erkranken führt wohingegen eine Unterdrückung diese reduzierte [443].

**II.** Auf einem zweiten möglichen Weg könnten lösliche, aber auch EB-gebundene Pmp21 Oligomere, vergleichbar zu Aβ, an den $PrP^C$ binden und in Folge einen toxischen Signalweg aktivieren, welcher letztlich in synaptischer Toxizität und neuronaler Dysfunktion resultiert. Zukünftige Studien werden zeigen, ob Pmp Oligomere in der Lage sind den $PrP^C$-Signalweg zu aktivieren, ob das Vorhandensein von monomerem oder oligomerem Pmp die Entstehung von Aβ Oligomeren beeinflusst und zuletzt, ob es möglich ist durch die Vorbehandlung chlamydialer EBs mit Aβ (vgl. [392]) eine nachfolgende Infektion zu reduzieren.

## 5.3 Ein Fünf-Komponenten-Impfstoff aus PmpA, PmpD, PmpG, PmpH und Ctad1 vermittelt einen langanhaltenden Infektionsschutz

Global betrachtet stellen chlamydiale Infektionen bis heute eine relevante Bedrohung dar. Laut WHO gab es im Jahr 2016 124 Millionen neue Infektionen durch *C. trachomatis*, wodurch es das meistverbreitete sexuell übertragbare Pathogen darstellt [444]. Erneute Infektionen, unentdeckte Erkrankungen und die damit verbundenen Folgen wie Unfruchtbarkeit oder Eileiterschwangerschaften machen intensive Impfstoffforschungen notwendig [6, 60]. Allerdings konnte sich innerhalb der letzten Jahrzehnte kein Antigen, Target, Adjuvans oder Form der Wirkstoff-Applikation als Favorit herauskristallisieren [445]. Wie in 1.7 erläutert, sind Pmps Adhäsine auf der Oberfläche von EBs, welche maßgeblich an der Bindung an die Wirtszelle sowie der Internalisierung beteiligt sind und damit entscheidend zu einer Infektion beitragen [1, 93, 275, 278]. Dies macht sie zu herausragenden Kandidaten für eine Impfstoffentwicklung.

In Manuskript III entwickelten wir in Kooperation mit Arbeitsgruppe Klos (Medizinische Hochschule Hannover) und Arbeitsgruppe Guzmán (Helmholtz-Zentrum für Infektionsforschung) einen Fünf-Komponentenwirkstoff (5cVAC), welcher sich aus *C. trachomatis* PmpA, PmpD, PmpG, PmpH und dem erst kürzlich beschriebenen neuen Adhäsin und Invasin Ctad1 zusammensetzte [102, 446] und mit dem mukosalen Adjuvans zyklisches Diadenosinmonophosphat kombiniert wurde. Eine wiederholte intranasale Impfung resultierte in einem bis zu fünf Monate anhaltenden effizienten Schutz von Mäusen gegen eine darauf folgende Infektion mit *C. trachomatis* Serovar E sowie zwei weiteren urogenitalen und einem Trachom-Serovar [446]. PmpD und Ctad1 zeigten nach der Impfung mit 5cVAC die stärkste spezifische IgA- und IgG-Reaktion. Vakzinierungsstudien mit zwei Komponenten (PmpD und Ctad1) resultierten 4 Tage nach Infektion in einer ähnlichen Gewichtszunahme wie bei Mäusen, welche mit 5cVAC

vakziniert wurden, wohingegen der Rückgang des „clinical score“ weniger deutlich ausgefallen war. Dies deutet darauf hin, dass mindestens PmpD oder Ctad1 sowie mindestens PmpA, PmpG oder PmpH im Impfstoff enthalten sein müssen um einen ausgeprägten Schutz zu vermitteln.

Die Notwendigkeit von mindestens 2 Komponenten könnte bedeuten, dass bei einer Blockierung spezifischer Pmps durch Antikörper, weitere Pmps dessen Funktion übernehmen könnten oder nicht alle Pmps für eine erfolgreiche Infektion in gleichem Maß notwendig sind. Dies unterstreicht die Notwenigkeit bei der Entwicklung eines Impfstoffes mehrere infektionsrelevante Proteine zu verwenden um auf diese Weise „Escape“- oder Ausweichsysteme zu neutralisieren.

Trotz der guten Wirksamkeit des hier entwickelten Impfstoffes gibt es weiterhin Optimierungsbedarf.

Die Verwendung von weiteren Pmps und die Entwicklung optimierter Fragmente könnte einen Immunschutz verbessern. Innerhalb der Passagierdomäne besitzen Pmps eine Vielzahl an FxxN- und GGA (I, L, V)-Motiven, welche für Eigenschaften wie Adhäsion und Oligomerisierung essentiell sind [275]. Es ist möglich, dass ein artifizielles Protein, welches hauptsächlich aus diesen Domänen besteht, eine bessere Immunisierung hervorrufen könnte.

Der in Favaroni *et al.* 2021 beschriebene „Escape-Mechanismus“ beschreibt eine chlamydiale EB-Oberfläche, welche eine Vielzahl unterschiedlicher homo- und heteromerer Pmp-Komplexe präsentiert, dadurch eine enorme Antigen-Vielfalt erzeugt und damit eventuell die Erkennung durch Antikörper des Immunsystems erschwert [278]. Ein Impfstoff, welcher nur einen Anteil der möglichen Pmp-Proteine verwendet, ist daher wahrscheinlich nicht in der Lage, einen vollständigen Schutz zu vermitteln.

Die Verwendung von mehreren bis allen Pmps als Grundlage für einen Impfstoff könnte durch eine breitere Produktion von Antikörpern einen optimierten Schutz erzeugen. Selbst bei einem solchen optimierten Schutz wäre es unklar, ob Antikörper, welche durch Impfung mit homomeren oligomeren Pmp-Proteinen entstanden, an heteromere Oligomere effizient binden könnten.

Es ist vorstellbar, dass der hier entwickelte Impfstoff auch bei genitalen Mäuseinfektionen schützend wirkt und auch mehrere *Ctr*-Serovare einschließt. Daher wird ein nächster Schritt ein urogenitales Mausmodell beinhalten.

Es gibt nach wie vor viele offene Fragen. Wie genau sieht die proteinöse Oberfläche chlamydialer EBs wirklich aus? Welche Pmps binden miteinander und in welchem Maß? Was sind die Auswirkungen dieser Komplexe? Ist die Entstehung von Alzheimer nur ein Kollateralschaden in der Bekämpfung des Wirtsorganismus gegen eine chlamydiale Infektion im Hirn? Diese Arbeit konnte einen kleinen Beitrag leisten diese Fragen teilweise aufzuklären. Zukünftige Forschungen werden genannte Fragestellungen vertiefen und sie kontinuierlich entschlüsseln.

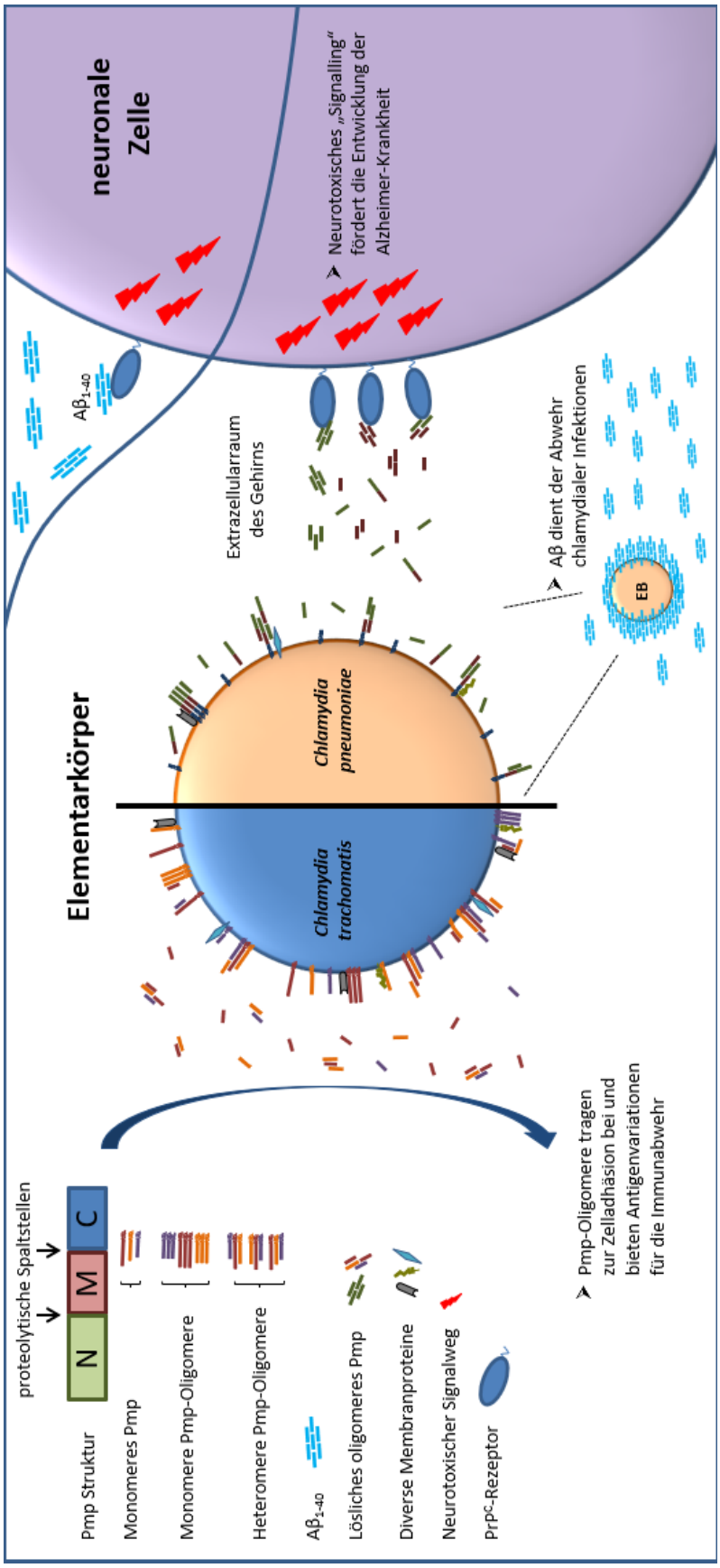


Abbildung 12: Zusammenfassendes Modell der Pmp-Präsentation und dessen Auswirkungen im Infektionsprozess

Pmps sind Adhäsine und zum Teil Invasine (d.h. nur Pmp21 wurde getestet und als Invasin bestimmt [1]), welche auf der Oberfläche aller chlamydialen Spezies identifiziert werden konnten. Aufgrund publizierter und in dieser Arbeit vorgestellten Untersuchungen an *C. pneumoniae* und *C. trachomatis* ist es möglich, das Pmps als Monomere, Oligomere und heteromere Oligomere auf der Oberfläche von EBs vorliegen. Diese unterschiedlichen Proteinformen können sowohl aus volllänge Pmp als auch in Kombination mit prozessierten Pmps vorliegen. Untersuchungen aus der Massenspektrometrie (in Verbindung mit der Proximity-Biotinylierungstechnik unter Verwendung der Peroxidase APEX2) legen nahe, dass Pmps spezifische andere Pmps in ihrer Bindung bevorzugen (z.B. PmpI mit PmpD) und auch Interaktionen zu anderen Membranproteinen vorstellbar sind. Die sich stark varrierende und verändernde EB Oberfläche bietet daher ein großes Maß an Antigen- Varibilität was eine Immunabwehr bzw. einen immunausweichenden Mechanismus darstellen könnte.

Chlamydiale Infektionen des Gehirns, wie sie bei *C. pneumoniae* beobachtet wurden, können die Entstehung der Alzheimer-Erkrankung fördern indem Pmp21-Oligomere an den $PrP^C$ binden und dadurch womöglich (wie bei Aβ) ein neurotoxisches „Signalling" auslösen. Zusätzlich ist es wahrscheinlich, das die vermehrte Ausschüttung von Aβ, als antimikrobiell beschiebenes Protein, eine Verteidigungsreaktion des Wirts gegen eine Infektion mit Chlamydien darstellt, welches wiederrum die Wahrscheinlichkeit der Entstehung von Alzheimer erhöhen könnte.

# Literaturverzeichnis


1. Molleken, K., E. Becker, and J.H. Hegemann, *The Chlamydia pneumoniae invasin protein Pmp21 recruits the EGF receptor for host cell entry.* PLoS Pathog, 2013. **9**(4): p. e1003325.
2. Bayramova, F., N. Jacquier, and G. Greub, *Insight in the biology of Chlamydia-related bacteria.* Microbes Infect, 2018. **20**(7-8): p. 432-440.
3. Elwell, C., K. Mirrashidi, and J. Engel, *Chlamydia cell biology and pathogenesis.* Nat Rev Microbiol, 2016. **14**(6): p. 385-400.
4. Bachmann, N.L., A. Polkinghorne, and P. Timms, *Chlamydia genomics: providing novel insights into chlamydial biology.* Trends Microbiol, 2014. **22**(8): p. 464-72.
5. Staub, E., et al., *Novel Chlamydia species isolated from snakes are temperature-sensitive and exhibit decreased susceptibility to azithromycin.* Sci Rep, 2018. **8**(1): p. 5660.
6. Cheong, H.C., et al., *Chlamydiaceae: Diseases in Primary Hosts and Zoonosis.* Microorganisms, 2019. **7**(5).
7. Lamoth, F. and G. Greub, *Amoebal pathogens as emerging causal agents of pneumonia.* FEMS Microbiol Rev, 2010. **34**(3): p. 260-80.
8. Grayston, J.T., et al., *Evidence that Chlamydia pneumoniae causes pneumonia and bronchitis.* J Infect Dis, 1993. **168**(5): p. 1231-5.
9. Baud, D. and G. Greub, *Intracellular bacteria and adverse pregnancy outcomes.* Clin Microbiol Infect, 2011. **17**(9): p. 1312-22.
10. Pospischil, A., et al., *Abortion in woman caused by caprine Chlamydophila abortus (Chlamydia psittaci serovar 1).* Swiss Med Wkly, 2002. **132**(5-6): p. 64-6.
11. Beeckman, D.S. and D.C. Vanrompay, *Zoonotic Chlamydophila psittaci infections from a clinical perspective.* Clin Microbiol Infect, 2009. **15**(1): p. 11-7.
12. Everett, K.D., R.M. Bush, and A.A. Andersen, *Emended description of the order Chlamydiales, proposal of Parachlamydiaceae fam. nov. and Simkaniaceae fam. nov., each containing one monotypic genus, revised taxonomy of the family Chlamydiaceae, including a new genus and five new species, and standards for the identification of organisms.* Int J Syst Bacteriol, 1999. **49 Pt 2**: p. 415-40.
13. Stephens, R.S., et al., *Divergence without difference: phylogenetics and taxonomy of Chlamydia resolved.* FEMS Immunol Med Microbiol, 2009. **55**(2): p. 115-9.
14. Browning, G.F., *Is Chlamydophila felis a significant zoonotic pathogen?* Aust Vet J, 2004. **82**(11): p. 695-6.
15. Bommana, S. and A. Polkinghorne, *Mini Review: Antimicrobial Control of Chlamydial Infections in Animals: Current Practices and Issues.* Front Microbiol, 2019. **10**: p. 113.
16. (CDC), D.o.H.a.H.S., *Sexually Transmitted Disease Surveillance, 2019*. April 2021.
17. Kreisel, K.M., et al., *Sexually Transmitted Infections Among US Women and Men: Prevalence and Incidence Estimates, 2018.* Sex Transm Dis, 2021. **48**(4): p. 208-214.
18. Torrone, E., et al., *Prevalence of Chlamydia trachomatis genital infection among persons aged 14-39 years--United States, 2007-2012.* MMWR Morb Mortal Wkly Rep, 2014. **63**(38): p. 834-8.
19. Kutlin, A., et al., *Molecular characterization of Chlamydophila pneumoniae isolates from Western barred bandicoots.* J Med Microbiol, 2007. **56**(Pt 3): p. 407-417.
20. Coles, K.A., P. Timms, and D.W. Smith, *Koala biovar of Chlamydia pneumoniae infects human and koala monocytes and induces increased uptake of lipids in vitro.* Infect Immun, 2001. **69**(12): p. 7894-7.

21. Bodetti, T.J., et al., *Molecular evidence to support the expansion of the hostrange of Chlamydophila pneumoniae to include reptiles as well as humans, horses, koalas and amphibians.* Syst Appl Microbiol, 2002. **25**(1): p. 146-52.
22. Longbottom, D. and L.J. Coulter, *Animal chlamydioses and zoonotic implications.* J Comp Pathol, 2003. **128**(4): p. 217-44.
23. Campos-Hernandez, E., et al., *Prevalence and molecular identification of Chlamydia abortus in commercial dairy goat farms in a hot region in Mexico.* Trop Anim Health Prod, 2014. **46**(6): p. 919-24.
24. Di Paolo, L.A., et al., *First report of caprine abortions due to Chlamydia abortus in Argentina.* Vet Med Sci, 2019. **5**(2): p. 162-167.
25. Nigg, C., *An Unidentified Virus Which Produces Pneumonia and Systemic Infection in Mice.* Science, 1942. **95**(2454): p. 49-50.
26. Barron, A.L., et al., *A new animal model for the study of Chlamydia trachomatis genital infections: infection of mice with the agent of mouse pneumonitis.* J Infect Dis, 1981. **143**(1): p. 63-6.
27. Mohamad, K.Y. and A. Rodolakis, *Recent advances in the understanding of Chlamydophila pecorum infections, sixteen years after it was named as the fourth species of the Chlamydiaceae family.* Vet Res, 2010. **41**(3): p. 27.
28. Phillips, S., et al., *Chlamydia pecorum gastrointestinal tract infection associations with urogenital tract infections in the koala (Phascolarctos cinereus).* PLoS One, 2018. **13**(11): p. e0206471.
29. Walker, E., et al., *Clinical, diagnostic and pathologic features of presumptive cases of Chlamydia pecorum-associated arthritis in Australian sheep flocks.* BMC Vet Res, 2016. **12**(1): p. 193.
30. Jelocnik, M., et al., *Molecular and pathological insights into Chlamydia pecorum-associated sporadic bovine encephalomyelitis (SBE) in Western Australia.* BMC Vet Res, 2014. **10**: p. 121.
31. Ohtani, A., et al., *Genetic and antigenic analysis of Chlamydia pecorum strains isolated from calves with diarrhea.* J Vet Med Sci, 2015. **77**(7): p. 777-82.
32. Fabijan, J., et al., *Chlamydia pecorum prevalence in South Australian koala (Phascolarctos cinereus) populations: Identification and modelling of a population free from infection.* Sci Rep, 2019. **9**(1): p. 6261.
33. Harkinezhad, T., T. Geens, and D. Vanrompay, *Chlamydophila psittaci infections in birds: a review with emphasis on zoonotic consequences.* Vet Microbiol, 2009. **135**(1-2): p. 68-77.
34. Reinhold, P., et al., *An experimentally induced Chlamydia suis infection in pigs results in severe lung function disorders and pulmonary inflammation.* Vet Res, 2008. **39**(3): p. 35.
35. Chahota, R., et al., *Involvement of multiple Chlamydia suis genotypes in porcine conjunctivitis.* Transbound Emerg Dis, 2018. **65**(1): p. 272-277.
36. Olive, A.J., et al., *Chlamydia trachomatis-induced alterations in the host cell proteome are required for intracellular growth.* Cell Host Microbe, 2014. **15**(1): p. 113-24.
37. Gruffydd-Jones, T., et al., *Chlamydophila felis infection. ABCD guidelines on prevention and management.* J Feline Med Surg, 2009. **11**(7): p. 605-9.
38. Lutz-Wohlgroth, L., et al., *Chlamydiales in guinea-pigs and their zoonotic potential.* J Vet Med A Physiol Pathol Clin Med, 2006. **53**(4): p. 185-93.
39. Rodolakis, A. and K. Yousef Mohamad, *Zoonotic potential of Chlamydophila.* Vet Microbiol, 2010. **140**(3-4): p. 382-91.
40. Sachse, K., et al., *Evidence for the existence of two new members of the family Chlamydiaceae and proposal of Chlamydia avium sp. nov. and Chlamydia gallinacea sp. nov.* Syst Appl Microbiol, 2014. **37**(2): p. 79-88.
41. Blasi, F., et al., *Epidemiology of Chlamydia pneumoniae.* Clin Microbiol Infect, 1998. **4 Suppl 4**: p. S1-S6.
42. Kuo, C.C., et al., *Chlamydia pneumoniae (TWAR).* Clin Microbiol Rev, 1995. **8**(4): p. 451-61.

43. Theunissen, H.J., et al., *Influence of temperature and relative humidity on the survival of Chlamydia pneumoniae in aerosols.* Appl Environ Microbiol, 1993. **59**(8): p. 2589-93.
44. Porritt, R.A. and T.R. Crother, *Chlamydia pneumoniae Infection and Inflammatory Diseases.* For Immunopathol Dis Therap, 2016. **7**(3-4): p. 237-254.
45. Balin, B.J., et al., *Chlamydia pneumoniae: An Etiologic Agent for Late-Onset Dementia.* Front Aging Neurosci, 2018. **10**: p. 302.
46. Shima, K., et al., *The Genetic Transformation of Chlamydia pneumoniae.* mSphere, 2018. **3**(5).
47. Myers, G.S., et al., *Evidence that human Chlamydia pneumoniae was zoonotically acquired.* J Bacteriol, 2009. **191**(23): p. 7225-33.
48. Wang, Y., et al., *Development of a transformation system for Chlamydia trachomatis: restoration of glycogen biosynthesis by acquisition of a plasmid shuttle vector.* PLoS Pathog, 2011. **7**(9): p. e1002258.
49. Witkin, S.S., et al., *Chlamydia trachomatis: the Persistent Pathogen.* Clin Vaccine Immunol, 2017. **24**(10).
50. Mohseni, M., S. Sung, and V. Takov, *Chlamydia*, in *StatPearls*. 2021: Treasure Island (FL).
51. Malhotra, M., et al., *Genital Chlamydia trachomatis: an update.* Indian J Med Res, 2013. **138**(3): p. 303-16.
52. Workowski, K.A., et al., *Sexually transmitted diseases treatment guidelines, 2010.* MMWR Recomm Rep, 2010. **59**(RR-12): p. 1-110.
53. Owusu-Edusei, K., Jr., et al., *The estimated direct medical cost of selected sexually transmitted infections in the United States, 2008.* Sex Transm Dis, 2013. **40**(3): p. 197-201.
54. Mabey, D. and R.W. Peeling, *Lymphogranuloma venereum.* Sex Transm Infect, 2002. **78**(2): p. 90-2.
55. Mestrovic, T. and S. Ljubin-Sternak, *Molecular mechanisms of Chlamydia trachomatis resistance to antimicrobial drugs.* Front Biosci (Landmark Ed), 2018. **23**: p. 656-670.
56. Stephens, R.S., et al., *Genome sequence of an obligate intracellular pathogen of humans: Chlamydia trachomatis.* Science, 1998. **282**(5389): p. 754-9.
57. Betts-Hampikian, H.J. and K.A. Fields, *The Chlamydial Type III Secretion Mechanism: Revealing Cracks in a Tough Nut.* Front Microbiol, 2010. **1**: p. 114.
58. Fields, K., M. Tan, and P. Bavoil, *Intracellular pathogens. I. Chlamydiales*. 2012.
59. Mitchell, C.M., et al., *In vitro characterisation of koala Chlamydia pneumoniae: morphology, inclusion development and doubling time.* Vet Microbiol, 2009. **136**(1-2): p. 91-9.
60. Tan, M. and P. Bavoil, *Intracellular pathogens I: chlamydiales*. Vol. 1. 2012: American Society for Microbiology Press.
61. Sixt, B.S., et al., *Metabolic features of Protochlamydia amoebophila elementary bodies--a link between activity and infectivity in Chlamydiae.* PLoS Pathog, 2013. **9**(8): p. e1003553.
62. Todd, W.J. and H.D. Caldwell, *The interaction of Chlamydia trachomatis with host cells: ultrastructural studies of the mechanism of release of a biovar II strain from HeLa 229 cells.* J Infect Dis, 1985. **151**(6): p. 1037-44.
63. Hybiske, K. and R.S. Stephens, *Mechanisms of host cell exit by the intracellular bacterium Chlamydia.* Proc Natl Acad Sci U S A, 2007. **104**(27): p. 11430-5.
64. Wyrick, P.B., *Chlamydia trachomatis persistence in vitro: an overview.* J Infect Dis, 2010. **201 Suppl 2**: p. S88-95.
65. Kintner, J., et al., *Commonly prescribed beta-lactam antibiotics induce C. trachomatis persistence/stress in culture at physiologically relevant concentrations.* Front Cell Infect Microbiol, 2014. **4**: p. 44.
66. Jacquier, N., et al., *Cell wall precursors are required to organize the chlamydial division septum.* Nat Commun, 2014. **5**: p. 3578.

67. Beatty, W.L., G.I. Byrne, and R.P. Morrison, *Morphologic and antigenic characterization of interferon gamma-mediated persistent Chlamydia trachomatis infection in vitro.* Proc Natl Acad Sci U S A, 1993. **90**(9): p. 3998-4002.
68. Vanover, J., et al., *Herpes simplex virus co-infection-induced Chlamydia trachomatis persistence is not mediated by any known persistence inducer or anti-chlamydial pathway.* Microbiology (Reading), 2008. **154**(Pt 3): p. 971-978.
69. Hatch, T.P., D.W. Vance, Jr., and E. Al-Hossainy, *Attachment of Chlamydia psittaci to formaldehyde-fixed and unfixed L cells.* J Gen Microbiol, 1981. **125**(2): p. 273-83.
70. Zhang, J.P. and R.S. Stephens, *Mechanism of C. trachomatis attachment to eukaryotic host cells.* Cell, 1992. **69**(5): p. 861-9.
71. Su, H., et al., *A recombinant Chlamydia trachomatis major outer membrane protein binds to heparan sulfate receptors on epithelial cells.* Proc Natl Acad Sci U S A, 1996. **93**(20): p. 11143-8.
72. Gitsels, A., N. Sanders, and D. Vanrompay, *Chlamydial Infection From Outside to Inside.* Front Microbiol, 2019. **10**: p. 2329.
73. Carabeo, R.A. and T. Hackstadt, *Isolation and characterization of a mutant Chinese hamster ovary cell line that is resistant to Chlamydia trachomatis infection at a novel step in the attachment process.* Infect Immun, 2001. **69**(9): p. 5899-904.
74. Moelleken, K. and J.H. Hegemann, *The Chlamydia outer membrane protein OmcB is required for adhesion and exhibits biovar-specific differences in glycosaminoglycan binding.* Mol Microbiol, 2008. **67**(2): p. 403-19.
75. Fadel, S. and A. Eley, *Chlamydia trachomatis OmcB protein is a surface-exposed glycosaminoglycan-dependent adhesin.* J Med Microbiol, 2007. **56**(Pt 1): p. 15-22.
76. Barbour, A.G., et al., *Chlamydia trachomatis has penicillin-binding proteins but not detectable muramic acid.* J Bacteriol, 1982. **151**(1): p. 420-8.
77. McCoy, A.J. and A.T. Maurelli, *Building the invisible wall: updating the chlamydial peptidoglycan anomaly.* Trends Microbiol, 2006. **14**(2): p. 70-7.
78. Klockner, A., et al., *AmiA is a penicillin target enzyme with dual activity in the intracellular pathogen Chlamydia pneumoniae.* Nat Commun, 2014. **5**: p. 4201.
79. Liechti, G.W., et al., *A new metabolic cell-wall labelling method reveals peptidoglycan in Chlamydia trachomatis.* Nature, 2014. **506**(7489): p. 507-10.
80. Tan, M., *Temporal gene regulation during the chlamydial developmental cycle.* Intracellular Pathogens I: Chlamydiales, 2012: p. 149-169.
81. Gitsels, A., et al., *Chlamydia: what is on the outside does matter.* Crit Rev Microbiol, 2020. **46**(1): p. 100-119.
82. Caldwell, H.D., J. Kromhout, and J. Schachter, *Purification and partial characterization of the major outer membrane protein of Chlamydia trachomatis.* Infect Immun, 1981. **31**(3): p. 1161-76.
83. Bavoil, P., A. Ohlin, and J. Schachter, *Role of disulfide bonding in outer membrane structure and permeability in Chlamydia trachomatis.* Infect Immun, 1984. **44**(2): p. 479-85.
84. Newhall, W.J. and R.B. Jones, *Disulfide-linked oligomers of the major outer membrane protein of chlamydiae.* J Bacteriol, 1983. **154**(2): p. 998-1001.
85. Puolakkainen, M., C.C. Kuo, and L.A. Campbell, *Chlamydia pneumoniae uses the mannose 6-phosphate/insulin-like growth factor 2 receptor for infection of endothelial cells.* Infect Immun, 2005. **73**(8): p. 4620-5.
86. Liu, X., et al., *Identification of Chlamydia trachomatis outer membrane complex proteins by differential proteomics.* J Bacteriol, 2010. **192**(11): p. 2852-60.
87. Christensen, S., et al., *Life inside and out: making and breaking protein disulfide bonds in Chlamydia.* Crit Rev Microbiol, 2019. **45**(1): p. 33-50.
88. Rockey, D.D., J. Lenart, and R.S. Stephens, *Genome sequencing and our understanding of chlamydiae.* Infect Immun, 2000. **68**(10): p. 5473-9.

89. Patel, A.L., et al., *Activation of epidermal growth factor receptor is required for Chlamydia trachomatis development.* BMC Microbiol, 2014. **14**: p. 277.
90. Li, X., et al., *Polymorphic Membrane Protein 17G of Chlamydia psittaci Mediated the Binding and Invasion of Bacteria to Host Cells by Interacting and Activating EGFR of the Host.* Front Immunol, 2021. **12**: p. 818487.
91. Molleken, K., E. Schmidt, and J.H. Hegemann, *Members of the Pmp protein family of Chlamydia pneumoniae mediate adhesion to human cells via short repetitive peptide motifs.* Mol Microbiol, 2010. **78**(4): p. 1004-17.
92. Becker, E., *Charakterisierung der chlamydialen Pmp Adhäsin Familie*, in *Funktionelle Genomforschung der Mikroorganismen*. 2013, Heinrich-Heine-Universität Düsseldorf.
93. Becker, E. and J.H. Hegemann, *All subtypes of the Pmp adhesin family are implicated in chlamydial virulence and show species-specific function.* Microbiologyopen, 2014. **3**(4): p. 544-56.
94. Fechtner, T., J.N. Galle, and J.H. Hegemann, *The novel chlamydial adhesin CPn0473 mediates the lipid raft-dependent uptake of Chlamydia pneumoniae.* Cell Microbiol, 2016. **18**(8): p. 1094-105.
95. Wuppermann, F.N., et al., *Chlamydia pneumoniae GroEL1 protein is cell surface associated and required for infection of HEp-2 cells.* J Bacteriol, 2008. **190**(10): p. 3757-67.
96. Bulut, Y., et al., *Chlamydial heat shock protein 60 activates macrophages and endothelial cells through Toll-like receptor 4 and MD2 in a MyD88-dependent pathway.* J Immunol, 2002. **168**(3): p. 1435-40.
97. Kol, A., et al., *Cutting edge: heat shock protein (HSP) 60 activates the innate immune response: CD14 is an essential receptor for HSP60 activation of mononuclear cells.* J Immunol, 2000. **164**(1): p. 13-7.
98. Maguire, M., et al., *Comparative cell signalling activity of ultrapure recombinant chaperonin 60 proteins from prokaryotes and eukaryotes.* Immunology, 2005. **115**(2): p. 231-8.
99. Costa, C.P., et al., *Role of chlamydial heat shock protein 60 in the stimulation of innate immune cells by Chlamydia pneumoniae.* Eur J Immunol, 2002. **32**(9): p. 2460-70.
100. Gerard, H.C., et al., *Apolipoprotein E4 enhances attachment of Chlamydophila (Chlamydia) pneumoniae elementary bodies to host cells.* Microb Pathog, 2008. **44**(4): p. 279-85.
101. Ajonuma, L.C., et al., *CFTR is required for cellular entry and internalization of Chlamydia trachomatis.* Cell Biol Int, 2010. **34**(6): p. 593-600.
102. Stallmann, S. and J.H. Hegemann, *The Chlamydia trachomatis Ctad1 invasin exploits the human integrin beta1 receptor for host cell entry.* Cell Microbiol, 2016. **18**(5): p. 761-75.
103. Mamelak, D., et al., *Hsp70s contain a specific sulfogalactolipid binding site. Differential aglycone influence on sulfogalactosyl ceramide binding by recombinant prokaryotic and eukaryotic hsp70 family members.* Biochemistry, 2001. **40**(12): p. 3572-82.
104. Kim, J.H., et al., *Chlamydia trachomatis co-opts the FGF2 signaling pathway to enhance infection.* PLoS Pathog, 2011. **7**(10): p. e1002285.
105. Subbarayal, P., et al., *EphrinA2 receptor (EphA2) is an invasion and intracellular signaling receptor for Chlamydia trachomatis.* PLoS Pathog, 2015. **11**(4): p. e1004846.
106. Carabeo, R., *Bacterial subversion of host actin dynamics at the plasma membrane.* Cell Microbiol, 2011. **13**(10): p. 1460-9.
107. Carabeo, R.A., et al., *Chlamydia trachomatis induces remodeling of the actin cytoskeleton during attachment and entry into HeLa cells.* Infect Immun, 2002. **70**(7): p. 3793-803.
108. Ford, C., et al., *Chlamydia exploits filopodial capture and a macropinocytosis-like pathway for host cell entry.* PLoS Pathog, 2018. **14**(5): p. e1007051.
109. Birkelund, S., H. Johnsen, and G. Christiansen, *Chlamydia trachomatis serovar L2 induces protein tyrosine phosphorylation during uptake by HeLa cells.* Infect Immun, 1994. **62**(11): p. 4900-8.

110. Fawaz, F.S., et al., *Infection with Chlamydia trachomatis alters the tyrosine phosphorylation and/or localization of several host cell proteins including cortactin.* Infect Immun, 1997. **65**(12): p. 5301-8.
111. Swanson, K.A., D.D. Crane, and H.D. Caldwell, *Chlamydia trachomatis species-specific induction of ezrin tyrosine phosphorylation functions in pathogen entry.* Infect Immun, 2007. **75**(12): p. 5669-77.
112. Lane, B.J., et al., *Chlamydial entry involves TARP binding of guanine nucleotide exchange factors.* PLoS Pathog, 2008. **4**(3): p. e1000014.
113. Graham, T.R. and M.M. Kozlov, *Interplay of proteins and lipids in generating membrane curvature.* Curr Opin Cell Biol, 2010. **22**(4): p. 430-6.
114. Cocucci, E., et al., *The first five seconds in the life of a clathrin-coated pit.* Cell, 2012. **150**(3): p. 495-507.
115. Hodinka, R.L., et al., *Ultrastructural study of endocytosis of Chlamydia trachomatis by McCoy cells.* Infect Immun, 1988. **56**(6): p. 1456-63.
116. Wyrick, P.B., et al., *Entry of genital Chlamydia trachomatis into polarized human epithelial cells.* Infect Immun, 1989. **57**(8): p. 2378-89.
117. Majeed, M. and E. Kihlstrom, *Mobilization of F-actin and clathrin during redistribution of Chlamydia trachomatis to an intracellular site in eucaryotic cells.* Infect Immun, 1991. **59**(12): p. 4465-72.
118. Hybiske, K. and R.S. Stephens, *Mechanisms of Chlamydia trachomatis entry into nonphagocytic cells.* Infect Immun, 2007. **75**(8): p. 3925-34.
119. Korhonen, J.T., et al., *Chlamydia pneumoniae entry into epithelial cells by clathrin-independent endocytosis.* Microb Pathog, 2012. **52**(3): p. 157-64.
120. Ward, M.E. and A. Murray, *Control mechanisms governing the infectivity of Chlamydia trachomatis for HeLa cells: mechanisms of endocytosis.* J Gen Microbiol, 1984. **130**(7): p. 1765-80.
121. Boleti, H., et al., *Chlamydia infection of epithelial cells expressing dynamin and Eps15 mutants: clathrin-independent entry into cells and dynamin-dependent productive growth.* J Cell Sci, 1999. **112 ( Pt 10)**: p. 1487-96.
122. Norkin, L.C., S.A. Wolfrom, and E.S. Stuart, *Association of caveolin with Chlamydia trachomatis inclusions at early and late stages of infection.* Exp Cell Res, 2001. **266**(2): p. 229-38.
123. Webley, W.C., L.C. Norkin, and E.S. Stuart, *Caveolin-2 associates with intracellular chlamydial inclusions independently of caveolin-1.* BMC Infect Dis, 2004. **4**: p. 23.
124. Gabel, B.R., et al., *Lipid raft-mediated entry is not required for Chlamydia trachomatis infection of cultured epithelial cells.* Infect Immun, 2004. **72**(12): p. 7367-73.
125. Matveev, S., et al., *The role of caveolae and caveolin in vesicle-dependent and vesicle-independent trafficking.* Adv Drug Deliv Rev, 2001. **49**(3): p. 237-50.
126. Stuart, E.S., W.C. Webley, and L.C. Norkin, *Lipid rafts, caveolae, caveolin-1, and entry by Chlamydiae into host cells.* Exp Cell Res, 2003. **287**(1): p. 67-78.
127. Peters, J., et al., *Type III secretion a la Chlamydia.* Trends Microbiol, 2007. **15**(6): p. 241-51.
128. Saka, H.A., et al., *Quantitative proteomics reveals metabolic and pathogenic properties of Chlamydia trachomatis developmental forms.* Mol Microbiol, 2011. **82**(5): p. 1185-203.
129. Clifton, D.R., et al., *A chlamydial type III translocated protein is tyrosine-phosphorylated at the site of entry and associated with recruitment of actin.* Proc Natl Acad Sci U S A, 2004. **101**(27): p. 10166-71.
130. Chen, Y.S., et al., *The Chlamydia trachomatis type III secretion chaperone Slc1 engages multiple early effectors, including TepP, a tyrosine-phosphorylated protein required for the recruitment of CrkI-II to nascent inclusions and innate immune signaling.* PLoS Pathog, 2014. **10**(2): p. e1003954.

131. Belland, R.J., et al., *Chlamydia trachomatis cytotoxicity associated with complete and partial cytotoxin genes.* Proc Natl Acad Sci U S A, 2001. **98**(24): p. 13984-9.
132. Clifton, D.R., et al., *Tyrosine phosphorylation of the chlamydial effector protein Tarp is species specific and not required for recruitment of actin.* Infect Immun, 2005. **73**(7): p. 3860-8.
133. Jiwani, S., et al., *Chlamydia trachomatis Tarp harbors distinct G and F actin binding domains that bundle actin filaments.* J Bacteriol, 2013. **195**(4): p. 708-16.
134. Hackstadt, T., *Initial interactions of Chlamydiae with the host cell In: Tan M, editor. Intracellular Pathogens I: Chlamydiales*. 2012, Washington, DC: ASM Press.
135. Thwaites, T.R., et al., *Vinculin Interacts with the Chlamydia Effector TarP Via a Tripartite Vinculin Binding Domain to Mediate Actin Recruitment and Assembly at the Plasma Membrane.* Front Cell Infect Microbiol, 2015. **5**: p. 88.
136. Jewett, T.J., et al., *The conserved Tarp actin binding domain is important for chlamydial invasion.* PLoS Pathog, 2010. **6**(7): p. e1000997.
137. McKuen, M.J., et al., *Fluorescence-Reported Allelic Exchange Mutagenesis Reveals a Role for Chlamydia trachomatis TmeA in Invasion That Is Independent of Host AHNAK.* Infect Immun, 2017. **85**(12).
138. Breton, C., et al., *Structures and mechanisms of glycosyltransferases.* Glycobiology, 2006. **16**(2): p. 29R-37R.
139. Bothe, M., et al., *DXD motif-dependent and -independent effects of the chlamydia trachomatis cytotoxin CT166.* Toxins (Basel), 2015. **7**(2): p. 621-37.
140. Thalmann, J., et al., *Actin re-organization induced by Chlamydia trachomatis serovar D--evidence for a critical role of the effector protein CT166 targeting Rac.* PLoS One, 2010. **5**(3): p. e9887.
141. Hansch, S., et al., *Chlamydia-induced curvature of the host-cell plasma membrane is required for infection.* Proc Natl Acad Sci U S A, 2020. **117**(5): p. 2634-2644.
142. Badour, K., et al., *Interaction of the Wiskott-Aldrich syndrome protein with sorting nexin 9 is required for CD28 endocytosis and cosignaling in T cells.* Proc Natl Acad Sci U S A, 2007. **104**(5): p. 1593-8.
143. Yarar, D., et al., *SNX9 activities are regulated by multiple phosphoinositides through both PX and BAR domains.* Traffic, 2008. **9**(1): p. 133-46.
144. Murra, G., *Identifizierung und Charakterisierung von Adhäsionsproteinen des humanpathogenen Erregers Chlamydia pneumoniae*. 2010: Heinrich-Heine-University Düsseldorf.
145. Kumar, Y. and R.H. Valdivia, *Actin and intermediate filaments stabilize the Chlamydia trachomatis vacuole by forming dynamic structural scaffolds.* Cell Host Microbe, 2008. **4**(2): p. 159-69.
146. Raulston, J.E., *Chlamydial envelope components and pathogen-host cell interactions.* Mol Microbiol, 1995. **15**(4): p. 607-16.
147. Tamura, A., et al., *Electron microscopic observations on the structure of the envelopes of mature elementary bodies and developmental reticulate forms of Chlamydia psittaci.* J Bacteriol, 1971. **105**(1): p. 355-60.
148. Glauert, A.M. and M.J. Thornley, *The topography of the bacterial cell wall.* Annu Rev Microbiol, 1969. **23**: p. 159-98.
149. Filip, C., et al., *Solubilization of the cytoplasmic membrane of Escherichia coli by the ionic detergent sodium-lauryl sarcosinate.* J Bacteriol, 1973. **115**(3): p. 717-22.
150. Caldwell, H.D. and P.J. Hitchcock, *Monoclonal antibody against a genus-specific antigen of Chlamydia species: location of the epitope on chlamydial lipopolysaccharide.* Infect Immun, 1984. **44**(2): p. 306-14.
151. Rund, S., et al., *Structural analysis of the lipopolysaccharide from Chlamydia trachomatis serotype L2.* J Biol Chem, 1999. **274**(24): p. 16819-24.
152. Wylie, J.L., G.M. Hatch, and G. McClarty, *Host cell phospholipids are trafficked to and then modified by Chlamydia trachomatis.* J Bacteriol, 1997. **179**(23): p. 7233-42.

153. Banhart, S., et al., *Sphingolipid Metabolism and Transport in Chlamydia trachomatis and Chlamydia psittaci Infections.* Front Cell Dev Biol, 2019. **7**: p. 223.
154. Lim, J.B. and J.B. Klauda, *Lipid chain branching at the iso- and anteiso-positions in complex Chlamydia membranes: a molecular dynamics study.* Biochim Biophys Acta, 2011. **1808**(1): p. 323-31.
155. Heine, H., et al., *Investigation on the agonistic and antagonistic biological activities of synthetic Chlamydia lipid A and its use in in vitro enzymatic assays.* J Endotoxin Res, 2007. **13**(2): p. 126-32.
156. Ingalls, R.R., et al., *The inflammatory cytokine response to Chlamydia trachomatis infection is endotoxin mediated.* Infect Immun, 1995. **63**(8): p. 3125-30.
157. Egan, A.J. and W. Vollmer, *The physiology of bacterial cell division.* Ann N Y Acad Sci, 2013. **1277**: p. 8-28.
158. Hesse, L., et al., *Functional and biochemical analysis of Chlamydia trachomatis MurC, an enzyme displaying UDP-N-acetylmuramate:amino acid ligase activity.* J Bacteriol, 2003. **185**(22): p. 6507-12.
159. McCoy, A.J., R.C. Sandlin, and A.T. Maurelli, *In vitro and in vivo functional activity of Chlamydia MurA, a UDP-N-acetylglucosamine enolpyruvyl transferase involved in peptidoglycan synthesis and fosfomycin resistance.* Journal of bacteriology, 2003. **185**(4): p. 1218-1228.
160. McCoy, A.J. and A.T. Maurelli, *Characterization of Chlamydia MurC-Ddl, a fusion protein exhibiting D-alanyl-D-alanine ligase activity involved in peptidoglycan synthesis and D-cycloserine sensitivity.* Mol Microbiol, 2005. **57**(1): p. 41-52.
161. McCoy, A.J., et al., *L,L-diaminopimelate aminotransferase, a trans-kingdom enzyme shared by Chlamydia and plants for synthesis of diaminopimelate/lysine.* Proc Natl Acad Sci U S A, 2006. **103**(47): p. 17909-14.
162. Patin, D., et al., *Functional and biochemical analysis of the Chlamydia trachomatis ligase MurE.* J Bacteriol, 2009. **191**(24): p. 7430-5.
163. Patin, D., et al., *Biochemical characterisation of the chlamydial MurF ligase, and possible sequence of the chlamydial peptidoglycan pentapeptide stem.* Arch Microbiol, 2012. **194**(6): p. 505-12.
164. Moulder, J.W., D.L. Novosel, and J.E. Officer, *Inhibition of the Growth of Agents of the Psittacosis Group by D-Cycloserine and Its Specific Reversal by D-Alanine.* J Bacteriol, 1963. **85**: p. 707-11.
165. Tamura, A. and G.P. Manire, *Effect of penicillin on the multiplication of meningopneumonitis organisms (Chlamydia psittaci).* J Bacteriol, 1968. **96**(4): p. 875-80.
166. Jacquier, N., P.H. Viollier, and G. Greub, *The role of peptidoglycan in chlamydial cell division: towards resolving the chlamydial anomaly.* FEMS Microbiol Rev, 2015. **39**(2): p. 262-75.
167. Moulder, J.W., *Why is Chlamydia sensitive to penicillin in the absence of peptidoglycan?* Infect Agents Dis, 1993. **2**(2): p. 87-99.
168. Diepold, A., et al., *Composition, formation, and regulation of the cytosolic c-ring, a dynamic component of the type III secretion injectisome.* PLoS Biol, 2015. **13**(1): p. e1002039.
169. Everett, K.D. and T.P. Hatch, *Architecture of the cell envelope of Chlamydia psittaci 6BC.* J Bacteriol, 1995. **177**(4): p. 877-82.
170. Bini, L., et al., *Mapping of Chlamydia trachomatis proteins by immobiline-polyacrylamide two-dimensional electrophoresis: spot identification by N-terminal sequencing and immunoblotting.* Electrophoresis, 1996. **17**(1): p. 185-90.
171. Nally, J.E., et al., *Characterization of the outer membrane proteome of Leptospira interrogans expressed during acute lethal infection.* Infect Immun, 2007. **75**(2): p. 766-73.
172. Aistleitner, K., et al., *Conserved features and major differences in the outer membrane protein composition of chlamydiae.* Environ Microbiol, 2015. **17**(4): p. 1397-413.

173. Johnson, M. *Detergents: Triton X-100, Tween-20, and More*. 2022-01-29 [cited 2022 24.11.2022]; Available from: https://www.labome.com/method/Detergents-Triton-X-100-Tween-20-and-More.html.
174. Sardinia, L.M., E. Segal, and D. Ganem, *Developmental regulation of the cysteine-rich outer-membrane proteins of murine Chlamydia trachomatis.* J Gen Microbiol, 1988. **134**(4): p. 997-1004.
175. Stephens, R.S., et al., *Diversity of Chlamydia trachomatis major outer membrane protein genes.* J Bacteriol, 1987. **169**(9): p. 3879-85.
176. Hatch, T.P., I. Allan, and J.H. Pearce, *Structural and polypeptide differences between envelopes of infective and reproductive life cycle forms of Chlamydia spp.* J Bacteriol, 1984. **157**(1): p. 13-20.
177. Birkelund, S., et al., *Analysis of proteins in Chlamydia trachomatis L2 outer membrane complex, COMC.* FEMS Immunol Med Microbiol, 2009. **55**(2): p. 187-95.
178. Parsons, L.M., F. Lin, and J. Orban, *Peptidoglycan recognition by Pal, an outer membrane lipoprotein.* Biochemistry, 2006. **45**(7): p. 2122-8.
179. Chen, D., et al., *Characterization of Pgp3, a Chlamydia trachomatis plasmid-encoded immunodominant antigen.* J Bacteriol, 2010. **192**(22): p. 6017-24.
180. Pourhajibagher, M. and A. Bahador, *Designing and in Silico Analysis of PorB Protein from Chlamydia Trachomatis for Developing a Vaccine Candidate.* Drug Res (Stuttg), 2016. **66**(9): p. 479-483.
181. Kawa, D.E. and R.S. Stephens, *Antigenic topology of chlamydial PorB protein and identification of targets for immune neutralization of infectivity.* The Journal of Immunology, 2002. **168**(10): p. 5184-5191.
182. Kubo, A. and R.S. Stephens, *Characterization and functional analysis of PorB, a Chlamydia porin and neutralizing target.* Mol Microbiol, 2000. **38**(4): p. 772-80.
183. Gentle, I.E., L. Burri, and T. Lithgow, *Molecular architecture and function of the Omp85 family of proteins.* Mol Microbiol, 2005. **58**(5): p. 1216-25.
184. Jacob-Dubuisson, F., et al., *First structural insights into the TpsB/Omp85 superfamily.* Biol Chem, 2009. **390**(8): p. 675-84.
185. Tanzer, R.J. and T.P. Hatch, *Characterization of outer membrane proteins in Chlamydia trachomatis LGV serovar L2.* J Bacteriol, 2001. **183**(8): p. 2686-90.
186. Skipp, P., et al., *Shotgun proteomic analysis of Chlamydia trachomatis.* Proteomics, 2005. **5**(6): p. 1558-73.
187. Beeckman, D.S., et al., *Identification and characterization of a type III secretion system in Chlamydophila psittaci.* Vet Res, 2008. **39**(3): p. 27.
188. Li, Z., et al., *The chlamydial plasmid-encoded protein pgp3 is secreted into the cytosol of Chlamydia-infected cells.* Infect Immun, 2008. **76**(8): p. 3415-28.
189. Ramsey, K.H., et al., *Plasmid CDS5 influences infectivity and virulence in a mouse model of Chlamydia trachomatis urogenital infection.* Infect Immun, 2014. **82**(8): p. 3341-9.
190. Zou, Y., et al., *Chlamydia trachomatis plasmid-encoded protein Pgp3 inhibits apoptosis via the PI3K-AKT-mediated MDM2-p53 axis.* Mol Cell Biochem, 2019. **452**(1-2): p. 167-176.
191. Zhou, H., et al., *PORF5 plasmid protein of Chlamydia trachomatis induces MAPK-mediated pro-inflammatory cytokines via TLR2 activation in THP-1 cells.* Sci China Life Sci, 2013. **56**(5): p. 460-6.
192. Cao, W., et al., *Chlamydial plasmid-encoded protein pORF5 induces production of IL-1beta and IL-18 via NALP3 inflammasome activation and p38 MAPK pathway.* Int J Clin Exp Med, 2015. **8**(11): p. 20368-79.
193. Godlewska, R., et al., *Peptidoglycan-associated lipoprotein (Pal) of Gram-negative bacteria: function, structure, role in pathogenesis and potential application in immunoprophylaxis.* FEMS Microbiol Lett, 2009. **298**(1): p. 1-11.

194. Sun, G., et al., *Structural and functional analyses of the major outer membrane protein of Chlamydia trachomatis.* J Bacteriol, 2007. **189**(17): p. 6222-35.
195. Su, H., et al., *Chlamydia trachomatis-host cell interactions: role of the chlamydial major outer membrane protein as an adhesin.* Infect Immun, 1990. **58**(4): p. 1017-25.
196. Su, H. and H.D. Caldwell, *In vitro neutralization of Chlamydia trachomatis by monovalent Fab antibody specific to the major outer membrane protein.* Infect Immun, 1991. **59**(8): p. 2843-5.
197. Baehr, W., et al., *Mapping antigenic domains expressed by Chlamydia trachomatis major outer membrane protein genes.* Proc Natl Acad Sci U S A, 1988. **85**(11): p. 4000-4.
198. Kim, S.K. and R. DeMars, *Epitope clusters in the major outer membrane protein of Chlamydia trachomatis.* Curr Opin Immunol, 2001. **13**(4): p. 429-36.
199. Pal, S., et al., *Immunization with the Chlamydia trachomatis major outer membrane protein, using adjuvants developed for human vaccines, can induce partial protection in a mouse model against a genital challenge.* Vaccine, 2006. **24**(6): p. 766-75.
200. Shaw, J., et al., *Dendritic cells pulsed with a recombinant chlamydial major outer membrane protein antigen elicit a CD4(+) type 2 rather than type 1 immune response that is not protective.* Infect Immun, 2002. **70**(3): p. 1097-105.
201. Pal, S., et al., *Vaccination of mice with DNA plasmids coding for the Chlamydia trachomatis major outer membrane protein elicits an immune response but fails to protect against a genital challenge.* Vaccine, 1999. **17**(5): p. 459-65.
202. Pal, S., et al., *Vaccination with the recombinant major outer membrane protein elicits long-term protection in mice against vaginal shedding and infertility following a Chlamydia muridarum genital challenge.* NPJ Vaccines, 2020. **5**: p. 90.
203. Everett, K.D., D.M. Desiderio, and T.P. Hatch, *Characterization of lipoprotein EnvA in Chlamydia psittaci 6BC.* J Bacteriol, 1994. **176**(19): p. 6082-7.
204. Hatch, T.P., *Disulfide cross-linked envelope proteins: the functional equivalent of peptidoglycan in chlamydiae?* J Bacteriol, 1996. **178**(1): p. 1-5.
205. Watson, M.W., P.R. Lambden, and I.N. Clarke, *Genetic diversity and identification of human infection by amplification of the chlamydial 60-kilodalton cysteine-rich outer membrane protein gene.* J Clin Microbiol, 1991. **29**(6): p. 1188-93.
206. Newhall, W.J.t., *Biosynthesis and disulfide cross-linking of outer membrane components during the growth cycle of Chlamydia trachomatis.* Infect Immun, 1987. **55**(1): p. 162-8.
207. Fechtner, T., et al., *Characterization of the interaction between the chlamydial adhesin OmcB and the human host cell.* J Bacteriol, 2013. **195**(23): p. 5323-33.
208. Allen, J.E. and R.S. Stephens, *Identification by sequence analysis of two-site posttranslational processing of the cysteine-rich outer membrane protein 2 of Chlamydia trachomatis serovar L2.* J Bacteriol, 1989. **171**(1): p. 285-91.
209. Ting, L.M., et al., *Interaction of outer envelope proteins of Chlamydia psittaci GPIC with the HeLa cell surface.* Infect Immun, 1995. **63**(9): p. 3600-8.
210. Stephens, R.S., et al., *Heparin-binding outer membrane protein of chlamydiae.* Mol Microbiol, 2001. **40**(3): p. 691-9.
211. Fadel, S. and A. Eley, *Differential glycosaminoglycan binding of Chlamydia trachomatis OmcB protein from serovars E and LGV.* J Med Microbiol, 2008. **57**(Pt 9): p. 1058-1061.
212. Natale, P., T. Bruser, and A.J. Driessen, *Sec- and Tat-mediated protein secretion across the bacterial cytoplasmic membrane--distinct translocases and mechanisms.* Biochim Biophys Acta, 2008. **1778**(9): p. 1735-56.
213. Green, E.R. and J. Mecsas, *Bacterial Secretion Systems: An Overview.* Microbiol Spectr, 2016. **4**(1).
214. Papanikou, E., S. Karamanou, and A. Economou, *Bacterial protein secretion through the translocase nanomachine.* Nat Rev Microbiol, 2007. **5**(11): p. 839-51.

215. Robinson, C. and A. Bolhuis, *Tat-dependent protein targeting in prokaryotes and chloroplasts.* Biochim Biophys Acta, 2004. **1694**(1-3): p. 135-47.
216. Sargent, F., et al., *Sec-independent protein translocation in Escherichia coli. A distinct and pivotal role for the TatB protein.* J Biol Chem, 1999. **274**(51): p. 36073-82.
217. Pop, O., et al., *The twin-arginine signal peptide of PhoD and the TatAd/Cd proteins of Bacillus subtilis form an autonomous Tat translocation system.* J Biol Chem, 2002. **277**(5): p. 3268-73.
218. Berks, B.C., T. Palmer, and F. Sargent, *Protein targeting by the bacterial twin-arginine translocation (Tat) pathway.* Curr Opin Microbiol, 2005. **8**(2): p. 174-81.
219. Meuskens, I., et al., *Type V Secretion Systems: An Overview of Passenger Domain Functions.* Front Microbiol, 2019. **10**: p. 1163.
220. Costa, T.R., et al., *Secretion systems in Gram-negative bacteria: structural and mechanistic insights.* Nat Rev Microbiol, 2015. **13**(6): p. 343-59.
221. Leo, J.C., I. Grin, and D. Linke, *Type V secretion: mechanism(s) of autotransport through the bacterial outer membrane.* Philos Trans R Soc Lond B Biol Sci, 2012. **367**(1592): p. 1088-101.
222. Grimwood, J. and R.S. Stephens, *Computational analysis of the polymorphic membrane protein superfamily of Chlamydia trachomatis and Chlamydia pneumoniae.* Microb Comp Genomics, 1999. **4**(3): p. 187-201.
223. Henderson, I.R. and A.C. Lam, *Polymorphic proteins of Chlamydia spp.--autotransporters beyond the Proteobacteria.* Trends Microbiol, 2001. **9**(12): p. 573-8.
224. Klauser, T., J. Pohlner, and T.F. Meyer, *The secretion pathway of IgA protease-type proteins in gram-negative bacteria.* Bioessays, 1993. **15**(12): p. 799-805.
225. Guerin, J., et al., *Two-Partner Secretion: Combining Efficiency and Simplicity in the Secretion of Large Proteins for Bacteria-Host and Bacteria-Bacteria Interactions.* Front Cell Infect Microbiol, 2017. **7**: p. 148.
226. Sijbrandi, R., et al., *Signal recognition particle (SRP)-mediated targeting and Sec-dependent translocation of an extracellular Escherichia coli protein.* J Biol Chem, 2003. **278**(7): p. 4654-9.
227. Tsirigotaki, A., et al., *Protein export through the bacterial Sec pathway.* Nat Rev Microbiol, 2017. **15**(1): p. 21-36.
228. Baud, C., et al., *Role of DegP for two-partner secretion in Bordetella.* Mol Microbiol, 2009. **74**(2): p. 315-29.
229. Ieva, R. and H.D. Bernstein, *Interaction of an autotransporter passenger domain with BamA during its translocation across the bacterial outer membrane.* Proc Natl Acad Sci U S A, 2009. **106**(45): p. 19120-5.
230. Oberhettinger, P., et al., *Intimin and invasin export their C-terminus to the bacterial cell surface using an inverse mechanism compared to classical autotransport.* PLoS One, 2012. **7**(10): p. e47069.
231. Pavlova, O., et al., *Mechanistic link between beta barrel assembly and the initiation of autotransporter secretion.* Proc Natl Acad Sci U S A, 2013. **110**(10): p. E938-47.
232. Weirich, J., et al., *Identifying components required for OMP biogenesis as novel targets for antiinfective drugs.* Virulence, 2017. **8**(7): p. 1170-1188.
233. Jain, S. and M.B. Goldberg, *Requirement for YaeT in the outer membrane assembly of autotransporter proteins.* J Bacteriol, 2007. **189**(14): p. 5393-8.
234. Lee, J., et al., *Substrate binding to BamD triggers a conformational change in BamA to control membrane insertion.* Proc Natl Acad Sci U S A, 2018. **115**(10): p. 2359-2364.
235. Henderson, I.R., et al., *Type V protein secretion pathway: the autotransporter story.* Microbiol Mol Biol Rev, 2004. **68**(4): p. 692-744.
236. Choi, P.S. and H.D. Bernstein, *Sequential translocation of an Escherchia coli two-partner secretion pathway exoprotein across the inner and outer membranes.* Mol Microbiol, 2010. **75**(2): p. 440-51.

237. Kang'ethe, W. and H.D. Bernstein, *Charge-dependent secretion of an intrinsically disordered protein via the autotransporter pathway.* Proc Natl Acad Sci U S A, 2013. **110**(45): p. E4246-55.
238. Grijpstra, J., et al., *Autotransporter secretion: varying on a theme.* Res Microbiol, 2013. **164**(6): p. 562-82.
239. Emsley, P., et al., *Structure of Bordetella pertussis virulence factor P.69 pertactin.* Nature, 1996. **381**(6577): p. 90-2.
240. Junker, M., et al., *Pertactin beta-helix folding mechanism suggests common themes for the secretion and folding of autotransporter proteins.* Proc Natl Acad Sci U S A, 2006. **103**(13): p. 4918-23.
241. Charbonneau, M.E., F. Berthiaume, and M. Mourez, *Proteolytic processing is not essential for multiple functions of the Escherichia coli autotransporter adhesin involved in diffuse adherence (AIDA-I).* J Bacteriol, 2006. **188**(24): p. 8504-12.
242. Dautin, N., et al., *Cleavage of a bacterial autotransporter by an evolutionarily convergent autocatalytic mechanism.* EMBO J, 2007. **26**(7): p. 1942-52.
243. Barnard, T.J., et al., *Autotransporter structure reveals intra-barrel cleavage followed by conformational changes.* Nat Struct Mol Biol, 2007. **14**(12): p. 1214-20.
244. Bernstein, H.D., *Looks can be deceiving: recent insights into the mechanism of protein secretion by the autotransporter pathway.* Mol Microbiol, 2015. **97**(2): p. 205-15.
245. Longbottom, D., et al., *Molecular cloning and characterization of the genes coding for the highly immunogenic cluster of 90-kilodalton envelope proteins from the Chlamydia psittaci subtype that causes abortion in sheep.* Infect Immun, 1998. **66**(4): p. 1317-24.
246. Longbottom, D., et al., *Identification of a multigene family coding for the 90 kDa proteins of the ovine abortion subtype of Chlamydia psittaci.* FEMS Microbiol Lett, 1996. **142**(2-3): p. 277-81.
247. Knudsen, K., et al., *Identification of two novel genes encoding 97- to 99-kilodalton outer membrane proteins of Chlamydia pneumoniae.* Infect Immun, 1999. **67**(1): p. 375-83.
248. Van Lent, S., et al., *Analysis of Polymorphic Membrane Protein Expression in Cultured Cells Identifies PmpA and PmpH of Chlamydia psittaci as Candidate Factors in Pathogenesis and Immunity to Infection.* PLoS One, 2016. **11**(9): p. e0162392.
249. Read, T.D., et al., *Genome sequences of Chlamydia trachomatis MoPn and Chlamydia pneumoniae AR39.* Nucleic Acids Res, 2000. **28**(6): p. 1397-406.
250. Thomson, N.R., et al., *The Chlamydophila abortus genome sequence reveals an array of variable proteins that contribute to interspecies variation.* Genome Res, 2005. **15**(5): p. 629-40.
251. Carlson, J.H., et al., *Comparative genomic analysis of Chlamydia trachomatis oculotropic and genitotropic strains.* Infect Immun, 2005. **73**(10): p. 6407-18.
252. Abdelsamed, H., J. Peters, and G.I. Byrne, *Genetic variation in Chlamydia trachomatis and their hosts: impact on disease severity and tissue tropism.* Future Microbiol, 2013. **8**(9): p. 1129-1146.
253. Tan, C., et al., *Variable expression of surface-exposed polymorphic membrane proteins in in vitro-grown Chlamydia trachomatis.* Cell Microbiol, 2010. **12**(2): p. 174-87.
254. Kiselev, A.O., et al., *Expression, processing, and localization of PmpD of Chlamydia trachomatis Serovar L2 during the chlamydial developmental cycle.* PLoS One, 2007. **2**(6): p. e568.
255. Nunes, A., et al., *Comparative expression profiling of the Chlamydia trachomatis pmp gene family for clinical and reference strains.* PLoS One, 2007. **2**(9): p. e878.
256. Vasilevsky, S., et al., *Chlamydial polymorphic membrane proteins: regulation, function and potential vaccine candidates.* Virulence, 2016. **7**(1): p. 11-22.
257. Carrasco, J.A., et al., *Altered developmental expression of polymorphic membrane proteins in penicillin-stressed Chlamydia trachomatis.* Cell Microbiol, 2011. **13**(7): p. 1014-25.
258. Gomes, J.P., et al., *Polymorphisms in the nine polymorphic membrane proteins of Chlamydia trachomatis across all serovars: evidence for serovar Da recombination and correlation with tissue tropism.* J Bacteriol, 2006. **188**(1): p. 275-86.

259. Struyve, M., M. Moons, and J. Tommassen, *Carboxy-terminal phenylalanine is essential for the correct assembly of a bacterial outer membrane protein.* J Mol Biol, 1991. **218**(1): p. 141-8.
260. Dautin, N. and H.D. Bernstein, *Protein secretion in gram-negative bacteria via the autotransporter pathway.* Annu Rev Microbiol, 2007. **61**: p. 89-112.
261. Leyton, D.L., A.E. Rossiter, and I.R. Henderson, *From self sufficiency to dependence: mechanisms and factors important for autotransporter biogenesis.* Nat Rev Microbiol, 2012. **10**(3): p. 213-25.
262. Hillman, R.D., Jr., Y.M. Baktash, and J.J. Martinez, *OmpA-mediated rickettsial adherence to and invasion of human endothelial cells is dependent upon interaction with alpha2beta1 integrin.* Cell Microbiol, 2013. **15**(5): p. 727-41.
263. Wells, T.J., M. Totsika, and M.A. Schembri, *Autotransporters of Escherichia coli: a sequence-based characterization.* Microbiology (Reading), 2010. **156**(Pt 8): p. 2459-2469.
264. Thornton, D.J., K. Rousseau, and M.A. McGuckin, *Structure and function of the polymeric mucins in airways mucus.* Annu Rev Physiol, 2008. **70**: p. 459-86.
265. Nielsen, H., *Predicting Secretory Proteins with SignalP.* Methods Mol Biol, 2017. **1611**: p. 59-73.
266. Kall, L., A. Krogh, and E.L. Sonnhammer, *Advantages of combined transmembrane topology and signal peptide prediction--the Phobius web server.* Nucleic Acids Res, 2007. **35**(Web Server issue): p. W429-32.
267. Soding, J., *Protein homology detection by HMM-HMM comparison.* Bioinformatics, 2005. **21**(7): p. 951-60.
268. Jefferys, B.R., L.A. Kelley, and M.J. Sternberg, *Protein folding requires crowd control in a simulated cell.* J Mol Biol, 2010. **397**(5): p. 1329-38.
269. Kallberg, M., et al., *Template-based protein structure modeling using the RaptorX web server.* Nat Protoc, 2012. **7**(8): p. 1511-22.
270. Team, R., *RStudio: Integrated Development Environment for R*. 2021, RStudio, PBC. p. Used code by Fabienne Kocher.
271. Kari, L., et al., *Chlamydia trachomatis polymorphic membrane protein D is a virulence factor involved in early host-cell interactions.* Infect Immun, 2014. **82**(7): p. 2756-62.
272. Crane, D.D., et al., *Chlamydia trachomatis polymorphic membrane protein D is a species-common pan-neutralizing antigen.* Proc Natl Acad Sci U S A, 2006. **103**(6): p. 1894-9.
273. Grimwood, J., L. Olinger, and R.S. Stephens, *Expression of Chlamydia pneumoniae polymorphic membrane protein family genes.* Infect Immun, 2001. **69**(4): p. 2383-9.
274. Montigiani, S., et al., *Genomic approach for analysis of surface proteins in Chlamydia pneumoniae.* Infect Immun, 2002. **70**(1): p. 368-79.
275. Luczak, S.E., et al., *The Chlamydia pneumoniae Adhesin Pmp21 Forms Oligomers with Adhesive Properties.* J Biol Chem, 2016. **291**(43): p. 22806-22818.
276. Swanson, K.A., et al., *Chlamydia trachomatis polymorphic membrane protein D is an oligomeric autotransporter with a higher-order structure.* Infect Immun, 2009. **77**(1): p. 508-16.
277. Paes, W., et al., *The Chlamydia trachomatis PmpD adhesin forms higher order structures through disulphide-mediated covalent interactions.* PLoS One, 2018. **13**(6): p. e0198662.
278. Favaroni, A. and J.H. Hegemann, *Chlamydia trachomatis Polymorphic Membrane Proteins (Pmps) Form Functional Homomeric and Heteromeric Oligomers.* Front Microbiol, 2021. **12**: p. 709724.
279. Kiselev, A.O., M.C. Skinner, and M.F. Lampe, *Analysis of pmpD expression and PmpD post-translational processing during the life cycle of Chlamydia trachomatis serovars A, D, and L2.* PLoS One, 2009. **4**(4): p. e5191.
280. Vandahl, B.B., et al., *The expression, processing and localization of polymorphic membrane proteins in Chlamydia pneumoniae strain CWL029.* BMC Microbiol, 2002. **2**: p. 36.
281. Wehrl, W., et al., *From the inside out--processing of the Chlamydial autotransporter PmpD and its role in bacterial adhesion and activation of human host cells.* Mol Microbiol, 2004. **51**(2): p. 319-34.

282. Organization, W.H., *Progress report of the implementation of the global strategy for prevention and control of sexually transmitted infections: 2006-2015: document for the World Health Assembly.* 2015.
283. Peipert, J.F., *Clinical practice. Genital chlamydial infections.* N Engl J Med, 2003. **349**(25): p. 2424-30.
284. Brunham, R.C., S.L. Gottlieb, and J. Paavonen, *Pelvic inflammatory disease.* N Engl J Med, 2015. **372**(21): p. 2039-48.
285. Brunham, R.C. and R. Rappuoli, *Chlamydia trachomatis control requires a vaccine.* Vaccine, 2013. **31**(15): p. 1892-7.
286. Liang, S., et al., *Considerations for the rational design of a Chlamydia vaccine.* Hum Vaccin Immunother, 2017. **13**(4): p. 831-835.
287. Nichols, R.L., et al., *Studies on trachoma. V. Clinical observations in a field trial of bivalent trachoma vaccine at three dosage levels in Saudi Arabia.* Am J Trop Med Hyg, 1966. **15**(4): p. 639-47.
288. Woolridge, R.L., et al., *Field trial of a monovalent and of a bivalent mineral oil adjuvant trachoma vaccine in Taiwan school children.* Am J Ophthalmol, 1967. **63**(5): p. Suppl:1645-50.
289. Mordhorst, C.H., *Experimental infections and immunogenicity of TRIC agents in monkeys.* Am J Ophthalmol, 1967. **63**(5): p. Suppl:1603-15.
290. Wang, S.P., J.T. Grayston, and E.R. Alexander, *Trachoma vaccine studies in monkeys.* Am J Ophthalmol, 1967. **63**(5): p. Suppl:1615-30.
291. Tan, M., J. Hegemann, and C. Suetterlin, *Chlamydia Biology: From Genome to Disease*. 2020, Norfolk, UK: Caister Academic Press. 570.
292. de la Maza, L.M. and E.M. Peterson, *Vaccines for Chlamydia trachomatis infections.* Curr Opin Investig Drugs, 2002. **3**(7): p. 980-6.
293. Pal, S., et al., *Immunization with the Chlamydia trachomatis mouse pneumonitis major outer membrane protein can elicit a protective immune response against a genital challenge.* Infect Immun, 2001. **69**(10): p. 6240-7.
294. Sun, G., et al., *Protection against an intranasal challenge by vaccines formulated with native and recombinant preparations of the Chlamydia trachomatis major outer membrane protein.* Vaccine, 2009. **27**(36): p. 5020-5.
295. Olsen, A.W., et al., *Protection Against Chlamydia trachomatis Infection and Upper Genital Tract Pathological Changes by Vaccine-Promoted Neutralizing Antibodies Directed to the VD4 of the Major Outer Membrane Protein.* J Infect Dis, 2015. **212**(6): p. 978-89.
296. Bunk, S., et al., *Immunoproteomic identification and serological responses to novel Chlamydia pneumoniae antigens that are associated with persistent C. pneumoniae infections.* The Journal of Immunology, 2008. **180**(8): p. 5490-5498.
297. Tan, C., et al., *Chlamydia trachomatis-infected patients display variable antibody profiles against the nine-member polymorphic membrane protein family.* Infect Immun, 2009. **77**(8): p. 3218-26.
298. Wheelhouse, N., et al., *Transcriptional analysis of in vitro expression patterns of Chlamydophila abortus polymorphic outer membrane proteins during the chlamydial developmental cycle.* Vet Res, 2009. **40**(5): p. 47.
299. Wheelhouse, N., et al., *Expression patterns of five polymorphic membrane proteins during the Chlamydia abortus developmental cycle.* Vet Microbiol, 2012. **160**(3-4): p. 525-9.
300. Paes, W., et al., *Recombinant polymorphic membrane protein D in combination with a novel, second-generation lipid adjuvant protects against intra-vaginal Chlamydia trachomatis infection in mice.* Vaccine, 2016. **34**(35): p. 4123-4131.
301. Muller, T., et al., *Vaccination with the polymorphic membrane protein A reduces Chlamydia muridarum induced genital tract pathology.* Vaccine, 2017. **35**(21): p. 2801-2810.

302. Pal, S., et al., *Comparison of the nine polymorphic membrane proteins of Chlamydia trachomatis for their ability to induce protective immune responses in mice against a C. muridarum challenge.* Vaccine, 2017. **35**(19): p. 2543-2549.
303. Eanes, E.D. and G.G. Glenner, *X-ray diffraction studies on amyloid filaments.* J Histochem Cytochem, 1968. **16**(11): p. 673-7.
304. Sipe, J.D. and A.S. Cohen, *Review: history of the amyloid fibril.* J Struct Biol, 2000. **130**(2-3): p. 88-98.
305. Sunde, M., et al., *Common core structure of amyloid fibrils by synchrotron X-ray diffraction.* J Mol Biol, 1997. **273**(3): p. 729-39.
306. Harada, R., et al., *Imaging Protein Misfolding in the Brain Using beta-Sheet Ligands.* Front Neurosci, 2018. **12**: p. 585.
307. Luis Del Pozo-Yauner, B.B., Adrián Ochoa-Leyva, Sandra Leticia Rodríguez-Ambriz, Julio Isael Pérez Carrión, Guadalupe Zavala-Padilla, Rosana Sánchez-López & Daniel Alejandro Fernández Velasco *The Structural Determinants of the Immunoglobulin Light Chain Amyloid Aggregation.* Physical Biology of Proteins and Peptides, 2015.
308. Smith, J.F., et al., *Characterization of the nanoscale properties of individual amyloid fibrils.* Proc Natl Acad Sci U S A, 2006. **103**(43): p. 15806-11.
309. Knowles, T.P. and M.J. Buehler, *Nanomechanics of functional and pathological amyloid materials.* Nat Nanotechnol, 2011. **6**(8): p. 469-79.
310. Hardy, J.A. and G.A. Higgins, *Alzheimer's disease: the amyloid cascade hypothesis.* Science, 1992. **256**(5054): p. 184-5.
311. Hurshman, A.R., et al., *Transthyretin aggregation under partially denaturing conditions is a downhill polymerization.* Biochemistry, 2004. **43**(23): p. 7365-81.
312. Chuang, E., et al., *Amyloid assembly and disassembly.* J Cell Sci, 2018. **131**(8).
313. Crespo, R., et al., *A generic crystallization-like model that describes the kinetics of amyloid fibril formation.* J Biol Chem, 2012. **287**(36): p. 30585-94.
314. So, M., D. Hall, and Y. Goto, *Revisiting supersaturation as a factor determining amyloid fibrillation.* Curr Opin Struct Biol, 2016. **36**: p. 32-9.
315. Yoshimura, Y., et al., *Distinguishing crystal-like amyloid fibrils and glass-like amorphous aggregates from their kinetics of formation.* Proc Natl Acad Sci U S A, 2012. **109**(36): p. 14446-51.
316. Young, L.M., A.E. Ashcroft, and S.E. Radford, *Small molecule probes of protein aggregation.* Curr Opin Chem Biol, 2017. **39**: p. 90-99.
317. Breydo, L. and V.N. Uversky, *Structural, morphological, and functional diversity of amyloid oligomers.* FEBS Lett, 2015. **589**(19 Pt A): p. 2640-8.
318. Chatani, E. and N. Yamamoto, *Recent progress on understanding the mechanisms of amyloid nucleation.* Biophys Rev, 2018. **10**(2): p. 527-534.
319. Morris, A.M., M.A. Watzky, and R.G. Finke, *Protein aggregation kinetics, mechanism, and curve-fitting: a review of the literature.* Biochim Biophys Acta, 2009. **1794**(3): p. 375-97.
320. Kelly, J.W., *Mechanisms of amyloidogenesis.* Nat Struct Biol, 2000. **7**(10): p. 824-6.
321. Serio, T.R., et al., *Nucleated conformational conversion and the replication of conformational information by a prion determinant.* Science, 2000. **289**(5483): p. 1317-21.
322. Lomakin, A., et al., *On the nucleation and growth of amyloid beta-protein fibrils: detection of nuclei and quantitation of rate constants.* Proc Natl Acad Sci U S A, 1996. **93**(3): p. 1125-9.
323. Jackson, M.P. and E.W. Hewitt, *Why are Functional Amyloids Non-Toxic in Humans?* Biomolecules, 2017. **7**(4).
324. Pham, C.L., A.H. Kwan, and M. Sunde, *Functional amyloid: widespread in Nature, diverse in purpose.* Essays Biochem, 2014. **56**: p. 207-19.
325. Otzen, D., *Functional amyloid: turning swords into plowshares.* Prion, 2010. **4**(4): p. 256-64.
326. Otzen, D. and R. Riek, *Functional Amyloids.* Cold Spring Harb Perspect Biol, 2019. **11**(12).

327. Barnhart, M.M. and M.R. Chapman, *Curli biogenesis and function.* Annu Rev Microbiol, 2006. **60**: p. 131-47.
328. Anderl, A., H. Kolmar, and H.L. Fuchsbauer, *The metal-binding properties of the long chaplin from Streptomyces mobaraensis: A bioinformatic and biochemical approach.* J Inorg Biochem, 2020. **202**: p. 110878.
329. Ashami, K., et al., *Droplet and fibril formation of the functional amyloid Orb2.* J Biol Chem, 2021. **297**(1): p. 100804.
330. Cereghetti, G., et al., *Reversible, functional amyloids: towards an understanding of their regulation in yeast and humans.* Cell Cycle, 2018. **17**(13): p. 1545-1558.
331. Grignaschi, E., et al., *A hydrophobic low-complexity region regulates aggregation of the yeast pyruvate kinase Cdc19 into amyloid-like aggregates in vitro.* J Biol Chem, 2018. **293**(29): p. 11424-11432.
332. Stansfield, I. and M.F. Tuite, *Polypeptide chain termination in Saccharomyces cerevisiae.* Curr Genet, 1994. **25**(5): p. 385-95.
333. Balbirnie, M., R. Grothe, and D.S. Eisenberg, *An amyloid-forming peptide from the yeast prion Sup35 reveals a dehydrated beta-sheet structure for amyloid.* Proc Natl Acad Sci U S A, 2001. **98**(5): p. 2375-80.
334. Daskalov, A., et al., *Identification of a novel cell death-inducing domain reveals that fungal amyloid-controlled programmed cell death is related to necroptosis.* Proc Natl Acad Sci U S A, 2016. **113**(10): p. 2720-5.
335. Shanmugam, N., et al., *Microbial functional amyloids serve diverse purposes for structure, adhesion and defence.* Biophys Rev, 2019. **11**(3): p. 287-302.
336. Blanco, L.P., et al., *Diversity, biogenesis and function of microbial amyloids.* Trends Microbiol, 2012. **20**(2): p. 66-73.
337. Picken, M.M., *The Pathology of Amyloidosis in Classification: A Review.* Acta Haematol, 2020. **143**(4): p. 322-334.
338. Iadanza, M.G., et al., *A new era for understanding amyloid structures and disease.* Nat Rev Mol Cell Biol, 2018. **19**(12): p. 755-773.
339. Nelson, R., et al., *Structure of the cross-beta spine of amyloid-like fibrils.* Nature, 2005. **435**(7043): p. 773-8.
340. Jucker, M. and L.C. Walker, *Self-propagation of pathogenic protein aggregates in neurodegenerative diseases.* Nature, 2013. **501**(7465): p. 45-51.
341. Knowles, T.P., M. Vendruscolo, and C.M. Dobson, *The amyloid state and its association with protein misfolding diseases.* Nat Rev Mol Cell Biol, 2014. **15**(6): p. 384-96.
342. Burre, J., M. Sharma, and T.C. Sudhof, *Cell Biology and Pathophysiology of alpha-Synuclein.* Cold Spring Harb Perspect Med, 2018. **8**(3).
343. O'Brien, R.J. and P.C. Wong, *Amyloid precursor protein processing and Alzheimer's disease.* Annu Rev Neurosci, 2011. **34**: p. 185-204.
344. Tiwari, S., et al., *Alzheimer's disease: pathogenesis, diagnostics, and therapeutics.* Int J Nanomedicine, 2019. **14**: p. 5541-5554.
345. Maroteaux, L., J.T. Campanelli, and R.H. Scheller, *Synuclein: a neuron-specific protein localized to the nucleus and presynaptic nerve terminal.* J Neurosci, 1988. **8**(8): p. 2804-15.
346. Burre, J., M. Sharma, and T.C. Sudhof, *Definition of a molecular pathway mediating alpha-synuclein neurotoxicity.* J Neurosci, 2015. **35**(13): p. 5221-32.
347. Spillantini, M.G., et al., *Alpha-synuclein in Lewy bodies.* Nature, 1997. **388**(6645): p. 839-40.
348. Wakabayashi, K., et al., *NACP, a presynaptic protein, immunoreactivity in Lewy bodies in Parkinson's disease.* Neurosci Lett, 1997. **239**(1): p. 45-8.
349. Singleton, A.B., et al., *alpha-Synuclein locus triplication causes Parkinson's disease.* Science, 2003. **302**(5646): p. 841.

350. Ibanez, P., et al., *Causal relation between alpha-synuclein gene duplication and familial Parkinson's disease.* Lancet, 2004. **364**(9440): p. 1169-71.
351. Desplats, P., et al., *Inclusion formation and neuronal cell death through neuron-to-neuron transmission of alpha-synuclein.* Proc Natl Acad Sci U S A, 2009. **106**(31): p. 13010-5.
352. Volpicelli-Daley, L.A., et al., *Exogenous alpha-synuclein fibrils induce Lewy body pathology leading to synaptic dysfunction and neuron death.* Neuron, 2011. **72**(1): p. 57-71.
353. Burre, J., M. Sharma, and T.C. Sudhof, *Systematic mutagenesis of alpha-synuclein reveals distinct sequence requirements for physiological and pathological activities.* J Neurosci, 2012. **32**(43): p. 15227-42.
354. Rey, N.L., et al., *Transfer of human alpha-synuclein from the olfactory bulb to interconnected brain regions in mice.* Acta Neuropathol, 2013. **126**(4): p. 555-73.
355. Zhu, X.C., et al., *Rate of early onset Alzheimer's disease: a systematic review and meta-analysis.* Ann Transl Med, 2015. **3**(3): p. 38.
356. Ayodele, T., et al., *Early-Onset Alzheimer's Disease: What Is Missing in Research?* Curr Neurol Neurosci Rep, 2021. **21**(2): p. 4.
357. Seltzer, B. and I. Sherwin, *A comparison of clinical features in early- and late-onset primary degenerative dementia. One entity or two?* Arch Neurol, 1983. **40**(3): p. 143-6.
358. de la Torre, J.C., *How do heart disease and stroke become risk factors for Alzheimer's disease?* Neurol Res, 2006. **28**(6): p. 637-44.
359. Revill, P., M.A. Moral, and J.R. Prous, *Impaired insulin signaling and the pathogenesis of Alzheimer's disease.* Drugs Today (Barc), 2006. **42**(12): p. 785-90.
360. Szczygielski, J., et al., *Traumatic brain injury: cause or risk of Alzheimer's disease? A review of experimental studies.* J Neural Transm (Vienna), 2005. **112**(11): p. 1547-64.
361. Miklossy, J., *Alzheimer's disease--a spirochetosis?* Neuroreport, 1993. **4**(7): p. 841-8.
362. Itzhaki, R.F., et al., *Herpes simplex virus type 1 in brain and risk of Alzheimer's disease.* Lancet, 1997. **349**(9047): p. 241-4.
363. Balin, B.J., et al., *Identification and localization of Chlamydia pneumoniae in the Alzheimer's brain.* Med Microbiol Immunol, 1998. **187**(1): p. 23-42.
364. Li, F., M. Hearn, and L.E. Bennett, *The role of microbial infection in the pathogenesis of Alzheimer's disease and the opportunity for protection by anti-microbial peptides.* Crit Rev Microbiol, 2021. **47**(2): p. 240-253.
365. Lustbader, J.W., et al., *ABAD directly links Aß to mitochondrial toxicity in Alzheimer's disease.* Science, 2004. **304**(5669): p. 448-452.
366. Malenka, R.C., *Bear MF.* LTP and LTD: an embarrassment of riches. Neuron, 2004. **44**: p. 5-21.
367. Chang, E.H., et al., *AMPA receptor downscaling at the onset of Alzheimer's disease pathology in double knockin mice.* Proceedings of the National Academy of Sciences, 2006. **103**(9): p. 3410-3415.
368. Oh, E.S., et al., *Amyloid precursor protein increases cortical neuron size in transgenic mice.* Neurobiol Aging, 2009. **30**(8): p. 1238-44.
369. Lee, J., et al., *Adaptor protein sorting nexin 17 regulates amyloid precursor protein trafficking and processing in the early endosomes.* J Biol Chem, 2008. **283**(17): p. 11501-8.
370. Koo, E.H., et al., *Precursor of amyloid protein in Alzheimer disease undergoes fast anterograde axonal transport.* Proc Natl Acad Sci U S A, 1990. **87**(4): p. 1561-5.
371. Ehehalt, R., et al., *Amyloidogenic processing of the Alzheimer beta-amyloid precursor protein depends on lipid rafts.* J Cell Biol, 2003. **160**(1): p. 113-23.
372. Thinakaran, G. and E.H. Koo, *Amyloid precursor protein trafficking, processing, and function.* J Biol Chem, 2008. **283**(44): p. 29615-9.

373. Jan, A., et al., *The ratio of monomeric to aggregated forms of Aβ40 and Aβ42 is an important determinant of amyloid-β aggregation, fibrillogenesis, and toxicity.* Journal of Biological Chemistry, 2008. **283**(42): p. 28176-28189.
374. Butterfield, D.A., *Amyloid beta-peptide (1-42)-induced oxidative stress and neurotoxicity: implications for neurodegeneration in Alzheimer's disease brain. A review.* Free Radic Res, 2002. **36**(12): p. 1307-13.
375. Walsh, D.M. and D.J. Selkoe, *Deciphering the molecular basis of memory failure in Alzheimer's disease.* Neuron, 2004. **44**(1): p. 181-93.
376. Yankner, B.A., et al., *Neurotoxicity of a fragment of the amyloid precursor associated with Alzheimer's disease.* Science, 1989. **245**(4916): p. 417-20.
377. Deshpande, A., et al., *Different conformations of amyloid beta induce neurotoxicity by distinct mechanisms in human cortical neurons.* J Neurosci, 2006. **26**(22): p. 6011-8.
378. Shankar, G.M., et al., *Amyloid-beta protein dimers isolated directly from Alzheimer's brains impair synaptic plasticity and memory.* Nat Med, 2008. **14**(8): p. 837-42.
379. Bao, F., et al., *Different beta-amyloid oligomer assemblies in Alzheimer brains correlate with age of disease onset and impaired cholinergic activity.* Neurobiol Aging, 2012. **33**(4): p. 825 e1-13.
380. Glabe, C.G., *Structural classification of toxic amyloid oligomers.* J Biol Chem, 2008. **283**(44): p. 29639-43.
381. Stefani, M., *Biochemical and biophysical features of both oligomer/fibril and cell membrane in amyloid cytotoxicity.* FEBS J, 2010. **277**(22): p. 4602-13.
382. Stephan, A., S. Laroche, and S. Davis, *Generation of aggregated beta-amyloid in the rat hippocampus impairs synaptic transmission and plasticity and causes memory deficits.* J Neurosci, 2001. **21**(15): p. 5703-14.
383. Giuffrida, M.L., et al., *Beta-amyloid monomers are neuroprotective.* J Neurosci, 2009. **29**(34): p. 10582-7.
384. Lombardo, S. and U. Maskos, *Role of the nicotinic acetylcholine receptor in Alzheimer's disease pathology and treatment.* Neuropharmacology, 2015. **96**(Pt B): p. 255-62.
385. Kostylev, M.A., et al., *Liquid and Hydrogel Phases of PrP(C) Linked to Conformation Shifts and Triggered by Alzheimer's Amyloid-beta Oligomers.* Mol Cell, 2018. **72**(3): p. 426-443 e12.
386. Silva, M.V.F., et al., *Alzheimer's disease: risk factors and potentially protective measures.* J Biomed Sci, 2019. **26**(1): p. 33.
387. Khan, S.S. and G.S. Bloom, *Tau: The Center of a Signaling Nexus in Alzheimer's Disease.* Front Neurosci, 2016. **10**: p. 31.
388. Heppner, F.L., R.M. Ransohoff, and B. Becher, *Immune attack: the role of inflammation in Alzheimer disease.* Nat Rev Neurosci, 2015. **16**(6): p. 358-72.
389. Li, H., et al., *Amyloid, tau, pathogen infection and antimicrobial protection in Alzheimer's disease -conformist, nonconformist, and realistic prospects for AD pathogenesis.* Transl Neurodegener, 2018. **7**: p. 34.
390. Panza, F., et al., *Time to test antibacterial therapy in Alzheimer's disease.* Brain, 2019. **142**(10): p. 2905-2929.
391. Dando, S.J., et al., *Pathogens penetrating the central nervous system: infection pathways and the cellular and molecular mechanisms of invasion.* Clin Microbiol Rev, 2014. **27**(4): p. 691-726.
392. Soscia, S.J., et al., *The Alzheimer's disease-associated amyloid beta-protein is an antimicrobial peptide.* PLoS One, 2010. **5**(3): p. e9505.
393. Bourgade, K., et al., *beta-Amyloid peptides display protective activity against the human Alzheimer's disease-associated herpes simplex virus-1.* Biogerontology, 2015. **16**(1): p. 85-98.
394. Bourgade, K., et al., *Protective Effect of Amyloid-beta Peptides Against Herpes Simplex Virus-1 Infection in a Neuronal Cell Culture Model.* J Alzheimers Dis, 2016. **50**(4): p. 1227-41.

395. Moir, R.D., R. Lathe, and R.E. Tanzi, *The antimicrobial protection hypothesis of Alzheimer's disease.* Alzheimers Dement, 2018. **14**(12): p. 1602-1614.
396. Ashraf, G.M., et al., *The Possibility of an Infectious Etiology of Alzheimer Disease.* Mol Neurobiol, 2019. **56**(6): p. 4479-4491.
397. Gerard, H.C., et al., *Chlamydophila (Chlamydia) pneumoniae in the Alzheimer's brain.* FEMS Immunol Med Microbiol, 2006. **48**(3): p. 355-66.
398. Hammond, C.J., et al., *Immunohistological detection of Chlamydia pneumoniae in the Alzheimer's disease brain.* BMC Neurosci, 2010. **11**: p. 121.
399. Little, C.S., et al., *Chlamydia pneumoniae induces Alzheimer-like amyloid plaques in brains of BALB/c mice.* Neurobiol Aging, 2004. **25**(4): p. 419-29.
400. Hahn, D.L., et al., *Chlamydia pneumoniae as a respiratory pathogen.* Front Biosci, 2002. **7**: p. e66-76.
401. Aronsson, F., et al., *Invasion and persistence of the neuroadapted influenza virus A/WSN/33 in the mouse olfactory system.* Viral Immunol, 2003. **16**(3): p. 415-23.
402. De Chiara, G., et al., *Infectious agents and neurodegeneration.* Mol Neurobiol, 2012. **46**(3): p. 614-38.
403. Haase, A.T., *Pathogenesis of lentivirus infections.* Nature, 1986. **322**(6075): p. 130-6.
404. Peluso, R., et al., *A Trojan Horse mechanism for the spread of visna virus in monocytes.* Virology, 1985. **147**(1): p. 231-6.
405. Rasmussen, S.J., et al., *Secretion of proinflammatory cytokines by epithelial cells in response to Chlamydia infection suggests a central role for epithelial cells in chlamydial pathogenesis.* J Clin Invest, 1997. **99**(1): p. 77-87.
406. Kumar, D.K., et al., *Amyloid-beta peptide protects against microbial infection in mouse and worm models of Alzheimer's disease.* Sci Transl Med, 2016. **8**(340): p. 340ra72.
407. Nochlin, D., et al., *Failure to detect Chlamydia pneumoniae in brain tissues of Alzheimer's disease.* Neurology, 1999. **53**(8): p. 1888.
408. Gieffers, J., et al., *Failure to detect Chlamydia pneumoniae in brain sections of Alzheimer's disease patients.* J Clin Microbiol, 2000. **38**(2): p. 881-2.
409. Ring, R.H. and J.M. Lyons, *Failure to detect Chlamydia pneumoniae in the late-onset Alzheimer's brain.* J Clin Microbiol, 2000. **38**(7): p. 2591-4.
410. Taylor, G.S., et al., *Failure to correlate C. pneumoniae with late onset Alzheimer's disease.* Neurology, 2002. **59**(1): p. 142-3.
411. Shima, K., G. Kuhlenbaumer, and J. Rupp, *Chlamydia pneumoniae infection and Alzheimer's disease: a connection to remember?* Med Microbiol Immunol, 2010. **199**(4): p. 283-9.
412. Biancalana, M. and S. Koide, *Molecular mechanism of Thioflavin-T binding to amyloid fibrils.* Biochim Biophys Acta, 2010. **1804**(7): p. 1405-12.
413. Van Gerven, N., et al., *The Role of Functional Amyloids in Bacterial Virulence.* J Mol Biol, 2018. **430**(20): p. 3657-3684.
414. LeVine, H., 3rd, *Thioflavine T interaction with synthetic Alzheimer's disease beta-amyloid peptides: detection of amyloid aggregation in solution.* Protein Sci, 1993. **2**(3): p. 404-10.
415. Nans, A., H.R. Saibil, and R.D. Hayward, *Pathogen-host reorganization during Chlamydia invasion revealed by cryo-electron tomography.* Cell Microbiol, 2014. **16**(10): p. 1457-72.
416. Golan, N., et al., *Structure and Conservation of Amyloid Spines From the Candida albicans Als5 Adhesin.* Front Mol Biosci, 2022. **9**: p. 926959.
417. Sapi, E., et al., *Borrelia and Chlamydia Can Form Mixed Biofilms in Infected Human Skin Tissues.* Eur J Microbiol Immunol (Bp), 2019. **9**(2): p. 46-55.
418. Al-Atrache, Z., et al., *Astrocytes infected with Chlamydia pneumoniae demonstrate altered expression and activity of secretases involved in the generation of beta-amyloid found in Alzheimer disease.* BMC Neurosci, 2019. **20**(1): p. 6.

419. Leissring, M.A., et al., *Enhanced proteolysis of beta-amyloid in APP transgenic mice prevents plaque formation, secondary pathology, and premature death.* Neuron, 2003. **40**(6): p. 1087-93.
420. Du, Y., et al., *alpha2-Macroglobulin as a beta-amyloid peptide-binding plasma protein.* J Neurochem, 1997. **69**(1): p. 299-305.
421. Carson, J.A. and A.J. Turner, *Beta-amyloid catabolism: roles for neprilysin (NEP) and other metallopeptidases?* J Neurochem, 2002. **81**(1): p. 1-8.
422. Wang, L., et al., *Epidermal growth factor receptor is a preferred target for treating amyloid-beta-induced memory loss.* Proc Natl Acad Sci U S A, 2012. **109**(41): p. 16743-8.
423. Lauren, J., *Cellular prion protein as a therapeutic target in Alzheimer's disease.* J Alzheimers Dis, 2014. **38**(2): p. 227-44.
424. Um, J.W., et al., *Alzheimer amyloid-beta oligomer bound to postsynaptic prion protein activates Fyn to impair neurons.* Nat Neurosci, 2012. **15**(9): p. 1227-35.
425. Rosener, N.S., et al., *A d-enantiomeric peptide interferes with heteroassociation of amyloid-beta oligomers and prion protein.* J Biol Chem, 2018. **293**(41): p. 15748-15764.
426. Kong, C., et al., *Binding between Prion Protein and Abeta Oligomers Contributes to the Pathogenesis of Alzheimer's Disease.* Virol Sin, 2019. **34**(5): p. 475-488.
427. Brody, A.H. and S.M. Strittmatter, *Synaptotoxic Signaling by Amyloid Beta Oligomers in Alzheimer's Disease Through Prion Protein and mGluR5.* Adv Pharmacol, 2018. **82**: p. 293-323.
428. Lauren, J., et al., *Cellular prion protein mediates impairment of synaptic plasticity by amyloid-beta oligomers.* Nature, 2009. **457**(7233): p. 1128-32.
429. Bate, C. and A. Williams, *Amyloid-beta-induced synapse damage is mediated via cross-linkage of cellular prion proteins.* J Biol Chem, 2011. **286**(44): p. 37955-37963.
430. Kudo, W., et al., *Cellular prion protein is essential for oligomeric amyloid-beta-induced neuronal cell death.* Hum Mol Genet, 2012. **21**(5): p. 1138-44.
431. Chung, E., et al., *Anti-PrPC monoclonal antibody infusion as a novel treatment for cognitive deficits in an Alzheimer's disease model mouse.* BMC Neurosci, 2010. **11**: p. 130.
432. Gimbel, D.A., et al., *Memory impairment in transgenic Alzheimer mice requires cellular prion protein.* J Neurosci, 2010. **30**(18): p. 6367-74.
433. Ferreira, D.G., et al., *alpha-synuclein interacts with PrP(C) to induce cognitive impairment through mGluR5 and NMDAR2B.* Nat Neurosci, 2017. **20**(11): p. 1569-1579.
434. Little, C.S., et al., *Age alterations in extent and severity of experimental intranasal infection with Chlamydophila pneumoniae in BALB/c mice.* Infect Immun, 2005. **73**(3): p. 1723-34.
435. Chacko, A., et al., *Chlamydia pneumoniae can infect the central nervous system via the olfactory and trigeminal nerves and contributes to Alzheimer's disease risk.* Sci Rep, 2022. **12**(1): p. 2759.
436. Gieffers, J., et al., *Chlamydia pneumoniae infection in circulating human monocytes is refractory to antibiotic treatment.* Circulation, 2001. **103**(3): p. 351-6.
437. Gieffers, J., et al., *Phagocytes transmit Chlamydia pneumoniae from the lungs to the vasculature.* Eur Respir J, 2004. **23**(4): p. 506-10.
438. MacIntyre, A., et al., *Chlamydia pneumoniae infection promotes the transmigration of monocytes through human brain endothelial cells.* J Neurosci Res, 2003. **71**(5): p. 740-50.
439. Eimer, W.A., et al., *Alzheimer's Disease-Associated beta-Amyloid Is Rapidly Seeded by Herpesviridae to Protect against Brain Infection.* Neuron, 2018. **99**(1): p. 56-63 e3.
440. Vojtechova, I., et al., *Infectious origin of Alzheimer's disease: Amyloid beta as a component of brain antimicrobial immunity.* PLoS Pathog, 2022. **18**(11): p. e1010929.
441. Spitzer, P., et al., *Amyloidogenic amyloid-beta-peptide variants induce microbial agglutination and exert antimicrobial activity.* Sci Rep, 2016. **6**: p. 32228.
442. Butterfield, S.M. and H.A. Lashuel, *Amyloidogenic protein-membrane interactions: mechanistic insight from model systems.* Angew Chem Int Ed Engl, 2010. **49**(33): p. 5628-54.

443. Jones, S.V. and I. Kounatidis, *Nuclear Factor-Kappa B and Alzheimer Disease, Unifying Genetic and Environmental Risk Factors from Cell to Humans.* Front Immunol, 2017. **8**: p. 1805.
444. Rowley, J., et al., *Chlamydia, gonorrhoea, trichomoniasis and syphilis: global prevalence and incidence estimates, 2016.* Bull World Health Organ, 2019. **97**(8): p. 548-562P.
445. Phillips, S., B.L. Quigley, and P. Timms, *Seventy Years of Chlamydia Vaccine Research - Limitations of the Past and Directions for the Future.* Front Microbiol, 2019. **10**: p. 70.
446. Lanfermann, C., et al., *Prophylactic Multi-Subunit Vaccine against Chlamydia trachomatis: In Vivo Evaluation in Mice.* Vaccines (Basel), 2021. **9**(6).

# Abbildungsverzeichnis

Abbildung 1: Taxonomische Einteilung der Ordnung Chlamydiales. ..... 12
Abbildung 2: Biphasische Vermehrungszyklus von Chlamydien. ..... 17
Abbildung 3: Schematisches Adhäsionsmodell für C. pneumoniae und C. trachomatis. ..... 21
Abbildung 4: Schematische Darstellung der chlamydialen Zellwand..... 26
Abbildung 5: Schematische Darstellung des Typ-5-Sekretionssystems. ..... 32
Abbildung 6: Anordnung der pmp-Gene im Genom von C. trachomatis serovar E DK-20. ..... 33
Abbildung 7: Schematische Darstellung der C. trachomatis Serovar E Pmps. ..... 35
Abbildung 8: Schematische Darstellung der Prozessierung von C. pneumoniae Pmp21. ..... 42
Abbildung 9: Schematische Darstellung einer Kreuz-β Konformation. ..... 45
Abbildung 10: Schematische Darstellung der klassischen Amyloid-Assemblierung und der nukleierenden Konformationsumwandlung zu Amyloid-Fibrillen..... 47
Abbildung 11: Zusammenfassende schematische Darstellung der APP-Prozessierung. ..... 51
Abbildung 12: Zusammenfassendes Modell der Pmp-Präsentation und dessen Auswirkungen im Infektionsprozess ..... 171

# Danksagung

Zu allererst bedanke ich mich herzlich bei meinem Doktorvater Prof. Dr. Johannes Hegemann. Nachdem mir das Arbeiten mit CPn0104 innerhalb meiner Masterarbeit sehr viel Freude bereitete, gab er mir die Chance meine wissenschaftliche Neugier und Leidenschaft in der Infektionsforschung in Form einer Promotion weiter auszuüben. Ich bedanke mich für die Diskussionen, Ratschläge und experimentellen Vorschläge während unserer Treffen, welche meinen wissenschaftlichen Horizont erweiterten, mir das Gefühl gaben an etwas Wichtigem zu Arbeiten und es mir ermöglichten, viele Kooperationen innerhalb meiner Promotions-Zeit aufzubauen.

Großer Dank gilt ebenfalls Prof. Dr. Klaus Pfeffer für die Übernahme des Koreferats und für die vielen guten experimentellen Ideen während unserer Meetings.

Ein großer Dank gilt ebenfalls Jun.-Prof. Dr. Wolfgang Hoyer, Filip Hasecke und Dr. Nadine Rösener. Die konstruktiven Diskussionen und das Arbeiten in und mit der physikalischen Biologie ermöglichte mir, meine Fragestellungen aus einem ganz neuen Blickwinkel zu betrachten, auf neuen Wegen zu Erforschen und zu Vertiefen. Die daraus resultierte lange anhaltende Kooperation schätze ich sehr.

Ebenfalls möchte ich mich bei den Arbeitsgruppen von Prof. Dr. Andreas Klos und Prof. Dr. Carlos Alberto Guzman bedanken. Zusammen waren wir in der Lage, einen Impfstoff zu entwickeln und damit einen Beitrag in der Bekämpfung gegen Chlamydien zu leisten.

Bedanken möchte ich mich auch bei Prof. Dr. Ursula Fleig für ihre konstruktive Kritik und Hilfsbereitschaft bei der Entwicklung meines Verteidigungsvortrages.

Besonderer Dank geht an meine Arbeitsgruppe AG-Hegemann und die AG-Fleig. Das Leben im stätigen gegenseitigen Austausch, die Hilfsbereitschaft, Kollegialität und manchmal auch Chaos und Unfug waren für mich über die Zeit wie eine zweite Familie geworden, welche ich mit schwerem Herzen vermissen werde. Selten findet man Kollegen im Leben, mit welchen man sich anfreundet, auch außerhalb der Uni super versteht und gerne Zeit verbringt.

Der größte Dank geht an meine Eltern und insbesondere an meine Mutter. Vielen lieben Dank für den stätigen Zuspruch, Ansporn, die Motivation und das offene Ohr, wenn es im Labor und drumherum stressig wurde oder Experimente mal nicht funktioniert haben.

Mein letzter Dank gilt natürlich den Korrektoren dieser Arbeit und Dir, lieber Leser, der vielleicht nichts mit Biologie am Hut hat aber sich mal eine Chlamydien-bezogene Dissertation durchlesen wollte :)

# Eidesstattliche Erklärung

Hiermit versichere ich, dass die vorliegende Arbeit von mir selbst verfasst wurde und dass ich keine anderen als die von mir angegebenen Hilfsmittel verwendet habe. Alle Stellen, die aus anderen Werken im Wortlaut oder dem Sinn entsprechend übernommen wurden, habe ich mit Quellenangaben kenntlich gemacht.

Sebastian Wintgens

(Düsseldorf, Mai 2023)